Universidad de Las Palmas de Gran Canaria

Escuela de Doctorado
Programa de Doctorado en Empresa, Internet y Tecnologías de las Comunicaciones

Tesis Doctoral

Analysis and Classification of Motor Dysfunctions in Gait by Using Wearable Sensors

Análisis y clasificación de las disfunciones motoras en caminar mediante sensores que envían información corporal

Tobias Steinmetzer

This dissertation is submitted for the degree of
International Doctor of Philosophy (PhD)

Director/a 1: Prof. Dr. Carlos M. Travieso-González
Director/a 2: Prof. Dr.-Ing. Ingrid Bönninger

El Director   El Codirector   El Doctorando

Las Palmas de Gran Canaria, Spain, Julio de 2020

LaTeX

Abstract

English

The life expectancy of the population is continuously increasing. This increasing life expectancy is related to the increasing quality of life and goes hand in hand with technical progress. Increasing life expectancy also gives rise to new problems that need to be overcome. One of the biggest problems is diseases of old age, which often result in pathological disorders in gait, such as Parkinson's disease. The diagnosis of Parkinson's disease is made using the Unified Parkinson's Disease Rating Scale (UPDRS). Nevertheless, medical decisions are subjective, as each physician evaluates a patient's gait differently. For this reason, it is essential to objectify this decision. Measuring the gait of a human by using sensors solves this problem. For this reason, this work deals with the development of a wearable system for mobile gait analysis. It is shown how such a system was implemented prototypically. The system consists of two wristbands, two insoles, and a smartphone. The wearables use Inertial Measurement Units (IMU) and Force Sensing Resistors (FSR). Furthermore, a method to synchronize these devices is presented. This ensures higher data quality and allows new approaches to analysis. To ensure that the devices work energy-efficiently, activity recognition based on Convolutional Neural Networks (CNN) was developed. The activity detection model can detect the activity *Gait* to all other activities with a probability of 94.7%. If the smartphone detects the activity *Gait*, a connection to the wearable sensors is automatically established, and the gait is recorded. When analyzing the gait, the first important step is to detect individual strides while walking. For this purpose, a CNN model was developed, which can detect strides with an accuracy of 95.8%. Based on these individual strides, it is possible to make a detailed analysis of the gait cycle. From the gait cycle, the parameters stride length, stride height, stride duration, stance phase duration, swing phase duration, Symmetry Ratio Index, Symmetry Index, Gait Asymmetry, Symmetry Angle and Normalized Dynamic Time Warping (DTW)Symmetry were calculated. Normalized (DTW) Symmetry is a proprietary method that compensates for the weaknesses of the Symmetry Ratio Index, Symmetry Index, GaitAsymmetry, and Symmetry Angle methods. The arm swing was classified using the Wavelet Transformation. Here, motor disorders in the arm could be detected with an accuracy of 90.3%. The stage of Parkinson's disease could be determined by means of the IMU sensors in the insole. Hierarchical clustering was carried out, and the DTWwas used as a metric. The Parkinson's stage could be detected with a specificity of 92%.

Spain

La esperanza de vida de la población aumenta constantemente. Esto está relacionado con el aumento de la calidad de vida y va de la mano con el progreso técnico. Sin embargo, el aumento de la esperanza de vida también da lugar a nuevos problemas que deben ser superados. Unos de los mayores problemas son las enfermedades de la vejez, que a menudo se relacionan con trastornos patológicos en la marcha, como la enfermedad de Parkinson. El diagnóstico de la enfermedad de Parkinson se hace usando la Escala Unificada de Calificación de la Enfermedad de Parkinson (UPDRS). No obstante, las decisiones médicas son subjetivas, ya que cada médico evalúa la marcha de un paciente de manera diferente. Por esta razón, es importante objetivar esta decisión. Medir la marcha de un humano por medio de sensores resuelve este problema. Por esta razón, esta tesis trata sobre el desarrollo de un sistema portátil para el análisis de la marcha. Con un sistema móvil, los diagnósticos también pueden hacerse por medio de la telemedicina en la vida diaria. En esta tesis se muestra cómo tal sistema fue implementado prototípicamente. El sistema consiste en dos muñequeras, dos plantillas y un teléfono inteligente. Los wearables usan Inertial Measurement Unit (IMU) y Force Sensing Resistor (FSR). Además, en la tesis se presenta un método para sincronizar estos dispositivos. Esto asegura una mayor calidad de los datos y permite nuevos enfoques de análisis. Para garantizar que los dispositivos funcionen con eficiencia energética, se implementó la detección de actividad basada en las Redes Neuronales Convolucionales (CNN). El modelo de detección de actividad es capaz de detectar la actividad Gait a todas las demás actividades de una probabilidad del 94.7%. Si el smartphone detecta la actividad Gait, se establece automáticamente una conexión con los sensores portátiles y se graba la marcha. Al analizar la marcha, el primer paso importante es detectar las zancadas individuales mientras se camina. Para ello se desarrolló una CNN, que es capaz de detectar zancadas con una precisión del 95,8%. Basándose en estos pasos individuales es posible hacer un análisis detallado del ciclo de marcha. A partir del ciclo de marcha se calcularon los parámetros longitud de la zancada, altura de la zancada, duración de la zancada, duración de la fase de apoyo, duración de la fase de balanceo, índice de relación de simetría, índice de simetría, asimetría de la marcha, ángulo de simetría y Normalized Dynamic Time Warping (DTW). Normalized Symmetry es un método propio que compensa las debilidades de los métodos del índice de relación de simetría, índice de simetría, asimetría de marcha y ángulo de simetría. El balanceo del brazo fue clasificado usando una transformación Wavelet. Aquí, los des órdenes motores en el brazo pudieron ser detectados con una precisión del 90.3%. El estado de la enfermedad de Parkinson podría determinarse por medio de los sensores IMU de la plantilla. Se llevó a cabo un hierarchical clustering y se utilizó el DTW como métrica. El estado de Parkinson podría ser detectada con una especificidad del 92%.

German

Die Lebenserwartung der Bevölkerung nimmt stetig zu. Dies hängt mit der steigenden Lebensqualität zusammen und geht einher mit dem technischen Fortschritt. Aus der immer höher werden Lebenserwartung ergeben sich aber auch neue Probleme. Eins der größten Probleme sind Alterskrankheiten, welche oft im Zusammenhang mit pathologischen Störungen im Gang stehen, wie zum Beispiel der Parkinsonkrankheit. Das Stadium der Parkinsonkrankheit wird mithilfe der Unified Parkinson's Disease Rating Scale (UPDRS) klssifiziert. Die ärztlichen Entscheidungen sind dennoch subjektiv, da jeder Arzt den Gang eines Patienten unterschiedlich bewertet. Daher ist es wichtig, diese Entscheidung zu objektivieren. Den Gang des Menschen mittels Sensoren zu messen, löst dieses Problem. Aus diesem Grund beschäftigt sich die Arbeit mit der Entwicklung eines tragbaren Systems zur mobilen Ganganalyse. Durch ein mobiles System können Diagnosen per Telemedizin im täglichen Leben erfolgen. In dieser Arbeit wird gezeigt, wie dieses System prototypisch umgesetzt wurde. Das System besteht aus zwei Armbändern, zwei Einlegesohlen und einem Smartphone. Die Wearables nutzen Inertial Measurement Units (IMU) und Force Sensing Resistors (FSR). Weiterhin wird in der Arbeit eine Methode präsentiert, um diese Geräte zu synchronisieren. Dies gewährleistet eine höhere Datenqualität und erlaubt neue Ansätze bei der Analyse. Damit die Geräte energieeffizient arbeiten, wurde eine Aktivitätserkennung basierend auf Convolutional Neural Networks (CNN) umgesetzt. Das Modell zur Aktivitätserkennung ist in der Lage, die Aktivität *Gait* von allen anderen Aktivitäten mit einer Wahrscheinlichkeit von 94,7% zu unterscheiden. Erkennt das Smartphone die Aktivität *Gait*, wird automatisch eine Verbindung zu den tragbaren Sensoren aufgebaut und der Gang aufgezeichnet. Bei der Analyse des Gangs ist der erste wichtige Schritt die Erkennung der einzelnen Schritte beim Gehen. Hierfür wurde ein CNN entwickelt, welches in der Lage ist, Schritte mit einer Genauigkeit von 95,8% zu erkennen. Anhand dieser einzelnen Schritte ist es möglich, eine detaillierte Analyse des Gangzyklus vorzunehmen. Aus dem Gangzyklus wurden die Parameter Schrittlänge, -höhe, -dauer, Standphasendauer, Schwungphasendauer, Symmetrie Ratio Index, Symmetrie Index, Gait Asymmetry, Summetry Angle und Normalized Dynamic Time Warping (DTW) Symmetry berechnet. Die Normalized (DTW) Symmetry ist ein eigenes Verfahren, welches die Schwächen der Methoden Symmetrie Ratio Index, Symmetrie Index, Gait Asymmetry und Summetry Angle ausgleicht. Der Armschwung wurde mithilfe der Wavelet Transformation klassifiziert. Hier konnten motorische Störungen im Arm mit einer Genauigkeit von 90,3% festgestellt werden. Das Parkinsonstadium konnte anhand der IMU-Sensoren in den Einlegesohlen festgestellt werden. Hier wurde eine hierarchische Clusterung durchgeführt und als Metrik die DTW verwendet. Das Parkinsonstadium konnte mit einer Spezifität von 92% festgestellt werden.

Acknowledge

In this part of my work, I would like to thank all people, without their help and support this work would not have been possible.

Contents

Acronyms

Acronym	Definition
AF	automatic framing
AF+CNN	Automatic Framing and Convolutional Neuronal Networks
BBS	Berg Balance Score
BLE	Bluetooth Low Energy
CNN	Convolutional Neuronal Networks
DGI	Dynamic Gait Index
DTW	Dynamic Time Warping
FFT	Fast Fourier Transformation
FRT	Functional Reach test
GA	Gait Asymmetry
HS	Heel strike
HMM	Hidden Markov Models
id	identification number
IMI	Internet- and Mobile-based Interventions
IQR	Interquartile range
MDR	Medical Device Regulation
MST	middle stance phase
MSW	middle swing phase
MMP	Min-Max Patterns
MD	motor dysfunctions
NDTWS	Normalized dynamic time warping symmetry
OS	operating system
PD	Parkinson's disease
RI	Ratio Index
RGB	Red Green Blue color space
ReLU	rectified linear unit
SLS	Single Leg Stance
SA	Symmetry Angle
SI	Symmetry Index
TPU	Thermoplastic elastomer based on urethane
3D	three-dimensional
TM	Threshold Model
TUG	Timed Up and Go
TO	Toe off
UPDRS	United Parkinson's Disease Rating Scale

1

Introduction

1.1. Background

> *"When Plato gave the tongue-in-cheek definition of man as 'featherless bipeds,' Diogenes plucked a chicken and brought it into Plato's Academy, saying, 'Behold! I've brought you a man,' and so the Academy added 'with broad flat nails' to the definition"*

> - Diogenes Laërtius [Laertius1925]

As the quote from Diogenes Laërtius [Laertius1925] shows, the human being is defined as unique. However, as unique as the human being is himself, so is his gait. The bipedal gait has always fascinated researchers. Anthropologists have since then developed numerous theories to explain why humans walk on two legs. One theory is that baby monkeys clung to their mothers during growing up. For this reason, the mothers were limited to collecting food. Therefore, they learned to stand on two legs. This enabled mothers to use their hands more effectively when searching for food [Lovejoy1981]. A second theory is that due to the reduction of the forests more than seven million years ago, primates could no longer swing from tree to tree. Thus, the food was also limited and the monkeys had to cover a distance on the ground. By standing on two legs, the primates could effectively move around. In addition, movement on two legs was more energy-efficient [Leakey1981].

The bipedal gait is a very complex process. Even though the gait is basically used to walk from one place to another. However, the requirements are different for each person and task. If the hands are free during walking, they can provide additional support for the gait. However, it is difficult for the body to keep its balance if it has to carry heavy objects. When carrying a hot coffee, the body must move as calmly as possible. The gait pattern depends on age, sex, height, physique, weight, mass distribution, living conditions, which profession is or was performed, environment (new or familiar place), mental condition [Gotz2006].

The complexity of gait requires the interaction of the nervous system, muscles, and the cardiorespiratory system. For this reason, diseases also manifest themselves in the human gait pattern [Pirker2017]. Injuries, diseases, or imbalance restricts human mobility. Which results in loss of general health [Lord2013], quality of life [Hirvensalo2000], cognitive disorders [Verghese2007], and the risk of falling [Beauchet2009]. From a clinical point of view, the analysis of human gait is of particular importance because gait disorders

in neurodegenerative diseases such as multiple sclerosis, amyotrophic lateral sclerosis, or Parkinson's disease (PD), occur in a high percentage of the older world population [Muro2014]. James Parkinson's first published the description of Parkinson's disease in his work in 1817. Symptoms such as tremor, temporary impaired posture, small strides, slowed gait, and the risk of falling were presented at six different patients [Parkinson1817]. Today, the United Parkinson's Disease Rating Scale (UPDRS) Part III [Goetz2008] assess motor ability as a result of Parkinson's disease, and the Hoehn and Yahr scale [Hoehn1998] is used to assess the stage of Parkinson's disease. Nevertheless, opinion is often subjective when assessing patients. Therefore, the results show low inter-rate reliability [Martinez1994, Richards1994].

Thus, a sensor-based method of measuring motor symptoms is essential for the objective evaluation of human gait. According to Maetzler [Maetzler2016], a technological system used in medical practices must have the following characteristics:

- provide valid and accurate results that are clinically relevant,

- contribute to an ecologically effective therapeutic decision (e.g., by influencing the patients health-related quality of life),

- offer a target range (i.e., a range to provide adequate information about a treatment response or disease course), and

- allow easy and repetitive use for medical staff and Parkinson's disease patients [Maetzler2016].

For this reason, this work is to develop a wearable system that measures the legs and arms motor function with quantitative methods. Based on these measured values, it should be possible to objectify the deciding process for the human gait in order to be able to conclude more accurately on motor dysfunctions.

1.2. Motivation

As covered in section 1.1, motor dysfunctions are usually assessed by the visual examination of physicians or gait specialists. The assessments are based on experience. Therefore, the assessment is subjective. For this reason, the focus of this thesis will be on the development of a sensor-based gait analysis system for objective gait analysis. In the context of the cooperation with the Niederlausitz Clinic Senftenberg, a system shall be developed, which can objectify the diagnosis of Parkinson's patients. As a requirement, the system should be wearable and suitable for everyday use because the clinic and other hospitals cannot set up an extra room for gait analysis. Furthermore, it should be inexpensive and easy to use, so that it is economical. Gait deviations such as asymmetry are one of the characteristic symptoms of patients with Parkinson's disease that contribute to the risk of falls [Zhang2018]. The gait analysis should be able to evaluate the patients' symmetry while moving, calculate several gait features, and evaluate if a patient has motor dysfunctions.

1.3. Hypotheses

In this thesis, the following hypothesis is tested: It is possible to evaluate the success of therapy, motor disorders, and Parkinson's stage by using wearables devices in daily life. The following terms are investigated and referenced in this thesis:

- It is possible to create wearables devices for the measurement of motion in every day.

- Wearables devices for motion measurement can be synchronized.

- The activity *Gait* can be extracted from all other activities

- The individual strides can be automatically extracted from the time series of the measured values.

- The time series can be used to determine the gait symmetry values of the gait symmetry more precisely than the features of the individual strides.

- The time series of the gait can be used to determine the stage of Parkinson's disease.

1.4. Objectives

In order to ensure a linear sequence of work to achieve each goal in a coherent manner, the following objectives have been defined:

Sensor selection: First of all, it has to be clarified, which sensors are used for gait analysis. For this reason, basic knowledge about sensors and systems for gait analysis must be collected. Based on this knowledge, a selection of sensors has to be made to solve the problem.

Create wearable hardware: The second task is to select the type of the devices and the positions for mounting them. For the solution to this problem, the biomechanical functionality of the body will have to be studied. A complete hardware solution will be developed due to the extensive knowledge of sensor technology and biomechanical functions. Once the hardware prototypes are developed, the firmware and an Android app for controlling the wearables have to be implemented. When the software development phase is completed, however, there is still the problem that the wearable devices do not work synchronously in time. Therefore, an algorithm for solving this problem has to be developed.

Study design: The next step is to create data sets, that are used for gait analysis. The following scenarios must be considered:

- A data set of everyday life that is to be created. Thereby, it should be achieved that with Android App, only the human gait is recognized again all other activities. This has the advantage that the wearables are only switched on when they are needed. Thus, should promotes an energy-efficient use of the sensors.

- A medical data set should be created. Analyses are then to be carried out on the basis of this data set. In order for the medical data set to be collected, the medical gait test must be defined, and the approval of the ethics committee must be obtained.

Data analysis: While the data is being collected step by step, the data analysis starts already. Here, individual strides should first be identified. This is the basis for calculating various gait parameters such as stride length, stride height, duration of gait phases, and gait symmetry. Furthermore, machine learning models for the classification of the data will be developed.

1.5. Structure of this work

In view of the broad scope of this work, it has been decided to write a separate state of the art for each chapter to ensure that the core message is retained. This should improve the reading flow and understanding.

To understand the biomechanics of the gait cycle, Chapter 2 - *Medicine and biomechanics fundamentals of gait* describes the phases and features of gait, symptoms of Parkinson's disease, and medical tests. In the following Chapter 3 - *Preliminary works*, previous works are presented. These form a basis for this work. In this work, there was research on gesture recognition and on measuring therapeutic success through gamification. For the realization of the Hardware different prototypes were developed. The first prototype consisted of the microcontrollers from Moticon. Afterward it was decided to build an own microcontroller. Both variants are presented in Chapter 4 - *Hardware*. Chapter 5 - *Study and data sets* present the used data sets. Two own data sets were recorded for the data analysis, and one public data set was used to confirm the results. To understand the complete algorithm, it is described in Chapter 6 - *Methodology*. To ensure that the wearables are energy efficient, they are only turned on when they are needed. For this purpose, an activity recognition with the smartphone was developed in Chapter 7 - *Activity recognition*. An essential prerequisite for the later analysis is that the wearables are synchronized. Chapter 8 - *Synchronization* provides the concept for this. Stride detection is the basis for the later calculation of gait features. For this reason, a special focus was placed on this chapter. For the stride detection in Chapter 9 - *Stride detection*, three algorithms were compared. Chapter 10 - *Stride features* give an overview of the calculated gait features. A separation is made between parameters in time and spatial. Although gait symmetry is gait features, it has been decided to

separate the chapter 11 - *Gait symmetry*, since this thesis introduces a new concept for the calculation. Chapter 12 - *Classification of motor dysfunctions in arm swing* describe how motor disorders can be identified by using wavelet transformation. The Parkinson's stage can be detected with the help of Dynamic Time Warping (DTW). Which is explain in Chapter 13 - *Clustering of Parkinson's stadium*. The results of the previous chapters are discussed in Chapter 14 - *Discussion*. Chapter 15 gives a conclusion of the work and Chapter 16 interesting points for future work.

Afterward the annex follows: In A. - *Ethics application*, the ethics application is attached. This was necessary to take recordings of people in the hospital with the wearable system. A Spanish summary of the work is B. - *Summary in Spanish/ Resumen en Español* shown. The confirmation of the residence abroad in Germany from the Erasmus program is in C. - *Erasmus* included. All publications are given in a list and full text in D. - *Publications*. The last annex E. - *Certificates* shows all certificates that were earned during the time of the doctorate.

2
Medicine and biomechanics fundamentals of gait

2.1. Time gait features

The human gait is a repeated process during walking. The analysis of the gait always focuses on a single leg. The gait can be divided into a stance phase and a swing phase, as shown in Figure 2.1. The stance phase represents 60 %, and the swing phase 40 % of the cycle. The division into stance and swing phase is very general. The gait cycle begins with the placement of the heel, the heel strike. When the foot is on the floor, and both legs are parallel, this is the mid-stance. The last ground contact before take-off is the terminal stance. Pre-swing is the moment when the foot swings back to the maximum point. If both legs are parallel during the swing phase, this is called mid-swing. Afterward the cycle starts again with the heel strike. Finally, there is a categorization in which the phase identification depends on the number of legs on the floor. If one leg is on the ground, this is the single support; if both are on the ground, this is the double support. Furthermore, the cadence is often given corresponds to the steps per minute.

2.2. Spatial gait features

Gait has not only time features. Various spatial parameters can also be measured, see Figure 2.2. The step length measures the distance between both legs. In contrast, the stride length is the distance of a single leg after a gait cycle. The step width measures the distance between both legs. The step angle indicates the angle of the foot to the walking direction.

2.3. Parkinson's Disease

Parkinson's disease progresses slowly and cannot be cured at present [Thumler2002]. In addition, the course of the disease and the symptoms it causes are individual for each patient, which means that a false diagnosis is made in many cases. Nevertheless, the individual stages of the disease can be distinguished and classified. The classification of the disease stages by Hoehn and Yahr scale [Hoehn1998] is still internationally recognized today. The stages are numbered from one to five and sorted by severity and spread of
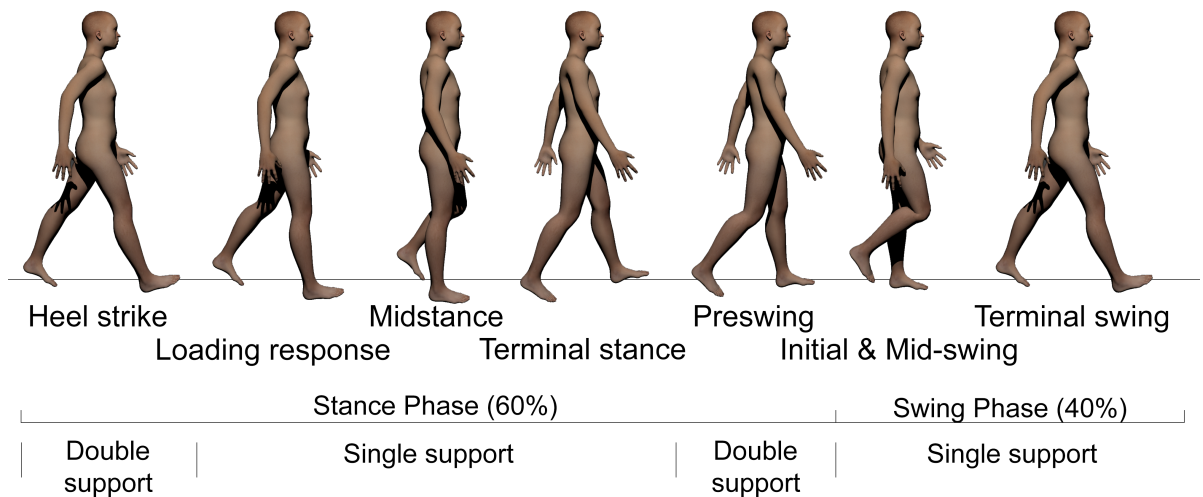
Figure 2.1.: Gait cycle of humans with gait phases.
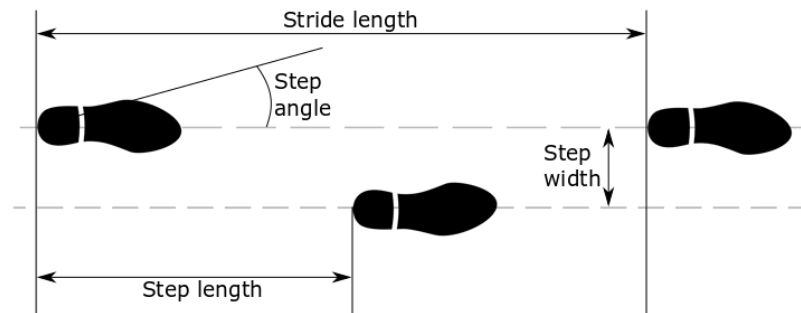
Figure 2.2.: Spatial gait features.

symptoms [Thumler2002]. The main motor symptoms of Parkinson's disease include akinesia, tremor, rigor, and postural reflexes disruption. Akinesia describes a slowing down of movement to immobility and must be present with at least one other motor symptom according to the brain-bank criteria in order to be diagnosed as Parkinson's disease. Akinesia overlaps in its meaning with hypokinesia and bradykinesia. Hypokinesia is defined as reduced movement amplitudes, or spontaneous movements. Bradykinesia describes slowed movements. In the case of involuntary, regular, and rhythmic movements, we speak of tremor. Depending on the form, the amplitude, frequency, and activation condition of tremors can vary. The amplitudes of tremors are distinguished between fine or coarse and the frequency between low frequency ($< 4\,\text{Hz}$) to high frequency ($> 7\,\text{Hz}$). The activation condition determines the shape of the tremor. Parkinson's disease can result in rest, hold, action, and intention tremors. Rest tremors occur when the muscles are completely relaxed. Holding tremors, on the other hand, occur when holding certain positions against gravity. Action tremors become apparent during a movement. In addition to the individual forms of tremor, they can be combined and in

special forms. In addition to the motor symptoms, non-motor symptoms can also be caused [Thumler2002]. A distinction is made between psychological, vegetative, sleep, sensory, visual, and olfactory disorders. In the context of this work, however, only the motor symptoms are in the foreground. Therefore, the non-motor symptoms will not be discussed in detail. L-Dopa therapy is currently one of the best measures to counteract the motor symptoms and to improve the movement of Parkinson's patients. However, the dosage of the drug can be tricky, as motor fluctuations can occur depending on the intake but also independent of it. The consequences of not optimally dosed and regulated medication are under- or over-mobility. For this reason, it is essential to monitor the progress of the disease in a Parkinson's patient and adjusts medication and therapies individually.

3

Preliminary works

The preliminary works are not directly related to the topic of the dissertation but have contributed to a deeper understanding of this area. The first work was to create a classifier for gesture recognition by using a Kinect camera [Steinmetzer2019c].Furthermore, the second work is concerned with measuring the success of therapy in patients with microangiopathy [Lohse2020].

3.1. Gamification

3.1.1. Introduction

The life expectancy of humans is increasing worldwide. Life expectancy predicted to grow in several countries with a probability of at least 65 % for women and 85 % for men [Kontis2018]. Chronic multimorbidity in industrialized countries is high, and prevalence increases with age [Dennis2016]. In Germany 80 % of healthcare costs are spent on chronic and long-term diseases. Current care is very inefficient, which means that 40 % of the resources used are lost [Helms2017]. The reasons are deficiencies in the theoretical approach, the training of nursing staff, medical logistics, and patient acceptance [Urban2016].

In recent years, health communication has developed into a separate field of research with a rather complex object of study. International research takes into account aspects of interpersonal and organizational communication [Jagt2018, Dempsey2018, Reid2018]. Attention, emotions, and motivation developed in the patient through communication with the therapist. The therapist uses conversation to generate interest, attitudes, and behavioral conversion. In long-term care, continuous feedback provided as part of the communication process. This can be achieved by modern media-supported integrated rhetoric [Ntoumanis2018, vanVelsen2019]. In addition to communication and the objective-argumentative exchange of information, an affective-emotional, multi-layered transmission of messages are required that comprehensively adapts to the recipient in real-time. More than 90 % of the factors influencing behavior have an unconscious effect. Only with the help of the remaining 10 % is it possible to justify and reflect on the action, although the recipients think that they are 100 % conscious and rational [Schultz2018, Stangor2019]. Identification, curiosity, autonomy, control, ego participation, fun, and joy relativize the experience of restrictions experienced by the patient through the treatment process. Persuasion is the targeted addressing of behavioral patterns to

achieve a desired behavior in the recipient [Wall2019]. Gamification transfers playful elements into a context that is not related to the game (for example medical assistance systems) to influence motivation, attitudes, and behavior [Grangeia2018]. It represents a persuasive strategy, which contains through its creative freedom a combination of several positively impacting behavior patterns. The following elements are essential for the success of gamification [Floryan2019]:

- Decision option and rules,

- Awards or achievements,

- Visualization of progress and target goal,

- Real-time feedback, and

- Immersion software technology.

Technology-based approaches offer an attractive opportunity to optimize aspects of health and quality of life, such as the use of the Internet- and Mobile-based Interventions (IMI). So far, IMIs have been used primarily in psychotherapy [Paganini2018, Domhardt2019, Ebert2018, Steubl2019].

To the best of our knowledge, there are no investigations to what extent IMIs can also apply to the long-term care of neurological patients. We investigate the questions whether a) playing elements in a positive treatment atmosphere can achieve in a context that is not related to the game, and b) by experiencing the overall therapeutic process, the patient's activity, and thus his adherence can be increased. Within a four-arm intervention study with 60 long-term neurological patients with symptomatic cerebral microangiopathy (affirmative ethics vote of 28.08.2017, ethic code EK 356092017 by institutional review board Ethics Committee Technical University Dresden) we used a standardized computer-aided sensor-motoric training. The analysis is carried out in detail:

- Whether therapy effects are triggered by training accompanying the main medical process in sensor-motoric disturbed patients with cerebral microangiopathy (CMA),

- The therapy effect differs from ambulatory training at the clinic campus under the supervision of a therapist and home training,

- Whether similar therapeutic effects achieved with and without the use of gamification, and

- The improvement of subjective quality of life perceived by patients with and without the use of gamification.

Besides, patients were questioned in a standardized guideline interview on patient preferences, treatment process, training program, motivational elements, and role of the therapist or avatar. This study will help us to analyze the degree of uncertainty of the

12

experimentation, and therefore, to analyze the degree of entropy of the sampling design [Chen2011].

It divided our proposal into the sections materials, methods, methodology, results, and discussion. In section materials, it describe the data used in our study and its distribution according to the asked questions [Lohse2020]. Then the medical methods and tests are explained in the section methods. The related test applications presented in the methodology section. In the last two sections the results of the pre- and post-tests are shown and discussed.

3.1.2. Material

Dataset

60 patients with symptomatic cerebral microangiopathy were admitted to the Centre for Neurology and Pain Therapy at the Niederlausitz Clinic GmbH for a one-week diagnostic and therapy optimization. The patients with symptomatic cerebral microangiopathy as a cerebral network disease with the preferably subcortical sensorimotor deficit were selected due to the functional deterioration of their sensorimotor competence. They were diagnosed and treated according to standardized guidelines. Patients were admitted to the study by the inclusion and exclusion criteria.

Inlusion criteria

- Legal age,

- Full consent and legal capacity,

- Information, and consent form,

- Clinically reliable diagnosis of cerebral microangiopathy (CMA), and

- Microangiopathic brain lesions confirmed by MRI:
    - Periventricular hypodensities of the medullary bed (leukoaraiosis), and
    - Lacunary syndrome with and without residual minimal-neurological deficiency

Exclusion criteria

- body mass > 135 kg,

- unbridgeable communication problems,

- vestibular dysfunctions (video head pulse test),

- cardiac pacemaker,

- Non-compensable visual limitations,

- orthopedic deficits of the lower extremities, and

- inability to stand independently without help

The subjects were divided into the following four groups, see Table 3.1: ambulant without gamification , ambulant with gamification , home without gamification, and home with gamification. The patients, whose home environment did not allow independent training with gamification, were assigned to the group ambulant without gamification. The recruitment for the remaining groups was random.

Table 3.1.: Test groups.

	Ambulant	*Home*	Total
WithoutGamification	14	16	30
WithGamification	14	16	30
Total	28	32	**60**

For the question of whether the therapy environment influences the success of the therapy, we divided the patient into two groups, *Ambulant* and *Home*. Furthermore, the groups are divided into $WithoutGamification$ and $WithGamification$ to analyze the therapeutic effect. In Table 3.2, different features of the groups with an average value and standard deviation are given. N defines the number of subjects per group.

Table 3.2.: Anthropometric data of the groups.

	Environment	
	Ambulant ($N = 28$)	*Home* ($N = 32$)
Age (Year)	72.43 ± 8.59	68.22 ± 10.89
Sex (m/f)	17/11	19/13
Size (cm)	170.18 ± 7.31	171.5 ± 6.23
Weight (kg)	85.89 ± 10.81	78.72 ± 12.54
BMI (m/kg)	29.72 ± 3.82	26.69 ± 3.5
	Gamification	
	$WithoutGamification$ ($N = 30$)	$WithGamification$ ($N = 30$)
Age (Year)	72.6 ± 8.67	67.77 ± 10.83
Sex (m/f)	18/12	18/12
Size (cm)	171.63 ± 6.75	170.13 ± 6.74
Weight (kg)	83.9 ± 11.95	80.23 ± 12.4
BMI (m/kg)	28.49 ± 3.87	27.71 ± 4.01

Devices

The training with gamification of the "Reha-Planet 2" program has performed with Kinect V2 sensors, with 30 video frames per second. Dynamic posturography was measured using a Posturomed © (Haider-Bioswing, Pullenreuth, Germany) [Melecky2019]. The therapy based on two specially developed therapy systems: "Reha-Planet 1" without persuasion (under the guidance of a therapist) and "Reha-Planet 2" with gamification, see Figure 3.1).

Figure 3.1.: "Reha-Planet 2" with Gamification

The program "Reha-Planet 2" was developed in [Lohse2019]. A therapist-avatar shows the exercises, which are performed by the patient at about the same time. Parallel to the therapist's avatar (recorded by a Kinect 2 camera), a patient avatar is displayed in real-time while the therapist also performs the exercises. On the patient avatar, the limbs that are correctly performing the exercises are highlighted in green and the incorrect postures are highlighted in red. If the exercises were performed incorrectly, arrows also indicate the direction in which the limbs have to move. Thus, the patient gets feedback to perform the exercise correctly.

3.1.3. Methods

Motor-driven and sensorimotor tests

During their stay in the hospital, patients received an introduction to a standardized, sensorimotor-centered training therapy. This training therapy was carried out once a day for six weeks as a four-armed intervention study on the hospital campus or at home. A training session of 30 minutes contained six exercises in the areas of general coordination, general or deficit-oriented muscle building, and sensorimotor training. For measurement of motor-driven functions, the following tests are performed:

- Single Leg Stance (SLS),

- 10-meter walk test ,

- Timed Up and Go test (TUG), and

- Functional Reach test (FRT).

One indicator of the ability to balance is the SLS. The time in seconds is measured concerning the patient's ability to stand on one leg. The patient performs the test on the left (SLS-L) and right (SLS-R) leg. During the 10-meter walking test, the velocity (V_{walking}) is measured in m/s while walking a distance of 10 meters. For the TUG test, subjects stand up from a chair, walk 3 meters, rotate 180 degrees, go back to the chair and sit down again. The TUG test measured the needed time s_{TUG} in seconds to complete the test. Based on a leaning task, FRT is proposed to measure the stability limit [Duncan1990]. This test measures the distance between the length of an extended arm at a maximum forward reach from a standing position while maintaining a fixed support base. The FRT is measured in centimeters. The following tests have been performed to measure sensorimotor stability:

- Berg Balance Score (BBS) - static stability relevant for everyday life,

- Dynamic Gait Index (DGI) - balance while walking, and

- Dynamic posturography - dynamic stability.

The BBS is used to assess the balance objectively. For this purpose, the patient has to perform several different tests. It is a list of 14 tests, each test consisting of a five-level ordinal scale from 0 to 4, where 0 indicates the lowest and 4 the highest level of function. The test takes about 20 minutes to complete [Berg1992]. For the Dynamic Gait Index, eight functional gait tests are performed by the patient and marked according to the lowest applicable category of three tests. The maximum total score that can be achieved is 24 [Shumway1995]. The Dynamic posturography measured the dynamic stability while the patient stands on an oscillating platform. A sudden acceleration of the platform results in a dynamic posturography [Reichmann2018]. The patient has to use their balance reactions to keep in the balance after the test is performed. For measurement, the resulting distance of the Posturomed platform from deflection to a standstill is measured in meters, see equation 3.1 [Boer2006]. A smaller distance during the test indicates a great postural stability ability. The stability is given in %. The highest stability is 100 %, see equation 3.2.

$$V_{\text{Postu}} = \frac{\sum_{i=2}^{n} \sqrt{(x_i - x_{i-1})^2 - (y_i - y_{i-1})^2)}}{n}$$

$$n...number\ of\ values$$
$$x_i - x_{i-1}...distance\ in\ x - direction$$
$$y_i - y_{i-1}...distance\ in\ y - direction$$

(3.1)

$$Stability = \frac{(4000 - \frac{\sum_{i=2}^{n} \sqrt{(x_i - x_{i-1})^2 - (y_i - y_{i-1})^2}}{n})}{40} \qquad (3.2)$$

Test of self-efficacy expectation

Qualitative, guideline-based social research interviews ensure that the participants have the freedom to answer the questions. The Short Form (36) Health Survey (SF-36) intended to ensure that the patient is not restricted in the reconstruction of experience and knowledge. The patient characteristics for self-efficacy expectations were completed by the patients using the standardized SF-36 questionnaire. The test consists of 36 questions and covers the areas of physical functioning, physical role, physical pain, general health, vitality, social functioning, emotional role, and psychological well-being.

Guideline interview

At the end of the therapy, a guideline interview was conducted with the patients. This interview aimed to get feedback on the therapy process. The essential parts of this interview were to determine patient preferences, get information about the treatment process, get an opinion about the IMI, determine motivations, and to be able to evaluate the therapist's role.

Statistical tests

For the analysis of therapy success, the groups *Ambulant* and *Home* are independent samples. The same applies to the groups *WithoutGamification* and *WithGamification*, see Table 3.2. Furthermore, the data is scaled, at least in an ordinal order. We were testing the data for normal distribution using the Shapiro-Wilk normal distribution test with a p-value of 0.05. The results showed that the data is not normally distributed. For this reason, the Wilcoxon rank-sum test was used for analyzing. A p-value of 0.05 was used for the Wilcoxon rank-sum test.

3.1.4. Methodology

The groups were selected equally according to the preference of the test persons. Unfortunately, it was not possible for two patients. They could not always come to the hospital campus for therapy. For this reason, the group size of the group *Home* is stronger than *Ambulant*. Before starting therapy, all patients were interviewed and pre-tested. The pre-test includes motor-driven, sensorimotor, and self-efficacy expectancy tests. Afterward, the patients completed 6 weeks of therapy with various motor exercises. At the end of the therapy, the post-test was performed and consisted of the motor-driven, sensorimotor, and self-efficacy expectancy test. Finally, the guideline interview was made.

3.1.5. Results

Age homogeneity

For the comparison of the groups it is checked whether the groups *Ambulant* and *Home* and the groups *WithoutGamification* and *WithGamification* are homogeneous, see Figure 3.2. The box plots show that the *Home* and *WithGamification* groups contain younger patients. After running the Wilcoxon rank-sum test to see if there are significant age differences between the groups, the conclusion is that the groups do not have significant age differences. The *Ambulant* and *Home* groups have a p-value of 0.136. The p-value is significantly higher than the threshold value of 0.05. The groups *WithoutGamification* and *WithGamification* have a p-value of 0.06981. The p-value is also greater than the threshold value of 0.05. Through the test, we were able to show that the group structure is coherent and that the age of the patients does not play a role in further consideration.
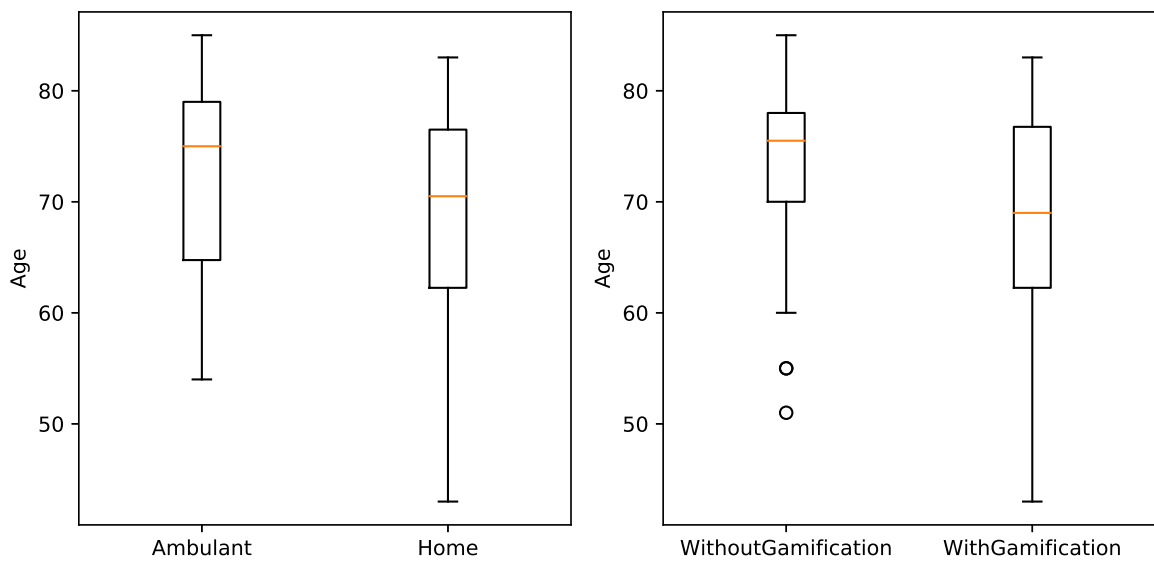
Figure 3.2.: Boxplot of the groups in regard to age.

Therapeutic effect

In Table 3.3, the values of the pre-test, post-test, and the p-values are shown. It was tested whether patients scored better on the tests after six weeks of therapy. A Wilcoxon rank-sum test was performed with a threshold of 0.05. All tests showed significant differences. The results showed that the training had a positive effect regardless of whether *Ambulant, Home, WithoutGamification*, or *WithGamification*.

Therapy with and without gamification

The results of the Wilcoxon rank-sum test for the significance level of 0.05 are shown in Table 3.4. It is tested if the therapy form *WithGamification* and *WithoutGamification*

Table 3.3.: Therapy effect of pre-test and post-test. Median, IQR and p-value were given.

	Pre-Test		Post-Test		
test	*median*	*IQR*	*median*	*IQR*	p-value
BBS	54	4.75	56	1.75	0.0001992
DGI	22	2.75	24	1.5	2.475e-05
V_{Walk}	1.08	0.17	1.17	0.19	0.000426
SLS-L	18	32.5	49.5	109.25	0.002942
SLS-R	16	34.5	52	103.75	6.017e-05
s_{TUG}	7.25	1.5	5.5	1.33	2.755e-05
FRT	33.5	6	38	3	6.011e-06
Dynamic posturography					
V_{Postu}	0.016	0.009	0.013	0.004	9.984e-07
Stability	7.25	1.5	5.5	1.33	2.755e-05

have differences at effectiveness. For this purpose, the differences were formed by pre-test and post-test. The table shows the median, Interquartile range (IQR), percentage change, and p-value. There is no significant difference between the groups. The kind of therapy has not influenced the success of the therapy.

Table 3.4.: Training effect *WithGamification* and *WithoutGamification*. Median, IQR and p-value were given.

	WithGamification			WithoutGamification			
test	*median*	*IQR*	%	*median*	*IQR*	%	p-value
BBS	1.5	4.5	5.82	2	2.75	5.22	0.587
DGI	2	2	13.89	2	1	9.27	0.68
V_{Walk}	0.106	0.178	11.55	0.113	0.165	11.87	0.847
SLS-L	8	38.25	276.44	8	22.5	223.39	0.994
SLS-R	28	49.5	215.7	5	19.375	396.71	0.08
s_{TUG}	-1.5	1.45	-20	-1.5	1.5	11.39	0.368
FRT	4.5	5.75	17.09	4.5	6.5	19.35	0.63
Dynamic posturography							
V_{Postu}	-0.039	0.069	-23.84	-0.03	0.057	-21.88	0.797
Stability	-1.5	1.45	-19.93	-1.5	1.5	-11.39	0.368

Home and ambulant training

For the analysis of whether the environment influences the training success, the difference between pre-test and post-test for the groups *Ambulant* and *Home* are calculated. The Wilcoxon rank-sum test is used with a significance level of 0.05. The results are shown in Table 3.5. The median, IQR, percentage change, and p-value are shown for each test. The DGI and FRT show significantly better results in the home environment. All

other test results are comparable. In most test cases, no significantly better results are achieved. Therefore we assume that the environment does not influence the success of the therapy.

Table 3.5.: *Ambulant* and *Home* training effects. Median, IQR and p-value were given.

| test | Ambulant | | | Home | | | |
	median	*IQR*	%	*median*	*IQR*	%	p-value
BBS	2	2.25	4.21	2	4.5	6.66	0.269
DGI	1	2	8.87	2	1	13.95	0.00595
V_{Walk}	0.099	0.167	8.75	0.12	0.137	14.31	0.165
SLS-L	8.5	27.25	160.4	8	39.125	328.24	0.523
SLS-R	8.5	40.625	194.44	10.5	36.25	404	0.946
s_{TUG}	-1.5	1.075	-8.31	-1.5	1.5	-22.08	0.101
FRT	3.5	4	11.77	6	6.25	23.86	0.00606
Dynamic posturography							
V_{Postu}	-0.035	0.049	-2.15	-0.034	0.078	-24.05	0.831
Stability	1.613	2.19	2.39	1.525	3.812	8.23	0.9

Self-efficacy expectation

Table 3.6 shows the results of the SF-36 questionnaire before and after the therapy. It was tested with the Wilcoxon rank-sum test at significance value 0.05. It can be seen that a significantly increased score was obtained in most categories. Exceptions are the columns *General state of health* and *Emotional role*. Thus it can be concluded that the therapy improved the subjective quality of life.

Table 3.6.: Therapy effect of the SF-36 questionnaire. Median, IQR and p-value were given.

| | Pre-Test | | Post-Test | | |
	median	IQR	median	IQR	p-value
Body function	55	45	75	30	0.001082
Vitality	40	31.25	50	26.25	0.01234
Psyche	64	36	76	32	0.00872
Body role function	25	75	75	100	0.005131
Pains	56.25	43.125	67.5	45	0.000219
General state of the health	45	26.25	55	25	0.1109
Social function	75	40.625	100	25	0.0001232
Emotional role	83.33	100	100	75	0.3878
Total	53.5	38.66	67.78	30.41	0.0001412

Next, we compared whether there were significant differences in the SF-36 questionnaire regarding the groups *WithoutGamification* and *WithGamification*. The differences

between the post-test and pre-test were used. The result is shown in Table 3.7. It can be seen that there are usually no significant differences in the individual categories. Exceptions are the columns *Pains* and *Social function*. When looking at the total score, significant differences are evident. This means that there are significant differences in the subjective quality of life in the choice of therapy. It remains to be noted that gamification has a positive effect.

Table 3.7.: Comparison of the therapy effect for the groups *WithoutGamification* and *WithGamification*. Median, IQR and p-value were given.

	WithGamification		WithoutGamification		
	median	IQR	median	IQR	p-value
Body function	10	3.75	7.5	38.75	0.778
Vitality	5	23.75	5	20	0.5272
Psyche	2	22	6	30	0.5272
Body role function	0	50	0	25	0.1782
Pains	56.25	43.125	67.5	45	0.000219
General state of the health	45	26.25	55	25	0.1109
Social function	75	40.625	100	25	0.0001232
Emotional role	83.33	100	100	75	0.3878
Total	53.5	38.66	67.78	30.41	0.0001412

Finally, it was checked whether there were differences in the environment concerning the SF-36 questionnaire. Therefore the groups *Ambulant* and *Home* were compared. The results are shown in Table 3.7. It was found that the environment has no significant influence on the subjective quality of life, see Table 3.8.

Table 3.8.: Comparison of the therapy effect for the groups *Ambulant* and *Home*. Median, IQR and p-value were given.

	Ambulant		Home		
	median	IQR	median	IQR	p-value
Body function	7.5	25	10	37.5	0.7662
Vitality	5	16.25	5	17.5	0.4788
Psyche	8	30	2	24	0.4788
Body role function	0	50	0	50	1.0
Pains	12.5	22.5	0	23.125	0.5202
General state of the health	0	25	0	16.25	0.7317
Social function	12.5	37.5	12.5	25	0.8913
Emotional role	0	41.67	0	8.33	0.6289
Total	9.28	19.5	9	26.22	0.8764

Standardized guideline interview

The guideline interviews allow for the process of long-term medical care the following conclusions:

- **Patient preferences, adherence:** The relationship of trust between the patient and the therapist is first based on competence and second on sympathy.

- **Treatment process:** Waiting time for an appointment, waiting time in the waiting room, time for direct physician-patient contact, and understanding feedback mechanisms under the stakeholders with sustainable viability.

- **Treatment process:** Waiting time for an appointment, waiting time in the waiting room, time for direct physician-patient contact, and understanding feedback mechanisms under the stakeholders with sustainable viability.

- **Training program:** With and without persuasion/gamification throughout effective and accepted by patients, important high usability, high precision in the mirroring also subtle training elements, and personal progress evaluation for the Patients in real-time.

- **Motivating elements, Persuasion, Gamification:** Sense of being integrated into a therapeutic fellowship, the freedom to vary with the feeling serious to be taken and finally to be able to use the therapy in to have a say in its concrete form, and patient's activity.

- **Role of the therapist/avatar:** The training therapist is the central point of contact for communication regarding training as part of the main process or as a secondary process. An avatar works more precisely in real-time progress assessment. It is preferred by the patient if the original therapist is also available on-demand (telemetrically if necessary).

3.1.6. Discussion

The use of particular IMI in sensor motor impaired patients with cerebral microangiopathy in the form of standardized sensor motor training over six weeks improved the medical outcome. This was evident both in the overall group and in the subgroups. It affected all motor-functional procedures used gait analysis, MPS, BBS, DGI, FRT, dynamic posturography, and SF-36. The first analysis of motivation and self-efficacy did not reveal any usable trends in the overall group. The subjective quality of life experienced by the patients improved significantly on average in the persuasive groups compared to the control groups. In the introduction we have shown that IMIs can improve the aspects of health and quality of life. This has been confirmed by our study in the case of cerebral microangiopathy [Paganini2018, Domhardt2019, Ebert2018, Steubl2019]. Furthermore, we can confirm the gamification contributes to the fact that the components of gamification have a positive effect on patients [Floryan2019].

The inclusion of gamification elements makes it easier for the patient to behave consistently adherent (central path of persuasion) after argumentative decision-making by including unconscious persuasion strategies: Patients trained more frequently and with a better outcome in the motor-functional tests and the subjective quality of life. In the process of long-term medical care, the patient expects plausible and comprehensible statements from the physician regarding the treatment path and goal and any accompanying effects/complications that may arise. From these results, it can conclude that personnel costs could be reduced by using gamification in therapy since therapy with a virtual trainer in the home environment is just as effective as the proposed ambulant training under the guidance of a therapist or in some cases, even more effective. In our opinion, a therapist should nevertheless supervise the initial training of the patient at the beginning to provide support for individual errors and problems in operation and execution.

3.1.7. Conclusion

Our results show that the proposed training therapy shows a low entropy value after six weeks. It is very interesting to analyze the results, from the point of view of the degree of entropy uncertainty in relation to the sample used. On the one hand, the tests carried out in *Ambulant* and *WithoutGamification* shows a more significant uncertainty to the totality of the samples. On the other hand, the uncertainty in *Home* and *WithGamification* is lower, which shows a low entropy behavior. It can be concluded that the proposed training therapy of symptomatic cerebral microangiopathy with the settings *Home* and *WithGamification* shows the most significant effect.

3.2. Gesture recognition

3.2.1. Motivation

Gestures are omnipresent in human non-verbal communication: We are confronted with gestures in aviation, in road traffic, e.g. police officers directing traffic, in sign language or when divers communicate under water. Therefore, in human-computer interaction it is essential for machines to comprehend gestures, e.g. in order to control robots, medical devices or entertainment systems. Technically, gesture recognition is based on 3D sensors combined with machine learning methods for classification. Progress in computer industry makes sensors cheaper and cheaper and therefore universally available. The classification algorithms on the other hand are required to deliver robust and reliable results.

3.2.2. Related Works

Gesture recognition has been accomplished by numerous methods which are well known from artificial intelligence and data mining, for a survey see [Mead2017] and [Sun2017]. Hidden Markov Models (HMM) are a powerful tool for describing the transition of

a system from one state into another. Since gestures like pointing from one object to the next, can naturally be described as transitions from state to state, HMM [Rabiner1989, Yamato1992] are commonly employed in gesture recognition, already since 1992 [Yang1994]. Jie Yang and Yangsheng Xu accomplished a similar task as considered here: Numbers, drawn by hand in the air, can be recognized with high accuracy using gesture recognition with HMM [Lee1999].

Cluster analysis has been performed in order to reduce the states for a gesture in HMM [Schlomer2008, Chen2018]. Dynamic gestures vary greatly in speed, magnitude and duration. The Dynamic Time Warping (DTW) algorithm in combination with HMM can overcome this problem. DTW measures similarity between two time series independently of duration and magnitude [Wang2018]. The authors of [Zhou2018] modified this combination of DTW and HMM by firstly extracting ideal gestures based on statistical methods and performing afterwards a classification with DTW and HMM. In a further approach, Adaptive clusters are used to find centroids of gestures, thus achieving better results in the classification of Chinese characters [Guo2018].

The use of HMM provides good results in the recognition of distinct gestures [Appenrodt2009]. However, if the same gesture is performed in different ways (e.g. clockwise or counterclockwise), clustering can be helpful [Prasad2009, Chen2018]. But according to our experiments the combination of clustering with HMM might impair the classification results.

Thus, in this paper we present Minimal Size Clustering in combination with HMM, which recognizes both distinct gestures or variants of the same gestures well. Furthermore, minimal size clustering enables us to remove wrong labeled data automatically.

We demonstrate the method on two data sets containing dynamic emblems, i.e. autonomous gestures, e.g. letters or numbers, which are carried out by one hand. We start with pre-processing of the data. In a next step we cluster the gestures to form different models of the same gesture. Next, we apply minimal size clustering and use then HMM for gesture classification.

3.2.3. Data sets

All recordings have been performed with ASUS Xtion Pro Live (data set 1) and Kinect V2 (data set 2) depth sensors with 30 video frames per second. The distance between person and camera was 200 to 300 cm. According to our experiments we defined the threshold ε for 0-movements, see section 3.2.4, to 15 mm. The system has been tested on two different datasets. We use 66% of the data sets for the training process and 34% for testing. The first data set consists of 9 simple gestures: up, down, left, right, push, pull, L, mirror L, and square. and contains 976 recordings gathered from 37 different individuals. The challenge here is that it might be difficult to recognize the same gesture when executed by a different individual.

The second data set consists of 300 recordings and 3 classes, namely the letters D, O and P, performed by one individual. We have chosen these classes, because these gestures are similar to each other. For every gesture the data set contains 100 recordings, 50 recordings clockwise and 50 anticlockwise.

Table 3.9.: Overview of data sets 1 and 2

Name	Recordings	Individuals	Classes	description
data set 1	976	37	9	simple gestures
data set 2	300	1	3	Letters D, O and P

3.2.4. Methods

Normalization

We consider the joint of the right hand. Data are recorded as 3D coordinates (in cm) with a frequency of 30 Hz:

$$\vec{g}(t) = (g^{x_s}(t), g^{y_s}(t), g^{z_s}(t)) \qquad (3.3)$$

for every time stamp t. These data are transformed into a body coordinate system whose origin is the midpoint of the two hip joints and the three body axes, transversal, longitudinal and sagittal, are the coordinate axes:

$$\vec{h}(t) = (h^{x_b}(t), h^{y_b}(t), h^{z_b}(t)). \qquad (3.4)$$

Compression

We convert movements of the skeleton joint given in the coordinates $\vec{h}(t)$ of the body coordinate system into 27 directions relatively to a given position, corresponding to a $3 \times 3 \times 3$ cube, see Figure 3.3. For two video frames at times t_1 and t_2 we consider the movement of a skeleton joint:

$$\vec{a} = \vec{h}(t_2) - \vec{h}(t_1) = (a^{x_b}(t), a^{y_b}(t), a^{z_b}(t)). \qquad (3.5)$$

The conversion of $\vec{a}_i$ into the 27 above directions is done using cosine similarity, where the symbol 0 is assigned to movements with $|\vec{a}| < \varepsilon$.

Working along the video frames we finally obtain a sequence $\boldsymbol{O}$ of directions coded by symbols 0 to 26 for the right hand skeleton joint:

$$\boldsymbol{O} = [s_1, \ldots s_N], \qquad (3.6)$$

where the number N depends on the duration of the gesture, see sequence in Table 3.10 [Lee1999].

Gesture Recognition

In order to detect the start and end of a gesture, we use static gestures: An open hand serves as initial or final state for a gesture. The complete workflow for gesture recognition can be seen in Figure 3.4.
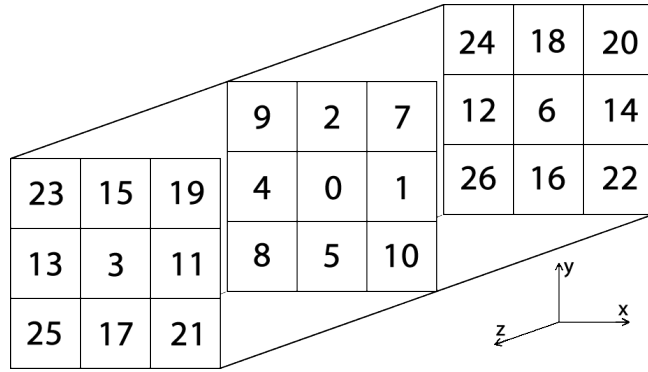
Figure 3.3.: The 27 *directions* can be shown in a $3 \times 3 \times 3$ cube, where 0 represents no movement. The symbol 1 stands for a movement to the right, 2 to the top, 3 backwards.

Table 3.10.: Clustering results for the gesture P.

Index	Cluster	Sequence
1	0	0, 18, 2, 2, 2, 15, 0, 0, 19, 11, 21, 5, 26, 12, 9
3	0	0, 2, 18, 2, 2, 19, 11, 21, 5, 26, 24, 9
2	0	20, 18, 18, 2, 2, 2, 19, 19, 11, 21, 5, 26, 26, 12, 9
4	0	0, 18, 2, 2, 2, 0, 0, 11, 11, 21, 5, 12, 9, 9, 0
5	0	0, 18, 2, 2, 2, 0, 11, 11, 21, 10, 26, 12
6	1	0, 18, 2, 2, 2, 0, 19, 11, 21, 5, 12, 4, 0, 0, 0, 0, 5, 5, 5, 17
7	1	20, 2, 2, 2, 2, 11, 11, 21, 5, 12, 4, 0, 0, 0, 5
8	1	17, 0, 0, 0, 0, 18, 20, 2, 2, 2, 0, 19, 11, 21, 5, 12, 4
9	1	1, 11, 19, 2, 24, 12, 26, 0, 22, 5, 5, 5, 21, 0, 0
10	1	0, 11, 11, 19, 2, 24, 12, 12, 0, 5, 5, 5, 5, 17
11	2	11, 11, 19, 9, 24, 12, 12, 0, 5, 5, 5, 17
12	2	11, 11, 19, 9, 12, 12, 0, 5, 5, 5, 5
14	2	21, 11, 19, 2, 24, 12, 12, 0, 5, 5, 5, 17, 0
13	2	1, 19, 2, 24, 12, 12, 0, 5, 5, 5, 5
15	3	1, 11, 19, 2, 24, 12, 0, 0, 5, 5, 5, 17, 0
18	3	1, 11, 19, 2, 9, 24, 12, 26, 0, 5, 5, 5, 17
19	3	10, 1, 11, 19, 2, 9, 12, 26, 26, 0, 5, 5, 5, 5
16	3	1, 11, 15, 2, 24, 12, 26, 0, 5, 5, 5, 5
17	3	1, 11, 11, 15, 2, 24, 12, 26, 0, 5, 16, 5, 17, 21, 0
20	4	10, 21, 11, 15, 2, 24, 12, 4, 0, 0, 16, 5, 5, 17

Hierarchical clustering is used to distinguish variants of a gesture, like drawing a letter P clockwise or anticlockwise, see Figure 3.5 [Johnson1967]. Clustering here is based on
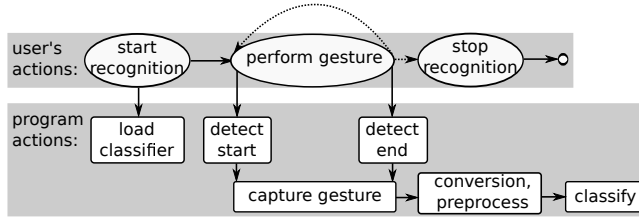
Figure 3.4.: Workflow of GestureRecognition.

the Jaccard metric, where we transform the gesture sequence into a set of subsequent 2-tupels of direction symbols:

$$
\boldsymbol{O} = (s_1, s_2, \ldots, s_N) \mapsto T(\boldsymbol{O}) \tag{3.7}
$$
$$
= \{(s_1, s_2), (s_2, s_3), \ldots (s_{N-1}, s_N)\} \tag{3.8}
$$

We use the standard Jaccard distance [Levandowsky1971] between two sequences $T(\boldsymbol{O}_k)$ and $T(\boldsymbol{O}_l)$, see Table 3.10. The number of clusters is determined according to [Mojena1977] with a threshold value 1.25 [Milligan1985]. Table 3.10 in the appendix shows an example for detecting gesture variants by hierarchical clustering.
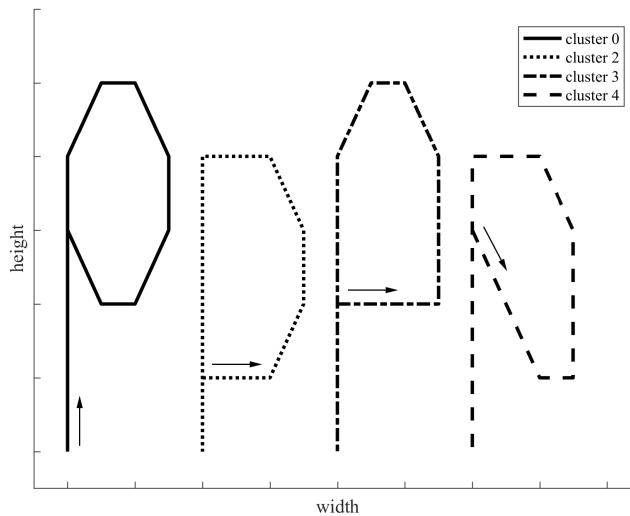
Figure 3.5.: Example for detecting different variants of a gesture by clustering: 2D visualization of the clusters 0, 2, 3 and 4 for the letter P. Cluster 1 is not shown. The sequences are shown in Table 3.10.

After performing clustering as described above, all clusters consisting of less elements than shows the result from the cluster analysis using 67 recordings for the P gesture. The minimal size (dashed line) at 8.375 is the mean over the cluster size. In this example we use three gesture clusters P0, P1, P2 for HMM training. So we can form several models for one gesture, see Figure 3.7.
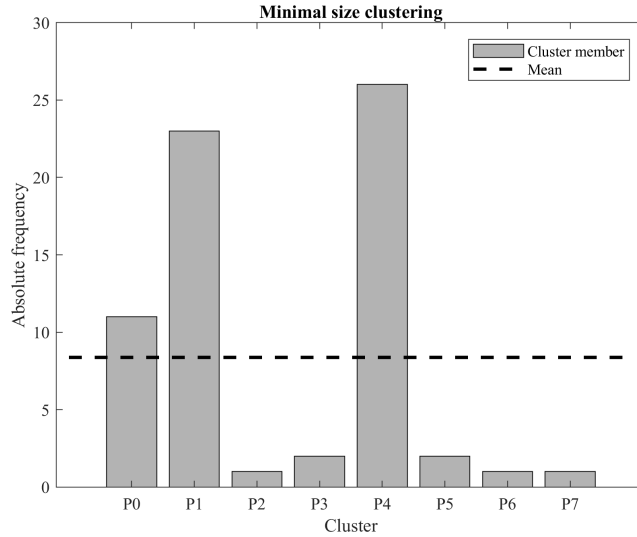
Figure 3.6.: Cluster size for letter P over 67 gestures with $\bar{x} = 8.375$.

For each variant of a gesture a Hidden Markov Model (HMM) λ_j is obtained by using Baum-Welch algorithm based on forward topology. Additionally, the so-called Threshold Model (TM) is trained by all data from the data set. The purpose of TM is to detect unknown gestures, for example we expect an unknown gesture to be classified as TM [Lee1999].
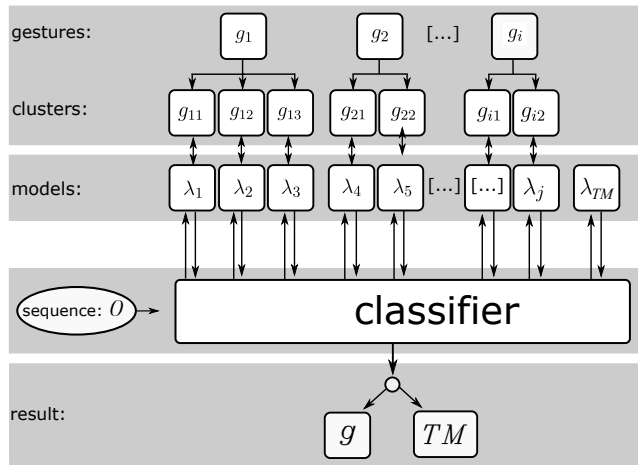
Figure 3.7.: The classifier consists of different models λ_j for each gesture g_i and variants (cluster) g_{ik}.

3.2.5. Results

Classification with and without Threshold Model

In order to demonstrate the effect of the TM, we trained a HMM with the classes P,O and D of data set 2. After training we classified additionally 28 unlearned gestures of class *push* and *pull* from data set 1. Figure 3.8 shows the results without threshold model. Each gesture has been assigned to a class, and as expected the unlearned gestures *push* and *pull* are all wrongly recognized. In contrast, the results with threshold model are shown in Fig. 3.9. It can be seen that the *push* and *pull* gestures were mainly classified as unknown and the results for trained gestures are slightly better than the classification without threshold model.

Figure 3.8.: Results for trained letters D, O and P and untrained gestures *push* and *pull* without threshold model.

Data set 1 - recognition of different gestures

For data set 1 the results show that the clustering process, which recognizes several variants for one gesture, improves the classification results. The video frame distances for the calculation of the directional vector $\vec{a}(t_n)$ does not influence the F-measure significantly. Figure 3.10 and 3.11 summarize the results. For the presentation of the results we used different distances of the video frames. Here we chose video frame distances from one to ten. The F-Measure is the multi-class F-score [Sokolova2009]. The results with HMM and HMM with minimal size clustering are very similar. On the other hand, HMM with clustering gives weaker results. Detailed results can be found in Table 3.11.
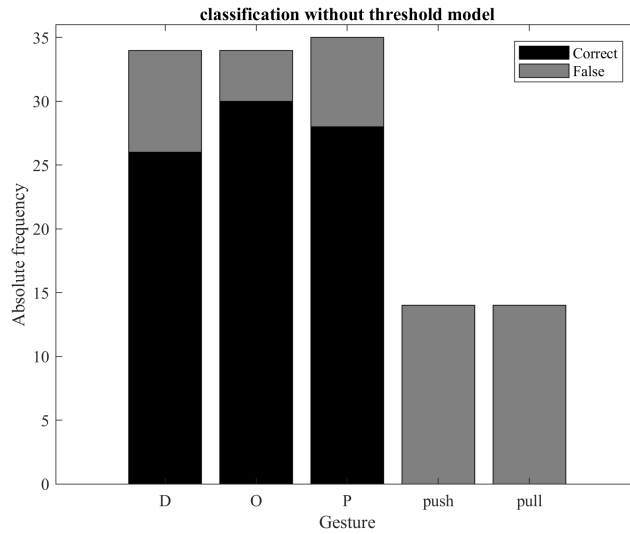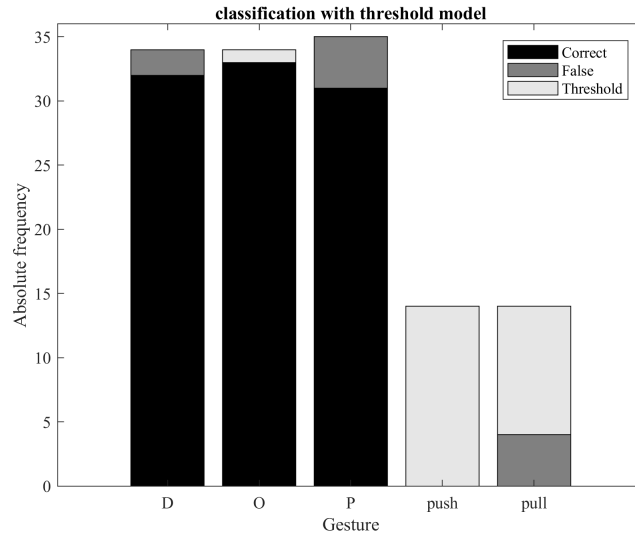
Figure 3.9.: Results for trained letters D, O and P and untrained gestures *push* and *pull* with threshold model.

Table 3.11.: Gesture recognition with and without clustering for data set 1.

	Clustering		Minimal size clustering		HMM	
FD	**FM**	**ER**	**FM**	**ER**	**FM**	**ER**
1	0.767	23.145	0.856	14.316	0.855	14.531
2	0.781	22.110	**0.865**	**13.459**	0.875	12.501
3	0.761	24.273	0.860	14.081	0.878	12.196
4	0.751	25.271	0.851	14.839	0.862	13.904
5	0.762	23.925	0.844	15.547	0.852	14.831
6	0.753	24.511	0.846	15.168	0.848	15.192
7	0.777	22.290	0.862	13.636	0.885	11.719
8	0.771	23.109	0.862	13.887	0.872	13.061
9	0.730	26.671	0.818	17.443	0.853	14.890
10	0.757	24.763	0.805	19.518	0.853	15.100

Data Set 2 - recognition of similar gestures

In this section, we present the results for the letter recognition, see Figure 3.12. Best results were obtained for small frame distances using clustering with an optimum value of 0.910 for the F-Measure and mean threshold clustering with a value of 0.910 for the F-Measure at two frames. The larger the frame distances, the lower is the F-Measure. This is due to the fact that information is lost with increasing distance of the frames. With very similar gestures we achieve the best results with HMM with minimal size

data set 1

Figure 3.10.: Results for the data set one; HMM, HMM + clustering and HMM + Minimal size clustering for video frame distance one to ten.

classification dataset 1 with threshold clustering model
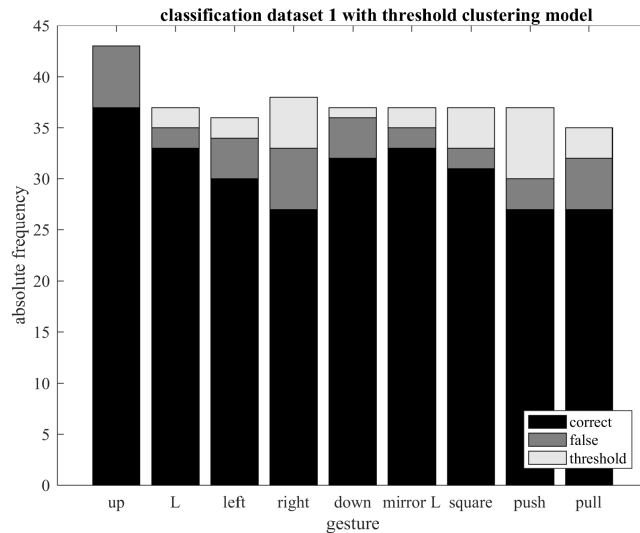
Figure 3.11.: Best result of crossvalidation minimal size clustering for video frame distance 2 and F-Measure 0.892. 34 (3.5%) misrecognized gestures; 26 (2.7%) gestures assigned to TM. Average number of cluster per gesture: 8.7 (1.8 with minimal size clustering).

clustering and HMM with clustering. On the other hand, the simple HMM is weaker. For detailed results see Table 3.12.

Table 3.12.: Gesture recognition with and without clustering for data set two.

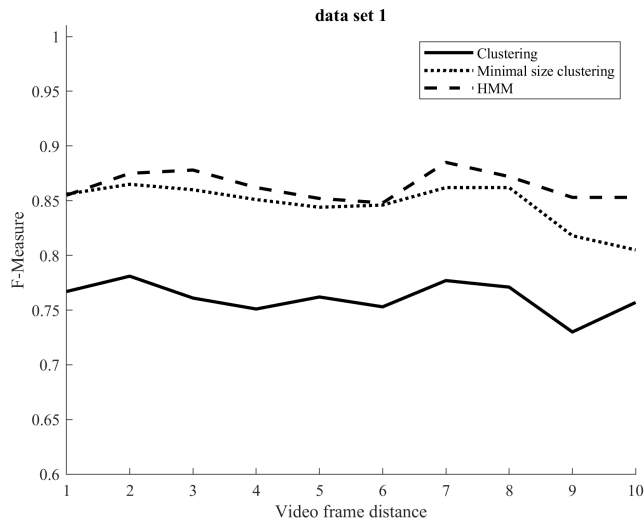|	Clustering		Minimal size clustering		HMM	
FD	FM	ER	FM	ER	FM	ER
1	0.837	16.004	0.898	10.039	0.763	22.145
2	0.910	8.670	**0.909**	**9.052**	0.868	13.320
3	0.878	12.403	0.850	14.925	0.807	19.051
4	0.876	12.430	0.877	12.261	0.832	16.877
5	0.774	22.898	0.873	12.887	0.807	19.386
6	0.787	22.690	0.848	15.393	0.766	23.617
7	0.704	29.782	0.804	19.768	0.772	23.215
8	0.770	23.121	0.775	22.918	0.708	29.581
9	0.711	28.717	0.756	24.689	0.788	21.667
10	0.694	30.837	0.802	19.948	0.719	28.225
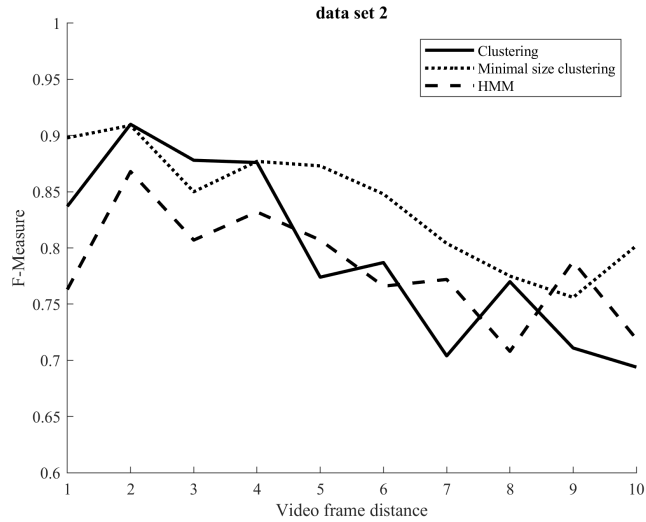
Figure 3.12.: Results for the data set two; HMM, HMM + clustering and HMM + Minimal size clustering for video frame distance one to ten.

3.2.6. Discussion

Characteristics of the developed model are:

- 3D-data are effectively transformed into a denoised and compressed form which is suitable for dynamic gesture recognition.

- Clustering with an adapted form of the Jaccard metric allows to distinguish variants of gestures and improves classification.
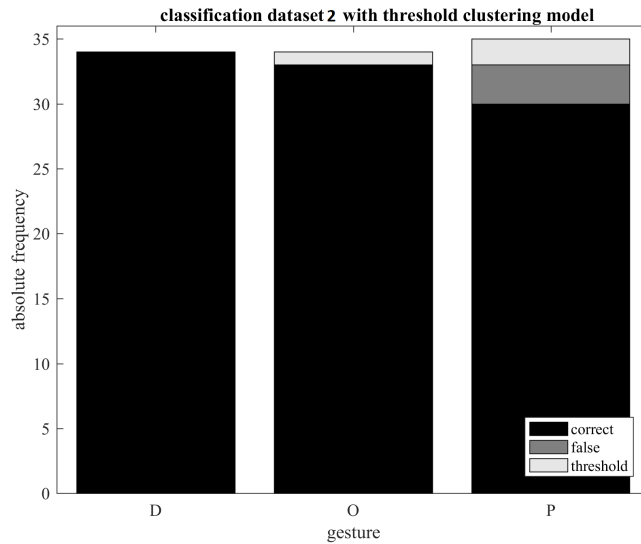
Figure 3.13.: Best result of crossvalidation for video frame distance two; F-Measure 0.97. Error(3%): 3 misrecognized gestures; three gestures assigned to TM. Average number of cluster per gesture: 8.3 (3.7 with minimal size clustering).

- Outliers are detected via clustering and removed in order to improve the recognition results.

With this work we have demonstrated that the combination of our proposed minimal size clustering and HMM is a very robust method for the recognition of different and similar gestures.

<div align="right">

4

</div>

Hardware and signals

Our motivation to create the hardware was to develop a wearable system that is able to analyze the human gait. It was important that the system can be used independently of the location. Not every hospital is able to run an expensive camera-based gait analysis laboratory. Due to demographic changes or the location as in rural areas. The tendency is therefore to look for possibilities to make tele diagnoses or to perform the treatment via tele-medicine. Furthermore, the system should be easy to use, so that even an unskilled patient can perform a gait analysis himself. The system should measure important biomechanical parameters of the gait. These were already introduced in Chapter 2. The more of these features the system is able to calculate, the more accurate the later evaluation will be.

4.1. Sensors

In order to analyze motor dysfunctions of gait, the first was to measure gait features. Already in 1992, motion and symmetry of the lower extremities were recorded with cameras and markers [Vagenas1992]. Technological advances and the cost-effective development of depth cameras have opened up new possibilities for motion analysis by Kinect from 2010. The depth camera extended the Red Green Blue color space (RGB) camera. Thus, the gait could be analyzed with new methods [Ince2017]. For the analysis of the human gait, the first step is to choose which sensors will be used for the analysis. In principle, a distinction is made here between wearable and non-wearable systems. In the following, the non-wearable systems are presented in the section 4.1.1 and the wearable systems in the section 4.1.2 with an overview of advantages and disadvantages.

4.1.1. Stationary

The non-wearable systems are further subdivided into camera based systems and floor sensors. The camera based systems offer different possibilities to analyze movements. One variant is to analyze the motion from RGB images by using image processing. A disadvantage is that the data is not three-dimensional (3D). Distances can only be determined with high difficulty [Muro2014]. For this reason, RGB cameras are often used as a supporting system. To analyze the gait, several cameras are used to create a sterocopic vision. Thereby it is possible to calculate distances easier [Muro2014].

The best results are achieved with Time-of-Flight Systems, Structured Light, or Infrared

Thermography. These systems are able to capture the environment in three dimensions and measure distances. Probably the most popular representative of this technology is the Kinect camera. The Kinect camera uses structured light to recognize people [Muro2014]. With the Kinect camera, gait analysis is possible without any additional hardware such as markers. However, the Kinect camera is rather inaccurate compared to a Vicon system, which is the gold standard in motion analysis [Buckley2019]. For this reason, 3D motion capture systems such as the Vison system are used for professional gait analysis. Disadvantages of the Vicon systems are a high price and that an extra room is needed for the measurements. Therefore, non-wearable sytems are not suitable for long-term measurements of gait in daily life [Buckley2019].

Often, several cameras are used at the same time this has different advantages. By using different cameras, the non-visible areas of a camera can be captured by additional cameras and this increases the data quality enormously. Furthermore, by using several cameras, errors in the analysis are compensated, which makes the data more robust [Muro2014]..

The second part of the Non-Wearable Systems are the floor sensors which are embedded in the floor as force plates. These are the gold standard when measure the ground reaction [Buckley2019]. For this reason, the data are also very high resolution [Buckley2019]. A disadvantage is that the purchase costs are very high [Buckley2019]. An alternative to the system are force measuring mats [Muro2014]. These mats are not very large, which means that gait analysis is only possible for individual strides.

4.1.2. Wearables

The second category of gait analysis sensors are wearables. These sensors are attached to the body or integrated into clothing. Thereby it is possible to analyse the gait independent of location.

An ultrasonic sensor measures the distance from sensor to another object. This makes it possible to measure the distance between the feet and the step frequency [Wahab2011]. Electromyogram (EMG) uses electrodes to measure the muscle contraction of the joints. They are used to measure angles between the limbs. However, electrodes must always be connected to the body, which is not suitable for measurement in everyday life. Since the electrodes have to be changed after a certain period of time and the application must be carried out professionally [Muro2014].

The most common way to measure gait using wearable sensors are the Inertial Measurement Unit (IMU) sensors. These usually consist of a combination of different sensors: 3D accelerometer, 3D gyroscope, and 3D magnetometer. The data from the individual sensors are usually merged using the Kalman Filter and this makes the data more robust. The IMU sensor allows the measurement of angle and acceleration data [Muro2014, Buckley2019, Sprager2015, Taborri2016]. This makes it possible to calculate distances, durations of gait phases and orientation data in Euler angles or quaternions. In a study the IMU sensors were validated against a camera based system. The result was, that the step length correlates with the system but a deviation of 5% must be accepted [Ferrari2013].

Force Sensitive Resistors (FSR) sensors are used to measure the ground reaction of the feet. These sensors change the value of the resistance when force is applied to them. This makes it possible to measure the force at different points. With the help of these sensors, conclusions can be drawn about the rolling motion of the foot and the distribution of force in the body [Muro2014].

In this thesis, a wearable system consisting of IMU and FSR sensors was chosen. The IMU sensors are inexpensive in contrast to a camera based system, space-saving, suitable for everyday use and provide sufficiently accurate measurement data. They are the counterpart of the camera-based systems. The FSR sensors enable the measurement of the force effect in the foot. This enables statements to be made about the rolling movement and balance of the test persons.

4.2. Related works of wearables

To analyze the gait with wearables there are a lot of different systems. But in general the focus is on the use of IMU and force sensors. Some researchers have attached IMU sensors to shoes or ankles using clamps or straps [Li2009, Rampp2014, Sabatini2005, Klucken2013, Tunca2017, Sijobert2015, Mariani2010, Ferrari2016, Ferster2015, Wang2015, Hsu2014, Trojaniello2014]. This makes it possible to measure the motion of the legs. Others concentrate more on the interpretation of the time gait features. The use of force sensors is suitable for this purpose [Jiang2018, Loiret2019, Mazumder2018b]. Furthermore, there are various wristbands that are equipped with IMU sensors to draw conclusions about motor disorders [Steinmetzer2019b, Tsipouras2012, Huang2012, Patel2009].

Then, there are even more complex systems. These often use a combination of sensors and sensor positions. The combination is often that in the foot both IMU and force sensors are mounted [Bamberg2008, Li2014, Steinmetzer2019a, Chelius2011, Hanlon2009] or that several IMUs are mounted on diffrent body parts [Steinmetzer2020, Takeda2014, Salarian2004, Li2014] to make a more accurate analysis.

In our researched works, no system could be found, which measures the movement of arms and legs using IMU and FSR sensors synchronously. For this reason, we decided to develop our own system.

4.3. Smartphone

For activity detection, we used various smartphones and tablets with the Android operating system to be independent of a specific device. However, the device must be able to provide linear acceleration and rotation data. We recorded both sensor data with a frequency of 50 Hz. To make the system energy efficient, we use smartphones for activity detection. If the smartphone has detected the activity *Gait*, the wearable devices record the data.

4.4. Mbientlab system

In the first experiments, we used a microcontroller with an integrated IMU sensor from Mbientlab the MetaMotionR microcontroller [Mbientlab2016]. These are equipped with a Bosch BMI160 3d accelerometer and 3D gyroscope and a Bosch BMM150 3D magnetometer. By using the Bosch Sensor Fusion Library which is available on board, we were able to record 3D orientation signals and 3D linear acceleration data with a frequency of 100 Hz on the microcontroller [Bosch2015]. Furthermore, the microcontroller provides the possibility to record four analog signals. These analog channels are used to record the data of the FSR sensors. The analog signals, orientation data, and linear acceleration could not be logged at the same time. Only two signal sources could be recorded simultaneously. Another problem is that only three devices can be synchronized with each other [Anwary2018b].

Nevertheless, we use the system to create the first data set, see section TUG 5.3. The possibility to record movement data of Parkinson's patients on both arms and legs, see Figures 4.1 and 4.2. The case for the insole, we printed with a German RepRap x350 Pro 3D printer. This helped to develop the first analyses, which we were able to learn from the signals and to develop ideas for better results.
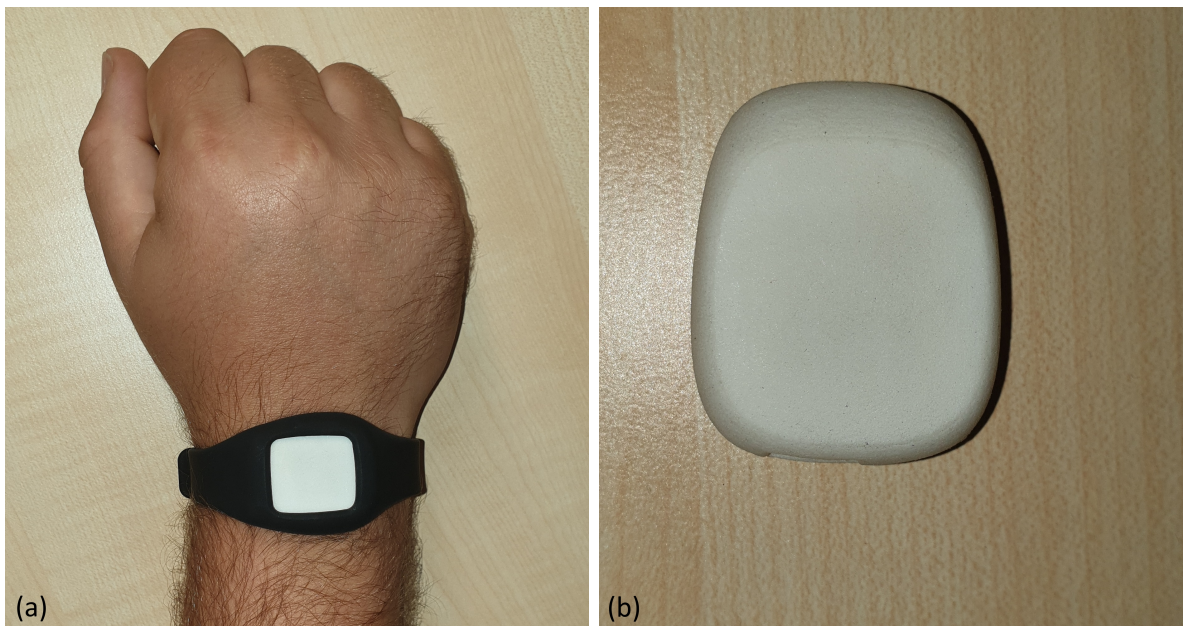

Figure 4.1.: (a) Wristband with the MetaMotionR sensor; (b) Position of the sensor during the measurement.

But since we want to realize a system consisting of four microcontrollers which are synchronized with each other and are able to record orientation data, linear acceleration and force data. Based on this idea a new system was realized.
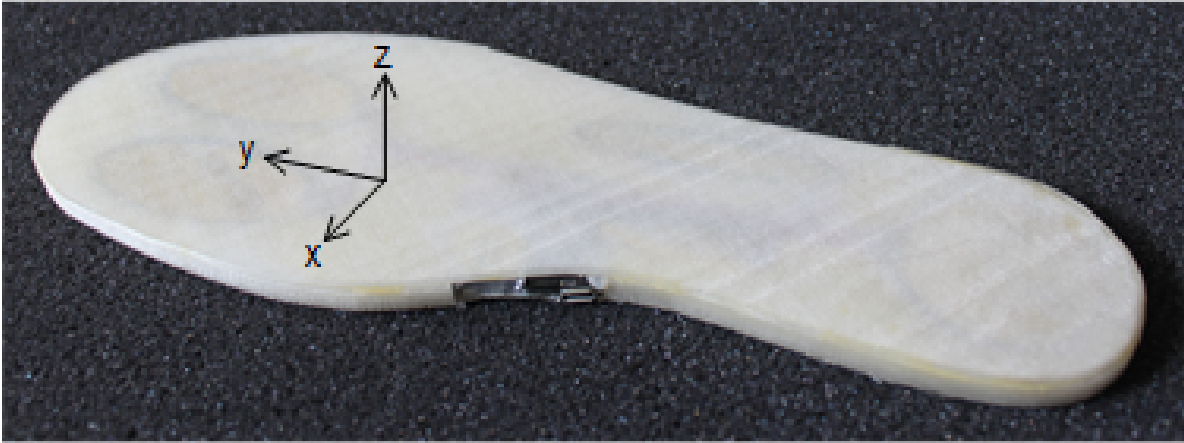
Figure 4.2.: Insole with MetaMotionR microcontroller and four FSR sensors.

4.5. Proprietary development

4.5.1. Insole

For the creation of our own wearable system, we have decided to produce an insole. The insole has been designed to hold ten force sensors and a BNO055 motion sensor. The microcontroller for data processing is placed outside the insole. The model for the insole is shown in Figure 4.3. The insole is made with a RepRap x350 per 3D printer. The Flexfill 98a was chosen as filament. This Ilament is based on Thermoplastic elastomer based on urethane (TPU). The elasticity of the material makes it ideal for use in the insole, because the rolling movement puts a lot of stress on the material. The four FSR sensors at the heel and at the ball are arranged parallel to each other so that the postural stability within the foot can be measured.

The circuit diagram for the insole is shown in Figure 4.4. Ten Interlink FSR 402 Short force sensors were used to measure the force data [Interlink2016]. The FSR sensors were designed as voltage dividers so that the resistance changes in the FSR sensors can be measured via the analog inputs of the Teensy 3.6 microcontroller. A Bosch BNO055 sensor is integrated into the insole for motion analysis [Bosch2015]. This sensor is a inertial sensor consisting of a gyroscope, accelerometer and a magnetometer. The sensor is located in the middle of the insole. Furthermore, the BNO055 sensor communicates via I2C interface with the Teensy 3.6 microcontroller. This sensor has a co-processor for sensor fusion which calculates absolute orientations and lineare acceleration values directly. The output is therefore angle velocity, acceleration, quaternions, euler angles and lineare acceleration at a frequency of 100 Hz. The data transmission to the smartphone and the entire communication works via Bluetooth LE. Here we use an Adafruit Bluefruit LE SPI Friend. With this board we can communicate with the Teensy 3.6 via an SPI interface. We also tested a UART interface but it is much slower and not suitable for our purposes.

The mounted insole is shown in Figure 4.5. The insoles are manufactured in three
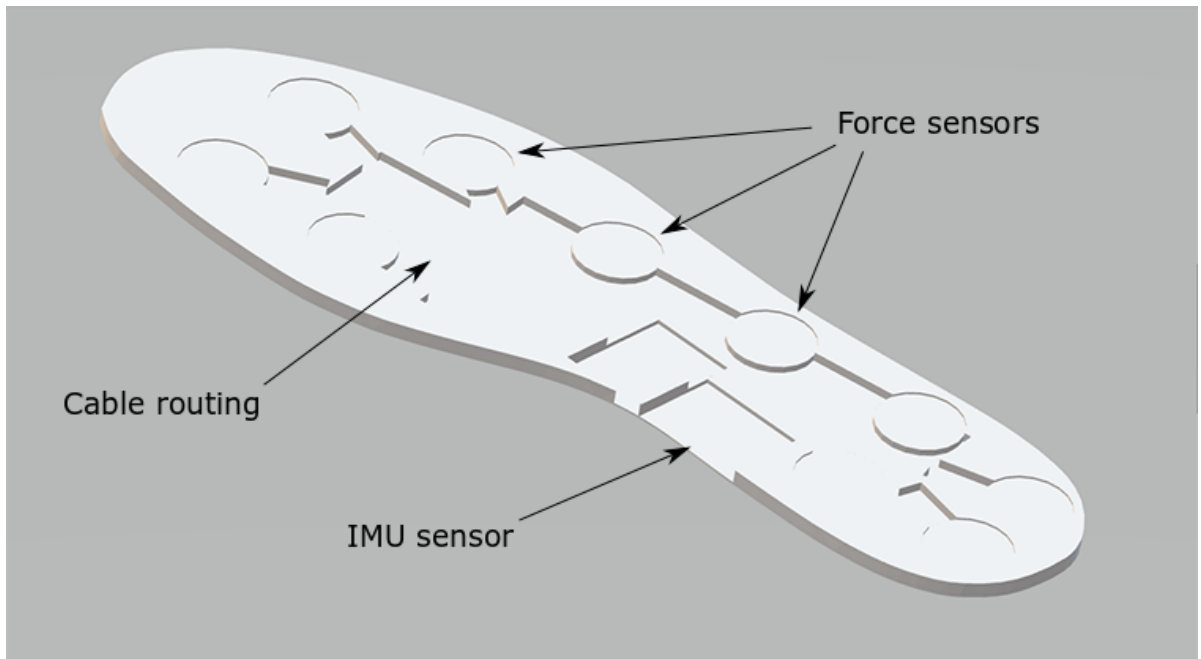
Figure 4.3.: 3D model of the insole.

different shoe sizes 37.5, 40, and 42.5 EU which was based on the common shoe sizes of the population.

4.5.2. Wristband

The circuit diagram of the wristband is the same as that of the insole. The difference between the two is that the wristband does not have force sensors. Figure 4.6 shows the circuit diagram. The advantage of the same pin layout is that only one firmware needs to be developed.

The mounted wristband is shown in Figure 4.7. Compared to the Mbientlab device, this one is larger. But for us to have full control over the device during development of the firmware, the advantages outweigh the disadvantages.

4.6. Sensor Signal

4.6.1. Insole

In the previous section we have shown how the hardware was developed. In this section we will discuss which signals the devices provide and what information is gained from them.

In Figure 4.8 shows the signals of the insole during the TUG test. All signals were recorded at a frequency of 100 Hz. In the Figure 4.8 (a-d) the following signals are shown: a) the 3D Euler angles, b) the 3D linear acceleration, c) the average force of heel (four
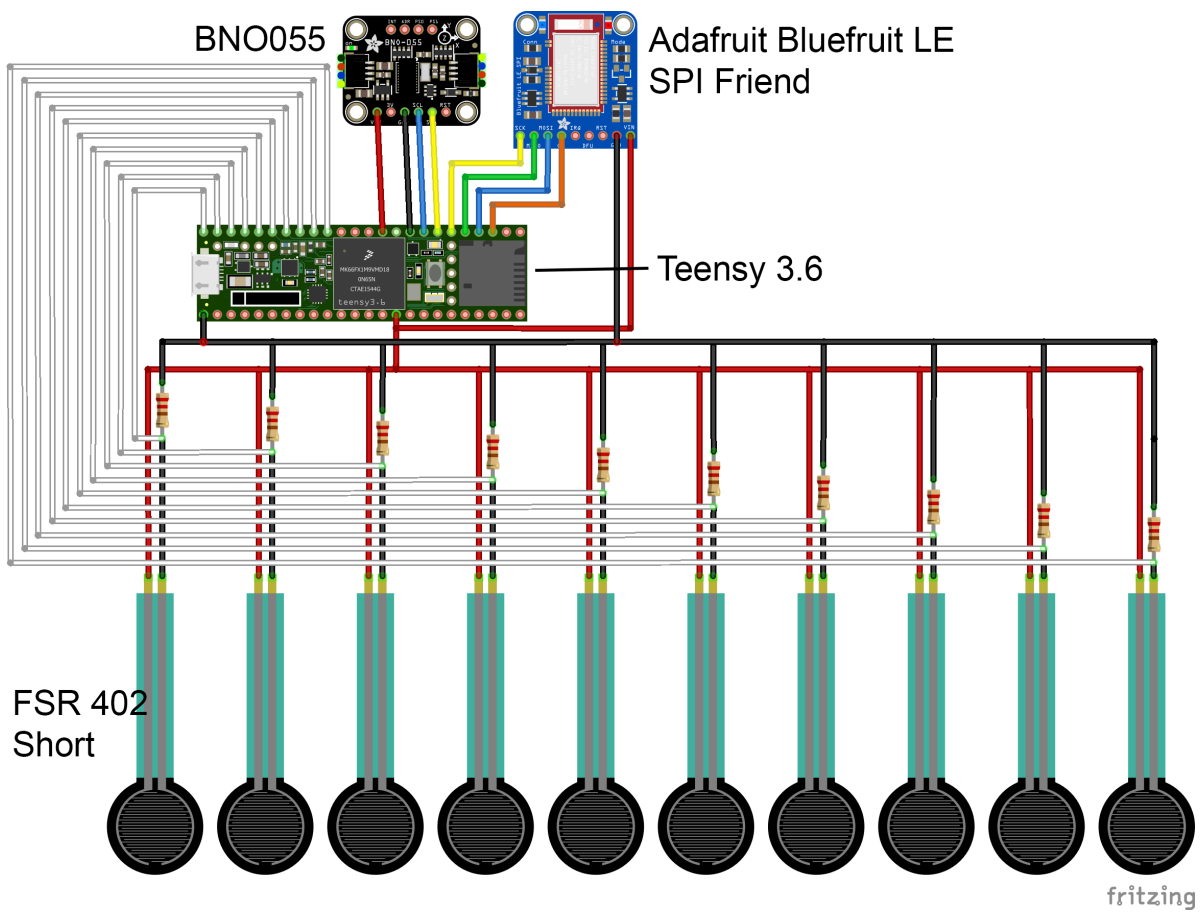
Figure 4.4.: Circuit diagram of the insole.
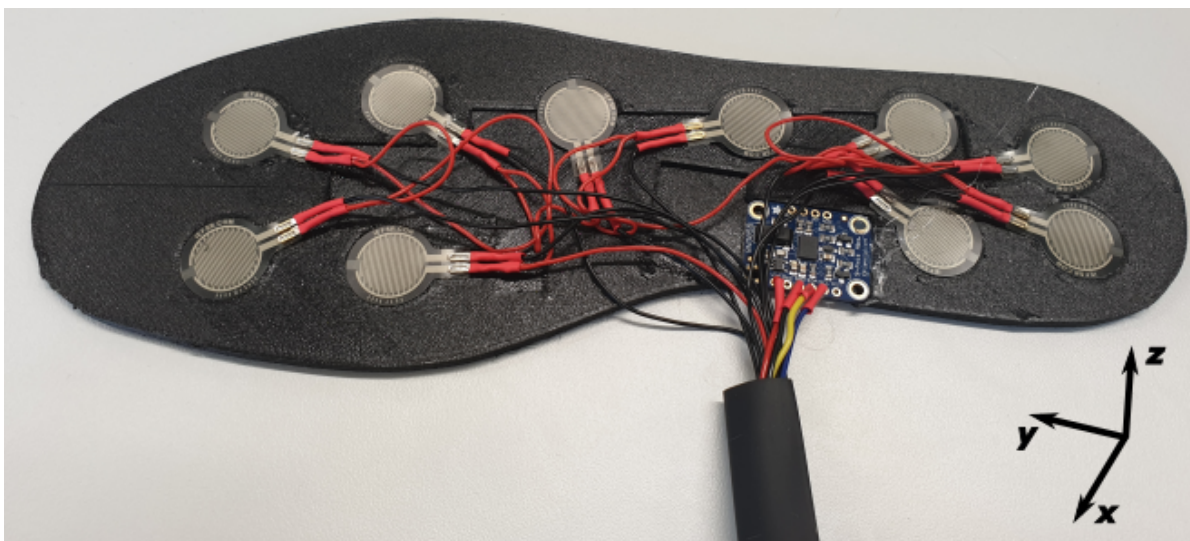
Figure 4.5.: Mounted insole with force sensors and IMU.
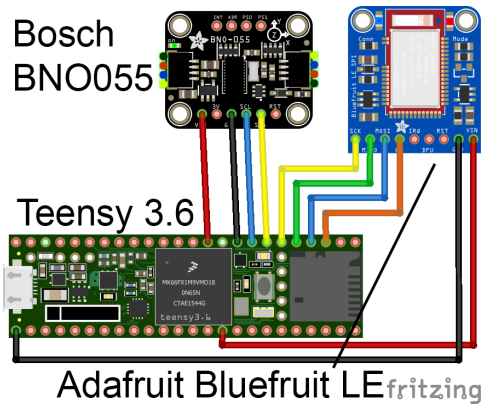
Figure 4.6.: Circuit diagram of the wristband.

sensors), metatarsus (two sensors) and bunion (four sensors), and d) the average of all ten force sensors.

4.6.2. Wristband

Figure 4.9 shows the signals of the wristband during the subjects performed the TUG test, 3D Euler angles and 3D linear acceleration of the arms were captured. The signals for the Euler angles and the linear acceleration were the result of the sensor fusion algorithm from Bosch. Both signals were recorded at a frequency of $100\,Hz$. The algorithm for the sensor fusion used the data from the accelerometer, gyroscope, and magnetometer. Figure 4.9 a) shows at the top the 3D Euler angles and at the bottom b) the 3D linear acceleration signals. The complete signal of one wristband during the TUG test is shown in Figure 4.9. Furthermore, Part (A) contains all recorded data and Part (B) the data between the black dotted lines, the active walking parts.
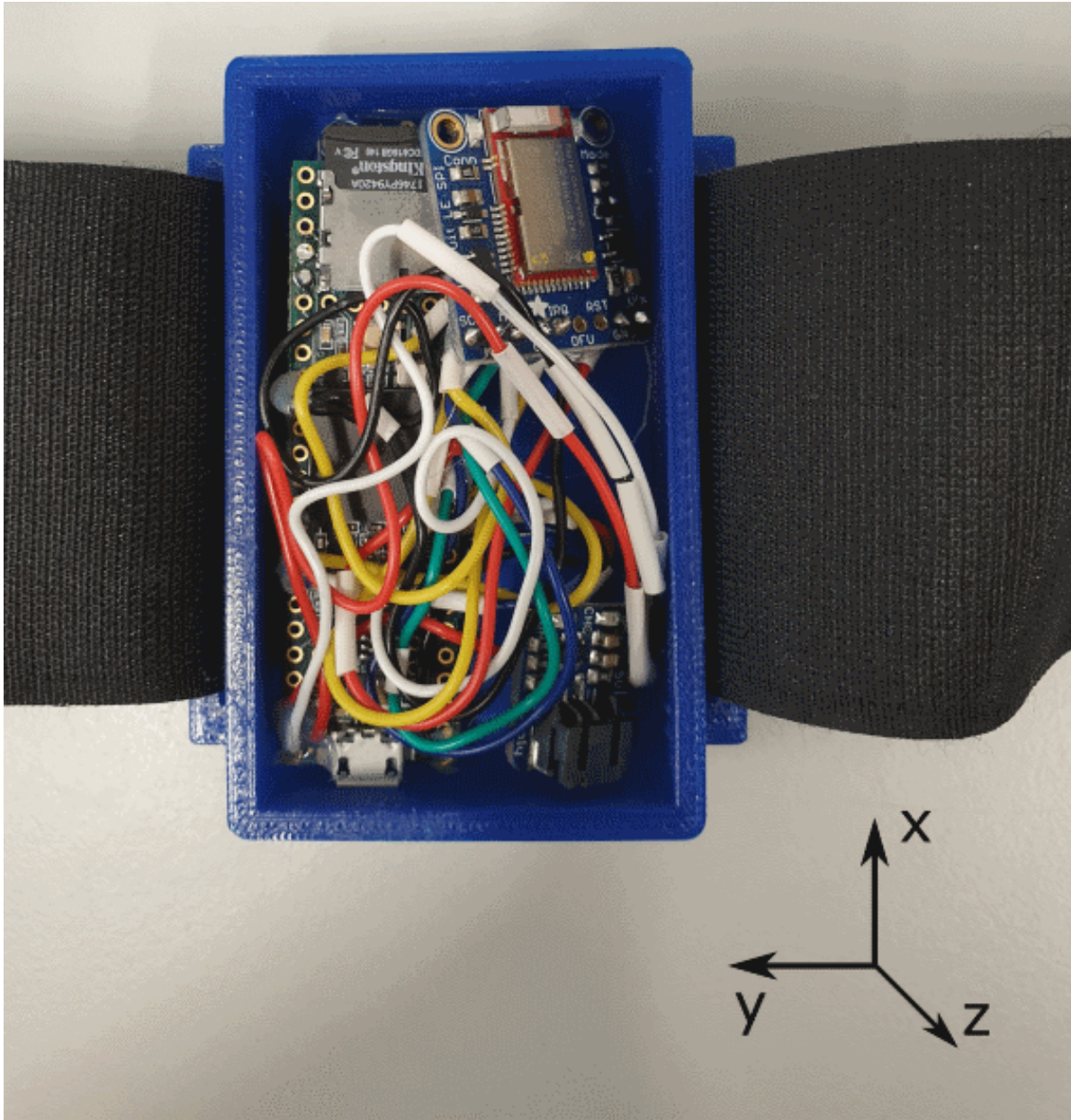
Figure 4.7.: Mounted wristband.
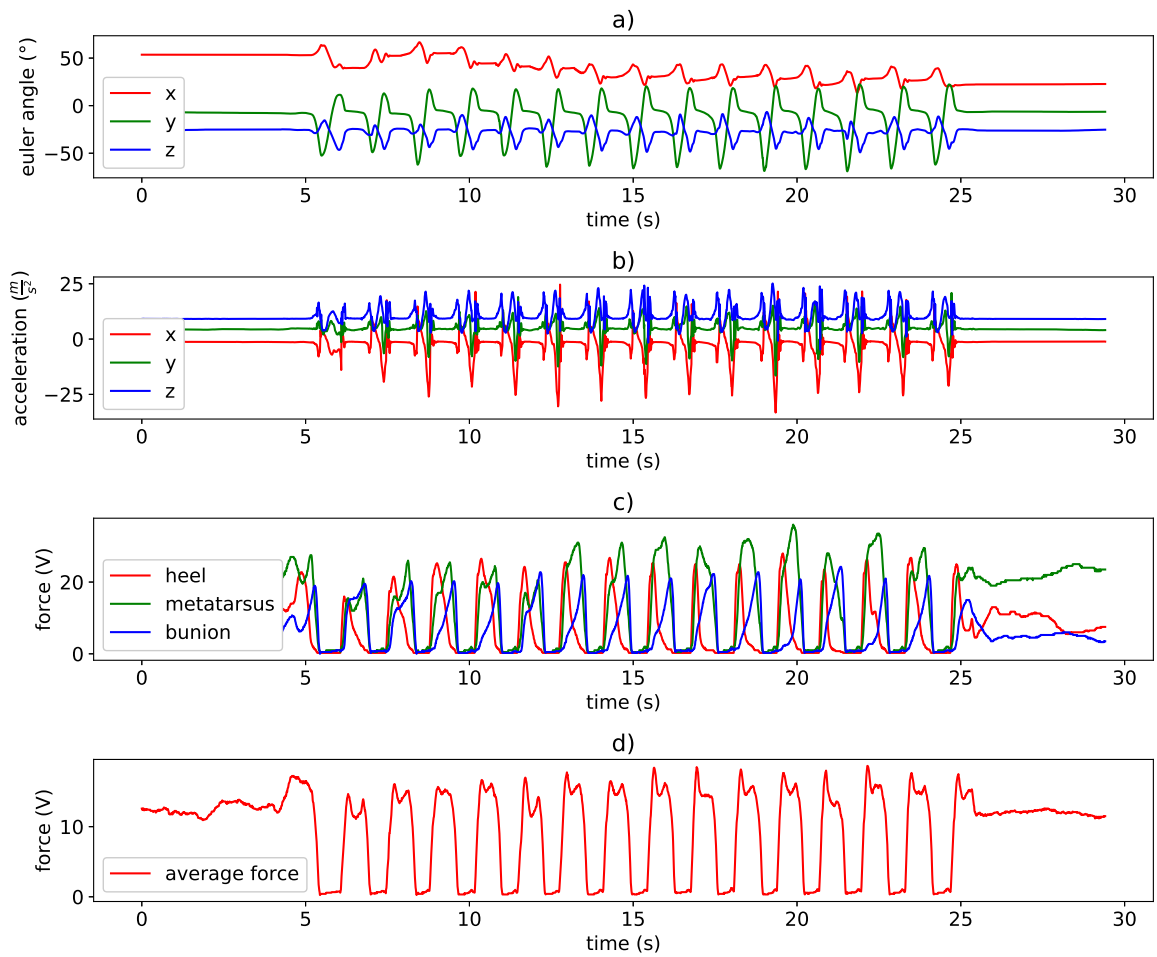
Figure 4.8.: a) Orientation data as Euler angles; b) linear acceleration; c) average force of heel (four sensors), metatarsus (two sensors) and bunion (four sensors); d) average of all force sensors
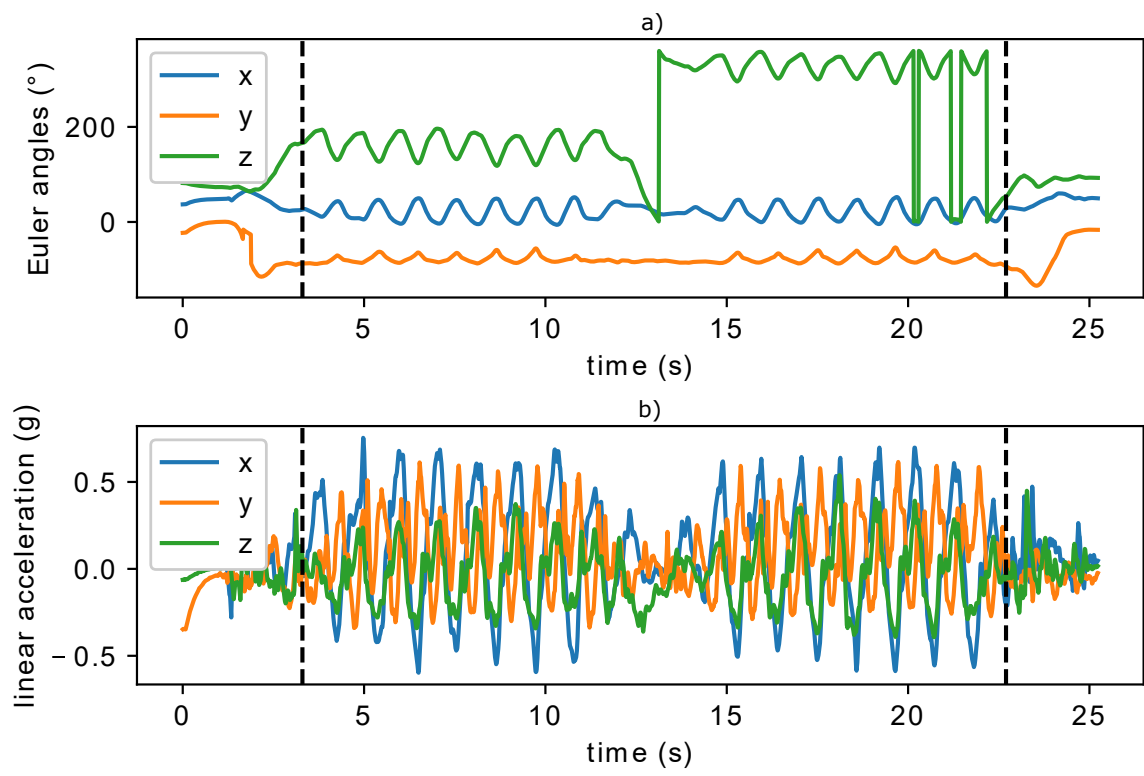
Figure 4.9.: Euler angles and linear acceleration of one wristband for the TUG test.

5

Study and data sets

In the previous Chapter 4 - Hardware and signals, the used hardware was shown. This chapter introduces the used data sets. In total, we create three data sets for gait analysis and use one public data.

5.1. Activity recognition

The first data set was created to record the motion of activities with the smartphone. In this data set, we use recordings of 20 healthy subjects. We recorded linear acceleration and rotation data of the Android operating system with a frequency of 50 Hz. In total, the following activities were recorded *gait, cycling, go stairs, lying, sitting, standing, smartphone lying around* (table or desk), *smartphone in use* (writing a message or play a game), and *use transport* (drive by car or train). We have reduced the problem to a binary problem and use in the following only the classes *gait* and *other*. The class *other* contains the activities *cycling, go stairs, lying, sitting, smartphone lying around, smartphone in use, standing, and use transport.*

For data collecting, we developed an Android App. The subjects specified the start, end, and type of activity via the App before each recording. Users had to select one activity from a list before starting the activity, see Figure 5.1 a). After the activity ends, the user had to confirm this by pressing a button, see Figure 5.1 b).

5.2. Daily life

For the daily life data set, we have a total of seven recordings of seven different healthy persons. The persons' age was between 25 and 54 years, and each person passed the test one time. During the experiment, the candidates had to pass the following test, see Figure 5.2. At the beginning of the test, the person sits on a chair for one minute. Then, the person gets up from the chair and stands for one minute. After that, the person walks back and forth for one minute. Then, the person goes upstairs three floors and then down the stairs. Next, the person walks for another minute again and ends up in front of a chair. The person spends one minute standing. In the second last step, the person repeatedly changes for one minute from a standing to a sitting position. Finally, the person sits for one minute on the chair.
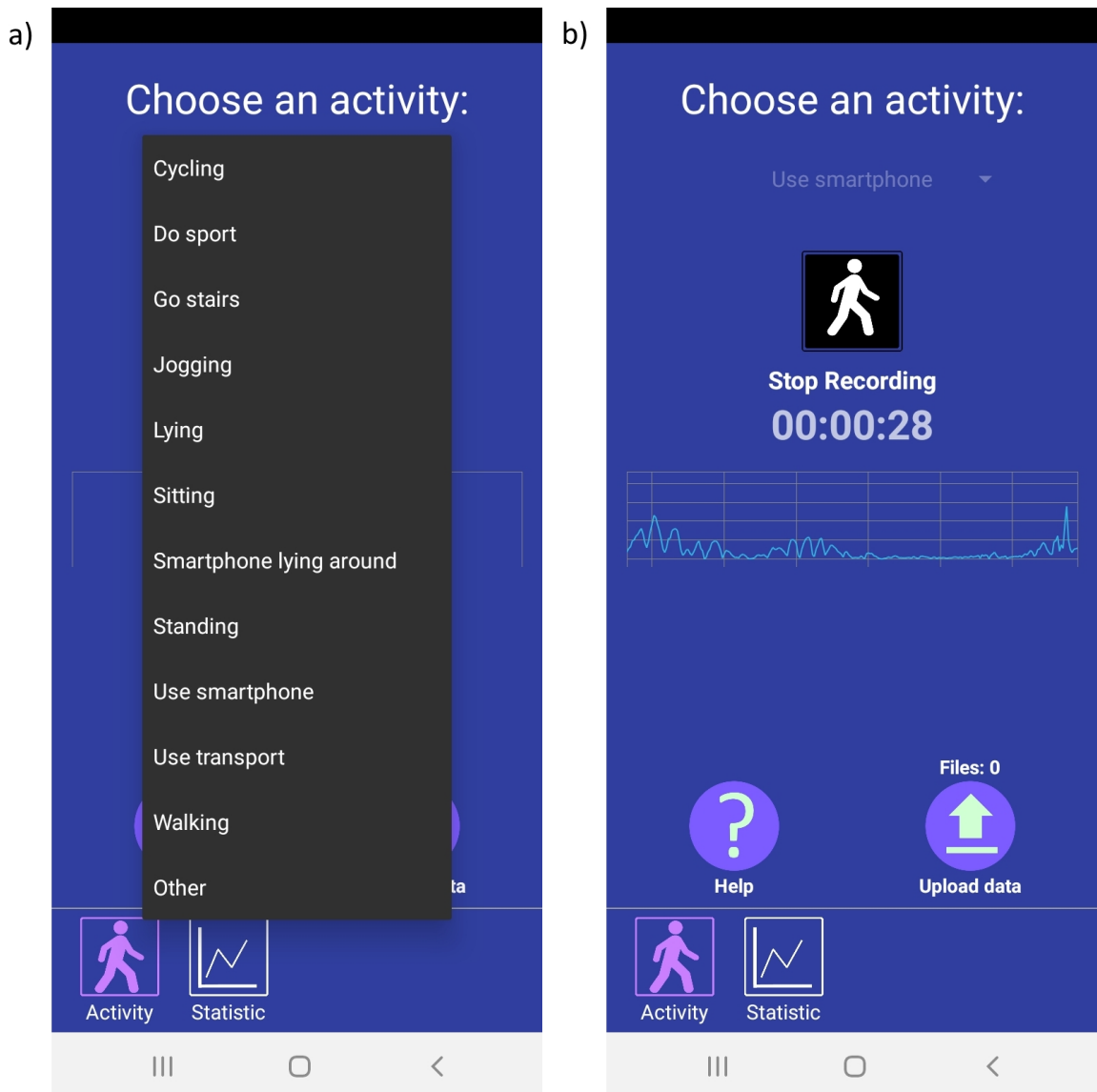
Figure 5.1.: Screenshots of the smartphone App to recording activities. a) select an activity to recording, b) stop recording after finish the activity.

5.3. Timed Up and Go

The physicians of the Niederlausitz Clinic used the Timed Up and Go (TUG) test to evaluate the subjects' motor dysfunctions as a part of the UPDRS. For the test, only a chair with a backrest and armrests was needed. At first, the test person was sitting on a chair. Upon a command from the test leader, the test person stood up and walked straight ahead for ten meters at an appropriate speed to a mark. At the mark, the test person turned around and walked ten meters straight ahead, back to the chair. The test person sat down in the chair. Then, the test and recording were finished. We divided the TUG into two different parts for later analysis of the data. Part (A) contained the
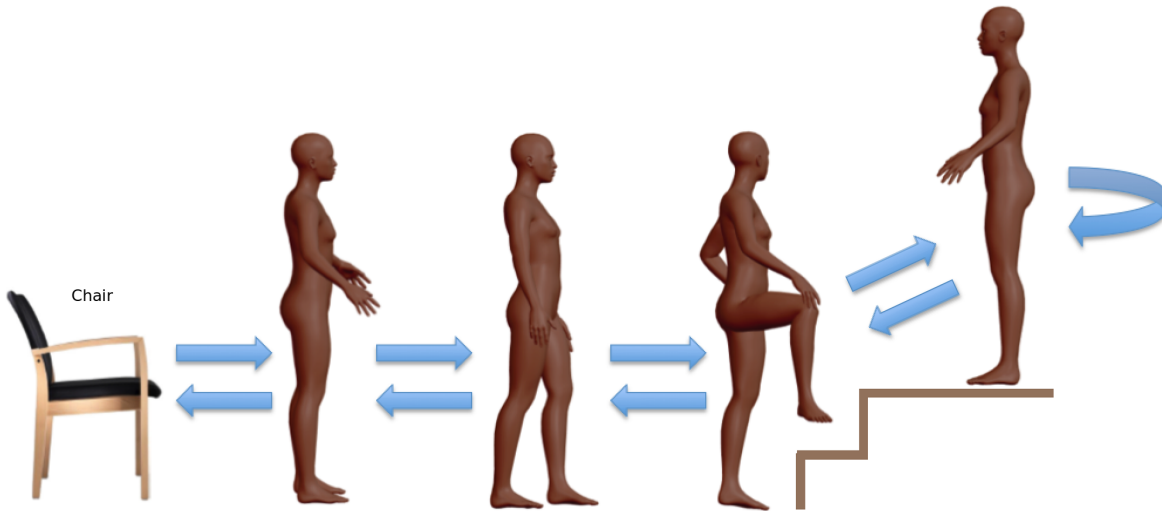
Figure 5.2.: Process of Daily Life Activities Test.

complete TUG, including standing up and sitting down in the chair. Part (B) included going straight to the mark, turning around, and going straight back to the chair. Parts (A) and (B) are shown in Figure 5.3. This splitting aimed to extract the gait data from the complete recording.

5.3.1. Recruiting

To create the data set for later analysis, we worked together with the Niederlausitz Clinic in the study "Development of a digital Parkinson Disease Assessment". The ethics application granted in December 2018 by Ethics Committee Brandenburg (Germany), see appendix A - Ethic application. The physicians evaluated all persons. A total of 39 different subjects with 250 recordings were available for the data set. Of these are 15 subjects with 80 recordings have motor dysfunctions, and 24 subjects with 170 recordings were used as a control group, see Table 5.1.

Table 5.1.: Amount of persons and records from the Parkinson's and control groups.

Label	Persons	Records
Motor dysfunction	15	80
Control	24	170

For the study, the gait of Parkinson's patients with different stages of the disease will be measured. In the different stages of Parkinson's disease, different symptoms are in the foreground. The subjects recruiting will be done by the Centre for Neurology and Pain Treatment of the Niederlausitz Hospital. The measurements for the study are performed under the supervision of medical personal and a physician. As a control group, subjects
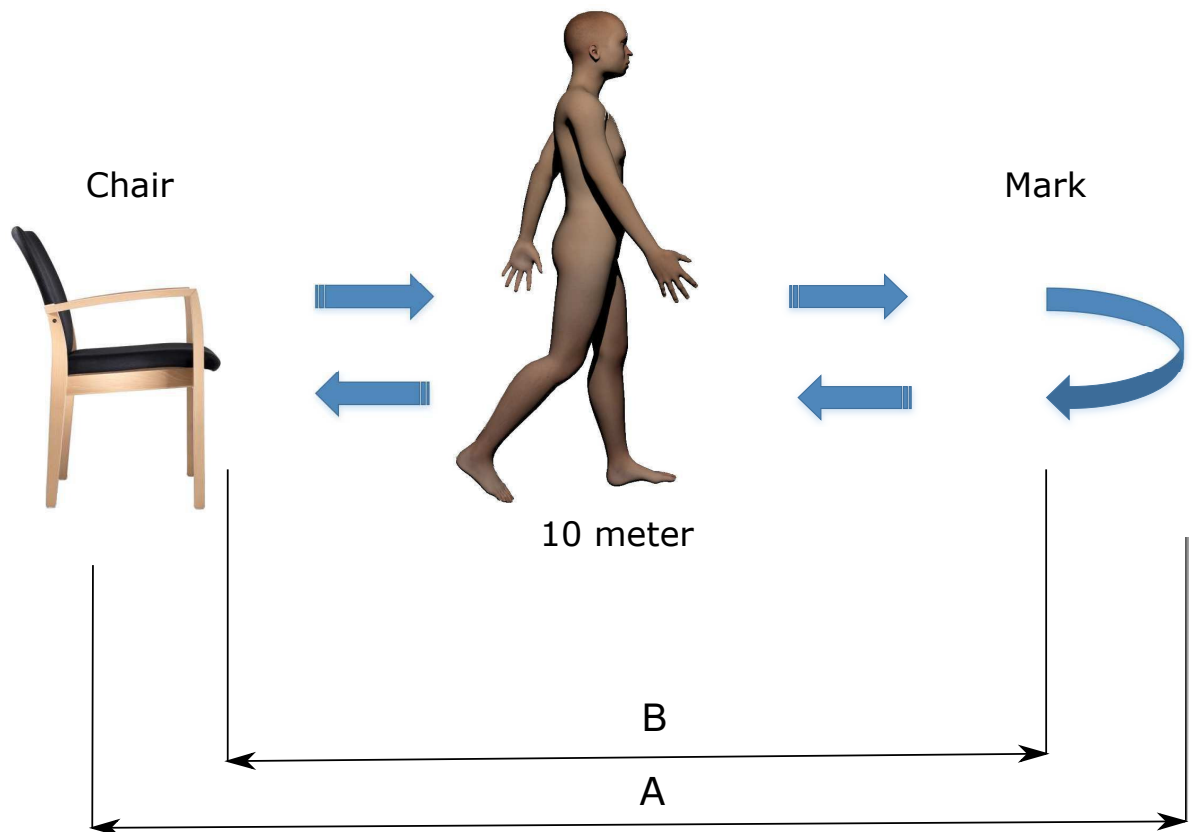
Figure 5.3.: Process of the TUG test.

of the same age are selected. These should not show any motor disorders. Patients were recruited to the study by the inclusion and exclusion criteria.

5.3.2. Inclusion criteria

- The subject gave the agreement for the study after being informed orally and in writing form about the aims and contents of the study.

- The subject has a clinically specific diagnosis of an idiopathic Parkinson's syndrome.

- There is no advanced normal pressure hydrocephalus and cerebral microangiopathy, which leads to another Movement disorder.

- The subject can walk.

5.3.3. Exclusion criteria

- Severe neurogenic contractures in the extremities that do not allow movements,

- Severe cognitive impairment with a mini-mental status < 20,

- Insurmountable communication difficulties, which make the instruction of the Preventing test persons from entering the test procedure,

- Acute injuries that affect the functionality of the limb restrict (for example fracture of the wrist),

- Illnesses within the last seven days (for example flu-like infection),

- Endoprostheses of the extremity,

- Drug consumption, or

- Pacemaker.

5.4. Public data set

To confirm the functionality of our algorithms for stride symmetry, we use a public data set. This data set consists of 93 patients with idiopathic Parkinson's disease and 73 subjects of the control group. The database includes the vertical ground reaction force records of subjects as they walked at their usual, self-selected pace for approximately two minutes on level ground, see Table 5.2. Underneath each foot were eight sensors (Ultraflex Computer Dyno Graphy, Infotronic Inc.) that measure force (in Newtons) as a function of time, see Figure 5.4. The output of each of these 16 sensors has been digitized and recorded at 100 samples per second, and the records also include two signals that reflect the sum of the eight sensor outputs for each foot. For details about the data format, see [Goldberger2003]. The results were divided into the studies Galit, Hausdorff, and Silvi. Within these studies, the study subjects were separated according to the control group and Parkinson's disease.

Table 5.2.: Demographics of the data set.

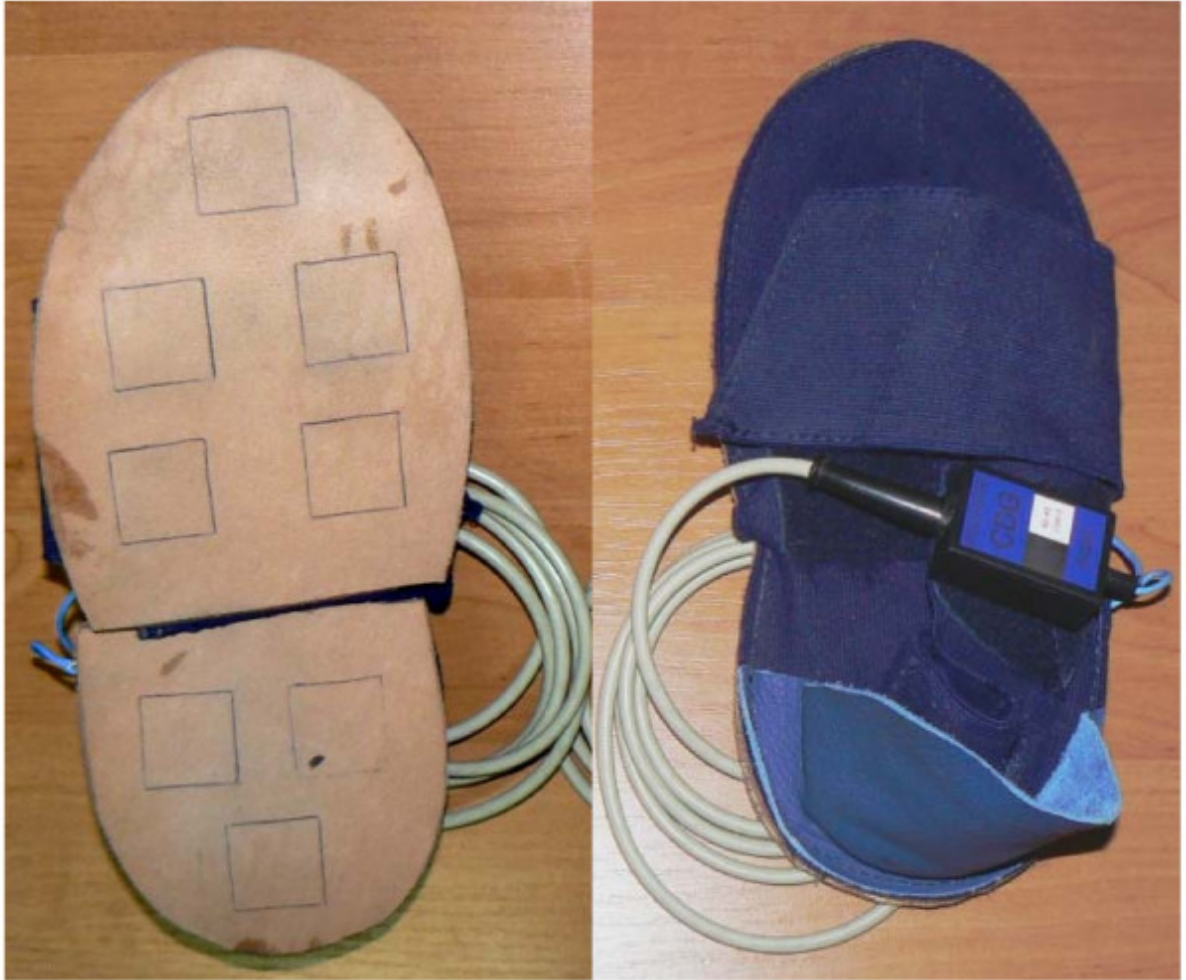| Study	Group	Count	Male/ Female	Age $(mean \pm std)$
Galit	PD	29	20/9	71.10 ± 8.06
	Control	18	10/8	71.56 ± 6.66
Hausdorff	PD	29	16/13	67.21 ± 9.15
	Control	26	12/14	64.58 ± 6.83
Silvi	PD	35	22/13	61.57 ± 8.86
	Control	29	18/11	57.93 ± 6.97
Total	PD	93	58/35	66.30 ± 9.50
	Control	73	40/33	63.66 ± 8.64

Figure 5.4.: Used hardware to create the data set [Jelen2008].

6

Methodology

The process for analysing gait data is based on the communication between our Android App and four wearable devices (two wristbands and two insoles), see Figure 6.1. We have separated the functional tasks of the smartphone, wearables, and data analysis with dotted lines.

At the beginning of the workflow, we make an activity recognition. Thus, we want to distinguish the activity *gait* again, the activity *other*. The activity *other* consists of the activities *cycling*, *go stairs*, *lying*, *sitting*, *standing*, *smartphone lying around* (table or desk), *smartphone in use* (writing a message or play a game), and *use transport* (drive by car, bus, or train). The activity detection is designed to keep the wearable sensors in standby mode until the activity *gait* is detected. This activity detection extends the usage time of the wearable devices. For recognition of activity gait, we have performed a five-fold cross-validation. For the results we have specified precision, recall, F1-Score and Accuracy.

However, the wearables work only as slaves, so the smartphone must always send a signal for starting a function. For this reason, the tasks *Start Recording*, *Stop Recording*, *Synchronization*, and *Data Transmission* are involved by both devices.

If a person is walking and the smartphone detects the activity *Gait*, the wearables are turned on, synchronized, and recording starts. When the activity *Other* is detected and the recording is running, then recording stops and the data is transferred to the smartphone for a later data analysis. After the transfer, the wearables are switched off.

From the recorded signals, strides have to be extracted. For this purpose we have evaluated different stride detection algorithms. To create our training data, we label manually our daily life activities and TUG test datasets into strides and no strides. Data are split into training and test data. In order to avoid biasing the results, we make sure that data assigned to an individual are either only in test data or only in training data. 70 % of the data were used for training and 30 % for testing. This type of separation makes the training data totally different from the test data. This means there are no redundant data to improve the results. Since there is a small dataset for the classification, we decided to use a k-fold cross-validation with mixing. We select seven folders for the daily life activity Test. We use five folders for training and two for the test.

For the gait phases, features, and symmetry calculation, we need a more accurate detection of the strides than with the activity recognition. For this reason, we perform a stride detection by using CNN to detect individual strides of the foot. After that, the

gait phases, features, and symmetry of the strides can be calculated. For classification of motor dysfunctions in arm swing we use the complete TUG-test. We decided to use 3-fold cross-validation for the classification to make the results of our applied methods reasonable. We used 66.6 % of the data for training and 33.3 % for testing. The Parkinson stadium clustering with insoles, a separate process is necessary. For this reason, the issues were listed separately.

For each measurement, we calculated the sensitivity, specificity (precision), recall, F1-score, and accuracy. For this, we used the confusion matrix in Table 6.1.

Table 6.1.: Binary confusion matrix.

	Labeled classes	
	Positive	Negative
predicted positive	TP true positive	FP false positive
predicted negative	FN false negative	TN true negative

Sensitivity Sensitivity (recall) is a widespread measurement in medicine. It indicates the ratio of predicted strides to all strides inside our test data:

$$recall = sensitivity = \frac{TP}{TP + FN}. \tag{6.1}$$

Specificity The specificity describes how well our system can distinguish steps from all other activities (no steps). It is the ratio of undetected strides in all test data where no steps were present:

$$specificity = \frac{TN}{FP + TN}. \tag{6.2}$$

Precision The precision is the proportion of correctly predicted steps to all predicted steps:

$$precision = \frac{TP}{TP + FP}. \tag{6.3}$$

Accuracy Accuracy is the ratio of all correctly recognized strides and all correctly recognized other activities (no stride) to all test data:

$$accuracy = \frac{TP + TN}{TP + FP + FN + TN}. \tag{6.4}$$

F1-score   The F1-Score is the harmonious average between precision and recall. In this way, both measures are combined into one value:

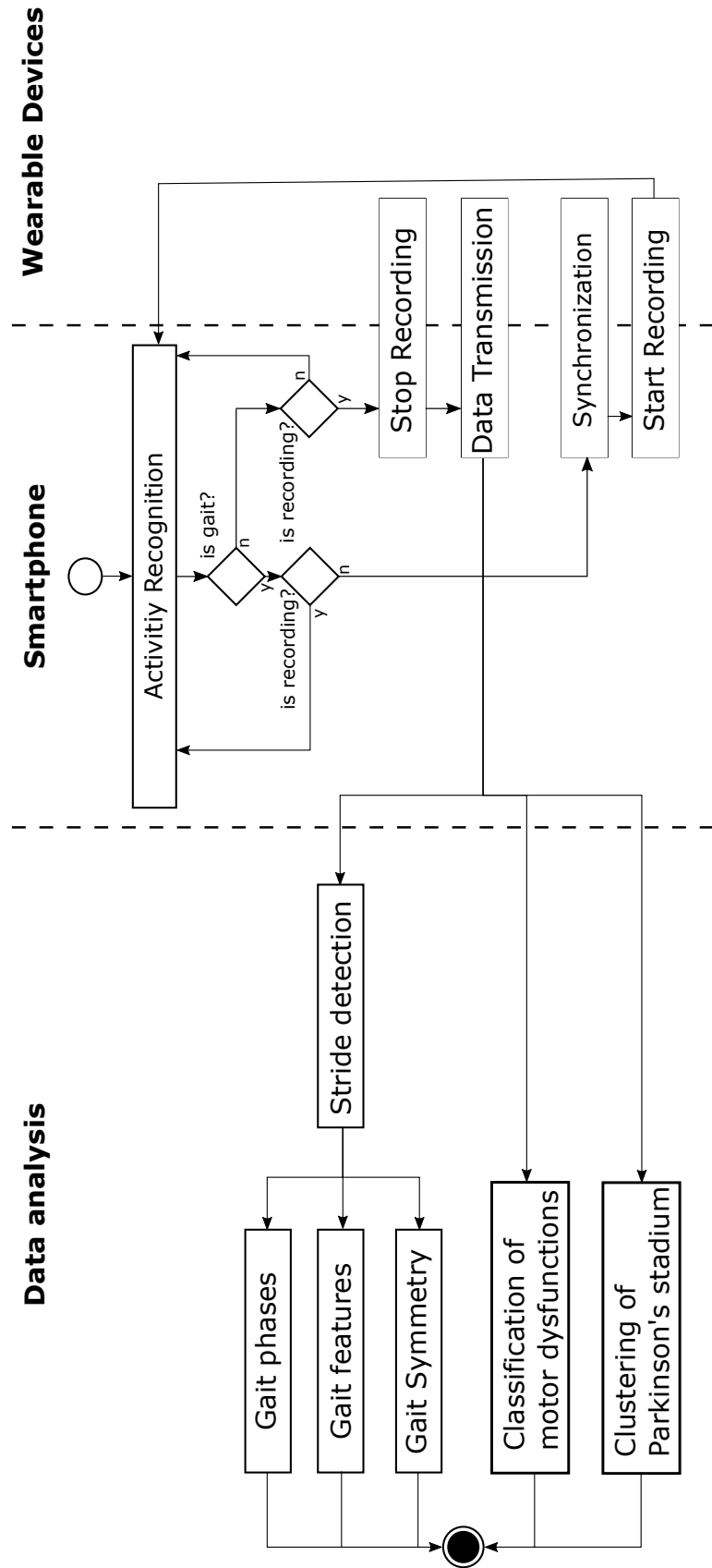$$F1 = 2 \cdot \frac{precision \cdot recall}{precision + recall}.$$

(6.5)

Figure 6.1.: Process of synchronize, record, and evaluate data.

7

Activity recognition

In the last chapter, the methodology of the work was presented. The wearable sensors are not energy efficient. This depends on the sensors that continuously send data to the microcontroller. Bluetooth Low Energy (BLE) has even high energy consumption. In order to ensure that, the microcontroller still works energy-efficiently, we only switch the wearable on when it is needed. Otherwise, the wearables remain in standby mode. Therefore, we developed an activity recognition for the smartphone [Steinmetzer2020]. The activity recognition will switch on the wearables only if the smartphone detects the activity *Gait*. This chapter explains the activity recognition.

7.1. Related works

Many smartphones have a gyroscope, accelerometer, and magnetometer. In many studies, this has been used to try to identify the activities of people [Gadaleta2018, Hassan2018, Cao2018]. One possibility to implement this is to choose a fixed window width of a signal and collect all statistical values for this window, which serve as a characteristic for the classification. The use of a neural network has proven to be useful here [Hassan2018, Cao2018]. Another possibility is the use of CNNs [Gadaleta2018]. Activity detection is usually used to reflect the time a person has been moving throughout the day. This is sufficient for an activity estimation of a person in general. The quality of smartphone sensors is adequate to estimate the activity of a person.

We take advantage of the activity recognition so that the wearables are not always switched on. As a result, the wearables are energy-efficient and are only used when the data is relevant for analysis.

7.2. Methods

In order to enable an energy-efficient use of the wearable devices, they are only powered when they are in use. The energy-efficient use means that the wearable devices only have to be switched on during recording. For this reason, we decided to use a binary activity classifier in the smartphone device. This classifier enables us to distinguish the activity *gait* from *other* like *cycling, go stairs, lying, sitting, smartphone lying around, smartphone in use, standing*, and *use transport*.

For the activity detection, we use the linear acceleration and rotation data of the Android operating system at a frequency of 50 Hz. As features, we use a fixed window

width of 10 s and an overlap of 50 %. The input is the complete window width and all axis of the sensor data for a 1D CNN classifier. Figure 7.1 shows the design of Convolutional Neural Network (CNN). We chose CNN because other researchers have also achieved excellent results with CNN [Gadaleta2018, Hassan2018].
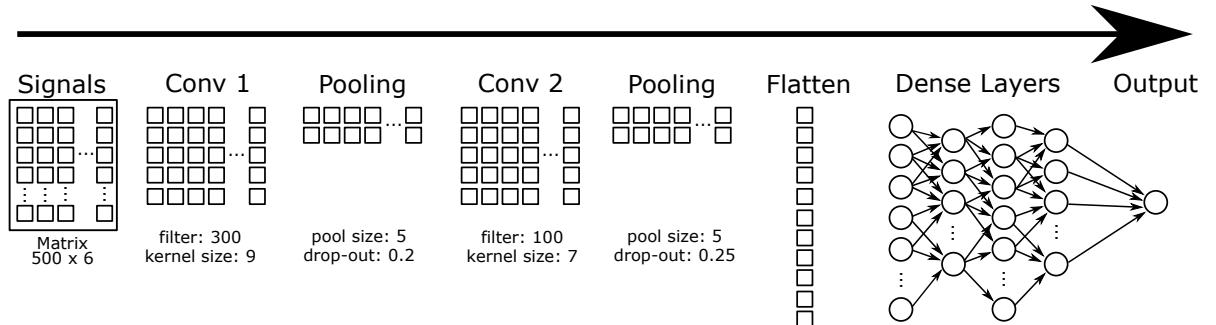
Figure 7.1.: Model of the CNN layers for activity recognition.

For the construction of the model, we use the activation function Rectified linear unit (ReLU) function except for the output layer. The first layer is a convolutional layer with 300 filters and a kernel size of nine. Next is a max-pooling with a size of five and a drop-out with 0.2. Then follows another convolution layer with 100 filters and a kernel size of seven. Then again, a max pooling with a size of 5 and a drop-out with a probability of 0.25. Next comes a flatting layer. In the following, there are different dense layers with 30, then 10, and finally 50 neurons. The last layer is the output layer, which uses a sigmoid function as the activation function.

For training, we have separated the data by persons. This ensures that the same person is not included in the training and test data set. We split the data that 66 % is used for training, and 34 % for testing. During training, we use different epochs and batch sizes. In our case, the setting of 100 epochs and 100 batch sizes has proven good results.

7.3. Results

For recognition of activity *gait*, we have performed a five-fold cross-validation. The results are shown in Table 7.1. For the results, we have specified precision, recall, F1-Score, and Accuracy. Each column show the average value and standard deviation.

Table 7.1.: Results for recognition of activity *gait*.

	Precision	**Recall**	**F1-Score**	**Accuracy**
CNN	0.958 ± 0.031	0.683 ± 0.023	0.884 ± 0.011	0.947 ± 0.005
[Hassan2018]	-	-	-	0.9585
[Cao2018]	-	-	-	0.9416

8

Synchronisation

The last chapter demonstrated how the wearables are used in an energy-efficient way by only switching them on when needed. The aim is to use the time series of the wearables to obtain conclusions about the subjects gait symmetry. Therefore, we want to use the complete time series of gait cycles to calculate the symmetry. However, for this, the wearables' signals have to be synchronous, which is not the case by default. For this reason, an algorithm is developed, which synchronizes the wearables with each other.

8.1. Related works

The video-based systems have a synchronized recording of all extremity movements. The disadvantage is that the measurements cannot be carried out in daily life. Only camera systems for laboratory measurements were found in the literature [Viteckova2016]. In contrast, wearable systems could be an alternative for making symmetry measurements of gait in daily life, but they are not time-synchronized.
In order to closing this gap, the microcontrollers must be synchronized with each other. Several approaches have already been pursued. A possible solution is to build up a sensor network in which the sensors are connected by wires [Viteckova2016]. Another work presents a system where a docking station serves as a charging station and synchronizes [Mancini2011]. The docking station can synchronize four wearable sensors, but it has a time drift after a longer runtime. Others use the system of MbientLab [Anwary2018b]. In order to determine whether the gait is symmetrical, we need four synchronized sensors, one for each limb. In earlier works, we had tested the system of Mbientlab, but it can only record three synchronized sensors [Anwary2018b].

In the following the advantages and disadvantages of the current systems are presented:

- Camera-based systems can measure the synchronized time series of each limb. However, they are stationary and, therefore, not suitable for measurements in daily life.

- A smartphone is useful for detecting gait activities. Nevertheless, it is too imprecise for clinical measurement.

- IMU systems are an alternative to camera-based systems. However, they have to be synchronized.

From the points mentioned above, it can be concluded that wearables are suitable for gait analysis but that a single device is inaccurate. For this reason, several wearables are used at different extremities. Therefore, wearables have to be synchronized. Ideally, only immediately before using the wearables, so that time drift is counteracted. For this reason, it is worth considering wireless synchronization via Bluetooth low energy.

8.2. Methods

8.2.1. Process

The synchronization takes place according to the following scheme, see Figure 8.1. The master device is the smartphone, and the slaves are the four wearable devices.

1. The master sends an empty Bluetooth packet to the first slave (reference slave) and the second slave.

2. Each slave replies with its device time (milliseconds since power-on) as soon as it receives the master is the packet.

3. The master receives the responses and measures the time difference between them.

4. To avoid random response times (for example, caused by physical influences), the process is repeated multiple times.

5. The median is the time difference between the reception of the packets by the reference slave and the second slave.

6. The master calculates the offset of the second device and sends it to the second device, see equation 8.2.

7. Now, the second slave knows its offset compared to the reference slave.

8. Steps one to seven are repeated with the first slave and the third slave.

9. Steps one to seven are repeated with the first slave and the fourth slave.

As a result, we get the offsets between the reference device and the other three measuring devices. The four measuring devices record data synchronously. Unfortunately, a drift can occur between the devices. In order to prevent this, the synchronization is repeated before each recording.

8.2.2. Verification test setup

To be able to measure the Bluetooth latency correctly, we have wired the microcontrollers to each other. Two microcontrollers are connected by wire using their serial output and input. The output pin of one device is connected with the input pin of the other device and vice versa. In the beginning, the outputs are set to "low". One of the two devices
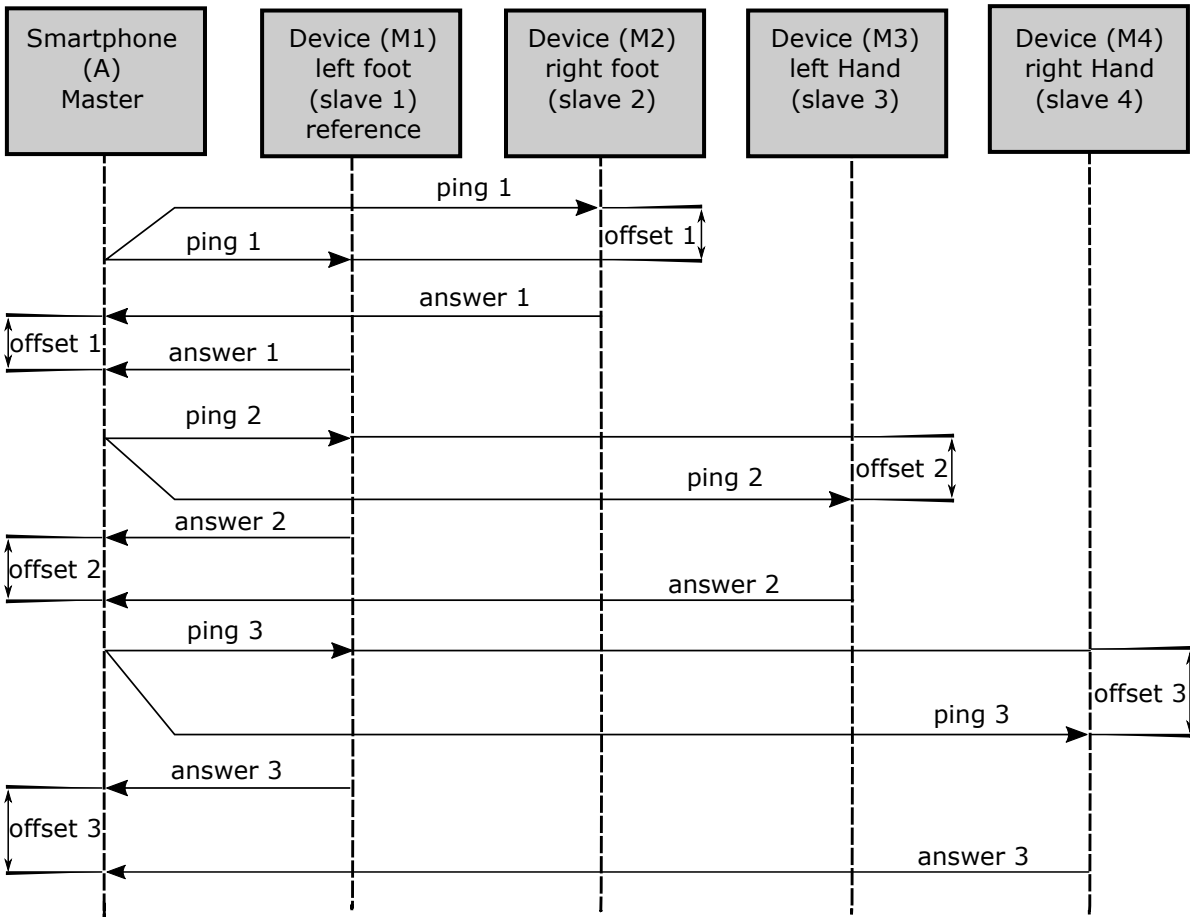
Figure 8.1.: Process of synchronization.

now initiates a "high" output and starts a timer. The other device registers this event by reading a "high" input and answers to the first device by setting its output pin to "high", too. The first device stops the timer as soon as it registers a "high" input. According to repeated measurements, the serial latency is lower than 1 ms. Because, this latency measurement does not influence the synchronization latency, it is ignored in the following section.

In the next step, we measure the latency and offset of the Android OS to send a Bluetooth packet to the microcontrollers. Furthermore, we also measure the time at which packets are received if the microcontrollers have sent them. For the measurement of the offset between the microcontrollers, we use the test setup from Section 8.2.2. For the test setup, the microcontrollers (M1) and (M2) were placed at the same distance to the Android smartphone (A). Therefore, M1 and M2 have the same signal strength. Otherwise, this can corrupt the result. The results of the measurement can be seen in Table 8.1. The first and second columns *A send M1* and *A send M2* are the timestamps of the Android OS in milliseconds (ms) when the commands were executed. *Diff 1* is the difference in ms between column $(AsendM2) - (AsendM1)$. The RL column is the wired offset between the two microcontrollers measured using the method in the Section

8.2.2. This offset is the real offset. *R1* and *R2* are the timestamps in milliseconds of the received Bluetooth packets of the microcontrollers. The last column l reflects the difference of the columns $R2 - R1$ in milliseconds. This offset, the Android OS uses to calculate the device offsets. Perfect synchronization is achieved when $RL = l$.

The measurement was repeated three times. Therefore each measurement is separated in the table by a double line. The columns RL and l show a correlation to each other. For this reason, it was written in bold. Table 8.1 shows that the packets are sent with different priorities by the Android OS. Thus, the column *Diff 1* does not correlate with RL. The values of the three measurements of *A send M1* and *A send M2* by Pearson correlation to give the following results 0.034, -0.272, -0.617. This means that there is no correlation. On the other hand, the columns l and RL correlate strongly by Pearson correlation with the following values 0.743, 0.580, 0.982.

This can be explained by the fact that the microcontrollers M1 and M2 process the commands sequentially, and thus all commands are equally authorized. Furthermore, it is possible to receive signals at the app in real-time because there are several threads available.

Out of this knowledge, we can say the receive time of the smartphone is the offset in which the microcontrollers sent the signal. We use this fact for synchronization. In summary, we can note that when sending packages of two microcontrollers at the same time, these also arrive simultaneously.

8.2.3. Synchronization algorithm

Based on the data from section 8.2.2, we can now propose a solution to synchronize two microcontrollers via bluetooth. The following steps describe the procedure of the algorithm:

1. The Android device A sends a packet to microcontrollers M1 and M2.

2. M1 sends a packet to A. The packet holds a timestamp of the system time $t1$ directly before sending it.

3. M2 sends a packet to A. The packet holds a timestamp of the system time $t2$ directly before sending it.

4. A receives a packet from M1 at a real-time $R1$.

5. A receives a packet from M2 at a real-time $R2$.

With this information, we can calculate our receive latency l:

$$l = R2 - R1 + c, \tag{8.1}$$

where c represents a possible error. The offset o from M1 and M2 can be calculated as follows: 8.2.

Table 8.1.: The Android OS is measured latency of two microcontrollers between the send and receives timestamps for three different executions. *A send M1* and *A send M2* are the timestamps when the Android OS executes the commands. *Diff 1* is the difference of $(A\ send\ M2) - (A\ send\ M1)$. *RL* is the wired latency between both microcontrollers when receiving the packets. *R1* and *R2* are the times when the Android OS has received the packets from the microcontrollers. Latency l is the difference of $R2 - R1$. The Bold columns show the correlation between *wired l* and calculated *l*.

A send M1	A send M2	DIFF 1	RL	R1	R2	l
1552473386320	1552473386332	12	**23**	1552473386373	1552473386396	**23**
1552473402974	1552473402985	11	**27**	1552473403025	1552473403054	**29**
1552473411800	1552473411804	4	**23**	1552473411851	1552473411872	**21**
1552473415820	1552473415829	9	**30**	1552473415863	1552473415897	**24**
1552473418088	1552473418100	12	**28**	1552473418131	1552473418160	**29**
1552473420520	1552473420527	7	**28**	1552473420564	1552473420593	**29**
1552473422598	1552473422604	6	**31**	1552473422638	1552473422672	**34**
1552473424513	1552473424523	10	**29**	1552473424557	1552473424585	**28**
1552473426282	1552473426295	17	**28**	1552473426327	1552473426355	**28**
1552473428201	1552473428209	8	**28**	1552473428239	1552473428267	**28**
1552475001845	1552475001849	4	**43**	1552475001888	1552475001929	**41**
1552475013106	1552475013111	5	**19**	1552475013159	1552475013179	**20**
1552475014617	1552475014624	7	**33**	1552475014658	1552475014730	**72**
1552475015951	1552475015964	13	**32**	1552475015996	1552475016029	**33**
1552475017448	1552475017460	12	**23**	1552475017495	1552475017517	**22**
1552475018910	1552475018920	10	**24**	1552475018958	1552475018979	**21**
1552475020302	1552475020309	7	**31**	1552475020346	1552475020380	**34**
1552475021704	1552475021713	9	**31**	1552475021751	1552475021780	**29**
1552475022982	1552475022995	13	**29**	1552475023021	1552475023049	**28**
1552475024662	1552475024670	8	**28**	1552475024709	1552475024737	**28**
1552477976517	1552477976523	6	**42**	1552477976564	1552477976605	**41**
1552477978212	1552477978222	10	**29**	1552477978258	1552477978287	**29**
1552477979992	1552477980003	11	**16**	1552477980046	1552477980067	**21**
1552477981607	1552477981616	9	**31**	1552477981651	1552477981685	**34**
1552477983153	1552477983165	12	**31**	1552477983193	1552477983227	**34**
1552477984567	1552477984581	14	**31**	1552477984611	1552477984645	**34**
1552477986029	1552477986036	7	**43**	1552477986078	1552477986120	**42**
1552477987445	1552477987455	10	**28**	1552477987486	1552477987515	**29**

Table 8.2.: Latency l between microcontroller M1 and M2.

Index	M1	M2	l	Wired l	c
1	1552919014830	1552919014946	116	81	35
2	1552919014999	1552919015047	48	8	40
3	1552919015776	1552919015154	-622	-665	43
4	1552919015838	1552919015897	59	55	4
5	1552919015950	1552919015972	22	20	2
6	1552919016005	1552919016014	9	6	3
7	1552919016055	1552919016064	9	7	2
8	1552919016098	1552919016106	8	5	3
9	1552919016147	1552919016156	9	8	1
10	1552919016191	1552919016199	8	4	4
11	1552919016240	1552919016262	22	21	1

$$o = (t2 - t1) + l. \tag{8.2}$$

Of course, in the proposed algorithm, errors can occur, resulting from disturbances in the magnetic field or other physical effects. Therefore, we perform the algorithm eleven times and use the median of the latency to determine the best synchronization between the devices $M1$ and $M2$.

8.3. Results

In Tables 8.2, 8.3, and 8.4 the measured values of synchronization are shown. In the tables, the first column is a numbered index. It is followed by the receiving time of the reference microcontroller and the third column of the to be synchronized microcontroller. Column four is the calculated latency of both microcontrollers, and column five is the wired measured latency over the wires. The last column shows the error from calculated to measured latency. For the most accurate timestamp, we calculate the median of the latencies l.

In Table 8.5 the latencies are shown sorted, and the median is printed bold. All three tables provide a positive error of 1 ms to the reference device. Thus, the total latency is 1 ms. In other measurements, we have a total error of 3 ms. Since we record the sensor data with 100 Hz, this error is tolerable for symmetry calculation.

Table 8.3.: Latency l between microcontroller M1 and M3.

Index	M1	M3	l	Wired l	c
1	1552919585669	1552919585703	34	34	0
2	1552919585731	1552919585728	-3	-5	2
3	1552919585770	1552919585781	11	8	3
4	1552919585824	1552919585827	3	4	1
5	1552919585862	1552919585877	15	16	1
6	1552919585924	1552919585914	-10	-8	2
7	1552919585961	1552919585978	17	17	0
8	1552919586024	1552919586014	-10	-8	2
9	1552919586061	1552919586078	17	17	0
10	1552919586124	1552919586114	-10	-9	1
11	1552919586161	1552919586171	10	9	1

Table 8.4.: Latency l between microcontroller M1 and M4.

Index	M1	M4	l	Wired l	c
1	1552988793978	1552988794019	41	41	0
2	1552988794060	1552988794056	-4	5	9
3	1552988794110	1552988794119	9	8	1
4	1552988794154	1552988794145	-9	-4	5
5	1552988794203	1552988794199	-4	-5	1
6	1552988794227	1552988794236	9	9	0
7	1552988794258	1552988794262	4	3	1
8	1552988794295	1552988794313	18	17	1
9	1552988794359	1552988794348	-11	-10	1
10	1552988794395	1552988794404	9	11	2
11	1552988794451	1552988794442	-9	-8	1

Table 8.5.: Latencies l between the microcontrollers (M1 and M2), (M1 and M3), and (M1 and M4).

M1 and M2			M1 and M3			M1 and M4		
Index	**l**	**c**	**Index**	**l**	**c**	**Index**	**l**	**c**
3	-622	43	6	-10	2	9	-11	1
8	8	3	8	-10	2	4	-9	5
10	8	4	10	-10	1	11	-9	1
6	9	3	2	-3	2	2	-4	9
7	9	2	4	3	1	5	-4	1
9	**9**	**1**	**11**	**10**	**1**	**7**	**4**	**1**
5	22	2	3	11	3	3	9	1
11	22	1	5	15	1	6	9	0
2	48	40	7	17	0	10	9	2
4	59	4	9	17	0	8	18	1
1	116	35	1	34	0	1	41	0

9
Stride detection

The last chapter was about the synchronization of the wearables and this chapter is focused on the stride detection. Both chapters are important basics for the later gait futures calculation in the Chapters 10, and 11. Gait recognition methods are divided into model-free and model-based approaches [Kovac2019, Kovac2014, Kovac2013, Seckiner2019]:

- Model-free approaches use gait representations such as silhouette, texture, and color to extract static gait features, and dynamic gait features such as joint trajectories [Seckiner2019, Tong2011]. Model-free approaches usually focus on changes in the appearance of individuals rather than on gait dynamics.

- Model-based approaches such as [Rastegari2019, Prakash2019, Gupta2019] create movement models to extract features [Kovac2019, Kovac2014, Kovac2013], for example stride length, height, and frequency. For diagnostic support and measurement of therapy success, we recommend model-based approaches because they are more resistant to changes in view and scale.

The goal of many kinds of research is gait analysis. Others are concerned about activity recognition. Stride detection recognizes as precisely as possible single strides in a time series. In contrast, activity recognition detects different kinds of movement, such as walking, standing, and jogging. A standardized test for the diagnosis of Parkinson's disease is the TUG test. This test is also used, for example, by [Mazumder2018b] to differentiate between healthy and Parkinson's patients. We also used this test by [Steinmetzer2018] under ideal hospital conditions for an approximate estimation of Parkinson's stadium.

We want to propose a system that recognizes the walking strides of Parkinson's patients in daily life [Steinmetzer2019a]. To the best of our knowledge, there is no other study detects strides:

- automatically,

- without a manual set threshold,

- independent of motor dysfunction,

- independent of the Parkinson's stage of the patient, and

- exclusively from walking activity (not from for example descending, ascending stairs, sitting activities).

9.1. Related works

Movement disorders that influence the patient's gait are measured with sensors such as gyroscopes, accelerometers, magnetometers, pressure sensors, and image sensors. Accelerometers and gyroscopes are often used in combination with a magnetometer [Barth2015, Bobic2018, Tao2018, Koroglu2018, Hannink2018, Watanabe2018]. The sensors can be integrated into smartphones [Tao2018, Kim2018] or attached to the ankle [Barth2015, Jiang2018, Hannink2018] or body [Koroglu2018]. In addition to the 2D image, a depth sensor is sometimes used for video recordings for gait analysis [Ince2017]. Force sensors are installed in insoles [Agostini2014, Mazumder2018b, Steinmetzer2018] and substrates [Muheidat2017].

A low-pass digital filter to eliminate the high-frequency noise components of raw accelerometer measurements is used in [Tao2018]. Furthermore, the authors ensure that only one peak is detected for every zero crossings of normal gravity.

By [Agostini2014], they define stride candidates by determining the beginning of the gait phase and calculate the stride duration. Strides with two phases and short duration are first merged with preceding strides and afterward with successive strides.

A stride recognition rate of 97 % is achieved in [Barth2015] with the multi-dimensional subsequence DTW with free walking. For this method, a fixed threshold value is used. Thus, worsens the results for abnormal movements or climbing stairs [Barth2015].

Mild Cognitive Impairment in gait is classified in [Gwak2018]. Photoplethysmography and gait (accelerometer and gyroscope) sensor data were recorded. The Butterworth filter was used to remove noise from the measured gait signals. To detect strides, a peak detection algorithm with minimum peak height and minimum peak distance was used.

For normal walking conditions, the stride frequencies have been assumed to range from 1 Hz to 3 Hz. By [Kim2018], gravitational acceleration is filtered by using a bandpass filter with a center frequency of 2 Hz and a bandwidth of 2 Hz. Strides are detected using the Stride Feature of Spectrogram methods and an Artificial Neural Network architecture. A gait mat delivers gait parameters analyzed in [Muheidat2017] such as speed, stride time, and stride length of the GAITRite® instrumented walkway system. In [Koroglu2018] foot and body-mounted IMUs are used for strides detection. Strides were labeled using a threshold. A residual neural network performed stride detection. For the training process, the cross-entropy function was used as the loss function.

In a preprocessing step by [Hannink2018], the signals from accelerometer and gyroscope are normalized and scaled to a fixed length of 256 samples per stride to ensure equally scaled and fixed-size input to the network. Mid-stance and heel-strike are detected. A two-layer Convolutional Neuronal Networks (CNN) followed by one fully connected layer and a readout-layer is chosen for stride detection. The advantage of Neural Networks, HMM, and regression-based systems is that they do not require a threshold.

In this proposal, we want to compare the most frequently used methods for stride detection, namely Min-Max Patterns (MMP), DTW, and CNN in order to be able to use the best variant of stride detection in daily life, independent of motor disorders.

9.2. Methods

In this section, we present three comparable methods Min-Max-Pattern (MMP), Dynamic Time Warping (DTW), and our method Convolutional Neural Networks (CNN). An overview of the different stride detection processes is shown Figure 9.1. This includes preprocessing, algorithms for stride detection, and the validation process.
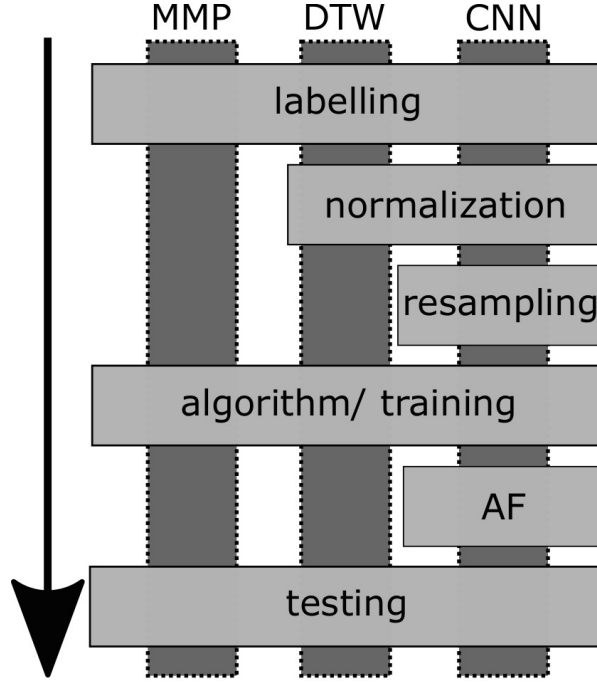

Figure 9.1.: Stride detection processes.

9.2.1. Preprocessing

Normalization

In order to enable the classifiers to work with uniform values, we normalize the data. For the normalization of the data, we use the Min-Max normalization. Thus our result vector has a value range from 0 to 1. The normalization is shown in equation 9.1, we calculate the normalization for every $x_i \ \forall \ i \in \{0, ..., N-1\}$ of the feature X. Where N is the length of feature X. Using the functions $min(X)$ and $max(X)$, which returns the absolute minimum and maximum of the feature X. The result is a normalized value $x_i^{norm} \in X^{norm}$ [Frochte2019]:

$$x_i^{norm} = \frac{x_i - min(X)}{max(X) - min(X)}. \tag{9.1}$$

Table 9.1.: Example of a distance matrix for selecting the ideal stride. The best choice is stride 1 with the minimum costs to all other strides.

	Stride 1	Stride 2	Stride 3	$\sum$
Stride 1	0	2	3	**5**
Stride 2	2	0	5	7
Stride 3	3	5	0	8

Resampling

After normalization, the individual signals are transformed to a uniform length of 100 values. This step is necessary because classifiers such as CNN always require the same tensors as input. For resampling, we use the Python library SciPy [Virtanen2019]. This method is based on Fast Fourier Transformation (FFT).

Ideal stride template

For the stride detection with the DTW, we need an ideal stride as a template. To estimate the ideal stride, we also use the DTW in combination with the labeled training data. Furthermore, we create a distance matrix $D_{stride}^{(M,N)}$, based on the costs for all strides to each other, where M is the number of rows and N the number of columns. The cost $D_{stride}^{(i,j)}$ is the distance between two strides by DTW. Then, we sum the costs of all columns for each row in vector $Cost_i$, as follows:

$$Cost_i = \sum_{j=0}^{N-1} D_{stride}^{(i,j)}, \forall\ i \in \{0, ..., M-1\}, j \in \{0, ..., N-1\}. \tag{9.2}$$

After that we choose the minimum of the vector $Cost$:

$$C_{ideal\_stride} = min(Cost_i) \forall\ i \in \{0, 1, ..., M-1\}. \tag{9.3}$$

This stride will be used as an ideal model for a stride. An example of our approach can be seen in table 9.1. In order to choose the ideal stride [Barth2015], we resampled the signals to a uniform length and averaged each index over all the strides.

9.2.2. Min-Max-Pattern

The simplest way to detect strides is to trace the MMP. This pattern is typical in human gait. However, this pattern also occurs in other motion sequences, for example climbing stairs. For this reason, this pattern is not an ideal choice [Barth2015]. Nevertheless, we have included the procedure for the sake of completeness.

The idea is that with a fixed window width, the time series is traversed over the y-axis of the orientation data. The index of the minimum and maximum within the window is for each window stored. We have set the window size to 90 values because this corresponds to 0.9 s, which is more than half duration of an average human stride. The
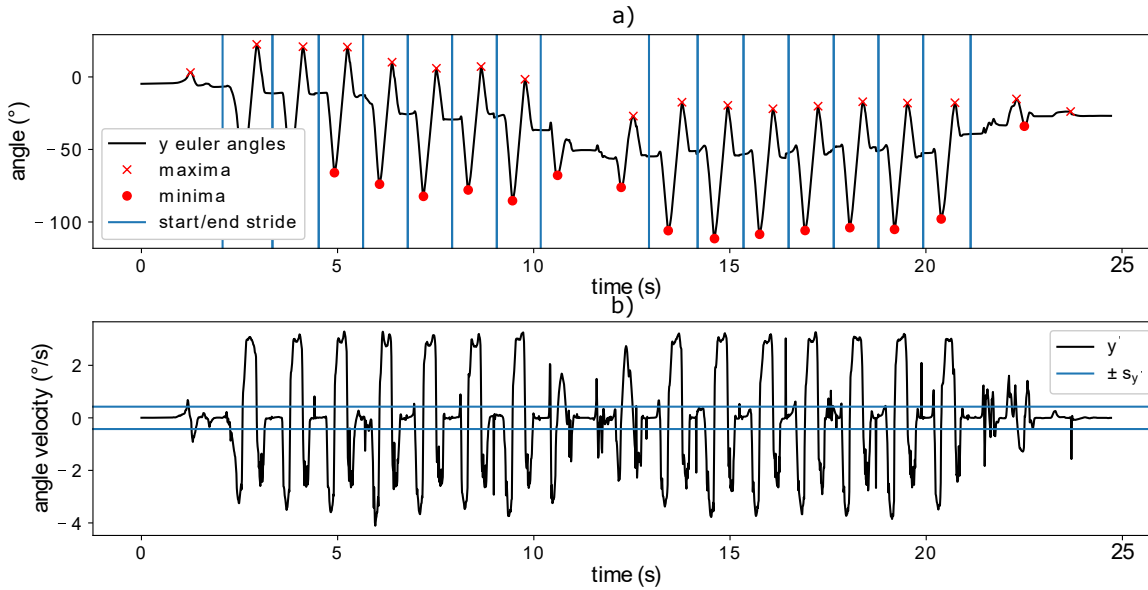
Figure 9.2.: Characteristics and results of the Min-Max-Pattern Recognition.

average duration is about 1.1 s with 110 values [Hausdorff1998]. Inside this window, all maxima and minima of a stride are expected to be included, without overlapping with a second stride.

The indices of all minima and maxima can then be displayed in a separate frequency table. All indices where the absolute frequency is higher than the average are potential strides. After that, a logical check is made, because each minimum must be followed by a maximum. Thus, ensures that minima and maxima are always present in pairs, see Figure 9.2 a). Next, the distance from each minimum to the corresponding maximum is determined. If this distance is outside the 90 % confidence interval of all strides used for training, it is assumed that it is not a stride. The 90 % confidence interval was chosen to remove extremely short or long steps. This confidence interval has proven to be useful in our tests.

We want to determine the corresponding stand phase for each MMP. In the standing phase, the angle change is almost zero. We form the derivation of the y-axis of the orientation data y' and calculate the standard deviation $s_{y'}$ of the y' sequence. Now, the ranges are selected between $y'_i > -s_{y'} \cdot 0.25$ and $y'_i < +s_{y'} \cdot 0.25$, see Figure 9.2 b). We have chosen the coefficient of 0.25 because we only look for areas close to zero. The person is standing phase is located in this area. Thus, we receive the areas of the standing phases. Finally, we select the mean index of the region within the standing phase between the MMP. This index indicates the start or end of a stride. We estimate the beginning of the first stride or the end of the last stride of a sequence of strides by the average length of the strides.
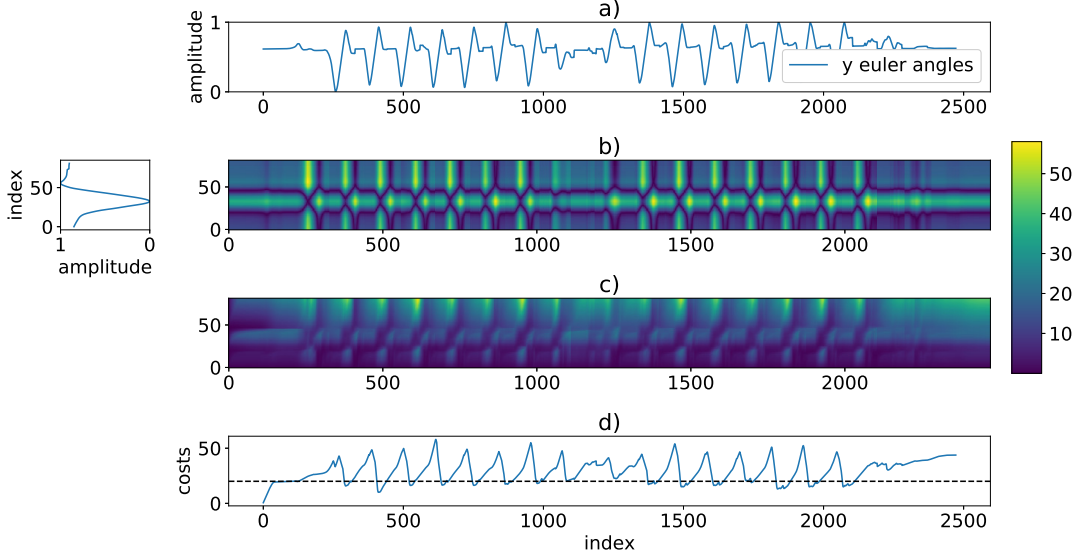
Figure 9.3.: DTW Algorithm between Ideal Stride and a test signal. a) raw y orientation signal; b) distance matrix between raw signal and template; c) accumulated distance matrix; d) Summed costs of the accumulated distance matrix.

9.2.3. Dynamic time warping

DTW is used to measure the similarity or distance of two signals based on the best path. The particular feature of the method is that the signals do not have to be the same length. In contrast, the Euclidean Distance always determines the distance between two points directly. For stride detection, we use the force, orientation, derivative orientation, and linear acceleration data. The DTW searches for the ideal path between two signals. The signals are first normalized before the algorithm for stride detection begins. Our algorithm is strongly based on the algorithm presented by Barth [Barth2015].

By using the ideal stride, see Section 9.2.1, we calculate the distance matrix $D(M, N)$ between the ideal stride and the test signal we want to analyze, see Figure 9.3, where M is the length of the ideal stride and N the length of the test signal.

Then, we calculate the Accumulated Cost Matrix $C(M, N)$. For this, we add the minimum costs from the distance matrix D. The lowest row of the matrix C results from the bottom row of the matrix D [Barth2015]:

$$C(0, n) = D(0, n) \ \forall \ n \in \{0, ..., N - 1\}. \tag{9.4}$$

The first column of the cost matrix C results from the sum of the previous element of matrix C and the current element of the matrix D as follows:

$$C(m, 0) = C(m - 1, 0) + D(m, 0) \ \forall \ m \in \{0, ..., M - 1\}. \tag{9.5}$$

All other elements of the cost matrix C are calculated from the minima of the neighborhood summed with the distance of the current element:
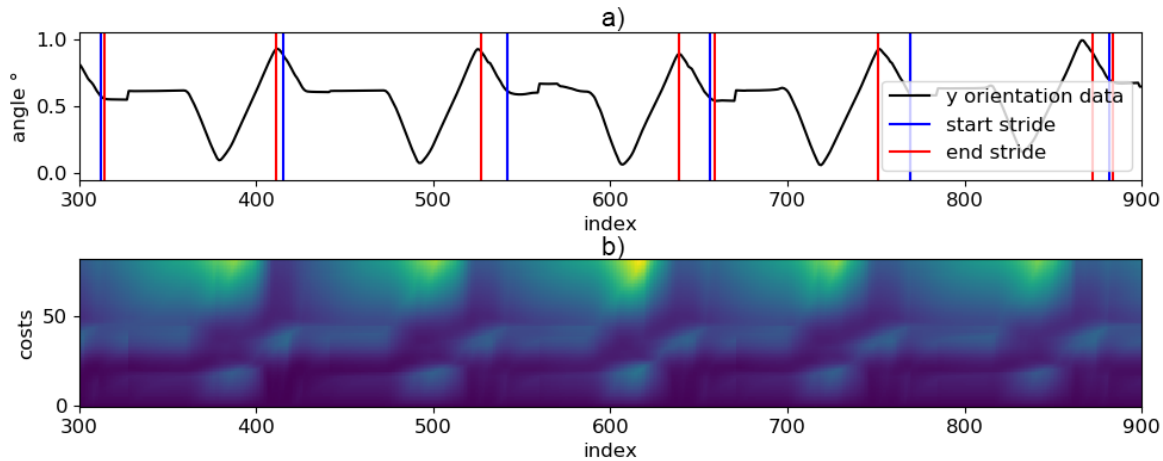
Figure 9.4.: Path between stride start and end.

$$C(m,n) = min(C(m-1,n), C(m-1,n-1), C(m,n-1)) + D(m,n)$$
$$\forall \; m \in 0, ..., M-1, n \in \{0, ..., N-1\}.$$

(9.6)

The result of the cost matrix C is shown in Figure 9.3 c).

As a result of the cost matrix, the summed costs are displayed in the last row, d). The first line of the cost matrix is in the last line of Figure 9.3. It can be seen in the last line of the figure. In the next step, a threshold value is selected to mark the end of a stride, see Figure 9.4 a). In our case, we chose the threshold of 17. A threshold value of 20, as recommended by Barth, was not useful in our case, as strides at the turn were often detected during the TUG test [Barth2015]. Finally, we follow the minimal path beginning at the end of the stride. Thus, we get the beginning of a stride, see Figure 9.4 a).

9.2.4. Convolutional neural network

CNNs are becoming more and more popular because they achieve significantly better results than traditional neural networks. Therefore, CNNs are used primarily for image recognition, but they are just as powerful at detecting signals. The difference between neural networks and CNNs is that CNNs learn local patterns. In contrast, traditional neural networks always use the entire input. The multilayer convolutional architecture allows us to increase the complexity of detection. Thus, it is possible to recognize in the first layer only patterns, and with the second or n-layer more and more complex objects [Abadi2016, Sze2017]. For our work with the CNNs we use the open-source python library Keras with TensorFlow [Chollet2015].

Preprocessing for CNN includes normalization and resampling, see Figure 9.5. Via resampling, all training data is resampled to a length of 100 values. For the classification with CNNs, we use a sequential network. As an activation function, we use the ReLU
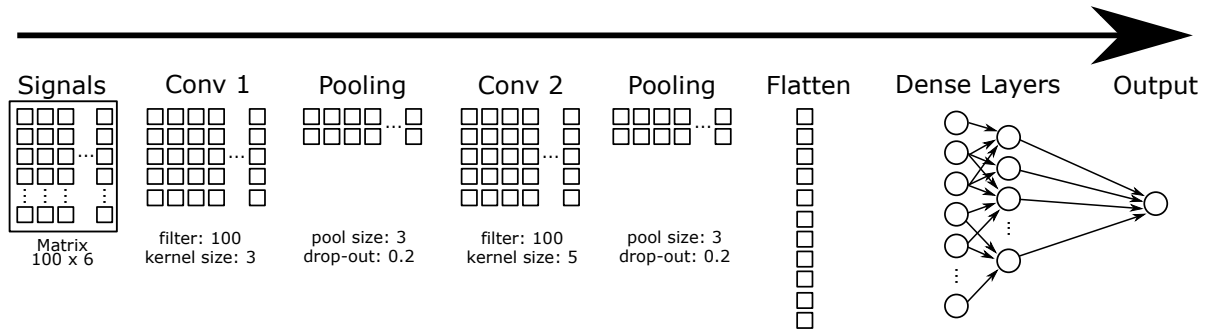
Figure 9.5.: Schema of the CNN layers.

function with except at the output layer, see equation 9.7, where x is the input. We use the sigmoid function at the output layer, see equation 9.8, because a ReLU function is not suitable. For the output layer, it is recommended to use a Sigmoid or Softmax function. The first one-dimensional convolutional layer creates 100 filters with a kernel size of three.

$$f(x) = max(0, x) \tag{9.7}$$

$$f(x) = \frac{1}{1 + e^{-x}} \tag{9.8}$$

To reduce the filters, we apply a max-pooling with a pool size of three and a drop-out with probability 0.2. After the second convolutional layer consists of 100 filters and a kernel size of five. This is followed by max-pooling again with a pool size of three. A drop-out follows this with probability 0.2, where single connections are randomly deleted [Srivastava2014]. After that, we have a flattening layer to adjust the dimensions for the neural network. Next, we have two dense layers. The first has 20 neurons and the second 30 neurons.

9.2.5. Automatic framing

In contrast to the MMP or DTW method, the CNN signals must have a uniform length. This uniform length is essential that the classifier always has the same inputs. In this case, we develop an algorithm, automatic framing (AF), that systematically cuts out small windows from our entire signal that the classifier can detect strides. The algorithm uses dynamic window sizes that even strides with different durations can be detected. The average duration of a stride is $1.1\,\mathrm{s} \pm 0.2\,\mathrm{s}$ [Hausdorff1998], which corresponds to 110 ± 20 values. Therefore, we use an average window size of 110 ± 30 values, so we capture all possible ranges. The window w can have the following sizes

$$w = \{80, 90, 100, 110, 120, 130, 140\}. \tag{9.9}$$

To increase performance, the algorithm always skips seven values when scanning the signal. Therefore, not every single increment is classified seven times. If the classifier

within a window detects a stride with a probability more than 70 %, the stride is stored in a list with start index, end index and probability of the stride. A recognition probability of 70 % is very low. In a later step, we select the stride with the highest probability. This deletes unnecessary strides. Based on the first detected stride, overlaps up to a maximum of

$$overlapping = detected\ stride + (average\ stride \cdot 0.8) \qquad (9.10)$$

is saved. The factor of 0.8 was selected so that a broad range is available for stride detection. Thus, a tolerance is given if a classification error has been made based on the average step duration [Hausdorff1998].

Because many strides represent the same stride by overlapping, we need to select the best fitting stride. For this reason, we choose the area from the first detected stride to the end of the overlap. Then, we select from this range this stride with the highest probability of being a stride. This stride is then defined as a valid stride. An example of the result is shown in Figure 9.6. To check the results of the algorithm, we use two test procedures. With the first method, we use the labeled data and for the second method, we use the original signals. Here we always mark the absolute minimum within one step ± 10 ms. If the predicted stride lies within this range, it is marked as a correct detected stride [Barth2015].

9.3. Results

In this section, we would like to present our results, which were achieved by using the data sets daily life and TUG test by using the presented methods.

9.3.1. Measured using IMU sensors

We do not use any force sensors to train the daily life data sets because the TUG test data set was made with an older version of the insole, see Chapter 4.4. Therefore, the data is comparable. Table 9.2 shows the results of the daily life data set. The MMP, DTW algorithm, and AF+CNN classification were compared. For the test, the complete time series were used. The sensitivity shows that the MMP and Automatic Framing and Convolutional Neuronal Networks (AF+CNN) algorithms perform best. The DTW algorithm performs comparatively well. Therefore, it can be assumed that the DTW algorithm does not always detect strides correctly. In contrast, the MMP and AF+CNN algorithms detect strides very well. The DTW algorithm has the highest specificity, followed by the AF+CNN algorithm. The MMP algorithm performs worse than all others. From this, it can be assumed that the DTW and AF+CNN algorithms detect other activities for example standing or going stairs well as no strides. However, the MMP algorithm has big problems with this. This result is identical to Barth's results [Barth2015]. With F1-Score and accuracy, the AF+CNN algorithm performs best, closely followed by the DTW algorithm. For this reason, we would recommend the AF+CNN algorithm for stride detection.
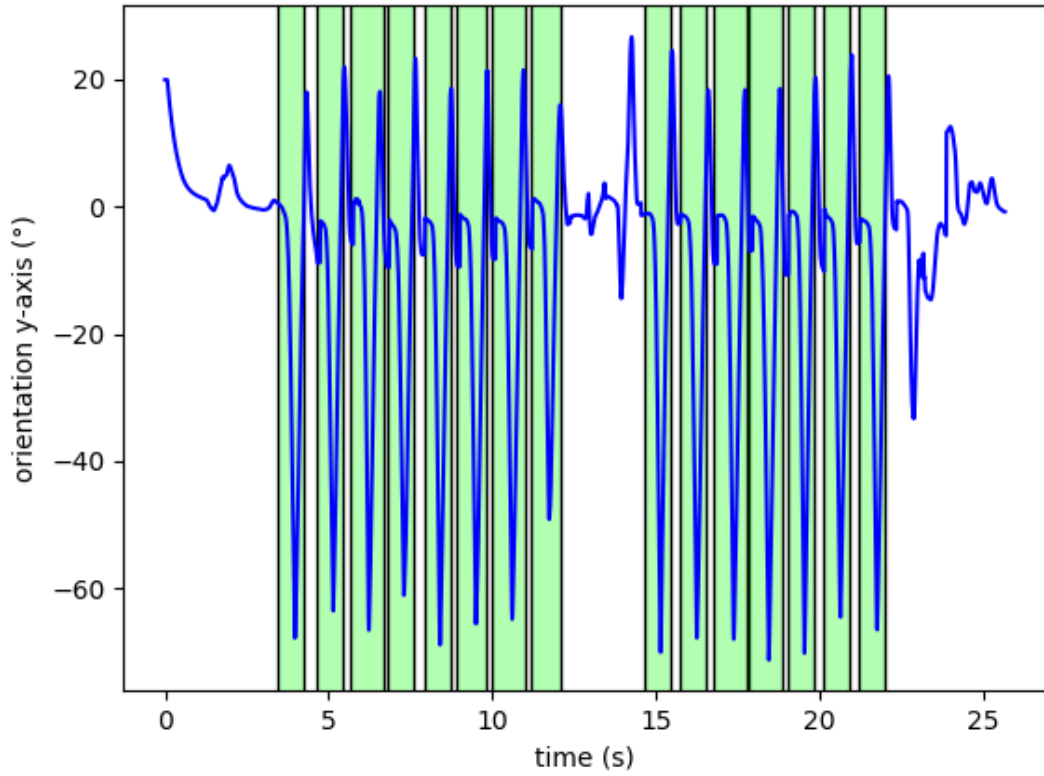
Figure 9.6.: Stride detection by CNN.

Table 9.2.: Daily life activities 1 with IMU sensors.

	Sensitivity	Specificity	Precision	F1-Score	Accuracy
MMP	0.990	0.771	0.658	0.791	0.838
DTW	0.896	**0.986**	**0.969**	0.931	0.956
AF+CNN	**0.992**	0.940	0.901	**0.944**	**0.958**

Table 9.3.: Daily life activities 2 with labeled data.

	Sensitivity	Secificity	Precision	F1-Score	Accuracy
AF+CNN (IMU)	0.978	0.994	0.978	0.974	0.988
AF+CNN (IMU+FSR)	**1.0**	**1.0**	**1.0**	**1.0**	**1.0**

Table 9.4.: Results of the data set TUG test with IMU sensors.

Data set	Group	Sensitivity	Specificity	Precision	F1-Score	Accuracy
MMP	PD	0.838	**0.895**	**0.925**	0.879	0.86
	no PD	0.844	0.778	0.871	0.857	0.820
DTW	PD	0.615	0.852	0.875	0.723	0.703
	no PD	0.663	**0.844**	0.887	0.759	0.727
AF+CNN	PD	**0.983**	0.812	0.899	**0.939**	**0.920**
	no PD	**0.968**	0.818	**0.91**	**0.938**	**0.916**

9.3.2. Measured using IMU and force sensores

These results show the improvement in the classification achieved when additional force sensors are used. The force sensors have been reduced to three different measuring points. For this purpose, we have calculated the average value of heel, metatarsus, and ball of the foot, as already described in Section 4.6. Table 9.3 shows a comparison of the AF+CNN method with and without force sensors. It is clear to see that the classification result for our test data was utterly correct. With the addition of force sensors, the gain in information increased significantly. This result can be related to the small data set of individuals tested, and all did not have motor dysfunctions.

9.3.3. Timed Up and Go test

The classifiers were not trained again during the test of the TUG test data set. We used the models from Section 9.3.1, in oder to show how independent they are of motor dysfunction or other appearance. Besides, the test took place in a completely different environment. The results were grouped by the classifier and whether a subject has Parkinson's disease or not, see Table 9.4.

The AF+CNN algorithm shows the best results for Parkinson disease (PD) and no Parkinson disease (no PD) at F1-Score and accuracy. From this, it can be concluded that the algorithm reacts well to changed data and is therefore very robust. However, it has a relatively weak specificity value because the AF+CNN algorithm wrongly counted other activities as a stride. The DTW algorithm scored worst in this test. This can be explained by the fact that the threshold was not optimized for the data. The algorithm can, therefore, react poorly to new data. This demonstrates the weakness of a fixed threshold in the algorithm. The same also applies to the MMP algorithm.

10

Calculation of stride features

The stride detection, which was presented in the last chapter, is the fundamental basis for estimate gait features of the gait cycle in this chapter. The calculation of different gait features has already been demonstrated in other works because this is an essential part of the gait analysis. The features allow the training of classifiers and help the physician during diagnosis. A fundamental requirement for this is that the data are valid. With the right choice of a classifier, such as a decision tree, the classification result is also easy to understand. This is a significant prerequisite for accepting a classifier for diagnostic support.

10.1. Related works

The features of the human gait can be divided into a time and space domain. Temporal gait parameters are the duration of different gait phases, such as the duration of gait cycle, stance phase, or swing phase. Spatial related gait parameters are stride length or stride height. There are different approaches to determine these features.

In order to calculate the duration of the swing phase and stance phase, the time of heel strike and toe off have to estimated. There are numerous approaches for this. Force sensors can be used with a fixed threshold value [Bamberg2008]. An other method is to calculate the velocity of the foot. If this velocity drops below a threshold value, the foot is in the stand phase, otherwise in the swing phase [Bamberg2008, Tunca2017]. Furthermore, the heel strike and toe off can be estimated from the minima and maxima of the acceleration and gyroscope data [Rampp2014, Salarian2004, Ferster2015, Wang2015, Hsu2014]. For the estimation of the stride length, the gyroscope and acceleration data are used to calculate the horizontal movement in the sensor's space by double integration [Bamberg2008, Rampp2014, Tunca2017, Sijobert2015, Mariani2010, Ferrari2015, Salarian2004, Ferster2015, Wang2015, Hsu2014]. The same procedure is used to calculate the stride height in the vertical [Mariani2010].
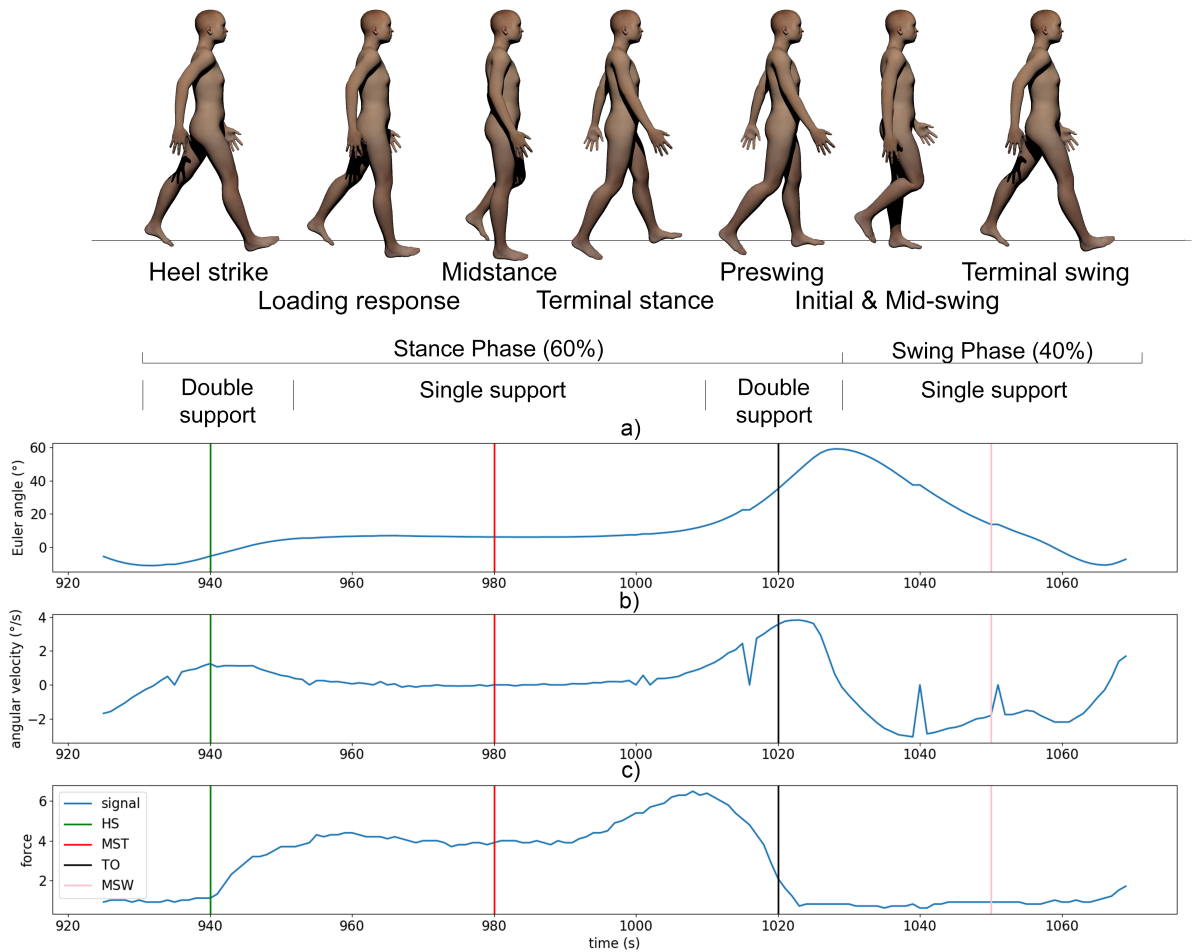
Figure 10.1.: Gait cycle with gait phases (HS, MST, TO, MSW), and signals of orientation data, angular velocity and force data.

10.2. Methods

10.2.1. Gait time features

For the calculation of the gait times, the times of Heel strike (HS), Toe off/ Terminal stance (TO), Mid-swing (MSW), and Midstance (MST) were estimated. A combination of orientation, angular velocity, and force data was used because each signal provides relevant information for particular gait features, see Figure 10.1.

Heel strike The HS is detected by the force sensors on the heel crossing a threshold value, Figure 10.1 c). The local minimum in the sagittal plane of the angular velocity between swing and stance phases is used to estimate the HS.

Toe off/ Terminal stance   The TO also detects the force sensors. If the force sensors on the toe cross a threshold, this is the TO, Figure 10.1 c). The angular velocity is also used to estimate the TO. The local minimum between stance and swing phase also indicates the TO. Furthermore, it is also possible to use the angular velocity data. In this case, the maximum corresponds to the TO, Figure 10.1 b).

Midstance   For the identification of the MST, the sum of all force sensors can be used. Within the stand phase, there is a local minimum between the two maxima, Figure 10.1 c). This characterizes the MST.

Mid-swing   The MSW can be estimated by calculating the average of HS and TO. Another possibility is to select a threshold value for zero Euler angle, or angluar velocity, Figure 10.1 a) and b).

Stance phase   The stance phase is calculated by calculating the difference between TO_i and HS_i.

Stand phase   The swing phase is calculated from the difference between HS_{i+1} and TO_i.

10.2.2. Spatial gait features

Basically, the calculation of the stride length follows the same principles as other works have shown before. But in contrast to the other works, the Bosch BNO055 provides orientation data and linear acceleration. For this reason, it is not necessary to subtract the gravity to get the linear acceleration. The orientation data are the result of the integration of the angular velocities. In addition, the orientation data is optimized by sensor fusion. The calculation for the stride length is based on the equations by Sijobert [Sijobert2015], but we use different signals, so we have adapted them.

The time of the MST is used as the starting point for calculating the stride length and height. Because of sensor drift and sensor inaccuracy, these are calculated at the beginning of the calculation minus the start value for the orientation data Θ and acceleration a, see equations 10.1 and 10.2. In order to calculate the step length and step height, we project the 3D signals onto a 2D space of the sagittal plane. For this reason, we use the y-axis of the orientation data as Θ and the x-axis and z-axis of the linear acceleration for the calculation.

$$\Theta_i = \Theta_i \Theta_0 \tag{10.1}$$
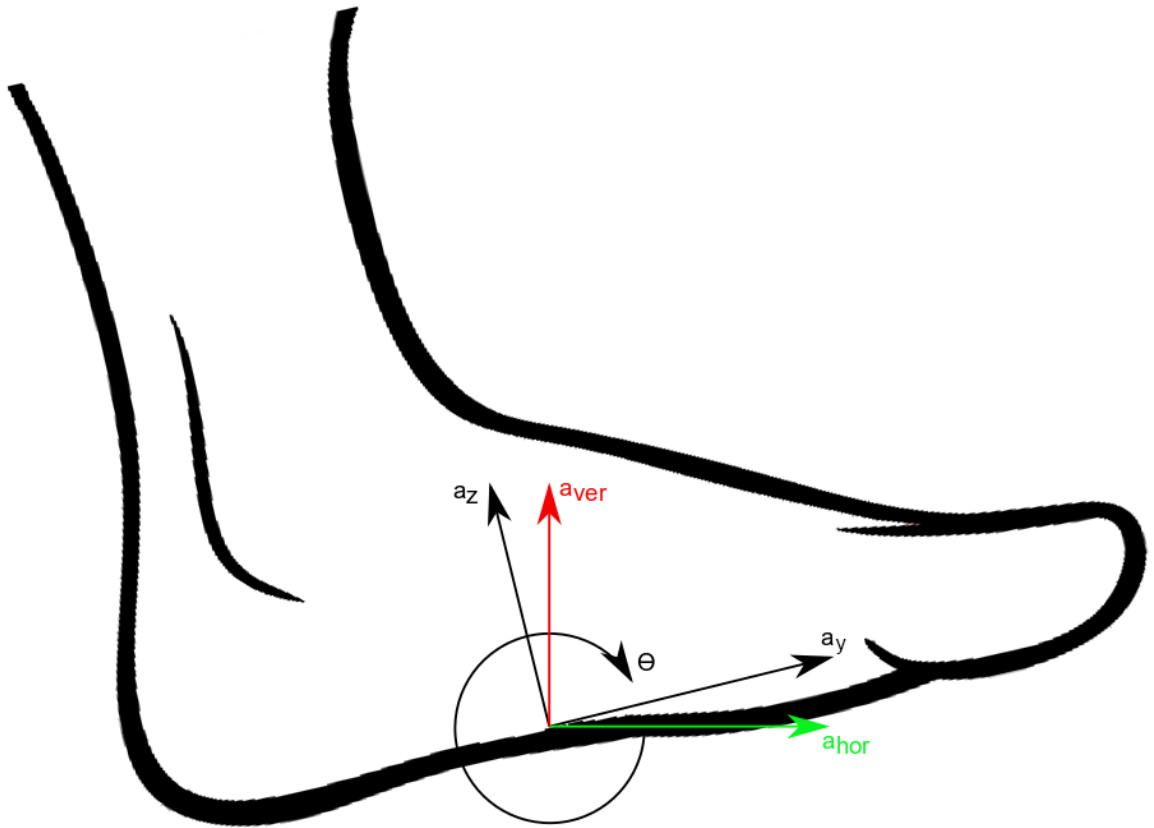
$$a_i = a_i a_0 \tag{10.2}$$

Figure 10.2.: Sensor axes for calculation of horizontal a_{hor} and vertical a_{ver} acceleration.

Stride length   The horizontal acceleration is calculated by

$$a^{hor} = cos(\Theta_i) \cdot a_i^y - sin(\Theta_i) \cdot a_i^z. \tag{10.3}$$

Next, the horizontal acceleration is integrated to obtain the horizontal velocity

$$v^{hor} = \int a_i^{hor} di. \tag{10.4}$$

To obtain the horizontal distance, the horizontal velocity has to be integrated

$$s^{hor} = \int v_i^{hor} di. \tag{10.5}$$

Stride height   The vertical velocity is calculated by

$$a^{ver} = cos(\Theta_i) \cdot a_i^z - sin(\Theta_i) \cdot a_i^y. \tag{10.6}$$

Next, the vertical acceleration has to be integrated to obtain the vertical velocity

$$v^{ver} = \int a_i^{ver} di. \tag{10.7}$$

To obtain the vertical distance, the vertical velocity has to be integrated

$$s^{ver} = \int v_i^{ver} di. \tag{10.8}$$

10.3. Results

The calculated gait features were first tested for variance homogeneity and normal distribution. In both cases, the p-value was less than 0.05. For this reason, the data are not variance homogeneous and normal distributed. A possible reason for the data not being normally distributed could be related to the small sample size. For this reason, the Wilcoxon signed-rank test was applied with a p-value of 0.05. In the statistical analysis, the left and right leg were separated. The results are shown in Tables 10.1 and 10.2. In these tables, the stride duration, stance phase duration, swing phase duration, stride length, and stride height were presented and separated into the groups control Group (CG) and Parkinson's disease (PD) with average and standard deviation. In the last column, the p-value is shown. It is noticeable that there are significant differences between CG and PD in stride duration, stance phase duration, and stride length. No significant differences were found for swing phase duration and stride height [Ngokingha2018].

Table 10.1.: Average and standard deviation of gait features of the right foot. It is split into control group (CG) and Parkinson's disease (PD) groups. The last column shows the p-value of the Wilcoxon signed-rank test.

Gait feature	CG	PD	p-value
Stride duration (s)	1.028 ± 0.087	1.087 ± 0.087	0.017
Stance phase duration (s)	0.581 ± 0.065	0.647 ± 0.066	$2.0e-04$
Swing phase duration (s)	0.447 ± 0.043	0.440 ± 0.038	0.976
Stride length (m)	1.149 ± 0.248	0.880 ± 0.221	$5.5e-06$
Stride height (m)	0.231 ± 0.120	0.250 ± 0.148	0.445

Table 10.2.: Average and standard deviation of gait features of the left foot. It is split into control group (CG) and Parkinson's disease (PD) groups. The last column shows the p-value of the Wilcoxon signed-rank test.

Gait feature	CG	PD	p-value
Stride duration (s)	1.046 ± 0.089	1.106 ± 0.085	0.013
Stance phase duration (s)	0.587 ± 0.064	0.648 ± 0.109	$4.0e-4$
Swing phase duration (s)	0.458 ± 0.044	0.459 ± 0.042	0.354
Stride length (m)	1.311 ± 0.226	0.981 ± 0.261	$4.2e-07$
Stride height (m)	0.149 ± 0.096	0.170 ± 0.078	0.229

11

Gait symmetry

The previously Chapters 8 - Synchronisation, 9 - Stride detection, and 10 - Calculation of stride features are the fundamental for this Chapter 11 - Gait symmetry. All these gained information are now used to calculate the symmetry of the legs. This allows us to compare symmetry based on discrete features with our own developed method to estimate the symmetry.

A symmetrical gait represents a high quality of life because all parts of the body must be in balance during gait. If regions of the body show motor dysfunctions, this leads to an asymmetrical gait pattern. The gait pattern reflects the general health [Lord2013], quality of life [Hirvensalo2000], cognitive disorders [Verghese2007], and the risk of falling [Beauchet2009]. The problem is currently used methods is that all these methods are based on the ratio of discrete gait features. We want to introduce a new way to calculate symmetry for wearable devices. Our method's outstanding feature is that the complete time series of the gait cycle is used for the symmetry analysis. This calculates the symmetry more accurately than using discrete based methods for symmetry calculation. An essential part of the method is the Dynamic time warping (DTW) [Keogh2005].

11.1. Related works

The situation is different when wearables assess diseases related to movement disorders. In this case, IMU sensors are attached to specific joints or integrated into clothing. To measure and store the time series of gait wearable containing microcontrollers in combination with IMU sensors are often used [Barth2015, Bobic2018, Tao2018, Koroglu2018, Hannink2018, Watanabe2018, Clemens2019, Crenshaw2006, Mancini2011, Anwary2018b, Anwary2018a, Anwary2018c, Steinmetzer2018]. In most cases, the motion of the lower extremities is measured [Barth2015, Bobic2018, Tao2018, Koroglu2018, Hannink2018, Watanabe2018, Steinmetzer2018]. Thereby conclusions can be made about the stride length, cadence, stride duration, gait phases, and symmetry [Barth2015, Hannink2018, Watanabe2018, Jiang2018].

The symmetry of arms and legs, as well as the symmetry of the upper and lower limbs with each other, investigate only a few papers [Lin2018b, Miller2018, Viteckova2016]. Changes of interlimb coordination in individuals with Parkinson's disease and healthy older adults while systematically manipulating walking speed are compared to determine the impact of Parkinson's disease symptoms on interlimb coordination [Lin2018b]. Markers were placed on the foot, heel, ankle, knee, hip, thigh, wrist, elbow, shoulder, and head.

A point estimate of the relative phase between body segments was calculated by using the moment at which the positive maxima were reached for the angle of each body segment. To assess change in asymmetry over time is the objective in [Miller2018]. The changes in movements are assessed by a single neurologist specializing in movement disorders. A robust ordinal logistic regression model that includes a control for clustering due to repeated observations within-person for evaluating the relative change in asymmetry is used.

Another system focuses on the study of the impact of PD on synkinesias (for example the symmetry of movement) during walking, and the effect of medication on the gait symmetry [Viteckova2016]. Every patient was tested and measured using IMU sensors in his on and off state. The trend symmetry value is calculated as a ratio of the variabilities of two eigenvectors, which are calculated from the kinematic motion data of the left and right limb. An up-to-date overview of symmetry analysis systems for movements is shown in [Viteckova2018]. For this reason, the use of synchronous signals to determine symmetry is very essential.

There are different methods for the calculation of symmetry. One approach is that different calculated features like step length, step duration, standing time, or swing time of the legs are put into relation [Loiret2019, Anwary2018b, Clemens2019]. The disadvantage of this method is that only average values of the calculated characteristics for the gait can be assessed, but not the entire time series. This is different for stationary systems, which are camera-based. With these systems, the complete body can be recorded synchronously [Crenshaw2006]. Both types of symmetry evaluation are useful. However, in our opinion, a direct comparison of the time series is most useful, because differences in the related arms and strides can be measured directly.

11.2. Methods

Discrete symmetry calculation by using various parameters is used for analysis gait with wearable devices. For comparison with our method, we introduce the methods Ratio index (RI), Symmetry index (SI), Gait asymmetry (GA), and Symmetry angle (SA), see equations 11.1 to 11.4. For the calculation of discrete symmetry, we use several features of the right and left foot. The smaller feature is x_{min}, and the bigger one x_{max}. In this way, we get a value between zero and one. X_i^{min} and X_i^{max} are, features consisting of swing phase duration, stand phase duration, and stride duration. X_i^{min} is the smaller value of feature i from the left and right stride. X_i^{max} is the larger value of feature i in the left and right stride. The advantage of the Symmetry angle over the other discrete symmetry calculations is that it does not matter which value is in the numerator and denominator.

Ratio Index To determine the RI, the smaller values of the feature i is divided by the higher one

$$RI = \frac{X_i^{min}}{X_i^{max}}. \tag{11.1}$$

Symmetry Index   The SI gives the difference between kinematic and kinetic parameters of the limbs. We have adjusted the value so that one represents a symmetrical gait and zero asymmetry

$$SI = 1 - \frac{|X_i^{min} - X_i^{max}|}{0.5 \cdot (X_i^{min} + X_i^{max})}. \tag{11.2}$$

Gait Asymmetry   The GA is similar to the Ratio Index. However, the logarithm was still calculated from the result

$$GA = 1 - ln\left(\frac{X_i^{max}}{X_i^{min}}\right). \tag{11.3}$$

Symmery Angle   The SA measures the relationship between two different limbs. Two exactly symmetrical parameters form an angle of $45\,°$. We have corrected the value, a symmetric value is again one and an asymmetric zero

$$SA = 1 - \frac{45° - arctan\frac{X_i^{min}}{X_i^{max}}}{90°}. \tag{11.4}$$

11.2.1. Normalized Dynamic Time Warping symmetry ratio

The focus of this chapter is not on stride detection. For this reason, a simple method is used because we have only force data. As soon as the sum of all force sensors is greater or equal to 100 N, this is considered the beginning of the stance phase. Conversely, swing phases are detected as soon as the sum of all force sensors is less than 100 N, see Figure 11.1.

The significant gaps in Figure 11.2 corresponds to the turning of the person at the end of the corridor. By using the interquartile range (IQR), the gaps are cut out. Usually, there are four to five such gaps per recording.

11.2.2. Preprocessing

Typically the DTW is used as a distance measurement. As higher the result is, as higher is the distance between the two signals. The more asymmetrical is the gait cycle. To better interpret the results of the symmetry, we normalize them. A value close to one shows a symmetrical motion and a value close to zero an asymmetrical motion. In order to be able to calculate the symmetry of the strides, the values would first have to be standardized and normalized. For standardization, we use the z-transformation, see
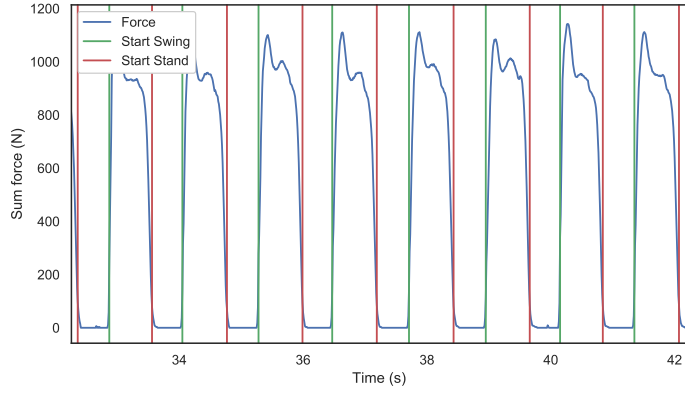
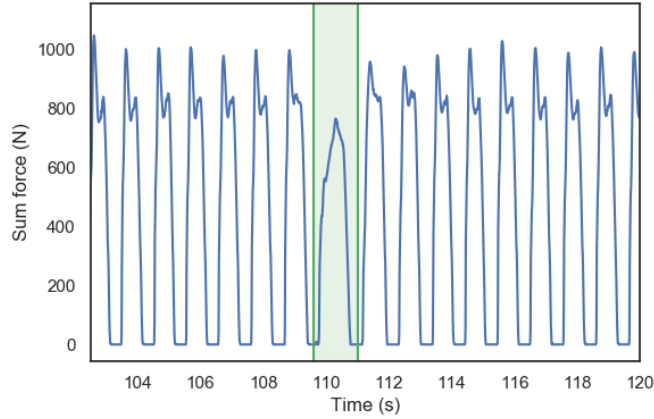Figure 11.1.: Force signal of gait with start and end of the stance and swing phases.

Figure 11.2.: Force signal of gait with gaps at the turning point.

equation 11.5. Through this standardization, the expected value of the data is $\bar{x} = 0$ and the standard deviation $s = 1$.

$$x_i^{std} = \frac{x_i - \bar{x}}{s}. \tag{11.5}$$

The time series of all records of all subjects are concatenated to form a uniform model for standardization and normalization. A min-max normalization is performed to ensure the value range between zero and one:

$$x_i^{norm} = \frac{x_i^{std} - min(X^{std})}{max(X^{std}) - min(X^{std})}. \tag{11.6}$$

11.2.3. Normalized Dynamic Time Warping

To measure the symmetry distance between the time series (strides) of the right and left foot, we use the DTW. DTW has become very well established in the analysis of time

series. In contrast to Euclidean distance, this method can compensate for time warping. This flexibility is a popular method for the analysis of time series in medicine, science, and industry. The idea with DTW is that not the distance of two indices is calculated, but the distance to the most fitting one. Thus allows comparing time series with each other if they recorded with different duration or frequency.

In the first step, the algorithm calculates distances between the time series $(x_i)_{1 \leq i \leq n}$ (force of the right foot) of length n and $(y_j)_{1 \leq j \leq m}$ (force of the left foot) of length m, resulting in a n times m matrix $D = D_{ij}$ containing distances D_{ij} between y_j and x_i. The distances within the matrix are calculated by the sum of the current distance and the minimum distance of a previous neighboring element [Keogh2005]:

$$D_{ij}^{norm} = dist(x_i, y_i) + min\{D_{i-1,j}, D_{i-1,j-1}, D_{i,j-1}\}. \tag{11.7}$$

A distance D_{ij} of zero means 100 % symmetry of the measured values. The higher the value D_{ij}, the lower is the symmetry of the limbs:

$$dist(x_i, y_i) = \frac{\sqrt{(x_i - y_j)^2}}{max(\{length(X), length(Y)\})}. \tag{11.8}$$

In order to get a result of one for symmetry and zero for asymmetry, the one minus result has to be calculated:

$$DTW_{ratio} = 1 - DTW_{n,m}^{norm}. \tag{11.9}$$

11.3. Results

11.3.1. Data set

In Table 11.1 the results of the data set from Chapter 5.4 are shown. The results were divided into the studies Galit, Hausdorff, Silvi, and total. Within these studies, the study subjects were separated according to the control group (CO) and Parkinson's disease (PD). It is noticeable that the results of the discrete symmetry calculation are similar to the DTW. Parkinson's disease groups in the studies show a higher asymmetry [Yogev2005, Hausdorff2007, Frenkel2005]. We have calculated the average value $\bar{x}$ and the standard deviation s.

11.3.2. Theoretical cases

In this section, we compare the results of the discrete methods and the DTW for the two feet of the theoretical signals. Figure 11.3 the path of the DTW from the signals are shown:

(a) Regular stride,

(b) Identical strides,

Table 11.1.: Results of the data set Galit (Ga), Hausdorff (Ju), Silvi (Si), and total for features Ratio index (RI), Symmetry index (SI), Gait asymmetry (GA), Symmetry angle (SA), and Normalized dynamic time warping symmetry (NDTWS).

Study	RI $\bar{x} \pm s$	SI $\bar{x} \pm s$	GA $\bar{x} \pm s$	SA $\bar{x} \pm s$	NDTWS $\bar{x} \pm s$
Gal CO	0.947 ± 0.028	0.938 ± 0.044	0.929 ± 0.068	0.981 ± 0.012	0.952 ± 0.020
Gal PD	0.942 ± 0.026	0.934 ± 0.033	0.931 ± 0.036	0.979 ± 0.010	0.960 ± 0.017
Hau CO	0.963 ± 0.008	0.960 ± 0.009	0.959 ± 0.010	0.987 ± 0.003	0.957 ± 0.017
Hau PD	0.953 ± 0.016	0.948 ± 0.019	0.947 ± 0.022	0.984 ± 0.006	0.955 ± 0.017
Sil CO	0.968 ± 0.025	0.964 ± 0.040	0.959 ± 0.062	0.989 ± 0.011	0.959 ± 0.018
Sil PD	0.941 ± 0.039	0.929 ± 0.062	0.919 ± 0.096	0.978 ± 0.017	0.954 ± 0.019
All CO	0.955 ± 0.016	0.949 ± 0.021	0.947 ± 0.025	0.984 ± 0.006	0.960 ± 0.018
Total PD	0.949 ± 0.027	0.942 ± 0.039	0.938 ± 0.055	0.982 ± 0.011	0.960 ± 0.016

(c) Amplitude shifted strides,

(d) Uniform amplitude shifted,

(e) Heel strike and toe off with same force on left foot, right foot fewer force, and

(f) Left foot has heel strike more force then toe off, right foot has toe off more force then heel strike.

The results for these signals are shown in Table 11.2. It can be seen that the discrete methods cannot correctly calculate the signals (c), (d), (e), and (f).

Table 11.2.: Results of the theoretical cases.

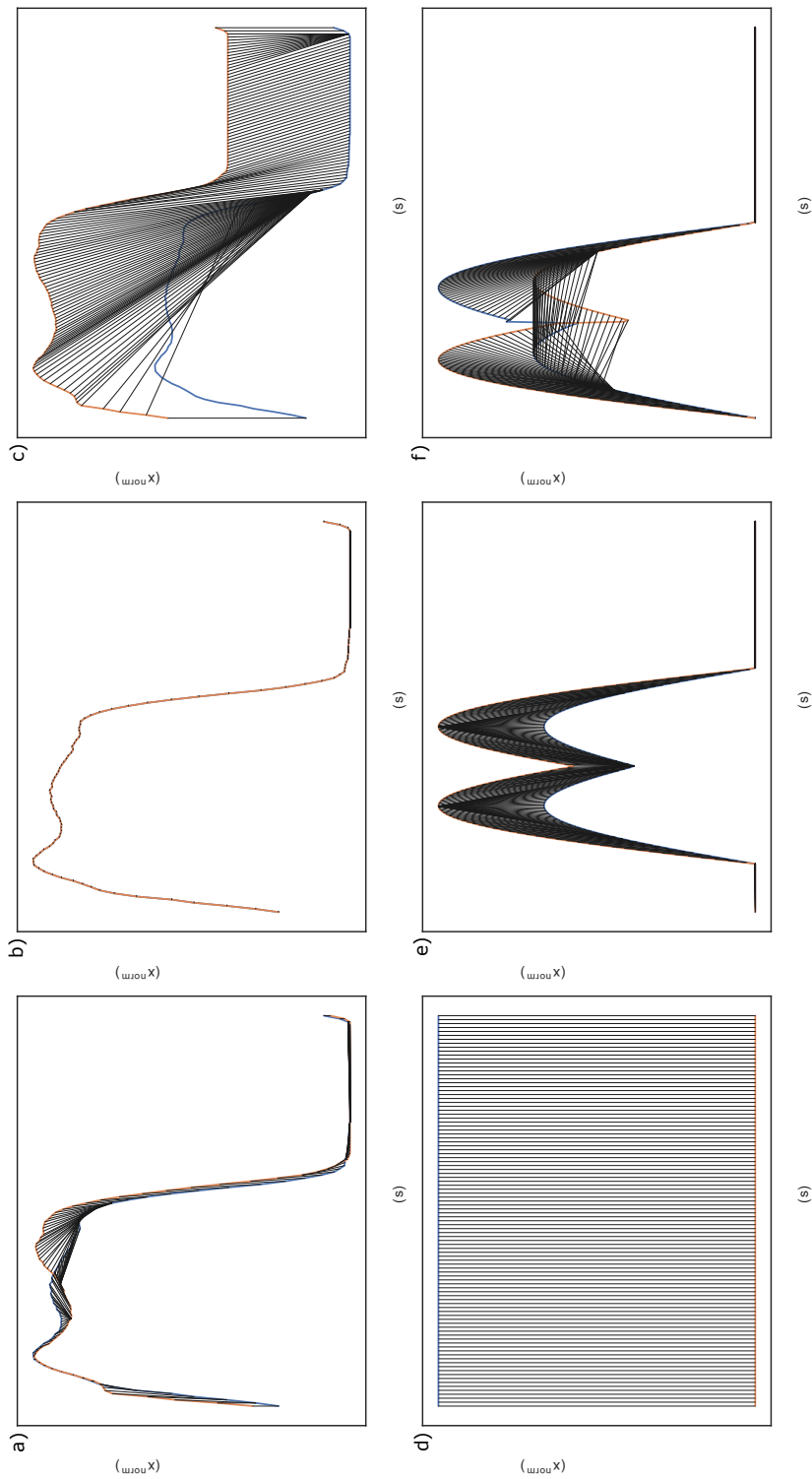| Signal	RI	SI	GA	SA	NDTWS
a	0.978	0.978	0.993	0.978	0.99
b	1.0	1.0	1.0	1.0	1.0
c	0.978	0.978	0.993	0.978	0.78
d	—	—	—	—	0.01
e	1.0	1.0	1.0	1.0	0.92
f	1.0	1.0	1.0	1.0	0.98

Figure 11.3.: Results of the DTW symmetry. (a) regular stride time series; (b) identical stride of right and left foot; (c) amplified, shifted strides; (d) uniform amplitude shifted; (e) heel strike and toe off with same force on left foot, right foot fewer force; (f) left foot has heel strike more force then toe off, right foot has toe off more force then heel strike.

12

Classification of motor dysfunctions in arm swing

Most of the research on gait analysis deals with the analysis of leg motion [Mazumder2018a, Jasni2019, Stoelben2019, Balzer2018, Prakash2019, Steinmetzer2018, Steinmetzer2019a]. However, the analysis of the arm movement is also important for the assessment of a gait disorder. Stationary systems that use cameras or ultrasound [Ospina2018, Spasojevic2015] [Baron2018, Lewek2010, Tsipouras2012, Castano2018, Dranca2018, Castano2019] [Roggendorf2012] but only a few mobile systems with inertial sensors [Huang2012, Bertomeu2015, Viteckova2016] are used to measure the arm swing. Therefore, this chapter explains how to classify motor dysfunctions in arm swing.

12.1. Reletaed works

By [Ospina2018], the arm swings of Parkinson's patients and healthy persons with the help of a Kinect camera were compared. Significant differences in amplitude and speed were observed. The arm movements of Parkinson's patients also often showed asymmetry. The Parkinson's disease group showed significant reductions in arm swing magnitude (left, $p = 0.002$; right, $p = 0.006$) and arm swing speed (left, $p = 0.002$; right, $p = 0.004$) and significantly greater arm swing asymmetry ($p < 0.001$). An accuracy of more than 90 % in distinguishing healthy people from persons with Parkinson's disease was also achieved using a Kinect camera by [Spasojevic2015]. Classification between healthy and non-healthy subjects is performed based on the five most relevant features and the two newly obtained features from linear discriminant analysis, using four different classifiers, support vector machine, multilayer perceptron, the radial basis neural network, and k nearest neighbor. Using the motion capture system Motek CAREN by [Baron2018], it was detected that Parkinson's patients have a different jerk and arm swing length compared to healthy people. The fact that Parkinson's patients in the early stages have a larger arm swing asymmetry could be confirmed by [Lewek2010] with the Vicon and the Baton Rouge motion lab system. The p-value for distinguishing healthy individuals from individuals with Parkinson's disease was 0.003. A Kinect system was used by [Castano2018] to detect the differences in speed, amplitude, and symmetry in arm movement between healthy people and people in the early stages of Parkinson's disease. By [Dranca2018], it was investigated which model method provided the best results when using a Kinect to detect Parkinson's disease stages.

The best results with an accuracy of 93.4 % were obtained with a special Bayesian network classifier using 10-fold cross-validation. The relevant features were related to left shin angles, left humerus angles, frontal and lateral bends, left forearm angles, and the number of steps during a spin. For the recordings by [Castano2019], a Kinect system was used in combination with an e-Motion capture program. The proposed system classifies PD into three different stages related to the freezing of gait. An accuracy of 93.4 % was reached using the features of the movement and position of the left arm, the trunk position for slightly displaced walking sequences, and the left shin angle for straight walking sequences. However, they obtained a better accuracy of 96.23 % for a classifier that only used features extracted from slightly displaced walking steps and spin walking steps.

By [Tsipouras2012], an automatic method for the treatment of levodopa-induced dyskinesia was developed. Gyroscopes were used on the abdomen and chest and the abdomen, chest, wrists, and ankles. In general, an average detection rate of 90 % for Parkinson's patients was achieved, and the average detection rate and the precision of the individual classes were 80 % and 77 %, respectively. Several classification techniques have been used for levodopa-induceddyskinesia assessment, including the naive Bayes classifier, k nearest neighbor, fuzzy lattice reasoning, decision trees, random forests, and neural networks using a multilayer perceptron.

The method used by [Roggendorf2012] consisted of guiding patients with early Parkinson's on a treadmill and measuring their movements with an ultrasound device on each side. The results were a reduced arm swing amplitude in the patients and a longer stride length compared to healthy people.

By [Huang2012], a sensor unit was used on each forearm. This sensor unit consisted of two triaxial G-Link accelerometers that were attached to an aluminum bar. Arm swing asymmetry, maximal cross-correlation, and instantaneous relative phase of bilateral arm swing were compared between PD and controls. PD subjects demonstrated significantly higher arm swing asymmetry ($p = 0.002$) and lower maximal cross-correlation ($p < 0.001$) than controls.

An accelerometer was placed on the upper arm, as well as a magnetic angular rate and gravity device on the shoulder by [Bertomeu2015]. The Denavit–Hartenberg model was used, and the algorithm was based on the pseudoinverse of the Jacobian by the acceleration of the upper arm. The accuracy of this method was demonstrated by the use of an optoelectronic system for control purposes.

A similar system to the one we developed was used by [Viteckova2016] with nearly the same sensors and sensor position. An eigenvector method was suggested to compare the axes of the left and right hand. The results showed a difference between people with Parkinson's disease and healthy people.

12.1.1. Methodology

After, we have presented our material and methods, we will now discuss in this section how we applied these methods. In the presentation of the data set, we already said that we divided our recording into two different parts. First, we classified Parts (A) and (B), which comprised the complete recording of the TUG test, see Chapter 5.3. The other

scenario was that we only used Part (B). In Part (B), only the gait was used. Figure 12.1 shows the complete algorithm of the classification. In principle, we distinguished between the signals of the Euler angles and the linear acceleration. First, we removed the jumps within a signal of the Euler angles and then calculated the derivation of the signal. This made the signal more comparable. These steps were not necessary for linear acceleration. Then, we set the signals to a uniform length. This was necessary so that the signals could be interpreted by CNN later during classification. After resampling, we calculated the wavelet transformation for each individual signal. We used the resulting scalograms for the classification. In the classifications, we analyzed three different cases. At first, we classified each signal individually by CNN. This allowed us to show which axis of the sensors was very important. In the second case of classification, we used the three best signals for a multi-channel CNN. The third case was that we used the three best signals for classification by voting.
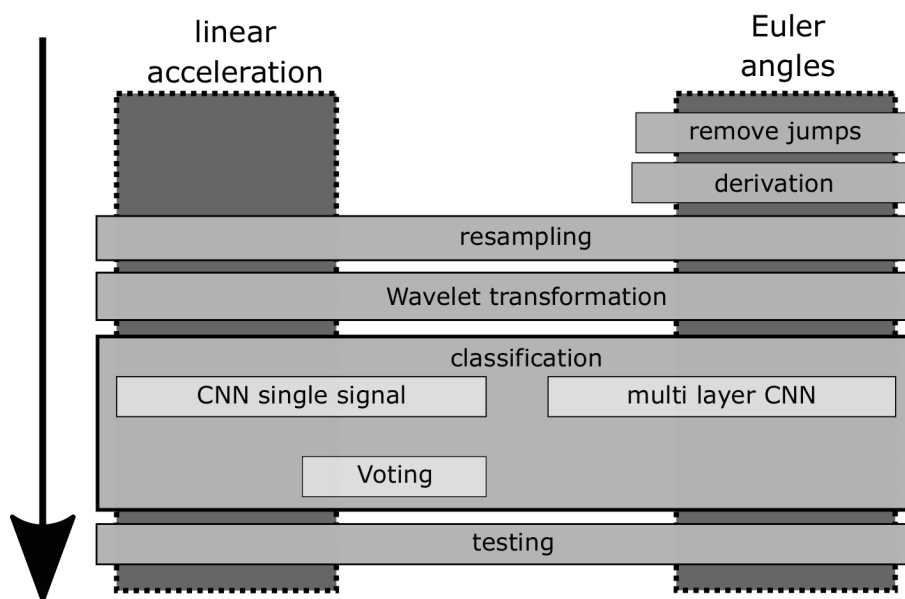

Figure 12.1.: Classification process for detecting motor dysfunctions in arm swinging.

12.2. Methods

12.2.1. Removing jumps

Figure 4.9 shows that some jumps existed in the signal of the z-axis of the Euler angle. This was because the value range of the sensor was between $0\,°$ and $360\,°$. This made the signal unstable. To correct this, we removed all jumps that were greater than a threshold of $300\,°$. In equation 12.1, our procedure is shown. If the absolute value of the difference of two successive sensor values $|x_i - x_{i+1}| > 300$, a correction of the signal was performed, where $i \in \{1, ..., N\}$. N indicates the length of the signal. The result of the cleanup is

given in Figure 12.2.

$$x_{i+1} = \begin{cases} x_{i+1} - 360 & for \ x_i < x_{i+1} \\ x_{i+1} + 360 & for \ x_i > x_{i+1} \end{cases} \tag{12.1}$$
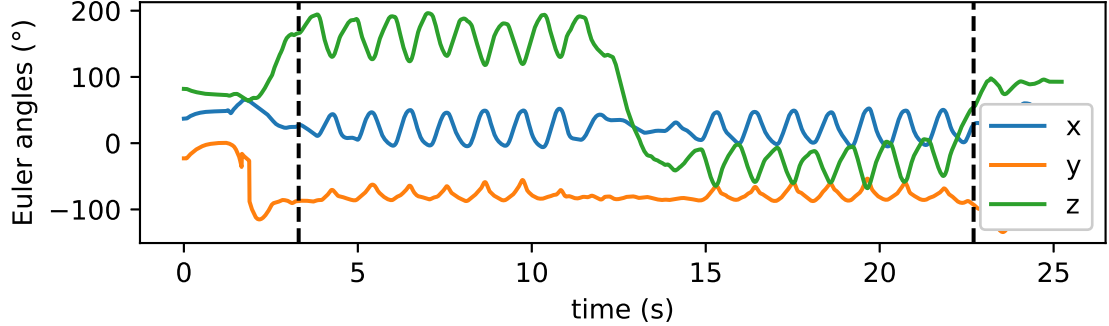

Figure 12.2.: Euler angles without jumps.

12.2.2. Derivation

It was not possible to create a classifier that could classify the subjects with motor and without motor dysfunctions by using the Euler angles, because the Euler angles were measured in absolute values. This means that the angles were not calibrated to a starting value at the beginning of the recording. For this reason, we calculated the derivative of each axis of the Euler angles. For this purpose, we calculated the difference between two successive measured values. The equation of the first order discrete derivative can be seen in equation 12.2, where N is the signal's length, x_i is the signal at index i, and x'_i is the value for the difference at i. The result of the derivation can be seen in Figure 12.3. The derivation makes the signals more comparable for different recordings. This is because the derivation uses the relative angle.

$$X'_i = x_{i+1} - x_i, i \in \{1, 2, ..., (N-1)\} \tag{12.2}$$

12.2.3. Resampling

Before CNN can interpret the data, the signal must have a uniform length. In order to do this, we resampled the data to a length of 512 values. For resampling, we used the Python library SciPy [Virtanen2019].

12.2.4. Wavelet Transformation

When considering static signals, the Fourier transformation is very well suited. There are hardly any static signals in the real world. Every signal changes its frequency dynamically
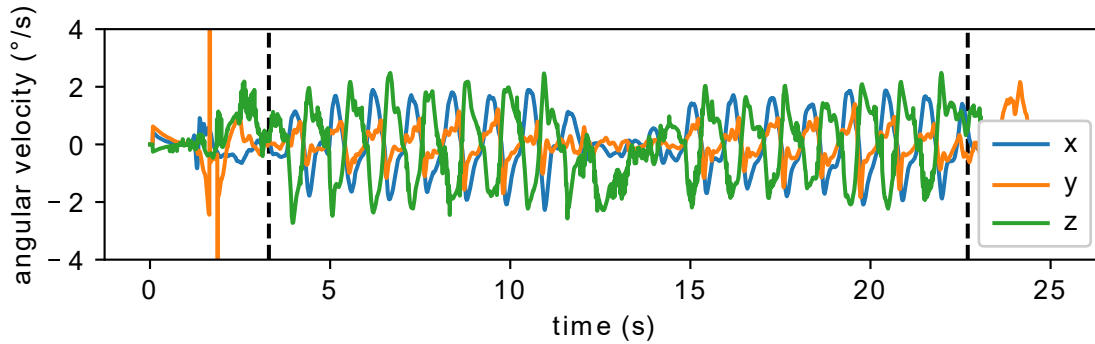
Figure 12.3.: Derivation of the Euler angles.

in time. This also applies to the human gait. The gait is a dynamic process. For this reason, it does not make sense to use Fourier analysis.

The origin of the data was a temporal series; therefore, we preferred the use of the wavelet transform in order to increase the information, by decomposition of the time-frequency. After the experiments, the accuracy showed a useful feature extracted from this transform. For the wavelet transformation, a signal was convoluted with a wavelet template. By selecting the kernel, we ensured that the ranges around 1.2 Hz, which is the frequency of the arm swing [Hausdorff1998], had a high amplitude. With this template, we calculated the wavelet transformation over the complete signal. In our case, these were the x-, y-, and z-axes of the derived Euler angle and the x-, y-, and z-axes of the linear acceleration of both wristbands. Figure 12.4 shows the scalograms of the individual signals of one wristband. On the y-axis, the frequencies are shown in Hertz and on the x-axis the time in seconds. For the calculation of the wavelet transformations, we used the Python library PyWavelets [Lee2019]. Figure 12.4 a) ,c) , and e) corresponds to the x-, y-, and z-axes of the derived Euler angles. We calculated for each signal the continuous wavelet transformation with the Morlet wavelet. It can be seen that there was a high amplitude from 0.25 Hz. In the lower frequency data < 0.25, the individual arm swings can be seen. Figure 12.4 b), d), and f) reflects the x-, y-, and z-axes of linear acceleration. We calculated for each signal the continuous wavelet transformation with the Morlet wavelet. With these data, it can be seen that the largest amplitude was in the range of 1 Hz. This corresponds to the natural arm swing since this corresponds to a frequency of approximately 1.2 Hz [Hausdorff1998].

12.2.5. Convolutional neural network

In image classification, as well as other signals, the application of CNNs has been very successful. The difference from common neuronal networks is that a CNN searches for a local pattern in the input signal. When using multiple CNN layers, one after the other, larger patterns can be detected [Abadi2016, Sze2017]. Thus, a CNN often provides better classification results than neuronal network. In our case, we achieved the best results with the use of three convolution layers. Then, we applied one neuronal network
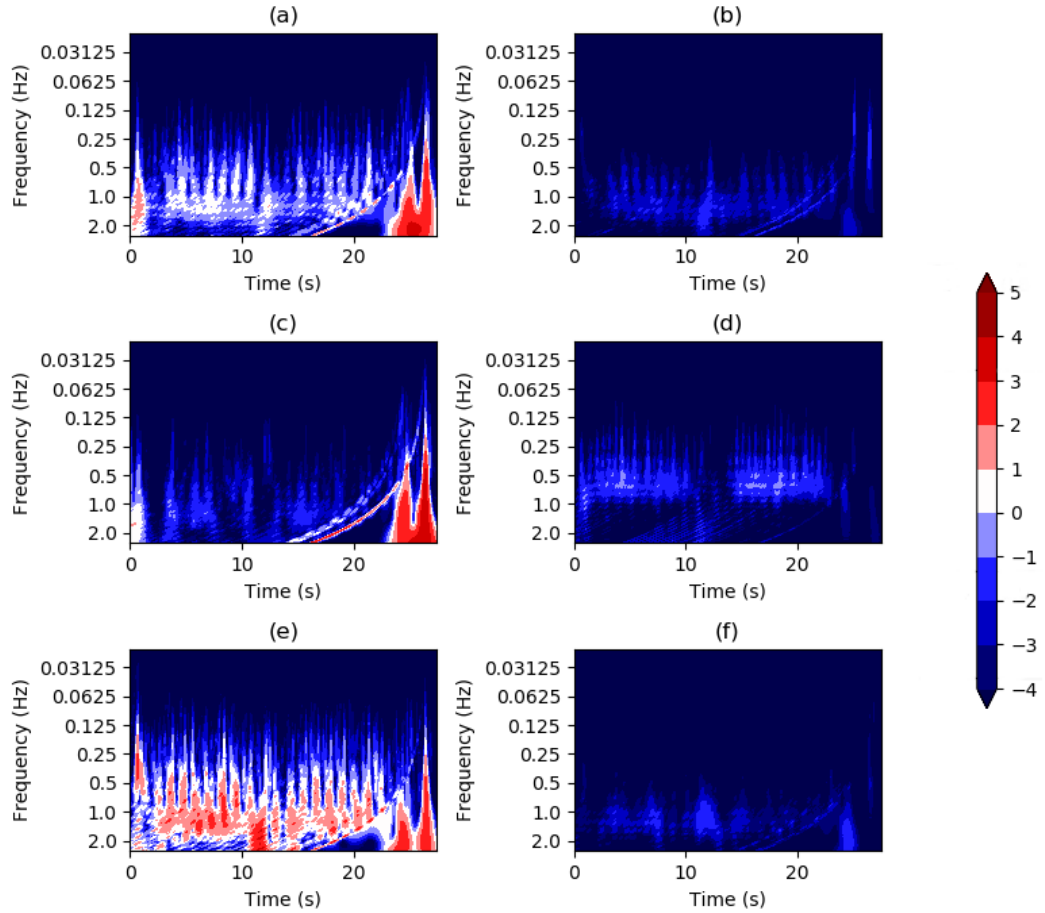
Figure 12.4.: (Scalograms of the individual signals for (a) x-axis of the derived Euler
angle; (b) y-axis of the derived Euler angle; (c) z-axis of the derived Euler
angle; (d) x-axis of linear acceleration; (e) y-axis of linear acceleration; and
(f) z-axis of linear acceleration.

with three encoders and one decoder. Our used CNN with the configuration is shown in
Figure 12.5. We used Python and the Keras library to create the CNN [Chollet2015].
We obtained the architecture for our CNN by systematically testing. We wanted to keep
the number of CNN layers as small as possible. However, with less than three layers, no
useful results were available.

In order to have a useful input for the CNN, we resampled the signal to a uniform
length of 512 values; see Section 12.2.3. We then applied a wavelet transformation to the
signal; see Section 12.2.4. This gave us a 128×512 matrix for the signal. We used this
matrix as input for the CNN. As the activation function, we used the ReLU function
for all convolution layers. We also used the ReLU function in the hidden layers of the
encoder and decoder. The equation of the ReLU function can be seen in equation 9.7.
The characteristic of the ReLU function is that the weight of the output is not negative.
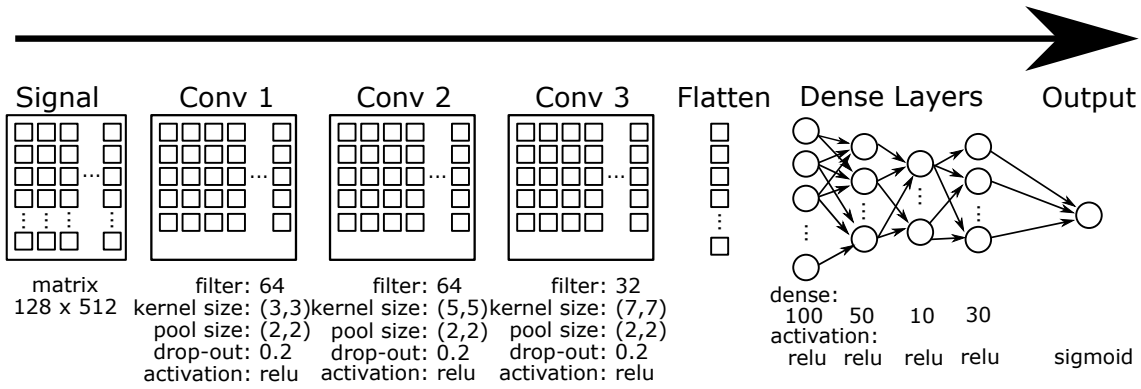In the output layer, we used the sigmoid function, see equation 9.8. After each convolution

Figure 12.5.: Construction of a single signal CNN for classification.

layer, we performed a two-dimensional max-pooling with a pool size of 2×2 and a drop out with a probability of 0.2.

The first convolutional layer searched for the smallest pattern from the signal. For convolution, we used a 3×3 matrix. In total, we created 64 different filters in the first convolutional layer. In the second convolutional layer, we increased our kernel size to 5×5 and created 64 filters again. The third convolutional layer had a kernel size of 7×7, and the filters created were reduced to 32 pieces. After the convolutional layers, we used a flatten layer so that the signal could be interpreted by the dense layers. In the dense layers, we started with three encoder layers with 100, 50, and 10 neurons, followed by a decoder layer with 30 neurons. Finally, we obtained our prediction in the output layer. Since we had a binary problem, a single neuron was used. For the training of the models, we used a batch size of 50 and 50 epochs. For training, we used an Intel Core i7-6700HQ with 2.6 GHz with four cores. Furthermore, the system used 16 GB RAM. The computer required approximately 45 min to train a model.

12.2.6. Multi-Channel CNN

In the last section, we presented our architecture for a single signal. To achieve better and more robust results, we wanted to use multiple channels x, y Euler angles, and x of linear acceleration for classification because these signals have the most characteristics of the gait. For this reason, we created an m-dimensional input. For the third dimension, we used the number of m different signals used. Figure 12.6 shows the construction. Another difference was that the first convolutional layer created 128 filters. The model was similar to the one in Figure 12.5. The computer required approximately 2 h to train a model. By using multiple channels, the classification result should be higher and more robust.

12.2.7. Weight voting

The multi-channel CNN was trained with 3 signals at the same time. The difference in voting was that for each signal, a separate model was trained, which was independent of
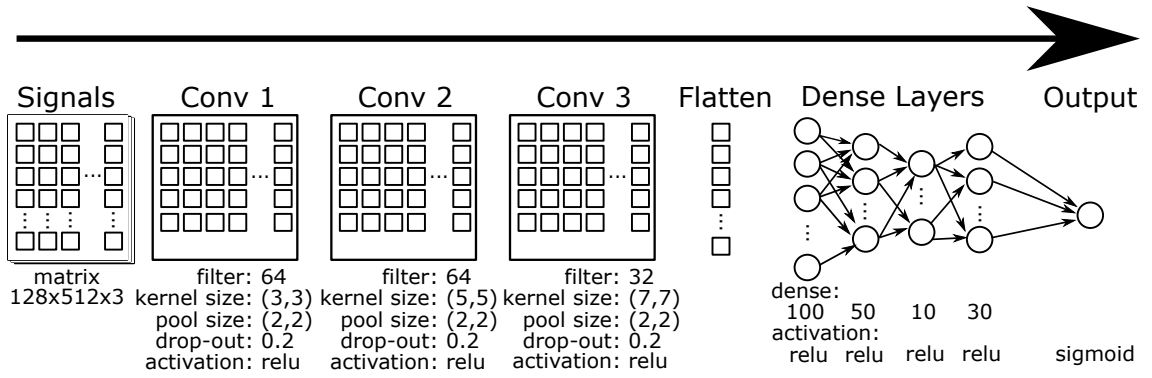
Figure 12.6.: Construction of a 3-channel CNN to use three different signals for classifi-
cation.

the other models. In our case, we had a binary problem, so the calculation for the voting
was easy. We used the predicted classes and calculated the average of all predictions;
see equation (12.3), where m_i is the prediction of a model from a classifier and M is the
number of classifiers.

$$v = \frac{1}{M} \sum_{i=1}^{M} m_i, i \in \{1, 2, ..., M\} \tag{12.3}$$

If $v \geq 0.5$, then the predicted class is motor dysfunctions (MD) and in all other cases,
no MD; see equation (12.4).

$$prediction = \begin{cases} MD, & v \geq 0.5 \\ noMD, & v < 0.5 \end{cases} \tag{12.4}$$

12.3. Results

12.3.1. Parts (A) and (B) of TUG

Single layer

To find out which sensor data were particularly useful for classification, we first separated
all signals from each other. The results are shown in Table 12.1. In the table, we applied
three-fold cross-validation to the sensor data. Furthermore, we optically separated the
results from the Euler angles and the linear acceleration with a double line. For each
signal, we calculated the precision, specificity, recall, F1-score, and accuracy. In every
cell, we show the mean

$$\bar{x} = \frac{1}{N} \sum_{i=1}^{N} x_i, i \in \{1, 2, ..., N\} \tag{12.5}$$

plus or minus the standard deviation

$$s = \sqrt{\frac{1}{1-N} \sum_{i=1}^{N} (x_i - \bar{x})^2}, i \in \{1, 2, ..., N\} \qquad (12.6)$$

, where N is the length of the signal. The columns with the best results are highlighted with bold. It can be seen that the x-axis of the Euler angle and the x-axis of the linear acceleration produced the best results. Furthermore, it can be seen that the z-axis of the Euler angle and linear acceleration provided the lowest results.

Table 12.1.: Results of a single signal by CNN classification. Parts (A) and (B) of the TUG test are used, see Chapter 5.3.

Signal	Sensitivity	Specificity	Recall	F1-Score	Accuracy
x Euler angles	**0.918** **±0.071**	**0.939** **±0.043**	**0.887** **±0.085**	**0.898** **±0.017**	**0.928** **±0.009**
y Euler angles	0.891 ±0.014	0.874 ±0.016	0.775 ±0.072	0.829 ±0.047	0.882 ±0.009
z Euler angles	0.57 ±0.505	0.844 ±0.186	0.606 ±0.527	0.587 ±0.514	0.821 ±0.173
x linear acceleration	**0.907** **±0.101**	**0.901** **±0.048**	**0.846** **±0.036**	**0.873** **±0.046**	**0.908** **±0.015**
y linear acceleration	0.857 ±0.031	0.888 ±0.056	0.841 ±0.066	0.848 ±0.032	0.877 ±0.027
z linear acceleration	0.795 ±0.118	0.863 ±0.044	0.74 ±0.043	0.761 ±0.037	0.841 ±0.009

Signal combination

In order to get better results in the classification, we decided to combine the individual layers. For the combination, there were several possibilities. On the one hand, it was possible to use an ensemble classifier like voting. On the other hand, we could use a multi-channel CNN. In Table 12.1, the x-axis of the Euler angles and the linear acceleration produced the best results. The third was the Euler angles of the y-axis. In this section, we used these three signals to improve our results. The results are shown in Table 12.2. We again used three-fold cross-validation for our results. Each cell represented the result as $\bar{x} \pm s$, see equations 12.5 and 12.6.

Table 12.2 shows the results of the signal combination classification. The three channel CNN achieved better results than the three signal voting. The three channel CNN was also better than any signal in Table 12.1.

Table 12.2.: Classification results by combining the x- and y-axis of Euler angles and the x-axis of linear acceleration. Parts (A) and (B) of the TUG test are used, see Chapter 5.3.

Layer	Sensitivity	Specificity	Recall	F1-Score	Accuracy
3 channel CNN	**0.934** **±0.047**	**0.932** **±0.013**	**0.899** **±0.026**	**0.928** **±0.043**	**0.933** **±0.024**
3 signal voting	0.915 ±0.078	0.9 ±0.02	0.821 ±0.052	0.862 ±0.026	0.902 ±0.018

12.3.2. Part (B) of TUG

Single layer

In this section, we present our results if only Part (B) of the TUG test was used for classification. In Table 12.3, you can see the results for a CNN classification for each axis of the sensors. As in Section 12.3.1, we used three-fold cross-validation and calculated the average $\bar{x}$ plus or minus the standard deviation s. The best results for each sensor and each column are marked with bold. Like the analysis of the complete TUG test, the x-axis provided the best results for Euler angles and linear acceleration. However, the results were not as accurate as in Section 12.3.1.

Table 12.3.: Results of a single signal by CNN classification. Only Part (B) of the TUG test is used, see Chapter 5.3.

Signal	Sensitivity	Specificity	Recall	F1-Score	Accuracy
x Euler angles	**0.873** **±0.027**	0.899 ±0.043	0.822 ±0.088	**0.844** **±0.039**	**0.887** **±0.018**
y Euler angles	0.793 ±0.037	0.855 ±0.016	0.756 ±0.046	0.772 ±0.006	0.831 ±0.015
z Euler angles	0.763 ±0.202	**0.943** **±0.049**	**0.904** **±0.088**	0.809 ±0.099	0.821 ±0.138
x linear acceleration	**0.909** **±0.012**	**0.9** **±0.044**	**0.822** **±0.088**	**0.862** **±0.053**	**0.903** **±0.032**
y linear acceleration	0.804 ±0.041	0.832 ±0.043	0.705 ±0.078	0.748 ±0.033	0.821 ±0.024
z linear acceleration	0.563 ±0.496	0.794 ±0.147	0.508 ±0.468	0.52 ±0.453	0.774 ±0.111

Signal combination

Table 12.4 shows the results of the signal combination of Part (B) of the TUG test. For the results, three-fold cross-validation was applied and for each cell, and the average $\bar{x}$ plus or minus the standard deviation s was calculated. The three signal voting performed best.

However, the results were marginally better than the single signal CNN classification in Table 12.3. Furthermore, the results were not as good as if the complete TUG test was used for the classification.

Table 12.4.: Classification results by combining the x- and y-axis of Euler angles and the x-axis of linear acceleration. Only Part (B) of the TUG test is used, see Chapter 5.3.

Layer	Sensitivity	Specificity	Recall	F1-Score	Accuracy
3 layer CNN	0.888 ±0.045	0.847 ±0.027	0.677 ±0.065	0.766 ±0.042	0.856 ±0.024
3 signal voting	**0.914 ±0.03**	**0.901 ±0.043**	**0.822 ±0.088**	**0.863 ±0.04**	**0.903 ±0.024**

13

Clustering of Parkinson's stadium

In this chapter, we use minimalistic sensor data to perform clustering based on the Parkinson's stadium. For this reason, we use only one axis from an insole. A problem with Parkinson's disease is that the stadium is often subjectively assessed. For this reason, we want to develop a system that supports the treating physician in his diagnosis and provides empirical measurement data. Because each person needs a different length for each stride, it would be impossible to work with the correlations without compressing or stretching the data, which would mean data manipulation. The advantage of the DTW algorithm is that a distance between two time series of different lengths can be calculated. As smaller this distance is, the more similar these time series are. The DTW algorithm calculates the ideal path between two time series.

13.1. Related works

This work is intended to make a further contribution to the analysis of gait disorders in Parkinson's disease. The aim is to support the treating physician in diagnosis and in assessing the severity of the movement disorder. The use of different sensors has proven useful in the analysis of human gait for many years [Boix2018]. In the first years, single or multiple cameras were often used to identify individuals by their gait [Kale2003, Boulgouris2005]. The Dynamic Time Warping (DTW) method has proven to be particularly useful in distinguishing the gait of individuals [Veeraraghavan2006, Muscillo2007]. Cameras were also used for the analysis of gait changes in neurodegenerative diseases. However, the accuracy is only sufficient to distinguish between healthy and sick persons [Rocha2015]. In recent years acceleration, gyroscope, and magnet sensors, Inertial Measurement Unit (IMU), have been used to analyze of movement disorders in Parkinson's disease[Ferrari2016, Ferster2015]. In [Ferrari2016], the Kalman filter is used to identify the gait asymmetry. The Fast Fourier Transformation (FFT) is used in [Ferster2015] to detect the freezing phases. Newest research again uses DTW, for example, for the segmentation of gait sequences [Haji2018] and recognition of asymmetry in gait [Barth2017]. For the detection of freezing phases, which occur mainly during turns, the turn was analyzed [Ferster2015, Haji2018]. In this chapter, the movement disorder stage is not to be determined based on individual characteristics such as asymmetry or freezing, but rather as the combination of all single disorders. The IMU sensors have been mounted on the shoe[Ferrari2016] or on the ankle [Ferster2015, Haji2018, Barth2017]. In this case, the sensor may slip during walking. This makes it difficult to detect the time point when

the foot touches the ground. For a more robust stride detection, we have integrated the sensor into an insole.

13.2. Methods

13.2.1. Preprocessing

For the present analysis, we used only the left insole's data, namely the linear acceleration of the y-axis, see Figure 13.1, for example, the forward acceleration, see Figure 4.5. The stride segmentation was performed with Min-Max Pattern (MMP) of Chapter 9.2.2 - Stride detection. The result of the stride detection can be seen in Figure 13.1. The starting point of a stride is the maximum value of the gait cycle in the figure the black lines. We use the complete straight walking. Start and end point of the complete straight walking analysis are marked with red lines in Figure 13.1. They are obtained by adding the average duration of a stride to the first or last detected maximum.
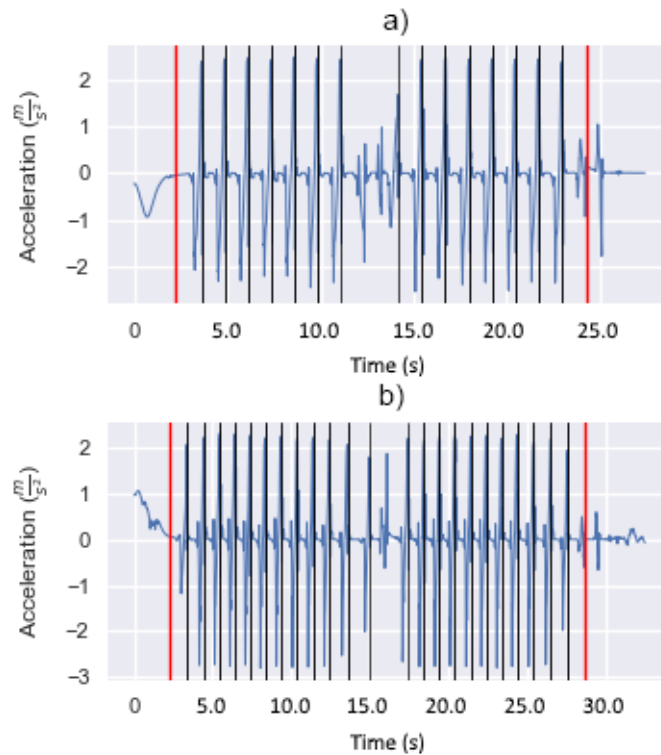

Figure 13.1.: Acceleration data of the y-axis and segmentation of the strides. The black lines indicate the start and end of a stride. The red lines indicate the start and end of a recording, a healthy subject a) and Parkinson's diasease subject b).

13.2.2. Dynamic time warping

Standard distance measures like Euclidean distance are not suitable to measure the distance between two time series, since the measured values are displaced in time, or the time series has a different length. For this reason, we used the DTW algorithm, see Chapter 11 - Symmetry.

13.2.3. Clustering

We performed hierarchical clustering [Handl2002]. Based on the distance of all single strides between two persons. This distance is obtained as the distance of all strides during the TUG for the two recordings. We performed hierarchical clustering according to the Complete-Linkage method and the Single-Linkage method and used the agglomerative algorithm.

In Figure 13.2, the result of clustering for strides with Single-Linkage of both subjects from section 13.2.1 can be seen. For easy understanding, the start, turn, and end of the recording are omitted, see Figure 13.3, white line and only single strides were used here. Here can be seen clearly that two large clusters were formed and one smaller one.

The result is shown in Figure 13.3. The green and red clusters show that the persons can be clearly distinguished from each other. Furthermore, even incorrectly interpreted strides in the blue cluster could be marked. These data are outliers from segmentation. Only one stride from HS is in the wrong cluster.

13.3. Results

We clustered the data with the hierarchical clustering method using the complete linkage and the DTW for distance measurement. For the analysis, we used all persons and the complete walking phase, see Figure 13.1 red lines. The result is shown in the dendrogram in Figure 13.5. In the dendrogram, we indicate the distances of the DTW algorithm of the clusters to each other on the y-axis. On the x-axis, we have marked each data set with the identification number (id) and the Parkinson stadium. This should help to understand the coherence of the data better. We have chosen a distance of 440 as a threshold to form the clusters because the results are very plausible in this constellation. This threshold gives us seven clusters as a result.

Tables 13.1 and 13.2 show confusion matrices for the result of the clustering of persons, Table 13.1, or recordings, Table 13.2. In Table 13.1, we have placed a confusion matrix for which only id's within clusters were displayed. It can be seen that the sensitivity is 57 %, and the specificity 90 %. At first glance, the sensitivity appears very low. However, it must be taken into account that the majority of the test cases are Parkinson's disease subjects, which were very well adjusted and showed hardly any motor dysfunctions, see Table 13.3. The specificity, on the other hand, is very convincing. The confusion matrix in Table 13.2 contains all recordings used during clustering. Here the sensitivity is 55 % and the specificity 92 %. The same reasoning applies here as to the confusion matrix in Table 13.1.
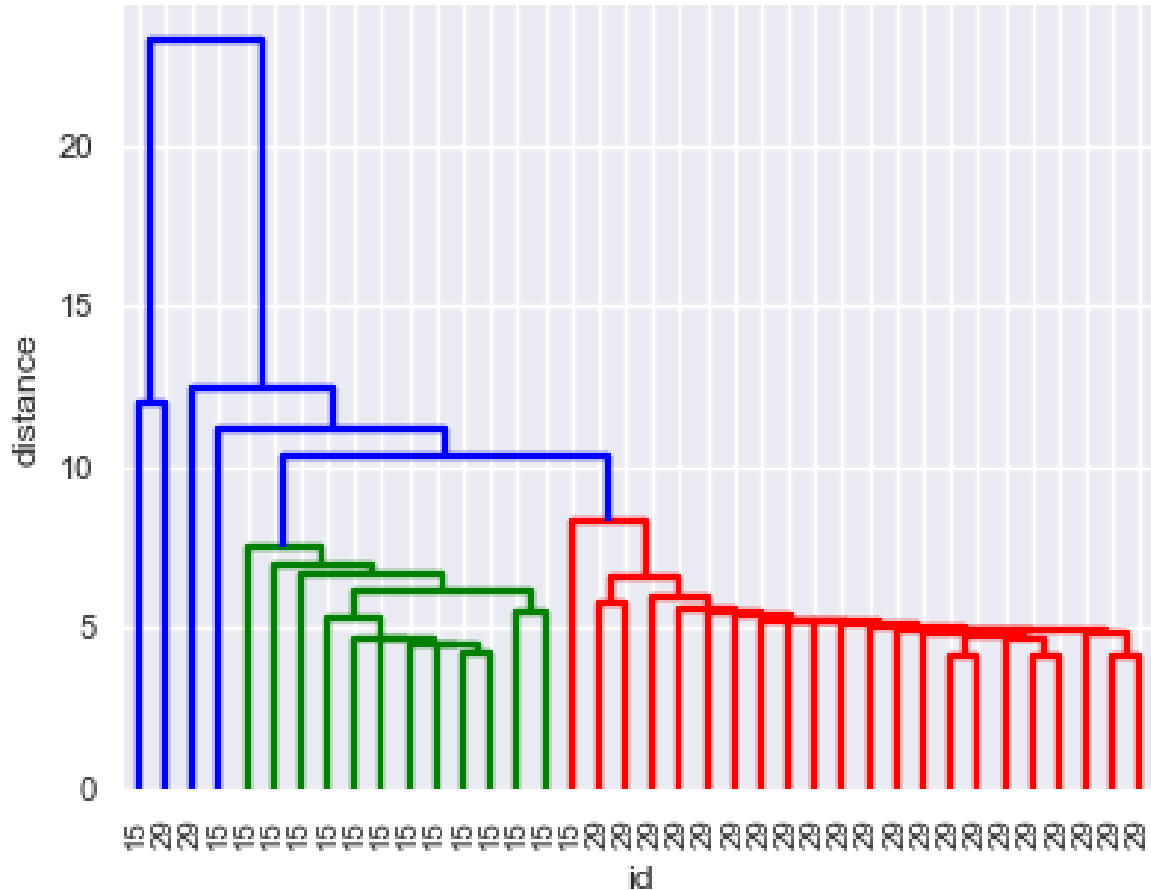
Figure 13.2.: The dendrogram shows the results of the cluster analysis. The strides of a healthy person (green) and a person with Parkinson's disease (red) were clustered. It can clearly be seen that two large clusters form and contain one smaller with outliers (blue).

Table 13.1.: Confusion matrix by id.

	PD stadium positiv	PD stadium negativ	$\sum$
Clustering positiv	11	2	14
Clustering negativ	8	19	32
$\sum$	19	21	46

We will take a closer look at the individual clusters, see Table 13.3 and Figure 13.5, and explain conspicuous assignments of data sets to clusters. The first green cluster contains mostly healthy and Parkinson's disease subjects, which do not have any particular motor disorders. The only exception is set (24,2.0), a Parkinson's disease subject, recorded on the day of his discharge from hospital. As a result, the Parkinson's disease subject was
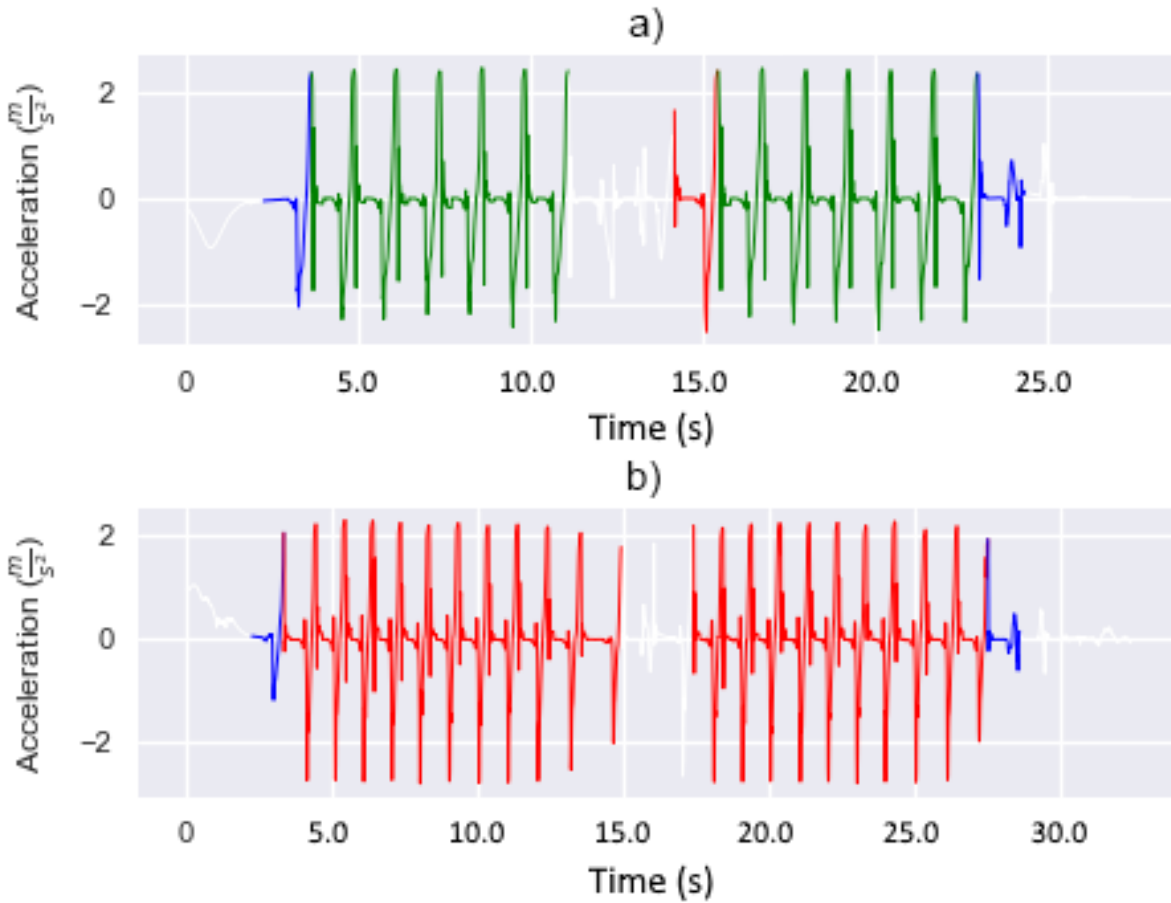
Figure 13.3.: Cluster result of healthy a) and Parkinson's disease b) subjects colored. the green cluster strides of healthy subject; red strides of Parkinson's disease subject; outliers are blue.

Table 13.2.: Confusion matrix by recording.

	PD stadium positiv	PD stadium negativ	$\sum$
Clustering positiv	25	4	29
Clustering negativ	20	49	69
$\sum$	45	53	98

optimally adjusted to the new medication and had no symptoms. The second (red) cluster consists of healthy and Parkinson's disease subjects, which have no particular motor abnormalities. Here the Parkinson's disease subject $(7, 3.0)$ stands out in particular. At the time of admission, this subject was newly adjusted to his medication. As a result, it was overdosed and over-movable. The third (turquoise) cluster consists only of test subjects of stadium one. According to our records, the subject $(10, 0)$ has a moderate

tremor but was set to Parkinson's stage zero by the medical doctor treating him. Cluster four (violet) contains only Parkinson's patients of stage three, where the healthy subject $(31, 0)$ is noticeable. The healthy subject has arthrosis in the legs and therefore had a high motor dysfunction. In clusters five blue, six yellow, and seven black, all Parkinson's disease subjects are assigned to the correct cluster, see Table 13.3.

Table 13.3.: Outstanding subjects

(Id, Stadium)	Cluster	Symptome
(48, nan)	1	No information about symptoms, fast-moving, and no apparent gait disorder.
(28, nan)	1	No information about symptoms, fast-moving, and no apparent gait disorder.
(24, 2)	1	Light hypokinesis, tremor slightly dominant on the right, light postural instability, new setting of medication, and recording on day of discharge from hospital.
(51, nan)	1	Tremor hand right, and no apparent gait disorder.
(50, nan)	2	No information about symptoms, and no apparent gait disorder.
(8, 1)	2	Rigor, and tremor.
(7, 3)	2	Over-movable due to overdosing.
(47, nan)	2	No information about symptoms, and no apparent gait disorder.
(10, 0)	3	Moderate tremor, and stadium 0 by doctor.
(29, nan)	4	Self-help group.
(49, nan)	4	Self-help group, light Tremor left, and medium postural instability.
(19, nan)	4	Self-help group, and tremor left.
(31, 0)	4	Artrosis in the legs.

In Figure 13.4, all time series data of the respective clusters are displayed jointly. The coincidence of pattern and time required to complete the TUG test within a cluster can be recognized in these diagrams.
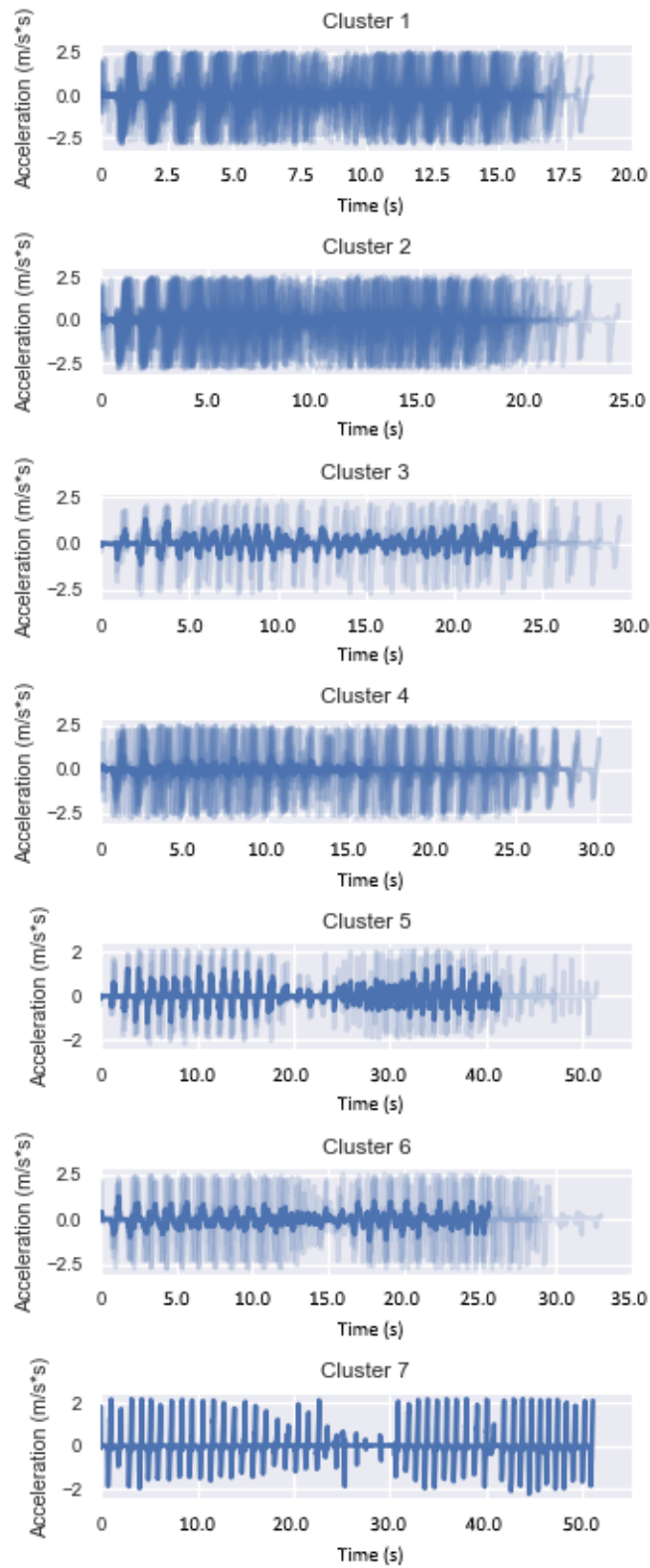
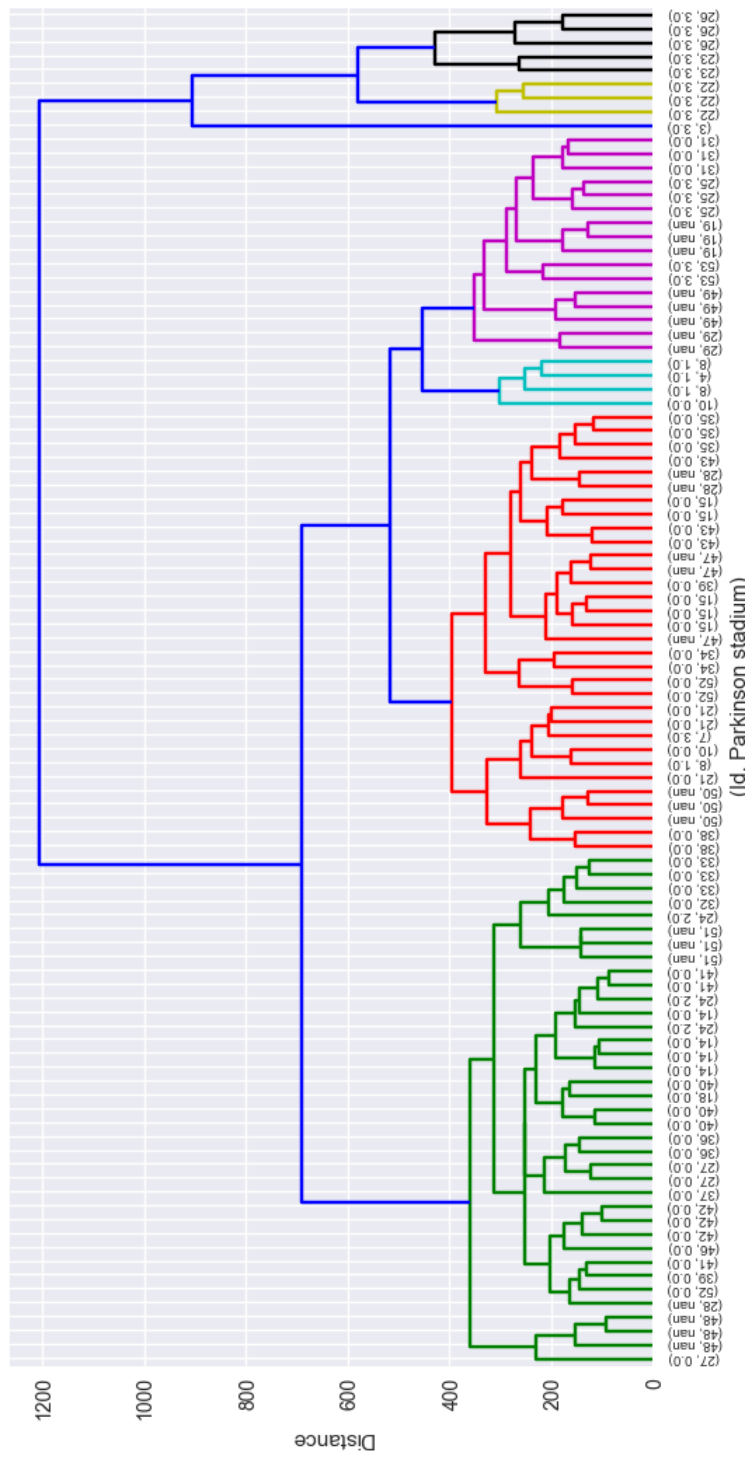Figure 13.4.: Time series of the clusters separately according to their assignment.

Figure 13.5.

112

14

Discussion

14.1. Hardware

As already shown in the state of the art, there are a multitude number of gait analysis systems [Muro2014, Buckley2019, Sprager2015, Taborri2016, Ferrari2013, Muro2014]. Furthermore, other work has mostly been limited to the analysis of the lower extremities and do not use a combination of wristband and insoles. However, this system still has two wristbands. These provide additional data of the upper extremities. Also, the used sensors are limited. Nevertheless, in this work, a system was created consisting of two insoles and two bracelets. What makes this system unique. The system used ten force sensors and an IMU sensor integrated into each insole and an IMU sensor integrated into each wrist band. In the literature research, no comparable system could be found.

Besides, we were able to produce insoles and wristbands for the hardware by using 3D printing. A disadvantage of this system is that the electronics in the used prototypes were soldered by hand. This resulted in cold solder joints or that the contact can broken.

14.2. Activity recognition

By developing an Android app for activity recognition, we were able to show that a smartphone can distinguish between activity *gait* and *other* activities such as *standing, lying, cycling,* or *writing messages.* With an accuracy of 94.7 %, we obtain similar results to other researchers [Hassan2018, Cao2018]. Activity recognition allows us to switch on the wearable sensors, and data recording only activity *gait* is recognized. This method is an energy-efficient solution.

14.3. Synchronization

Furthermore, we present a solution to synchronize several wearables sensors. In the literature, this problem has already been recognized, and there were several approaches. However, the problem is that the devices of Mbientlab can only synchronize three devices [Anwary2018b]. We synchronize four wearables for four extremities. Another solution was to synchronize the time during charging by cable [Mancini2011]. However, this solution has the disadvantage that in more extended use, a drift of the clock occurs. We

synchronize the wearables before each recording (recognition of activity *gait*). This way, we start each recording without drift of the clock.

14.4. Stride detection

In our opinion, the stride detection is a critical point in the analysis of the human gait, since all further parameters are inside this. If a stride is not well recognized, further mistakes will occur in a more detailed analysis. The presented methods have shown that the problem of stride detection can be solved with many different methods. AF+CNN achieved the best performance in our tests. The advantage of the AF+CNN classifier is that it does not require a threshold value. Furthermore, the Automatic framing algorithm makes it possible to analyze the data during recording. Furthermore, we have shown that the combination of force and IMU sensors can increase the results even more so that our test produce small errors. As comfortable to carry measuring instruments for persons with motoric dysfunctions as in Parkinson's disease, we propose a combination of force and IMU sensors. As an automatic stride detection process for daily life use, we propose a joint of Automatic framing, normalization, resampling, and CNN.

14.5. Gait features

With the results of the Gait features we could confirm the results of other works [Rampp2014, Salarian2004, Ferster2015, Wang2015, Hsu2014, Bamberg2008, Rampp2014, Tunca2017, Sijobert2015, Mariani2010, Ferrari2015, Salarian2004, Ferster2015, Wang2015, Hsu2014]. The features step length, step height, number of steps, step duration, duration of the stance phase and swing phase, and times of Heel Strike, middle stance phase, toe off, and middle swing phase could be added. These features are useful for the physician to detect gait disorders, as they are also used to make diagnoses. The features can also be used for classification.

14.6. Symmetry

In most of the papers dealing with symmetry, they use the stride length, stride duration, and different gait phases to calculate the ratio of the left and right leg [Barth2015, Hannink2018, Watanabe2018, Jiang2018]. In contrast, our symmetry calculation considers the complete time series. However, the synchronization of the sensors is essential for this. For stride detection, we use a combination of automatic framing and CNN. The use of CNN's for stride detection has proven to be very useful for us. Other work has already been able to benefit from the technology [Steinmetzer2019a]. The symmetry of the legs is analyzed with DTW. In the results we show that the results for RI, SI, GA, SA, and DTW are very similar for the given data set. The results confirm the results of other studies [Blazkiewicz2014, Hubble2015].

However, the weaknesses of the discrete symmetry calculation are visible in the results in section 11.3.2. If the parameters were chosen incorrectly in the symmetry calculation, asymmetries of the gait may not be visible. We could demonstrate this phenomenon in the second part of the results. In figure 11.3 at (c), (e), and (f) the discrete symmetry was always 1.0, but the signals were different in the amplitude. These differences could not be measured. By using our presented method, the whole signal was used for the symmetry calculation. Thus, it was possible to calculate not only the symmetry differences in the time as well as in the amplitude domain. For discrete symmetry calculation, a wide spectrum of features is important for a robust symmetry calculation. With our proposed method this is not necessary. We were able to demonstrate that our presented method is a useful extension for the calculation of gait symmetry with wearable sensors.

14.7. Classification of motor dysfunctions

In Tables 12.1 and 12.3, the x-axis always shows the best results of the arm swing analysis. The x-axis corresponds to the movement in the sagittal plane. According to the literature, the essential human gait characteristics are also present in this plane [Zhang2007, Tafazzoli2010]. For this reason, it is a logical conclusion that the features with the highest significance are present on this axis. We compared the results with the complete TUG test, Parts (A) and (B), was used for the classification, as well as if we only used the gait, Part (B), for the classification. The results showed that for the classification of motor dysfunctions, the gait alone gave quite good results with an accuracy of 90.3%. However, when looking at the complete test, we obtained even better results with 93.3% accuracy. From this, we concluded that the complete TUG test was necessary for the analysis of motor dysfunctions.

Furthermore, we classified each signal separately. During the classification, we found out that the x-axis of the Euler angle and linear acceleration gave the best results, independent of whether Parts (A) and (B), as well as only Part (B), were used for the classification. From this, we concluded that the x-axis was the most relevant.

The conclusion was that we obtained better results through the combination of the signals compared to single signals. In the classification of Parts (A) and (B), the three-channel CNN proved to be the best solution. When classifying with only Part (B), voting was the best choice. Table 14.1 shows our classification results compared to the corresponding state of the art. Our results were comparable to the results from large, expensive, and stationary video-based systems.

Our system delivered better results than the wearable system that also classified the data [Tsipouras2012]. We could not compare the other works because they focused on a statistical evaluation of the data. CNN, in combination with wavelet transformations, was a powerful technique for arm swing analysis.

Table 14.1.: Comparison of classification results with other works.

Reference	Description	Accuracy
[Spasojevic2015]	Kinect camera	90 %
[Dranca2018]	Kinect, Bayesian network	93.4 %
[Castano2019]	Kinect and e-Motion capture program	96.23 %
[Tsipouras2012]	Gyroscope	90 %
Our system	IMU sensors	93.3 %

14.8. Classification of Parkinson's stadium

Finally, it can be concluded that the sensor insole used for this study is very well suited for measuring motor dysfunctions. Hierarchical clustering, in combination with Single-Linkage and DTW, is useful for detecting outliers within a recording. In combination with Complete-Linkage and DTW, hierarchical clustering makes a clear distinction between subjects and the stadium of gait disorder. We also demonstrated that the linear acceleration data at a rate of 100 Hz are sufficient to draw conclusions about a person's motor health. With this data rate, it is theoretically even possible to evaluate the data in real-time. It proved to be sufficient to use only data collected from one foot to distinguish the different levels of gait disorder.

15
Conclusion

The central hypothesis for this work is: It is possible to evaluate the success of therapy, motor disorders, and Parkinson's stage by using wearables devices in daily life.

For the data analysis, a medical data set was created with Parkinson's disease patients and a control group. Another data set was recorded in daily life. These data sets allowed a detailed analysis of the data. Furthermore, a public data set was used for force sensors. The results of all data sets were consistent. It was impossible to calculate the success of the therapy because the sample size of our longitudinal study was too small (one subject). However, it can be assumed that the presented methods can answer this question if a suitable data set is available.

It is possible to develop wearable devices to measure the motion of gait in daily life. In contrast to a complex gait analysis system like the Vicon, a cheap alternative could be developed, which can be used independently of location. This system consists of two wristbands with IMU sensors and two insoles with IMU and force sensors. With the IMU sensors, it is possible to record the motion of the arms and legs. The force sensors allow us to measure the ground reaction of the feet.

Wearable devices for motion measurement can be synchronized [Steinmetzer2020] and annex D. For the wearables, a firmware was developed, together with a developed Android app, it is possible to control the wearables. The app also allows the synchronization of the wearables with each other. The synchronization enables the calculation of the gait symmetry on a new level. The synchronization of the wearables is accurate to a maximum of 3 ms.

The activity *Gait* can be extracted from all other activities [Steinmetzer2020] and annex D. Furthermore, our Android app allows the classification of human activities. The activity *Gait* is calculated with an accuracy of 94.7 %. The activity detection allows us to turn on the wearables only when needed. Thus, the wearables are used energy efficiently.

Strides of healthy and subjects with motor dysfunctions can automatically detect [Steinmetzer2019a] and annex D. With stride detection by IMU sensors and a CNN classifier, we could achieve an accuracy of 92 %. If we combined the IMU and FSR sensors, the accuracy increased to 100 %.

The time series can be used to determine the gait symmetry more precisely than the discrete symmetry based on several features. The data sets were used to determine several gait parameters such as stride duration, stride length, stride height, times of gait phases, and symmetry parameters. Furthermore, a new way of calculating symmetry

was developed by using DTW. This requires an essential requirement that the wearables work synchronously, and the single strides of a person are filtered out of the complete time series.

The time series can be used to determine the Parkinson's disease stadium. We were able to achieve a specificity of 92 % [Steinmetzer2018] and annex D. From the insoles motions analysis, it was possible to identify the Parkinson stadium of the subjects. By analyzing the arm motion through wavelets, it is possible to make conclusions about motor dysfunctions in arm swing. We achieved results with 93:3% accuracy [Steinmetzer2019b] and annex D.

This hypothesis can be partially confirmed. In this thesis, it could be shown that significant differences in gait characteristics between a Parkinson's patient and a control group are present with the help of statistical tests. Furthermore, with the help of hierarchical clustering and DTW, the Parkinson stage could be clustered. Motor dysfunctions in the gait could be determined with the help of wavelet transformation. The presented methods can be applied in daily life because the activity detection allows the wearables to work energy-efficient, and the synchronization of the wearables via Bluetooth LE ensures high data quality.

16
Future Works

In this work, we show that the developed system works, and we are able to analyze human gait and motor disorders. So far, the system is only a prototype that consists of several completed breakout boards. This was only soldered at the correct interfaces. In the future, a design for an own board should be developed. This could be produced by machine. This would make the microcontroller less error-prone regarding damaged solder points. It would also pave the way for an industrial product that can be used for diagnosis and the measurement of therapeutic success.

In order for the device to be used in medicine, it must also be certified with the Medical Device Regulation (MDR). For this purpose, the gait analysis system must be able to calculate valid values. For this reason, the system has to be validated against a gold standard. Data have already been recorded, but the validation of the data is still pending. Validation of the data is essential and an important element for further work. In future works, it should be proved how the symmetry calculation with the DTW works in multidimensional signals.

With the symmetry calculation with the DTW, we could show that our method compensates for the weaknesses of the other systems and is a useful extension for measuring symmetry. For this reason, the method should be further researched. Several sensor signals should be used simultaneously for the calculation of the symmetry. This would make the value even more accurate, since not only the ground reaction times are used. Also, the behavior of the feet in the air through the orientation and acceleration data.

Finally, the classification of the Parkinson's disease stadium should also be revised. Currently, the stadium is only classified according to the y-axis of linear acceleration. This type of classification is risky because one axis should not rely on one signal alone. A classification with all gait features of time and spatial domain would be the best way from the medical point of view. By using simple classifiers such as k nearest neighbor, decision tree, or Bayes network, the results can be easily understood, and the process is available to the physician for decision making. This makes the system transparent and comprehensible.

A
Ethic application

LANDESÄRZTEKAMMER BRANDENBURG
Körperschaft des öffentlichen Rechts

Hauptgeschäftsstelle

Landesärztekammer Brandenburg, Geschäftsstelle Cottbus
Postfach 10 14 45, 03014 Cottbus

BTU Cottbus - Senftenberg
Frau Prof. Dr. Ing. Ingrid Bönninger
Großhainer Straße 57
01968 Senftenberg
Deutschland

Ihr Zeichen:	
Ihre Nachricht vom:	
Unser Zeichen:	S 11(a)/2016 ma-fr
Unsere Nachricht vom:	
Referat:	Ethikkommission
Bearbeiter:	Friedrich, Steffi
Telefon:	0355 78010-151
Telefax:	0355 78010-159
E-Mail:	ethik@laekb.de
Datum:	24.08.2016

Entwicklung eines Digitalen Parkinson-Disease-Assessments

unser Zeichen: S 11(a)/2016

Sehr geehrte Frau Professor Bönninger,

die nachgereichten Unterlagen sind am 12.08.2016 in der Geschäftsstelle der Ethikkommission.

Die Ethikkommission der Landesärztekammer Brandenburg hat den o. g. Antrag gem. § 15 der Berufsordnung der Landesärztekammer Brandenburg nochmal in der Sitzung am **24.08.2016** beraten.

Gegen die Beteiligung des Prüfzentrums

Klinikum Niederlausitz GmbH Krankenhaus Senftenberg
Krankenhausstr. 10
01968 Senftenberg
- **Prüfer: Herr Prof. Dr. med. Markus Reckhardt**
- **Prüfer: Herr Prof. Dr. med. habil. Fritjof Reinhardt**

erhebt die hiesige Kommission keine Bedenken. Die Ethikkommission erteilt jedoch nachfolgenden Hinweis.

<u>Hinweis:</u>
Der Prüfplan und die Patienteninformation sind nochmals auf redaktionelle Fehler kritisch zu überarbeiten. Den überarbeitenden Unterlagen sehen wir entgegen.

Die Kommission wünscht Ihnen bei der Durchführung Ihres Forschungsvorhabens viel Erfolg. Für die Übermittlung eines Abschlussberichtes wäre Ihnen die Ethikkommission sehr verbunden.

Wir gehen davon aus, dass Sie den an der Studie beteiligten Prüfärzten unser Votum zur Kenntnis bringen.

Die ärztliche und juristische Verantwortung des Prüfleiters bleibt durch die Stellungnahme der Ethikkommission unberührt.

Die Ethikkommission der Landesärztekammer Brandenburg orientiert sich an den ICH-GCP-Richtlinien.

Mit freundlichen Grüßen

Prof. Dr. med. Michael Matthias
Vors. d. Ethikkommission der LÄKB

Eingereichte Unterlagen:
- Anschreiben vom 12.08.2016
- Geänderte Patienteninformation und Einwilligungserklärung
- Geänderte Seite 7 des Studienprotokolls

ALLG_AnwendungsBeobachtung.dotm

Mitglieder der Ethik-Kommission der Landesärztekammer Brandenburg

Sitzungstermin: 24.08.2016

Prof. Dr. med. Michael Matthias	Facharzt für Innere Medizin/Hämatologie
Prof. Dr. med. habil. Ulf Burchardt	Facharzt für Innere Medizin/Nephrologie
Prof. Dr. med. habil. Thomas Erler	Facharzt für Kinder- und Jugendmedizin
Priv.-Doz. Dr. med. Gudrun Richter	Fachärztin für Neurologie, Psychiatrie und Psychotherapie
Dr. med. Sigrun Voß	Fachärztin für Allgemeinmedizin
Gaby Güttler	Pastorin

123

PF Ethik

Von:	boenning <Ingrid.Boenninger@b-tu.de>
Gesendet:	Freitag, 21. Dezember 2018 14:21
An:	PF Ethik
Cc:	Tobias Steinmetzer
Betreff:	Bitte um Verlängerung der Studiendauer
Anlagen:	VerlaengerungBTU_ParkinsonStudie2018.pdf

Wir bestätigen den Eingang und die Kenntnisnah des Schreibens / der aufgeführten Unterlagen. Es bestehen keine ethischen Bedenken.

Mit freundlichen Grüßen

Vors. der Ethikkommission

Sehr geehrte Frau Friedrich,

mit dem angehängten Schreiben möchte ich die Ethik-Kommission um eine Verlängerung unserer Studie bitten.

Zuvor wünsche ich Ihnen ein wunderschönes und erholsames Weihnachtsfest.

Mit freundlichen Grüßen
Ingrid Bönninger
--
Prof. Dr.-Ing. Ingrid Boenninger

Institute of Medical Technology
Brandenburg University of Technology Cottbus - Senftenberg Universitaetsplatz 1, 01968 Senftenberg, Germany

phone: +49-3573-85613
fax: +49-3573-85609
mail: ingrid.boenninger@b-tu.de

1

[Entwicklung eines Digitalen Parkinson-Disease-Assessments]

Landesärztekammer Brandenburg
Hauptgeschäftsstelle Ethik-Kommission
Dreifertstraße 12
z.Hd. Frau Friedrich
03044 Cottbus

Prof. Dr.-Ing. Ingrid Bönninger
phone: +49-3573-85613
fax: +49-3573-85609
mail: ingrid.boenninger@b-tu.de

Senftenberg, 21.12.2018

**Antrag auf Erweiterung der Untersuchung im Rahmen der Studie
Entwicklung eines Digitalen Parkinson-Disease-Assessments**

Sehr geehrte Frau Friedrich,

für die obige Studie, die am 24.8.2016 von der Ethikkommission der Landesärztekammer Brandenburg für den Zeitraum bis Oktober 2018 (mit einem Zusatzantrag zur Tremormessung 2017) genehmigt wurde, bitten wir um eine Verlängerung bis Oktober 2020.

Der Grund für die Verlängerung sind verbesserte Messgeräte und –methoden, von denen wir eine exaktere Analyse der jeweiligen Bewegungsstörungen erwarten.
Die Verbesserungen der Geräte bestehen in:
- höhere Abtastrate
- Zwischenspreicherung größerer Datenmengen in SD-Karte im Messgerät für Langzeitmessungen
- mechanisch stabilere Einlegesohlen

Alle anderen Teile der Studie bleiben identisch.

Wir bitten Sie um eine Prüfung dieses Antrages durch die Ethikkommission der Landesärztekammer Brandenburg.

Mit freundlichen Grüßen

Prof. Dr. Ingrid Bönninger

B

Summary in Spanish/ Resumen en Español

Universidad de Las Palmas de Gran Canaria

DOCTORADO EN EMPRESAS, INTERNET Y TECNOLOGÍAS DE LAS COMUNICACIONES

DESCUELA DE DOCTORADO DE LA UNIVERSIDAD DE LAS PALMAS DE GRAN CANARIA

Análisis y clasificación de las disfunciones motoras en caminar mediante sensores que envían información corporal

Doctorando/a

Fdo.: Tobias Steinmetzer

Director/a

Fdo.: Prof. Dr. Carlos M. Travieso-González
   Fdo.: Prof. Dr.-Ing. Ingrid Bönninger

Las Palmas de Gran Canaria, Spain, a 15. Julio de 2020

1 Introducción

1.1 Antecedentes

En los últimos años, la importancia de análisis de la manera de caminar para apoyar los diagnósticos médicos ha aumentado significativamente.

Aunque la marcha es básicamente sólo caminar de un lugar a otro la marcha bipedal es un proceso muy complejo. Los requisitos son diferentes para cada persona y tarea. Si las manos están libres durante la caminata, pueden apoyar adicional la marcha. Sin embargo, es difícil para el cuerpo mantener su equilibrio si tiene que llevar objetos pesados. La forma de andar depende de la edad, el sexo, la altura, físico, peso, distribución de la masa, condiciones de vida (qué profesión se tiene o ha realizado), ambiente (un nuevo lugar o un lugar conocido), condición mental [Gotz2006].

La complejidad de la marcha requiere la interacción del sistema nervioso, los músculos y el sistema cardio-respiratorio. Por esta razón, las enfermedades también se manifiestan en el patrón de la forma de caminar [Pirker2017]. Las lesiones, enfermedades o desequilibrios limitan la movilidad humana. Esto se manifiesta en la pérdida de la salud general [Lord2013], la calidad de vida [Hirvensalo2000], problemas cognitivos [Verghese2007], y el riesgo de caídas [Beauchet2009]. Desde un punto de vista clínico del análisis de la marcha humana es de particular importancia, debido a que los problemas de marcha en enfermedades neurodegenerativas, como la esclerosis múltiple, la amiotrófica lateral esclerosis o la enfermedad de Parkinson, ocurren en un alto porcentaje de la población de personas mayores [Muro2014].

James Parkinson publicó por primera vez, la descripción de la enfermedad de Parkinson enfermedad, en su trabajo en 1817. Se presentaron síntomas como temblores, alteraciones temporales de la postura, pequeñas zancadas, marcha lenta y riesgo de caídas en seis pacientes diferentes [Parkinson1817]. Hoy en día la United Parkinson's Disease Rating Scale (UPDRS) Part III [Goetz2008] se utiliza para evaluar las habilidades motoras. La puntuación UPDRS se utiliza para determinar la etapa de la enfermedad de Parkinson utilizando la escala Hohn Yahr [Hoehn1998]. Por lo tanto, los resultados muestran una baja fiabilidad entre los mismos [Martinez1994, Richards1994].

Por esta razón, un método basado en sensores para medir los síntomas motores es esencial para la evaluación objetiva de la marcha humana. De acuerdo con Maetzler, un sistema tecnológico utilizado en las prácticas médicas debe tener las siguientes características:

- proveer resultados válidos y precisos que sean clínicamente relevantes

- contribuir a una decisión terapéutica efectiva

- ofrecen un rango objetivo (es decir, un rango para proveer información adecuada sobre un tratamiento o curso de la enfermedad)

- permiten un uso fácil y repetitivo para el personal médico y/o los pacientes de la Enfermedad de Parkinson (PD) [Maetzler2016].

Por esta razón, el objetivo de esta tesis es el desarrollo de un sistema de sensores en diferentes partes del cuerpo (wearable), que mide y analiza tanto la función motora de las piernas como de los brazos con métodos cuantitativos. Así debería ser posible objetivar el proceso de decisión basado en el andar de las personas y así, discernir con más precisión sobre las disfunciones las disfunciones en la motricidad.

El capítulo 1 de esta tesis explicará la motivación que ha tenido el autor, se presentará la hipótesis para esta tesis y los objetivos.

1.2 Motivación

En la actualidad, las disfunciones motoras suelen evaluarse mediante el examen visual de médicos o especialistas en la marcha. Las evaluaciones se basan en la experiencia. Por lo tanto, la evaluación es subjetiva. Por esta razón, el objetivo de esta tesis es el desarrollo de un sistema de análisis de la marcha basado en sensores. En el contexto de la cooperación con la Clínica Niederlausitz Senftenberg, se desarrollará un sistema capaz de objetivar el diagnóstico de pacientes de Parkinson.

El sistema debe ser portátil. Además, debería ser barato y fácil de usar en la vida diaria. Las desviaciones de la marcha o el caminar, como la asimetría, es uno de los síntomas característicos de los pacientes con PD que contribuyen al riesgo de caídas [Zhang2018]. El análisis de la marcha debe ser capaz de evaluar la simetría de los pacientes mientras se mueven, calcular varias características de la marcha, y evaluar si un paciente tiene disfunciones motoras.

1.3 Hipótesis

Es posible evaluar el éxito de la terapia, los desórdenes motores y el estadio de Parkinson mediante el uso de sensores sobre el cuerpo de la persona (o wearables), en la vida cotidiana

Los siguientes puntos se investigan y se referencian en esta tesis:

1. Es posible crear wearables para la medición del movimiento en el uso de la vida diaria.

2. Wearables para la medición del movimiento pueden ser sincronizadas.

3. La actividad "caminar" puede extraerse de todas las actividades de movimiento

4. Los pasos individuales pueden ser extraídos automáticamente de la serie de tiempo de los valores medidos.

5. De las series temporales de la marcha se pueden determinarse los valores de simetría de la marcha más exacto que de las características de los pasos individuales.

6. De las series temporales de la marcha, se puede determinar el estadio de Parkinson.

1.4 Objetivos

Con el fin de asegurar una secuencia lineal de trabajo para lograr cada objetivo de manera coherente, se han definido los siguientes objetivos.

Selección de los sensores: En primer lugar, hay que aclarar qué sensores se utilizan para el análisis de la marcha. Por esta razón, se deben adquirir conocimientos básicos sobre los sensores y sistemas para el análisis de la marcha. Basándose en este conocimiento, una selección de sensores tiene que hacer para resolver el problema.

Crear wearable hardware: La segunda tarea es seleccionar el tipo de hardware y las posiciones para montarlos en el cuerpo humano.

Cuando se desarrollan los prototipos de hardware, el firmware y una aplicación Android para controlar los wearables tiene que ser implementada. Cuando la fase de desarrollo del software es completa, todavía existe el problema de que los wearables no funcionan de forma sincronizada en el tiempo. Por lo tanto, hay que desarrollar un algoritmo para resolver este problema.

Study design: El siguiente paso es crear conjuntos de datos que se utilicen para el análisis de la marcha. Se deben considerar los siguientes escenarios:

1. se creará un conjunto de datos de la vida cotidiana. Por lo tanto, se debe lograr que con la aplicación Android sólo se reconoce el andar de las personas de todas las actividades a analizar.

2. se debe crear un conjunto de datos con supervisión médica. A continuación, se deben realizar el análisis sobre la base de este conjunto de datos. Para que se pueda recoger el conjunto de datos médicos, se debe definir la prueba de la forma de andar bajo el punto de vista médico, y se debe obtener la aprobación del comité ético.

   Análisis de datos: Primero se deben identificar los pasos individuales. Esta es la base para el cálculo de varios parámetros de la marcha como la longitud de los pasos, la altura de los pasos, duración de las fases de la marcha y la simetría de la marcha. Además, se desarrollarán modelos de la clasificación.

2 Estado del Arte

2.1 Hardware

Ya en 1992, se registró el movimiento y la simetría de las extremidades inferiores con cámaras y marcadores [Vagenas1992]. Los avances tecnológicos y el desarrollo rentable de las cámaras de profundidad han abierto nuevas posibilidades para el análisis de movimiento por Kinect desde 2010. La cámara de profundidad extendió la cámara RGB. Así, la forma de andar podría ser analizada con nuevos métodos [Ince2017].

Para el análisis de la forma de caminar de las personas, el primer paso es elegir qué sensores se usarán para el análisis. En principio, aquí se hace una distinción entre sistemas lo que se puede llevar y los que no. La segunda categoría del sistema de análisis de la forma de caminar o marcha, son los wearables. Estos sensores están conectados al cuerpo o integrados en la ropa. De este modo, es posible analizar la marcha independientemente de la ubicación. Un sensor de ultrasónido mide la distancia del sensor a otro objeto. Esto permite medir la distancia entre los pies y la frecuencia de pasos [Wahab2011]. El electromiograma (EMG) utiliza electrodos para medir la contracción muscular. Esto hace posible medir los ángulos entre las extremidades. Sin embargo, los electrodos deben estar siempre conectados al cuerpo, lo que no es adecuado para la medición en la vida cotidiana. Ya que los electrodos tienen que ser cambiados después de un cierto período de tiempo y por un profesional[Muro2014]. La forma más común de medir la marcha utilizando wearables son los sensores de la Unidad de Medición Inercial (IMU). Estos suelen consistir en una combinación de diferentes sensores: Acelerómetro 3D, giroscopio 3D y magnetómetro 3D. Los datos de los sensores individuales normalmente se fusionan usando el filtro de Kalman. Esto hace que los datos sean más robustos. El sensor IMU permite la medición de datos de ángulo y aceleración [Muro2014, Buckley2019, Sprager2015, Taborri2016]. Esto hace posible calcular distancias, duraciones de fases de marcha y datos de orientación en ángulos de Euler. En un estudio, los sensores de la UMI fueron validados contra un sistema basado en cámaras. El resultado fue que la longitud del paso se correlaciona con el sistema, pero debe aceptarse una desviación del 5% [Ferrari2013]. Los sensores de Resistencias Sensibles a la Fuerza (FSR) se usan para medir la reacción de los pies en el suelo. Estos sensores cambian el valor de la resistencia cuando se les aplica una fuerza. Esto permite medir la fuerza en diferentes puntos. Con la ayuda de estos sensores, se pueden sacar conclusiones sobre el movimiento de rodadura del pie y la distribución de la fuerza en el cuerpo [Muro2014]. En esta tesis se eligió un sistema compuesto por sensores IMU y FSR. Los sensores IMU son baratos en contraste con un sistema basado en cámaras, ahorran espacio, son adecuados para el uso diario y proveen datos de medición suficientemente precisos. Son la contrapartida de los sistemas basados en cámaras. Los sensores FSR permiten medir el efecto de la fuerza en el pie. Esto permite obtener conclusiones sobre el movimiento de balanceo y el equilibrio de las personas de prueba.

2.2 Reconocimiento de actividades

Muchos móviles inteligentes o smartphones tienen un giroscopio, un acelerómetro y un magnetómetro. En muchos trabajos, esto se ha utilizado para identificar las actividades de las personas [Gadaleta2018, Hassan2018, Cao2018]. Una posibilidad para implementar esto es elegir un ancho de ventana fijo y recoger todos los valores estadísticos para esta ventana, que sirven como característica para la clasificación. El uso de una red neuronal ha demostrado ser útil [Hassan2018, Cao2018]. Otra posibilidad es el uso de la CNN [Gadaleta2018]. La detección de actividad se utiliza generalmente para medir el tiempo que una persona se ha estado moviendo durante el día. Esto es suficiente para una estimación de la actividad de una persona en general. La calidad de los sensores de los

smartphones es adecuada para estimar la actividad de una persona.

2.3 Sincronización

Los sistemas basados en video tienen una grabación sincronizada de todos los movimientos de las extremidades. La desventaja es que las mediciones no pueden realizarse en la vida diaria. En la literatura sólo se encontraron sistemas de cámaras para mediciones de laboratorio [Viteckova2016]. Los sistemas portátiles, en cambio, podrían ser una alternativa para hacer mediciones de simetría de la marcha en la vida diaria, pero no están sincronizados en el tiempo.

Para cerrar esta brecha, los microcontroladores deben estar sincronizados entre sí. Ya se han aplicado varios métodos para ello. Una posible solución es construir una red de sensores en la que los sensores estén conectados por cables [Viteckova2016]. Otro trabajo presenta un sistema en el que una estación de acoplamiento sirve como estación de carga y para la sincronización [Mancini2011]. La estación de acoplamiento puede sincronizar cuatro sensores, pero tiene una diferencia de tiempo después de un tiempo de funcionamiento más largo. Otros usan el sistema de MbientLab [Anwary2018b]. Para determinar la simetría de la marcha, se necesitan cuatro sensores sincronizados (uno en cada extremidad). En trabajos anteriores, se habían probado el sistema de Mbientlab, pero sólo puede registrar tres sensores sincronizados [Anwary2018b].

Ventajas y desventajas de los sistemas actuales:

- Los sistemas basados en cámaras pueden medir series temporales sincronizadas de cada extremidad. Pero son estacionarios y por lo tanto no son adecuados para las mediciones en la vida cotidiana.

- Un teléfono inteligente es útil para detectar actividades de marcha. Pero es demasiado impreciso para la medición clínica.

- Los sistemas IMU son una alternativa a los sistemas basados en cámaras. Pero tienen que estar sincronizados.

Para calcular la simetría de la marcha de las series temporales utilizando sensores incrustados en las prenda en la vida diaria, proponemos un sistema con dos pulseras con sensores IMU, dos plantillas con un IMU y diez sensores de fuerza, y un smartphone para la detección de actividades. Para las mediciones sincronizamos todos los sensores si la actividad caminar se detecta en la vida diaria. Proponemos un método para calcular la simetría de todos los valores medidos del ciclo de la caminata en lugar del cálculo de la simetría con parámetros.

2.4 Detección de los pasos

Los desórdenes del movimiento que influyen en la marcha del paciente se miden con sensores como giróscopos, acelerómetros, magnetómetros, sensores de presión y sensores de imagen. Los acelerómetros, los giróscopos se utilizan a menudo en combinación con un magnetómetro [Barth2015, Bobic2018, Tao2018, Koroglu2018, Hannink2018, Watanabe2018].

Los sensores pueden estar integrados en los teléfonos inteligentes [Tao2018, Kim2018] o fijados en el tobillo [Barth2015, Jiang2018, Hannink2018] o en el cuerpo [Koroglu2018]. Para las grabaciones de vídeo para el análisis de la marcha, a veces se utiliza un sensor de profundidad además de la imagen 2D [Ince2017]. Los sensores de fuerza se instalan en las plantillas [Agostini2014, Mazumder2018b, Steinmetzer2018] y en el suelo [Muheidat2017].

El objetivo de la integración de muchas tecnologías es la detección de los pasos, otras se centran en el reconocimiento de actividades. La detección de pasos reconoce de forma precisa, un solo paso en una serie de tiempo. Por el contrario, el reconocimiento de actividad detecta diferentes tipos de movimiento, por ejemplo, caminar, estar de pie, trotar.

Una prueba estandarizada para el diagnóstico de la enfermedad de Parkinson es el test "Time Up and Go". Esta prueba también es utilizada, por ejemplo, por [Mazumder2018b] para diferenciar entre los pacientes sanos y los de Parkinson. También usamos esta prueba en [Steinmetzer2018] bajo condiciones hospitalarias ideales para una aproximada estimación del estadio de Parkinson.

En [Tao2018] se utiliza un filtro digital de paso bajo para eliminar los componentes de ruido de alta frecuencia de las mediciones del acelerómetro.A partir de esto, los autores se aseguran de que sólo se detecte un pico por cada cruce de cero de la gravedad. En [Agostini2014] definen los candidatos a los pasos de determinan el comienzo de la fase de andar y calculan la duración del paso. Los pasos con dos fases y una corta duración se fusionan primero con los pasos anteriores y después con los sucesivos. Se logra una cuota de reconocimiento de zancadas del 97% en [Barth2015] con la subsiguiente DTW multidimensional con libre marcha. Con este método un valor umbral es fijado. Esto empeora los resultados de los movimientos anormales o de subir escaleras [Barth2015].

El Mild Cognitive Impairment (MCI) en la marcha se clasifica en [Gwak2018]. Se registraron los datos de los sensores de fotopletismografía (PPG) y de la marcha (acelerómetro y giroscopio). El filtro de Butterworth se utilizó para eliminar el ruido de las señales de marcha medidas. Para detectar pasos, se utilizó un algoritmo de detección de picos que funciona con la mínima de la altura de pico y la distancia mínima de los picos. Para condiciones normales de caminata, las frecuencias de los pasos han sido asumidas para variar entre 1 Hz y 3 Hz. En el [Kim2018] la aceleración gravitatoria está registrada usando un filtro de paso de banda con una frecuencia central de 2 Hz y un ancho de banda de 2 Hz. Los pasos se detectan usando los métodos de "Stride Feature of Spectogram" y una arquitectura de Red Neural Artificial (ANN). Los parámetros de marcha analizados en [Muheidat2017] como la velocidad, el tiempo de paso y la longitud del paso son dados por una alfombra sobre la que se realizan los pasos, usando el sistema GAITRite®. En [Koroglu2018] las UMI montadas en el pie y el cuerpo se utilizan para la detección de pasos. Los pasos se etiquetaron usando un umbral. La detección de pasos fue realizada por una residual red neuronal. Para el proceso de entrenamiento, se utilizó la función de entropía cruzada como loss funtion. En un paso de preprocesamiento en [Hannink2018] las señales del acelerómetro y el giroscopio se normalizan. Se escalan a una longitud fija de 256 muestras por paso para asegurar una entrada a la red de tamaño fijo y a igual escala. Se detectan la postura media (Mid-stance (MS)) y el tacón (heelstrike (HS)). Para

la detección de pasos se elige una red convolucional (CNN) de dos capas seguida de una capa totalmente conectada y una capa readout-layer. La ventaja de las redes neuronales (NN), los modelos ocultos Markov (HMM) y los sistemas basados en la regresión es que no requieren un umbral.

En esta propuesta queremos comparar los métodos más utilizados para detección de pasos, Patrones Mín-Máx (MMP), Deformación Dinámica del Tiempo (DTW), Redes Neuronales Convolucionales (CNN) para poder utilizar la mejor variante de detección de zancadas en la vida diaria, independiente de los trastornos motores.

2.5 Características de la marcha

Las características del andar humano pueden dividirse en un dominio de tiempo y espacio. Los parámetros temporales de la marcha son la duración de las diferentes fases de la marcha, como la duración de un ciclo de marcha, la fase de postura o la fase de balanceo. Los parámetros de marcha relacionados con el espacio son la longitud o la altura del paso. Hay diferentes métodos de aproximación a determinar estas características. Para determinar el golpe de talón y la punta del pie, con el fin de calcular la duración de la fase de apoyo y de la fase de balanceo, hay varias posibilidades. Los sensores de fuerza pueden utilizarse con un valor umbral fijo [Bamberg2008]. Otro método es calcular la velocidad del pie. Si esta velocidad cae por debajo de un valor umbral, el pie está en la fase de reposo (stand phase) [Bamberg2008, Tunca2017]. Además, de los mínimos y máximos de los datos de aceleración y del giroscopio el golpe de talón y el dedo del pie puede ser determinado [Rampp2014, Salarian2004, Ferster2015, Wang2015, Hsu2014]. Para la determinación de la longitud del paso, se utilizan los datos del giroscopio y la aceleración para calcular el movimiento horizontal en el espacio del sensor por integración doble [Bamberg2008, Rampp2014, Tunca2017, Sijobert2015, Mariani2010, Ferrari2015, Salarian2004, Ferster2015, Wang2015, Hsu2014]. El mismo procedimiento se utiliza para calcular la altura del paso en la vertical [203].

2.6 Simetría de la marcha

La situación es diferente cuando los wearables evalúan enfermedades relacionadas con los desórdenes del movimiento. Para medir y guardar las series de tiempo de la marcha que se llevan, a menudo se utilizan microcontroladores en combinación con sensores IMU [Barth2015, Bobic2018, Tao2018, Koroglu2018, Hannink2018, Watanabe2018, Clemens2019, Crenshaw2006, Mancini2011, Anwary2018b, Anwary2018a, Anwary2018c, Steinmetzer2018]. En la mayoría de los casos, el movimiento de la parte baja se miden en las extremidades [Barth2015, Bobic2018, Tao2018, Koroglu2018, Hannink2018, Watanabe2018, Steinmetzer2018]. De esta manera se pueden sacar conclusiones sobre la longitud del paso, la cadencia, la duración del paso, las fases de la marcha y la simetría [Barth2015, Hannink2018, Watanabe2018, Jiang2018]. Hay métodos diferentes para el cálculo de la simetría. Una forma de evaluialo es mediante las diferentes características calculadas como la longitud del paso, la duración del paso, el

tiempo de estar de pie, o el tiempo de oscilación de las piernas se ponen en relación [Loiret2019, Anwary2018b, Clemens2019].

La desventaja de este método es que sólo los valores medios de las características calculadas para la marcha puede ser evaluada, pero no toda la serie temporal. Esto es diferente para los sistemas estacionarios, que están basados en cámaras. Con estos sistemas, el cuerpo completo puede ser grabado sincrónicamente [Crenshaw2006]. Ambos tipos de evaluación de la simetría son útiles. Sin embargo, en nuestra opinión, una comparación directa de las series temporales es más útil, porque se pueden medir las diferencias en los brazos y piernas relacionados directamente. La simetría de los brazos y las piernas, así como la simetría de la parte superior e inferior extremidades es investigada por sólo unas pocas referencias [Lin2018a, Miller2018, Viteckova2016]. Cambios en la coordinación de las extremidades de personas con PD y adultos mayores sanos comparan sistemáticamente la velocidad de marcha para determinar el impacto de los síntomas de la PD en la coordinación de las extremidades [Lin2018a]. Se colocaron marcadores en el pie, talón, tobillo, rodilla, cadera, muslo, muñeca, codo, hombro y cabeza. Se calculó un punto, denominado el punto estimado de las fases relativas (PERP), entre los segmentos corporales utilizando el momento en que se reciben el máximo positivo ángulo de cada segmento corporal. Evaluar el cambio en la asimetría a lo largo del tiempo es el objetivo en [Miller2018]. Los cambios en los movimientos son evaluados por un solo neurólogo especializado en los desórdenes del movimiento. Un modelo de regresión logístico que incluye un control para un clustering mediante observaciones repetidas, dentro de la persona para evaluar el cambio relativo en la asimetría se ha desarrollado. Otro sistema se centra en el estudio del impacto de la PD en las sincinesias (es decir, la simetría del movimiento) durante la marcha, y el efecto de la medicación en la simetría de la marcha [Viteckova2016]. Cada paciente fue examinado y medido con sensores IMU en su estado ON y OFF. El valor de la simetría de la tendencia se calcula como una relación de las variabilidades de dos autovectores, que se calculan a partir de los datos de movimiento cinemático de la extremidad izquierda y derecha. Un resumen reciente de la simetría para sistemas de análisis de movimientos, se muestra en [Viteckova2016]. El uso de puntos de tiempo sincronizados para la determinación de la asimetría es la prioridad. Eso significa que la transmisión de datos tiene que estar sincronizada.

2.7 Detección de estadio de Parkinson por DTW

Este trabajo tiene por objeto contribuir al análisis de los desórdenes de la marcha en la enfermedad de Parkinson. El objetivo es ayudar el posible diagnóstico del médico y en la evaluación de la gravedad del desorden del movimiento. El uso de diferentes sensores ha demostrado ser útil en el análisis de la marcha humana durante muchos años [Boix2018]. En los primeros años, se utilizaban a menudo una o varias cámaras para identificar a los individuos por su forma de andar [Kale2003, Boulgouris2005]. El método Dynamic Time Warping (DTW) ha demostrado ser particularmente eficaz para distinguir la forma de andar de los individuos [Veeraraghavan2006, Muscillo2007]. También se utilizaron cámaras para el análisis de cambios de la marcha en las enfermedades neurodegenerativas. Sin embargo, la precisión es sólo suficiente para distinguir entre personas sanas y enfermas

[Rocha2015]. En los últimos años los sensores de aceleración, giroscopio y magnetómetros (unidad de medición inercial- IMU) se han utilizado para el análisis de los desórdenes del movimiento en la Parkinson enfermedad [Ferrari2016, Ferster2015]. En [Ferrari2016] el filtro de Kalman se utiliza para identificar la asimetría de la marcha. La transformada rápida de Fourier se utiliza en [Ferster2015] para detectar las fases de freezing. Las últimas investigaciones utilizan de nuevo el DTW, por ejemplo, para la segmentación de las secuencias de marcha y para el reconocimiento de la asimetría en la marcha [Barth2017]. Para la detección de las fases de freezing, que ocurren especialmente durante los giros, y por tanto, se analizó el giro [Ferster2015, Haji2018]. En este documento, la etapa del desorden de movimiento no se determinará sobre la base de características individuales como la asimetría o la freezing, sino más bien como la combinación de todos los desórdenes individuales. Los sensores del IMU se ha montado en el zapato [Ferrari2016] o en el tobillo [Ferster2015, Haji2018, Barth2017]. En este caso, el sensor puede caer durante la marcha. Esto dificulta la detección del punto de tiempo cuando el pie toca el suelo.

Para una detección de paso mas robusta, hemos integrado el sensor en una plantilla. En este trabajo usamos datos de sensores minimalistas para realizar un clustering basadas en el estadio de Parkinson. Por esta razón, usamos sólo un eje de una plantilla. Un problema con la enfermedad de Parkinson es que el estadio es a menudo evaluado subjetivamente. Por esta razón, queremos desarrollar un sistema que apoye al médico en su diagnóstico y que proporcione datos de medición empírica. Porque cada persona necesita una longitud diferente para cada paso, sería imposible trabajar con las correlaciones sin comprimir o estirar los datos, lo que significaría la manipulación de los datos. La ventaja del algoritmo de DTW, es que puede medir un número de distancia entre dos series temporales de longitudes diferentes. Cuanto más pequeña es esta distancia, más similares son estas series temporales. El algoritmo DTW busca el camino ideal entre dos series temporales.

2.8 Disfunción motora en el balanceo del brazo

La mayor parte de la investigación sobre el análisis de la marcha trata sobre el análisis del movimiento de las piernas [Mazumder2018a, Jasni2019, Stoelben2019, Balzer2018, Prakash2019, Steinmetzer2018, Steinmetzer2019a]. Sin embargo, el análisis del movimiento del brazo también es importante para la evaluación de un desorden de la marcha. Los sistemas estacionarios que utilizan cámaras o ultrasonidos [Ospina2018, Spasojevic2015, Baron2018, Lewek2010, Tsipouras2012, Castano2018, Dranca2018, Castano2019, Roggendorf2012] y móviles se utilizan sistemas con sensores inerciales [Huang2012, Bertomeu2015, Viteckova2016] para medir el balanceo del brazo. En [Ospina2018], se comparó los balanceos de brazo de los pacientes de Parkinson y las personas sanas con la ayuda de una cámara Kinect. Se observaron diferencias significativas en la amplitud y la velocidad. Los movimientos de los brazos de los pacientes de Parkinson también mostraron a menudo asimetrías. El grupo PD mostró reducciones significativas en la magnitud de la oscilación del brazo (izquierda, p = 0,002; derecha, p = 0,006) y en la velocidad de oscilación del brazo (izquierda, p = 0,002; derecha, p = 0,004) y una asimetría de oscilación del brazo significativamente mayor (ASA) ($p < 0,001$). También se logró una precisión de más del 90% para distinguir a las personas sanas de las personas con PD usando una cámara Kinect en [Spasojevic2015].

La clasificación entre sujetos sanos y no sanos se realiza en base a las cinco características más relevantes y las dos nuevas características obtenidas de la LDA, utilizando cuatro clasificadores diferentes, máquina de vector soporte (SVM), perceptrón multicapa (MLP), la red neural de base radial (RB) y el vecino más cercano (KNN). Usando el sistema de captura de movimiento Motek CAREN en [Baron2018], se detectó que los pacientes con Parkinson tienen un tirón y un balanceo del brazo diferente en comparación con las personas sanas. El hecho de que los pacientes de Parkinson en las primeras etapas tengan un ASA más grande podría ser combinado en [Lewek2010] con el Vicon y el Baton Rouge sistema de laboratorio de movimiento. El p-valor fue de 0,003, para ver la independencia de los individuos sanos frente a los que tienen la enfermedad de Parkinson. Un sistema Kinect fue utilizado en [Castano2018] para detectar las diferencias de velocidad, amplitud y simetría en el movimiento de los brazos entre las personas sanas y las que se encuentran en las primeras etapas de la enfermedad de Parkinson. En [Dranca2018], se investigó qué método proveía los mejores resultados cuando se usaba una Kinect para detectar las etapas de la enfermedad de Parkinson. Los mejores resultados con una precisión del 93,4% se obtuvieron con un clasificador de redes Bayesianas, usando una validación cruzada de 10 divisiones. Las características relevantes estaban relacionadas con los ángulos de la espinilla izquierda, ángulos del húmero izquierdo, curvas frontales y laterales, ángulos del antebrazo izquierdo y el número de pasos durante un giro. Para las grabaciones en [Castano2019], se utilizó un sistema Kinect en combinación con un programa de captura de e-Motion. El sistema propuesto clasifica la Parkinson's disease en tres estados diferentes relacionados con la freezing de la marcha (FoG). Se ha logrado una precisión del 93,4% usando las características del movimiento y la posición del brazo izquierdo, la posición del tronco para secuencias de caminata ligeramente desplazadas, y la ángulo de la espinilla izquierda para las secuencias de caminata recta. Sin embargo, obtuvieron una mejor precisión del 96,23% para un clasificador que sólo usó características extraídas de los pasos y de los giros al caminar.

En [Tsipouras2012], se desarrolló un método automático para el tratamiento de la discinesia inducida por levodopa (LID). Se usaron giroscopios en el abdomen y el pecho y el abdomen, las muñecas y los tobillos. En general, se logró una cuota media de detección del 90% para los pacientes de Parkinson, y la cuota media de detección y la precisión de las clases individuales (LID, Parkinson, sano) fueron del 80% y el 77%, respectivamente. Se han utilizado varias técnicas de clasificación para evaluación de LID, incluyendo el clasificador Naive Bayes, KNN, fuzzy lattice reasoning (FLR), árboles de decisión, random forests (RF), y una red neuronal usando un perceptrón multicapa (MLP). El método utilizado en [Roggendorf2012] consistía en guiar a los pacientes con Parkinson temprano en una cinta de correr y medir sus movimientos con un dispositivo de ultrasonido en cada lado. Los resultados fueron una reducción de la amplitud del balanceo de los brazos de los pacientes y una mayor longitud de los pasos en comparación con las personas sanas.

En [Huang2012], se utilizó una unidad de sensor en cada antebrazo. Esta unidad sensorial consistía en dos acelerómetros triaxiales G-Link que estaban unidos a una barra de aluminio. La asimetría del balanceo del brazo (ASA), la correlación cruzada máxima (MXC) y la fase relativa instantánea (IRP) del balanceo bilateral del brazo se

compararon entre la PD y las personas de control. Los sujetos con PD demostraron una ASA significativamente más alta (p = 0,002) y una MXC más baja (p < 0,001) que las personas de control.

Se colocó un acelerómetro en la parte superior del brazo, así como un dispositivo de velocidad angular magnética y gravedad (MARG) en el hombro en [Bertomeu2015]. Se utilizó el modelo Denavit- Hartenberg, y el algoritmo se basó en el pseudoinverso del Jacobiano por la aceleración de la parte superior del brazo. Un sistema similar se utilizó en [Viteckova2016] con casi los mismos sensores y la misma posición. Se sugirió un método autovectores para comparar los ejes de la mano izquierda y la derecha. Los resultados mostraron una diferencia entre las personas con la enfermedad de Parkinson y las personas sanas.

3 Metodología

Todo el proceso de reconocimiento de los datos de la marcha se basa en la comunicación entre nuestra aplicación para Android y cuatro wearables (dos pulseras, figura 1 y dos plantillas, figura 2). La figura 3 muestra el proceso. Las tareas funcionales del smartphone, los wearables y el análisis de datos están separados por una línea de puntos. Sin embargo, los wearables trabajan sólo como esclavos, así que el smartphone siempre debe enviar una señal para iniciando una función. Por esta razón las tareas Iniciar grabación, Detener grabación, Sincronización y Transmisión de datos están implicadas en ambos dispositivos.
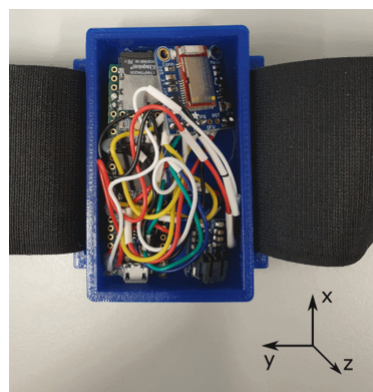
Figura 1 Pulsera con sensor IMU
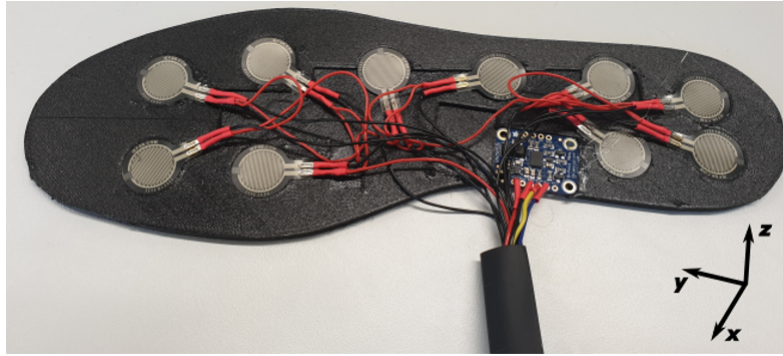
Figura 2 Plantilla con fuerza y IMU sensores.

Al principio del trabajo, se hace un reconocimiento de la actividad. Por lo tanto, se quieren distinguir la actividad de andar de otras actividades. Otras actividades pueden ser las actividades de montar en bicicleta, subir escaleras, acostarse, sentarse, pararse, el smartphone está tumbado (en una mesa o escritorio), el smartphone en uso (escribiendo un mensaje o jugando un juego), o usar el transporte (conducir en coche, autobús o tren). La detección de actividad de andar es diseñada para mantener los sensores en modo de espera hasta que la actividad de andar sea detectada. Esta detección de actividad prolonga el tiempo de uso de los dispositivos., porque sólo se guardan los valores medidos de la actividad andar. Cuando una persona hace de actividad andar, la aplicación comprueba si una grabación está en proceso. Si no, los dispositivos que se han incrustrado primero, y luego comienza la grabación del movimiento. Cuando la actividad de otro tipo, como la marcha ha sido detectada, y la grabación está en proceso, la grabación se detuvo, y los datos transmitido al smartphone para el análisis de datos.

Para las fases de la marcha, las características y el cálculo de la simetría, se necesita una detección más precisa de los pasos que durante el reconocimiento de la actividad. Por esto razón, realizamos una detección de pasos usando la CNN. Después de eso, las fases de la marcha, las características y la simetría de los pasos puede ser calculado.
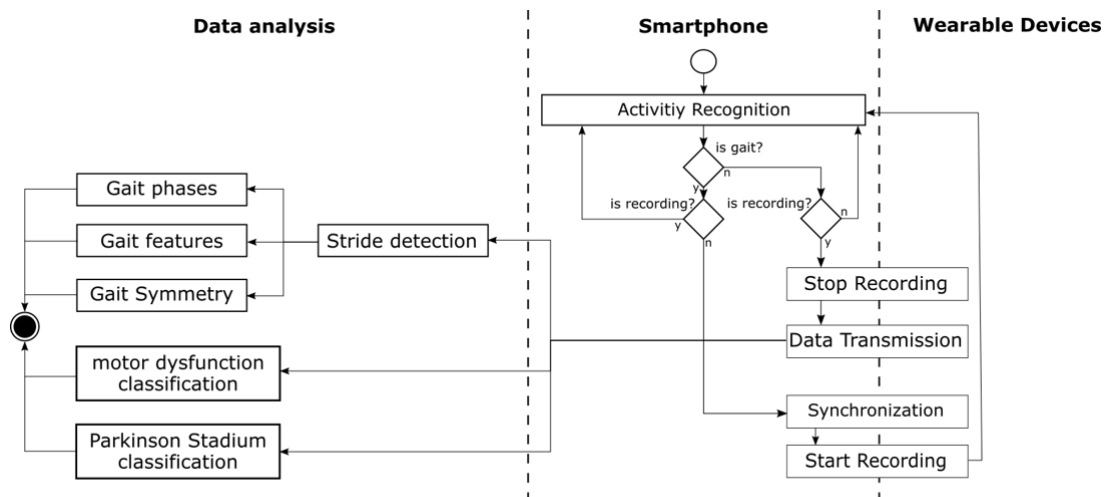
Figura 3 Proceso general del análisis de la marcha

141

Para la clasicación de las disfunciones motoras en el balanceo del brazo y la clasicación del estadio de Parkinson con plantillas, es necesario un proceso independiente.

4 Base de datos

4.1 Base de datos para el reconocimiento de actividades

En este conjunto de datos, usamos las grabaciones de 20 sujetos sanos para probar el sistema. Para esta propuesta, desarrollamos una aplicación para Android. Los sujetos especificaron el comienzo, el final y el tipo de actividad a través de la aplicación antes de cada grabación. Grabamos los datos de aceleración lineal y rotación del sistema operativo de Android con una frecuencia de 50Hz. Los usuarios tendrán que especificar qué actividad van a realizar. En total, se registraron las siguientes actividades: andar, ir en bicicleta, ir por las escaleras, acostarse, sentarse, pararse, smartphone en uso (mesa o escritorio), smartphone en uso (escribir un mensaje o jugar a un juego), y usar el transporte (conducir en coche o tren). Hemos reducido el problema a un problema binario y usamos en las siguientes clases sólo andar y otras. La clase "otras" contiene las actividades de ciclismo, ir a las escaleras, acostarse, sentarse, smartphone estático, smartphone en uso, de pie y en transporte.

4.2 Base de datos de Timed Up and Go (TUG)

Decidimos usar la prueba del TUG, figura 4, como una prueba adecuada para registrar los datos de la marcha. Entre otras cosas, se utiliza para evaluar el rendimiento motor de las United Parkinson Disease Rating Scale (UPDRS). Para la prueba, sólo se necesitaba una silla con respaldo y apoyabrazos. Primero, la persona de la prueba estaba sentada en una silla. A la orden de quien dirige el experimento, la persona que realiza la prueba se levanta y camina en línea recta durante diez metros a una velocidad apropiada hasta una marca. En la marca, la persona que realiza la prueba, se da la vuelta y camina diez metros en línea recta, de vuelta a la silla. El sujeto que hace la prueba, se sienta y finalmente la prueba y la grabación terminan. Para crear un conjunto de datos para su posterior análisis, trabajamos junto con la Clínica Niederlausitz en el estudio "Desarrollo de una evaluación digital de la enfermedad de Parkinson" (solicitud de ética concedida en diciembre de 2018 por el Comité de Ética de Brandenburgo). Todas las personas fueron evaluadas por los médicos. Se disponía de un total de 39 personas diferentes con 250 grabaciones para la data set. De ellos, había 15 pacientes con disfunción motora con 80 grabaciones y 24 personas con 170 grabaciones como grupo de control.
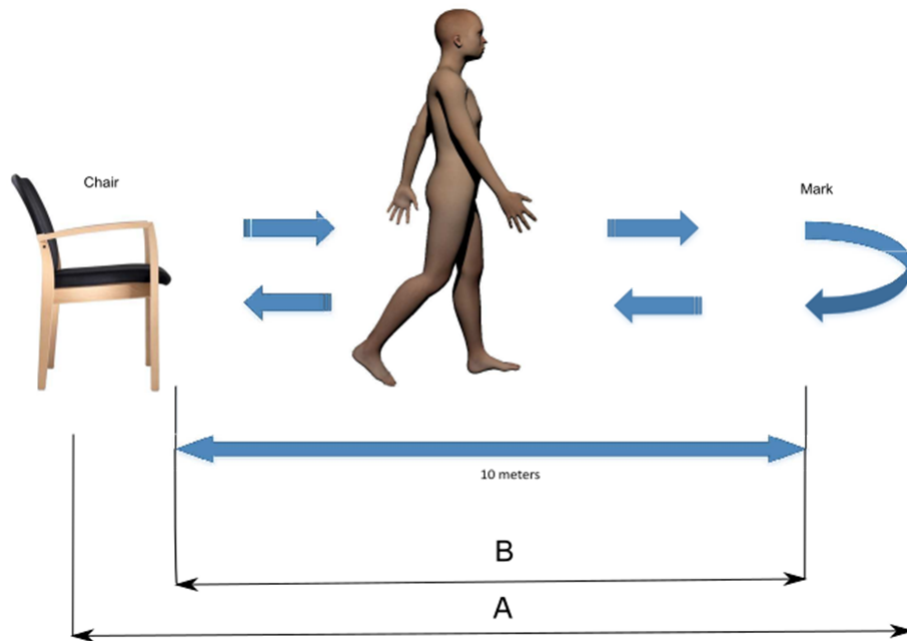
Figura 4 El proceso de la prueba Timed Up and Go (TUG)

4.3 Base de datos de la vida cotidiana

Para la data set de las actividades de la vida diaria tenemos un total de 7 grabaciones de 7 personas sanas diferentes. La edad de las personas estaba entre 25 y 54 años. En total, cada persona pasó la prueba una vez. Durante el experimento los sujetos tuvieron que pasar la siguiente prueba. Al principio de la prueba, la persona se sienta en una silla durante un minuto. Luego la persona se levanta de la silla y se pone de pie por un minuto. Después de eso, la persona camina de un lado a otro durante un minuto. Luego, la persona sube las escaleras tres pisos y luego baja las escaleras. Luego, la persona camina un minuto más y termina frente a una silla. La persona pasa un minuto de pie. En el penúltimo paso, la persona cambia repetidamente durante un minuto de una posición de pie a una de sentado. Finalmente, la persona se sienta por un minuto en la silla.

4.4 Base de datos público de la fuerza

Para el cálculo de la simetría de la marcha usamos la fuerza de los datos del sensor. Para ello utilizamos una data set público. Se trata de 93 pacientes con PD idiopática, y 73 sujetos del grupo de control. La base de datos incluye los datos de la fuerza de reacción del suelo vertical de los sujetos mientras caminaban a su ritmo habitual, auto-seleccionado, durante aproximadamente 2 minutos en suelo llano, ver Tabla I. Debajo de cada pie había 8 sensores (Ultraflex ComputerDyno Graphy, Infotronic Inc.) que miden la fuerza (en Newtons) en función del tiempo. La salida de cada uno de estos16 sensores ha sido digitalizada y grabada a 100 muestras por segundo, y las grabaciones también incluyen dos señales que reflejan la suma de las salidas de los 8 sensores para cada pie. Para

143

detalles sobre el formato de los datos, véase [Goldberger2003].

Table 1: Demographics of the data set

Group	Count	Male/ Female	Age ($mean \pm std$)
PD	93	58/35	66.30 ± 9.50
Control	73	40/33	63.66 ± 8.64

5 Métodos

5.1 Reconocimiento de actividades

Para posibilitar el uso energético de los wearables que se llevan puestos, sólo se activa cuando están en uso. Para un uso eficiente de la energía, los wearables que se pueden usar, sólo tienen que ser activadas durante la grabación. Por esta razón, decidimos usar un clasificador de actividad binario en el smartphone. Este clasificador nos permite distinguir la actividad de andar de otras como ir en bicicleta, ir por las escaleras, acostarse, sentarse, de pie, smartphone en estático, smartphone en uso y usando en el transporte.
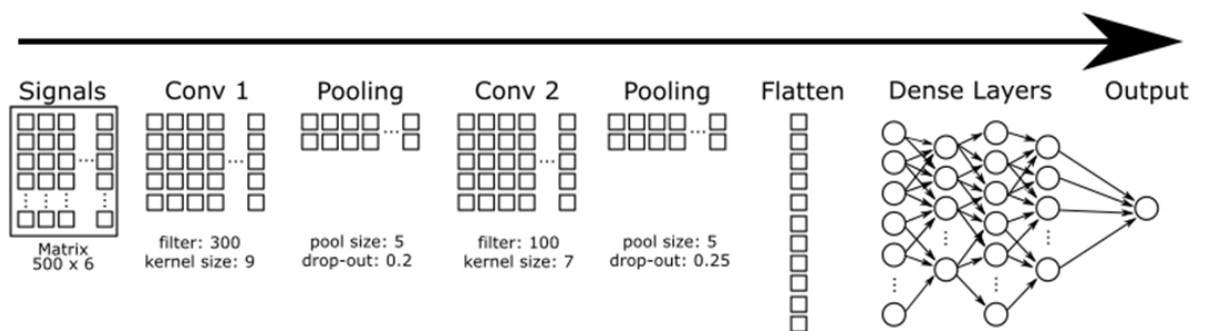
Figura 5 Modelo para que la CNN detecte la actividad *Gait*

Para la detección de la actividad, utilizamos los datos de la aceleración lineal y los datos de rotación del sistema operativo Android (OS) a una frecuencia de 50Hz. Como características, usamos un ancho de ventana fijo de 10s y un solapamiento del 50%. Usamos el tamaño completo de la ventana y todos los ejes de los datos del sensor como entrada para un clasificador 1D CNN. La figura 5 muestra el diseño de la CNN. Elegimos CNN porque otros investigadores también han logrado buenos resultados con la CNN [Gadaleta2018, Hassan2018]. Para la formación, hemos separado los datos por personas. Esto asegura que la misma persona no está incluida en el conjunto de datos de entrenamiento y pruebas. Dividimos los datos en que el 66% se utiliza para el entrenamiento y el 34% para las pruebas. Durante el entrenamiento, usamos diferentes épocas y tamaños del batch. En nuestro caso, el ajuste de 100 épocas y 100 del tamaño del batch, han dado buenos resultados.

5.2 Reconocimiento de pasos

En esta sección queremos presentar dos métodos comparables, Min-Max-Pattern (MMP) y Dynamic Time Warping (DTW), y nuestro método Convolutional Neural Networks (CNN) para el reconocimiento de pasos. Esto incluye el preprocesamiento, los algoritmos para la detección de pasos y el proceso de validación. En la figura 3 se presenta una visión general de los diferentes procesos de detección de pasos.

MMP   La forma más simple de detectar trazas es rastrear un patrón Mínimo-Máximo (MMP). Este patrón es típico en la marcha humana. Sin embargo, este patrón también se presenta en otras secuencias de movimiento, por ejemplo, subir escaleras. Por esta razón, este patrón no es una elección ideal [Barth2015]. Sin embargo, hemos incluido el procedimiento para completarlo.

DTW   Las señales se normalizan primero antes de que el algoritmo de detección de pasos comienza. Nuestro algoritmo está fuertemente basado en el algoritmo presentado por Barth [Barth2015].

CNN   Las CNN se están popularizando cada vez más porque logran resultados significativamente mejores que los NN tradicionales. Las CNN se utilizan principalmente para el reconocimiento de imágenes, pero son igual de potentes en la detección de señales.
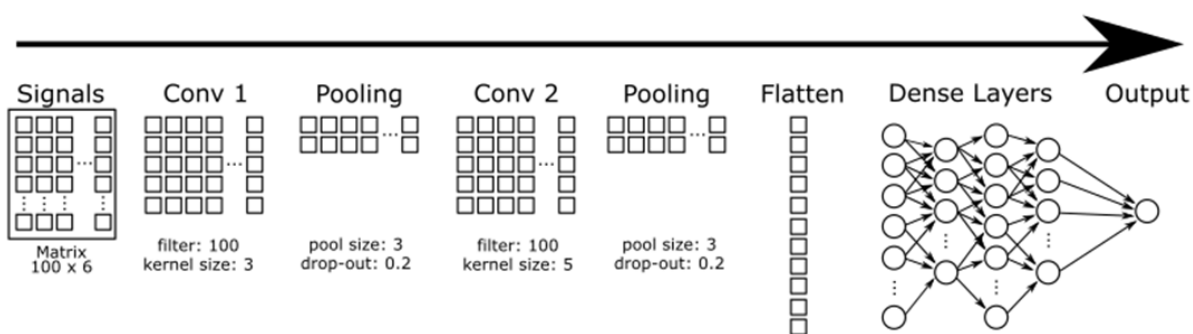
Figura 6 Modelo para que la CNN reconozca los pasos

La diferencia entre las NN y las CNN es que las CNN aprenden patrones locales. Por el contrario, las NN tradicionales siempre usan la entrada completa. La arquitectura convolucional multicapa le permite aumentar la complejidad de la detección. Así, es posible reconocer en la primera capa sólo los patrones, y con la segunda o n-capa más y más objetos complejos [Abadi2016, Sze2017]. Para nuestro trabajo con las CNN usamos la librería de keras en Python de código abierto con Tensor Flow, figura 6.

5.3 Características de la marcha

5.3.1 Características del tiempo de marcha

Para el cálculo de los tiempos de marcha, se estimaron los tiempos de golpe de talón (HS), dedo del pie (TO), valor medio de fase de balanceo (MSW) y fase de postura media (MST). Se utilizó una combinación de datos de orientación, velocidad angular y fuerza, porque cada señal da información relevante para características particulares de la marcha, figura 7.

Heel Stike (HS) El HS es detectado por los sensores de fuerza en el talón cruzando un valor umbral. Además, el mínimo local en el plano sagital de la velocidad angular entre la fase de balanceo y la fase de apoyo se utiliza para estimar el HS.

Toe off (TO) / Terminal Stance El dedo del pie o el TO también es detectado por los sensores de fuerza. Si los sensores de fuerza en el dedo del pie cruzan un umbral, este es el TO. La velocidad angular también se utiliza para estimar el TO. El mínimo local entre la postura y la fase de balanceo también indica el TO.

Middle Stance phase (MST) Fase de postura media o MST puede ser estimado calculando el promedio de HS y TO.

Middle swing phase (MSW) Fase de oscilación media. Para la identificación del MSW, se puede utilizar la suma de todos los sensores de fuerza. Dentro de la fase de oscilación hay un mínimo local entre los dos máximos. Esto caracteriza al MSW. Además, también es posible utilizar los datos de orientación. En este caso el máximo corresponde a la fase media de balanceo.

Stance phase Fase de apoyo. La fase de apoyo se calcula calculando la diferencia entre TO_i y HS_i.

Swing phase Fase de reposo La fase de reposo se calcula a partir de la diferencia entre HS_{i+1} y TO_i.

146
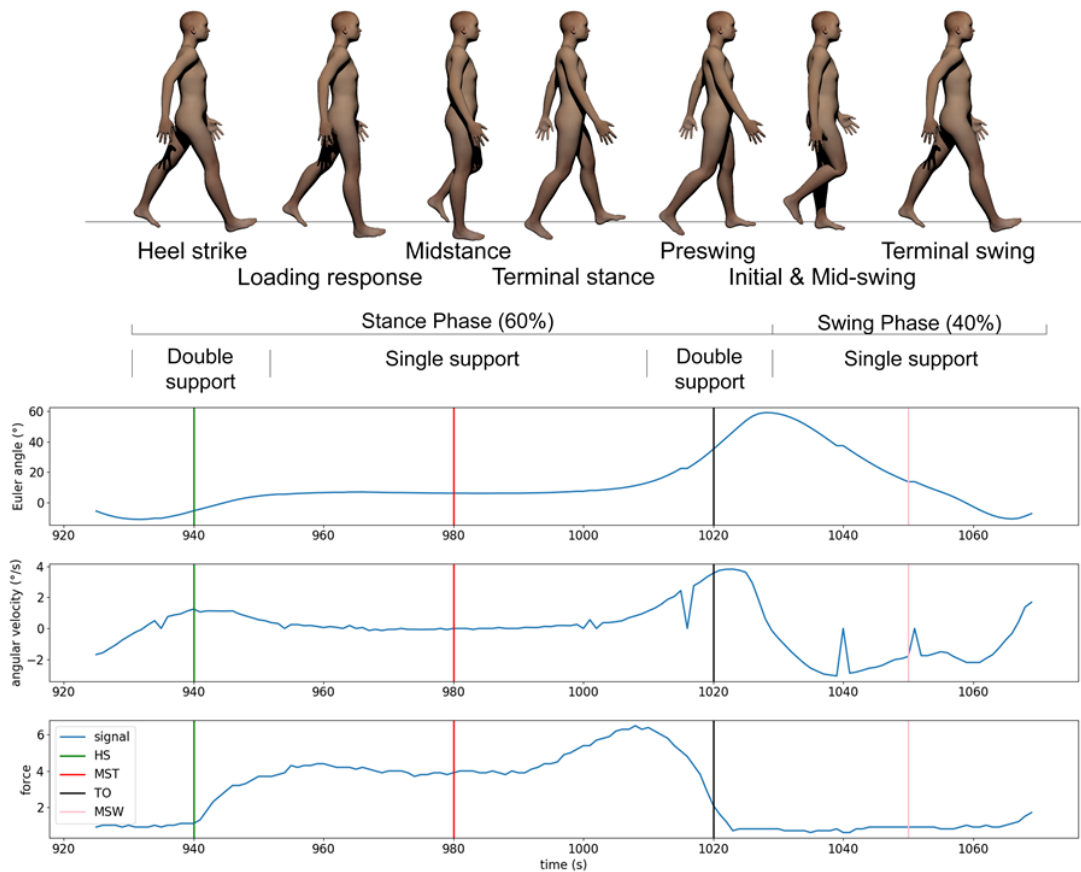
Figura 7 ciclo de marcha, fases de marcha (HS, MST, TO, MSW), y datos de señal de orientación, velocidad angular y datos de fuerza

5.3.2 Características de la marcha espacial

Básicamente, el cálculo de la longitud de los pasos sigue los mismos principios que otros trabajos han mostrado antes. Pero en contraste con las otras obras, el BNO Bosch 055 provee datos de orientación y aceleración lineal. Por esta razón, no es necesario restar la gravedad para obtener la aceleración lineal. Los datos de orientación son el resultado de la integración de las velocidades angulares. Además, los datos de orientación se optimizan mediante la fusión de los sensores.

El tiempo del MST se utiliza como inicio para calcular la longitud y la altura de la zancada. Debido a la deriva del sensor y a la inexactitud del mismo, se calculan al principio del cálculo menos el valor de inicio para los datos de orientación y aceleración a, ver fórmula 1 y 2.

$$\Theta_i = \Theta_i - \Theta_0 \quad (1)$$

$$a_i = a_i - a_0 \quad (2)$$

Stride length Longitud de los pasos La aceleración horizontal se calcula por:

$$a^{hor} = cos(\Theta_i) \cdot a_i^x - sin(\Theta_i) \cdot a_i^z$$

(3)

A siguiente, la aceleración horizontal se integra para obtener la velocidad horizontal.

$$v^{hor} = \int a_i^{hor} di.$$

(4)

Para obtener la distancia horizontal, la velocidad horizontal tiene que ser integrada

$$s^{hor} = \int v_i^{hor} di.$$

(5)

Stride height La velocidad vertical se calcula por

$$a^{ver} = cos(\Theta_i) \cdot a_i^z - sin(\Theta_i) \cdot a_i^x$$

(6)

A continuación, la aceleración vertical tiene que ser integrada para obtener la velocidad vertical

$$v^{ver} = \int a_i^{ver} di.$$

(7)

Para obtener la distancia vertical, la velocidad vertical tiene que ser integrada.

$$s^{ver} = \int v_i^{ver} di.$$

(8)

5.4 Simetría de la marcha

Para el cálculo de la simetría discreta usamos los parámetros xmax y xmin. De esta manera obtenemos un valor entre 0 y 1, porque el valor pequeño es siempre usado en el numerador.

Ratio Index (RI) Índice de Ratio. Para determinar el RI, los valores contrarios de los pies se dividen por cada uno de ellos, ver la ecuación 9.

$$RI = \frac{X_{min}}{X_{max}}$$

(9)

Symmetry Index (SI) Índice de Simetría. El SI da la diferencia entre los parámetros cinemáticos y cinéticos de las extremidades. Hemos ajustado el valor para que 1 represente un marcha simétrica y asimetría 0, ver ecuación 10.

$$SI = 1 - \frac{|X_{min} - X_{max}|}{0.5 \cdot (X_{min} + X_{max})}$$

(10)

Gait Asymmetry La Asimetría de la marcha es similar al Índice de Ratio. Sin embargo, el logaritmo todavía se calculó a partir del resultado.

$$GA = ln\left(\frac{X_{min}}{X_{max}}\right)$$

(11)

Symmetry Angle (SA) Ángulo de simetría. La SA mide la relación entre dos diferentes miembros. Dos parámetros exactamente simétricos forman un ángulo de 45. Tenemos que corregir el valor, un valor simétrico es 1 y un 0 asimétrico, ver ecuación 12.

$$SA = \frac{45° - arctan\frac{X_{min}}{X_{max}}}{90°}$$

(12)

5.5 Simetría DTW normalizada

Para medir la distancia de simetría entre las series temporales (pasos) del pie derecho y del izquierdo, usamos el DTW. La DTW se ha establecido muy bien en el análisis de señales de series temporales. A diferencia de la distancia euclidiana, este método puede compensar la distorsión temporal. Basado en esta flexibilidad, es un método conocido para el análisis de las series temporales en la medicina, la ciencia y la industria. La idea con DTW es que no se calcula la distancia de dos índices, sino la distancia a la más adecuada. Así permite comparar las series temporales entre sí si se registran con diferente duración o frecuencia. Antes de que la simetría sea calculada por DTW, las series temporales son primero estandarizadas y normalizada. En el primer paso, el algoritmo calcula las distancias entre la serie temporal $(x_i)1 \leq j \leq n$ (fuerza del pie derecho) de longitud $(y_j)1 \leq j \leq m$ (fuerza del pie izquierdo) de longitud m, resultando en una matriz de n veces m $D = D_{ij}$ conteniendo distancias D_{ij} entre y_j y x_i.

$$D_{ij}^{norm} = dist(x_i, y_i) + min\{D_{i-1,j}, D_{i-1,j-1}, D_{i,j-1}\}$$

(13)

Una distancia D_{ij} de 0 significa una simetría del 100% de los valores medidos. Cuanto más alto es el valor D_{ij} , más baja es la simetría de los extremidades. Entonces la distancia debe ser dividida por el número de la longitud máxima de la señal.

$$dist(x_i, y_i) = \frac{\sqrt{(x_i - y_j)^2}}{max(\{length(X), length(Y)\})}$$

(14)

Para obtener un resultado de 1 para la simetría y 0 para la asimetría, este se calcula usanod la ecuación 15.

$$DTW_{ratio} = 1 - DTW_{n,m}^{norm}$$

(15)

5.6 Balanceo del brazo

Después de haber presentado nuestro material y métodos, ahora discutiremos en esta sección cómo aplicamos estos métodos. En la presentación del conjunto de datos, nosotros ya dijo que dividimos nuestra grabación en dos partes diferentes. Primero, nosotros las partes clasificadas (A) y (B), que comprendían el registro completo de la prueba del TUG.

El otro escenario era que sólo usábamos la Parte (B). En la Parte (B), sólo el se usó el modo de andar. La figura 8 muestra el algoritmo completo de la clasificación. En principio, distinguimos entre las señales de los ángulos de Euler y la aceleración lineal. Primero, eliminamos los saltos dentro de una señal de los ángulos de Euler y luego calculamos la derivación de la señal. Esto hizo que la señal fuera más comparable. Estos pasos no eran necesarios para la aceleración lineal. Entonces, fijamos las señales a una longitud uniforme. Esto era necesario para que las señales pudieran ser interpretadas por la CNN más tarde durante la clasificación. Después del resampling, calculamos la wavelet transformación para cada señal individual. Usamos las escalas resultantes para la clasificación. En las clasificaciones, analizamos tres casos diferentes. Al principio, clasificamos cada señal individualmente por la CNN. Esto nos permitió mostrar qué eje de los sensores era muy importante. En el segundo caso de clasificación, usamos las tres mejores señales para una CNN multicanal. El tercer caso fue que usamos las tres mejores señales para la clasificación por medio de la votación.
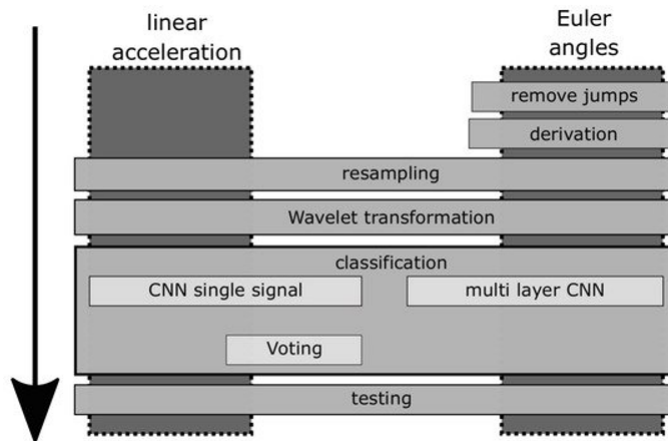
Figura 8 Proceso de clasificación para detectar disfunciones motoras en el balanceo del brazo.

5.7 DTW para reconocer el estadio de PD

Realizamos hierarchical clustering [Handl2002]. Basado en la distancia de todos los pasos entre dos personas. Esta distancia se obtiene como la distancia de todos los pasos durante el TUG para las dos grabaciones. Realizamos la hierarchical clustering de acuerdo con el método de Complete-Linkage, así como con el de Single-Linkage y utilizar el algoritmo aglomerado. Para facilitar la comprensión, se omiten el inicio, el giro y el final de la grabación y aquí sólo se utilizaron pasos sencillos.

6 Discusión

6.1 Hardware

Como ya se ha demostrado en el Estado del Arte, hay un gran número de sistemas de análisis de la marcha [Muro2014, Buckley2019, Sprager2015, Taborri2016, Ferrari2013, Muro2014]. También los sensores utilizados son claramente limitados. Sin embargo, en esta obra se realizó un sistema que consiste en dos plantillas y dos pulseras sin cables. Lo que hace que este sistema sea único. El sistema utilizaba 10 sensores de fuerza y un sensor IMU integrado en cada plantilla y un sensor IMU integrado en cada pulsera. En la investigación de la literatura no hay un sistema similar, con lo que es innovador. Además, otros trabajos se han limitado en su mayoría al análisis de las extremidades inferiores. Sin embargo, este sistema todavía tiene dos pulseras. Estas proveen datos adicionales de las extremidades superiores. Pudimos producir plantillas y muñequeras para el hardware mediante la impresión en 3D. Una desventaja de este sistema es que la electrónica de los prototipos usados fue soldada a mano. Esto dio lugar a uniones de soldadura en frío o que el contacto tuviera roto.

6.2 Reconocimiento de actividades

Al desarrollar una aplicación Android para el reconocimiento de actividades, pudimos mostrar que un smartphone puede distinguir entre la actividad de andar y otras actividades como estar de pie, acostarse, andar en bicicleta o escribir mensajes. Con una precisión del 94.7% obtenemos resultados similares a los de otros investigadores [Gadaleta2018, Hassan2018, Cao2018]. El reconocimiento de actividad nos permite encender los sensores de los wearables sólo cuando se reconocen la actividad marcha. Esta propuesta es una solución en materia de eficiencia energética.

6.3 Sincronización

Cuando se registran datos con varios sensores, se tiene el problema de la sincronización temporal. En la literatura, este problema ya ha sido reconocido, y hubo varios métodos. Sin embargo, el problema es que los dispositivos de Mbientlab sólo pueden sincronizar tres dispositivos [Anwary2018b]. Otra solución fue sincronizar el tiempo durante la carga por cable [Mancini2011]. Sin embargo, esta solución tiene la desventaja de que en un uso más extendido, se produce una deriva del reloj. Presentamos una solución para sincronizar varios sensores incrustados en prendas. Sincronizamos cuatro prendas, para las cuatro extremidades. Sincronizamos los wearables antes de cada grabación (reconocimiento de la actividad de marcha). De esta manera, empezamos cada grabación sin deriva del reloj.

6.4 Reconocimiento de pasos

Los métodos presentados han demostrado que el problema de la detección de pasos puede resolverse de muchas formas diferentes. El mejor performance en nuestras pruebas fue logrado por el AF-CNN. La ventaja del clasificador AF-CNN es que no requiere un valor umbral. Además, el AF-Algoritmo permite analizar los datos durante la grabación. Además, hemos demostrado que la combinación de la fuerza y los sensores IMU puede aumentar los resultados aún más, aunque se pueden producir pequeños errores. En nuestra opinión, el reconocimiento del paso es el punto más importante en el análisis de la marcha humana, porque todos los parámetros dependen del paso. Si no se reconoce bien el paso, se producirán más errores en un análisis más detallado. Como una cómoda posibilidad para usar instrumentos de medición para las personas con motor disfunciones como en la enfermedad de Parkinson, proponemos una combinación de fuerza y sensores IMU en pulseras y plantillas.

6.5 Características de la marcha

Con los resultados de las características de la marcha podríamos confirmar los resultados de otros trabajos [Rampp2014, Salarian2004, Ferster2015, Wang2015, Hsu2014, Bamberg2008, Rampp2014, Tunca2017, Sijobert2015, Mariani2010, Ferrari2015, Salarian2004, Ferster2015, Wang2015, Hsu2014]. También se incluyeron las características de longitud del paso, altura del paso, número de los pasos, duración del paso, duración de la fase de

apoyo y la fase de balanceo, y tiempos de golpe de talón, valor medio de fase de apoyo, dedo del pie y valor medio de fase de balanceo. Estas características ayudan al médico a detectar las anomalías de la marcha, ya que también se utilizan para los diagnósticos.

6.6 Simetría

En la mayoría de los trabajos que tratan de la simetría, utilizan la longitud del paso, la duración del paso y las diferentes fases de la marcha para calcular la relación entre la pierna izquierda y la derecha [Barth2015, Hannink2018, Watanabe2018, Jiang2018]. Para esto la sincronización de todos los sensores es esencial.

Para la detección de pasos, usamos una combinación de enmarcado automático y CNN. El uso de CNN para la detección de pasos ha demostrado ser muy útil para nosotros [Steinmetzer2019a]. Otros trabajos ya han podido beneficiarse de la tecnología [Steinmetzer2018].

La simetría de las piernas se analizamos con DTW. Nuestros resultados para RI, SI, GA, SA, y DTW confirman los resultados de otros estudios de simetría discreta [Blazkiewicz2014, Hubble2015] para la misma base de datos estudio 2019/20.

Si los parámetros fueron elegidos incorrectamente en el cálculo de simetría, las asimetrías de la marcha pueden no ser visibles. Podríamos demostrar este fenómeno en la segunda parte de los resultados. En la figura 9 en (c), (e), y (f) la simetría discreta fue siempre 1.0, pero las señales eran diferentes en la amplitud. Estas diferencias no podían ser calculados usando la simetría discreta. Usando nuestro método presentado, la señal completa fue usada para el cálculo de la simetría. Así, fue posible calcular no sólo las diferencias de simetría en el tiempo, así como en el dominio de la amplitud.
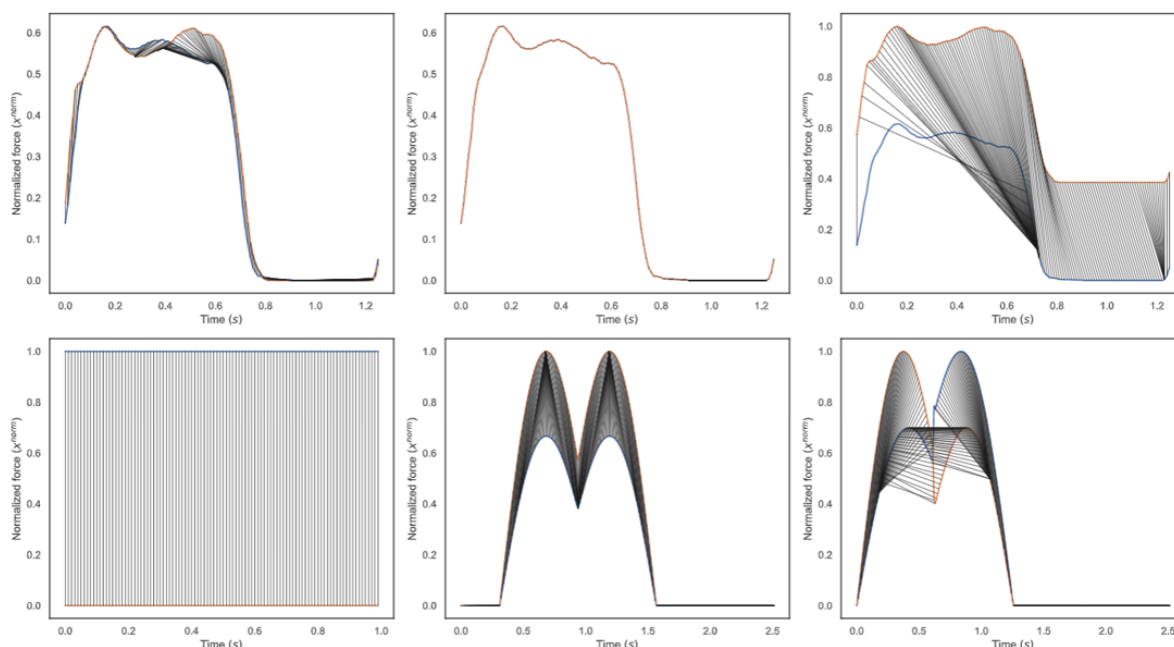
Figura 9 Resultados de la simetría usando DTW

En este trabajo pudimos demostrar que nuestro método presentado es una extensión útil para el cálculo de la simetría de la marcha con sensores que se pueden llevar puestos. En futuros trabajos se debería probar cómo el cálculo de la simetría con el DTW funciona en señales multidimensionales. Además, el cálculo de la simetría no sólo debe aplicarse a los sensores de fuerza, sino que también debe aplicarse a las señales de orientación, aceleración lineal, velocidad y posición.

6.7 Balanceo del brazo

El eje x siempre muestra los mejores resultados. El eje x corresponde al movimiento en el plano sagital. Según la literatura, las características más importantes de la marcha humana también están presentes en este plano [Zhang2007, Tafazzoli2010]. Por esta razón, es una conclusión lógica que las características de mayor importancia están presentes en este eje. Presentamos nuestros resultados en la sección anterior.

Comparamos los resultados cuando la prueba completa del TUG, Partes (A) y (B), fue usada para la clasificación, así como si sólo usáramos la actividad andar recto, Parte (B), para la clasificación. Los resultados mostraron que, para la clasificación de las disfunciones motoras, la actividad andar recto daba resultados bastante buenos con una precisión del 90,3%, pero cuando se mira la prueba completa hemos obtenido resultados aún mejores con una precisión del 93,3%. A partir de esto, concluimos que la prueba completa del TUG era necesaria para el análisis de disfunciones motoras.

Además, clasificamos cada señal por separado. Durante la clasificación, descubrimos que el eje x (movimiento en el plano sagital) del ángulo de Euler y la aceleración lineal daban los mejores resultados, independientemente de si las partes (A) y (B), así como sólo la parte (B) se usaron para la clasificación. A partir de esto, concluimos que el eje x era el más relevante.

La conclusión fue que obtuvimos mejores resultados a base de la combinación de las señales en comparación con las señales individuales. En la clasificación de las partes (A) y (B), la CNN de tres capas resultó ser la mejor solución Al clasificar con sólo la Parte (B), la votación fue la mejor opción. Los trabajos, que usaron sistemas estacionarios con sólo camera Kinect [Spasojevic2015] recibieron una precisión de 90%, con la combinación de camera Kinect y redes bayesianas [Dranca2018] , se obtuvo un 93,4%, con camera Kinect y programa e-Motion capture [Castano2019] 96,23%. Nuestro sistema reconoció los persones con lesiones de movimiento con una precisión del 93,3% y así es comparable a los sistemas estacionarios y provee mejor resultados que el sistema con giroscopio [Tsipouras2012] , que obtuvo una precisión del 90%.

No pudimos hacer una comparación con los otros trabajos porque se centraron en una evaluación estadística de los datos en lugar de una clasificación. La CNN en combinación con wavelet transformación es una poderosa técnica para el análisis del balanceo del brazo.

6.8 Reconocimiento de estado de Parkinson usando DTW

Finalmente se puede concluir que la plantilla del sensor utilizada para este estudio es muy adecuada para medir las disfunciones motoras. Hierachical clustering en combinación con Single-Linkage y DTW es útil para detectar los valores atípicos dentro de una grabación. Hierachical clustering en combinación con Complete-Linkage y DTW hace una clara distinción entre los sujetos y el estadio del desorden de la marcha. También demostramos que los datos de aceleración lineal a una velocidad de 100Hz son suficientes para sacar conclusiones sobre la salud motora de una persona. Resultó suficiente utilizar sólo los datos recogidos de un pie para distinguir los diferentes niveles de desorden de la marcha. Esto está probablemente relacionado con el hecho de que la pierna sana tiene que compensar los movimientos de la pierna enferma y por lo tanto no se mueve normalmente.

Se podrían lograr más mejoras utilizando datos adicionales sensores, como los ángulos absolutos y los datos de presión, así como utilizando los datos de los sensores de ambos pies. Otras clasificaciones posibles son k-Nearest-Neighbor o redes neuronales y así sucesivamente. Además, también podría aumentarse el número de dimensiones para su uso práctico a fin de aumentar la tasa de reconocimiento.

7 Conclusión

Durante el trabajo, se pudo validar la hipótesis de esta tesis docotral, y se pudieron resolver muchos problemas. En contraste con un complejo sistema de análisis de la marcha como el Vicon, se pudo desarrollar una alternativa de sensores portátil, cómodo para llevar en la vida diaria por los pacientes y más económico que un sistema estacionario. Con este sistema es posible evaluar el éxito de la terapia, los desórdenes motores y el estadio de Parkinson mediante el uso de wearables en la vida cotidiana. Se desarrolló una Android aplicación, que puede extraerse la actividad caminar de todas las actividades de movimiento con una precisión del 94,7%. Sincronizamos cuatro prendas para cuatro extremidades, por el desarrollo de una Android aplicación de smartphone. La sincronización de los wearables tiene una deriva del tiempo de un máximo de 3ms. Sincronizamos los wearables antes de cada grabación (reconocimiento de la actividad caminar). De esta manera, empezamos cada grabación sin la deriva del tiempo. Los pasos individuales pueden ser extraídos automáticamente por uso de CNN de la serie de tiempo de los valores medidos. Reconocemos los pasos individuales con una precisión del 98,8%. De las series temporales de la marcha se pueden determinarse los valores de simetría de la marcha más exacto que de las características de los pasos individuales. Determinamos varios parámetros de la marcha, como la duración y la longitud y la altura de los pasos, los tiempos de las fases de la marcha y los parámetros de simetría. Además, se desarrolló una nueva forma de calcular la simetría mediante el uso de series temporales y DTW, que, a diferencia del uso de parámetros, evita valores de simetría incorrectos en casos especiales. De las series temporales de la marcha se pueden determinar el estadio de Parkinson por uso de DTW con una sensibilidad del 90%.

C
Erasmus

Certificado de estancia
Movilidad de estudiantes para prácticas en empresa

CERTIFICADO DE ESTANCIA - CERTIFICATE OF ATTENDANCE
PROGRAMA ERASMUS PRÁCTICAS

Academic year: 2019/2020
Name of the host company/institution: Brandenburg University of Technology Cottbus-Senftenberg
Host Country: Germany

I. LLEGADA - ARRIVAL

- TO BE COMPLETED AT ARRIVAL TIME -

IT IS HEREBY CERTIFIED THAT:

Mr./Ms. Tobias Steinmetzer

from the University of Las Palmas de Gran Canaria **has arrived as a ERASMUS-PRACTICUM trainee** at your company/institution in the Department (s) Institute of Medical Technology **Date of arrival**: 01/09/2019

Name of the signatory: Prof. Dr. Ingrid Bönninger
Function: Erasmus coordinator for ULPGC

Date
08/05/2020

Stamp and Signature of Training Programme Tutor

Brandenburgische Technische Universität
Cottbus-Senftenberg
Fakultät 1
Institut für Medizintechnologie
Universitätsplatz 1
01968 Senftenberg

II. SALIDA - DEPARTURE

- TO BE COMPLETED AT DEPARTURE TIME -

IT IS HEREBY CERTIFIED THAT:

Mr./Ms. Tobias Steinmetzer

from the University of Las Palmas de Gran Canaria has **been a ERASMUS-PRACTICUM trainee** at your company/institution, **between** 01/09/2019 **and** 30/04/2020 in the Department (s) Institute of Medical Technology, Brandenburg University of Technology Cottbus-Senftenberg

Name of the signatory: Prof. Dr. Ingrid Bönninger
Function: Erasmus coordinator for ULPGC

Date
08/05/2020

Stamp and Signature of Training Programme Tutor

Brandenburgische Technische Universität
Cottbus-Senftenberg
Fakultät 1
Institut für Medizintechnologie
Universitätsplatz 1
01968 Senftenberg

158

D
Publications

- Steinmetzer, T., Bonninger, I., Priwitzer, B., Reinhardt, F., Reckhardt, M. C., Erk, D., & Travieso, C. M. (2018, July). Clustering of Human Gait with Parkinson's Disease by Using Dynamic Time Warping. In 2018 IEEE International Work Conference on Bioinspired Intelligence (IWOBI) (pp. 1-6). IEEE.

- Steinmetzer, T., Bönninger, I., Reckhardt, M., Reinhardt, F., Erk, D., & Travieso, C. M. (2019). Comparison of algorithms and classifiers for stride detection using wearables. Neural Computing and Applications, 1-12.

- Steinmetzer, T., Maasch, M., Bönninger, I., & Travieso, C. M. (2019). Analysis and Classification of Motor Dysfunctions in Arm Swing in Parkinson's Disease. Electronics, 8(12), 1471.

- Steinmetzer, T., Piatraschk, S., Bönninger, I., Travieso, C. M., & Priwitzer, B. (2019, July). Gesture Recognition with 3D Sensors using Hidden Markov Models and Clustering. In 2019 IEEE International Work Conference on Bioinspired Intelligence (IWOBI) (pp. 000127-000132). IEEE.

- Steinmetzer, T., Wilberg, S., Bönninger, I., & Travieso, C. M. (2020). Analyzing gait symmetry with automatically synchronized wearable sensors in daily life. Microprocessors and Microsystems, 103118.

- Lohse, P., Steinmetzer, T., Reichmann, H., Reckhardt, M., Bönninger, I., & Reinhardt, F. (2020). Optimierung der Langzeitbetreuung von neurologischen Patienten durch internet-und mobile-basierte Interventionen ohne und mit persuasiven Elementen einschließlich der Gamification. Fortschritte der Neurologie· Psychiatrie.

DEVELOPING NATURE-INSPIRED INTELLIGENCE BY NEURAL SYSTEMS

Comparison of algorithms and classifiers for stride detection using wearables

Tobias Steinmetzer[1,2] · Ingrid Bönninger[1] · Markus Reckhardt[1,4] · Fritjof Reinhardt[1,4] · Dorela Erk[4] ·
Carlos M. Travieso[3]

Abstract

Sensor-based systems for diagnosis or therapy support of motor dysfunctions need methodologies of automatically stride detection from movement sequences. In this proposal, we developed a stride detection system for daily life use. We compared mostly used algorithms min–max patterns, dynamic time warping, convolutional neural networks (CNN), and automatic framing using two data sets of 32 healthy and 28 Parkinson's disease (PD) persons. We developed an insole with force and IMU sensors to record the gait data. The PD patients carried out the standardized time up and go test, and the healthy persons a daily life activities test (walking, sitting, standing, ascending and descending stairs). As an automatically stride detection process for daily life use, we propose a first stride detection using automatic framing, and after normalization and resampling data a CNN is used. A $F1$-score of 0.938 (recall 0.968, precision 0.910) for time up and go test and of 0.944 (recall 0.992, precision 0.901) for daily life activities test were obtained for CNN. Compared to the other detection methods, up to 6% F-measure improvement was shown.

Keywords Stride detection · Gait analysis · Inertial sensors · Parkinson's disease · Validation · Dynamic time warping · Time up and go test · Convolutional neural networks

1 Introduction

Parkinson's disease (PD) is a chronic neurodegenerative and progressive disease that affects 10 million persons all over the world [1]. At an advanced stage of Parkinson's disease, affected individuals can be unable to control their movements. Movement disorders in Parkinson's can include tremor, rigidity (reduced movement due to muscle tension), akinesia (immobility) and postural instability [2]. The aim of our cooperation with the Center of Neurology and Pain Management of the Niederlausitz Clinic Senftenberg is to support the diagnosis and measurement of the long-term therapeutic success of the motor side of idiopathic Parkinson's syndrome. During the last decade, a large number of technology-based tools have been developed to measure motion disorders in PD in order to make diagnosis more objective [11]. A second goal of the development of devices for the measurement of movement disorders is to measure the therapy success in order to motivate the patient to actively participate in the therapy [2].

Gait recognition methods are divided into model-free and model-based approaches [3–6].

- Model-free approaches use gait representations such as silhouette, texture, and colour to extract static gait features, and dynamic gait features such as joint trajectories [6, 7]. Model-free approaches usually focus on changes in the appearance of individuals rather than on gait dynamics.

✉ Tobias Steinmetzer
tobias.steinmetzer101@alu.ulpgc.es;
tobias.steinmetzer@b-tu.de

1 Brandenburg University of Technology Cottbus-Senftenberg, Institute of Medical Technology, Universitätsplatz 1, 01968 Senftenberg, Germany

2 University of Las Palmas de Gran Canaria, Empresa, Internet y Tecnologías de las Comunicaciones, Las Palmas de Gran Canaria, Spain

3 University of Las Palmas de Gran Canaria, Signals and Communication Department, IDeTIC, Las Palmas de Gran Canaria, Spain

4 Niederlausitz Clinic, Center of Neurology and Pain Management, Senftenberg, Germany

- Model-based approaches such as [8–10] create movement models to extract features [3–5], e.g. stride length, height, and frequency. For diagnostic support and measurement of therapy success, we recommend model-based approaches because they are more resistant to changes in view and scale.

Movement disorders that influence the patient's gait are measured with sensors such as gyroscopes, accelerometers, magnetometers, pressure sensors and image sensors. Accelerometers and gyroscopes are often used in combination with a magnetometer [12–17]. The sensors can be integrated into smartphones [14, 18] or attached to the ankle [12, 16, 19] or body [15]. For video recordings for gait analysis, a depth sensor is sometimes used in addition to the 2D image [20]. Force sensors are installed in insoles [21–23] and substrates [24].

The goal of many researches is a stride detection, and others are concerned on activity recognition. Stride detection recognizes as exactly as possible single strides in a time series. In contrast, activity recognition detects different kinds of movement, e.g. walking, standing, jogging. A standardized test for the diagnosis of Parkinson's disease is the time up and go test. This test is also used, for example, by [22] to differentiate between healthy and Parkinson's patients. We also used this test in [23] under ideal hospital conditions for an approximate estimation of Parkinson's stage.

In this proposal, we want to compare the most frequently used methods for stride detection, namely min–max patterns (MMP), dynamic time warping (DTW), convolutional neuronal networks (CNN) in order to be able to use the best variant of stride detection in daily life, independent of motor disorders.

A low-pass digital filter to eliminate the high-frequency noise components of raw accelerometer measurements is used in [14]. Thereafter, the authors ensure that only one peak is detected for each zero crossing of normal of gravity.

In [21], they define stride candidates by determining the beginning of the gait phase and calculate the stride duration. Strides with two phases and a short duration are first merged with preceding strides and afterwards with successive strides.

A stride recognition rate of 97% is achieved in [12] with the multi-dimensional subsequence DTW with free walking. Using this method, a threshold value is fixed. This worsens the results for abnormal movements or climbing stairs [12].

Mild Cognitive Impairment (MCI) in gait is classified in [25]. Photoplethysmography (PPG) and gait (accelerometer and gyroscope) sensor data were recorded. The Butterworth filter was used to remove noise from the measured gait signals. To detect strikes, a peak detection algorithm that works with minimum peak height and minimum peak distance was used.

For normal walking conditions, the frequencies of the stride have been assumed to range from 1 to 3 Hz. In [18], gravitational acceleration is filtered by using a bandpass filter with a center frequency of 2 Hz and a bandwidth of 2 Hz. Strides are detected using the Stride Feature of Spectrogram methods and an artificial neural network (ANN) architecture.

Gait parameters analysed in [24] such as speed, stride time and stride length are delivered by a gait mat of the GAITRite® instrumented walkway system.

In [15], foot- and body-mounted IMUs are used for stride detection. Strides were labelled using a threshold. The stride detection was performed by a residual neural network. For the training process, cross-entropy function was used as the loss function.

In a preprocessing step in [16], the signals from accelerometer and gyroscope are normalized and scaled to a fixed length of 256 samples per stride to ensure equally scaled and fixed size input to the network. Mid-stance (MS) and heel-strike (HS) are detected. For stride detection, a two-layer convolutional network followed by one fully connected layer and a readout-layer is chosen.

The advantage of neural networks (NN), hidden Markov models (HMM) and regression-based systems is that they do not require a threshold.

In order to be able to carry out gait measurements at home without laboratory conditions, we have designed insoles with installed sensors. To find the best method of stride detection, we compare in this proposal the most used methods min–max patterns, dynamic time warping, convolutional neuronal networks, and daily life activities test on the basis of two data sets from 32 healthy and 28 PD persons.

We would like to propose a system that recognizes the walking strides of Parkinson's patients in daily life. To the best of our knowledge, there is no other study detecting strides

1. automatically
2. without a manually set threshold
3. independent of motor dysfunction
4. independent of the Parkinson's stage of the patient
5. exclusively from walking activity (not from, e.g. descending, ascending stairs, sitting activities)

This work is divided into six sections. Section 2 describes the developed hardware, the tests performed by patients and healthy persons. The preprocessing procedures normalization, resampling, and ideal stride forming are described in Sect. 3. The stride detection methods we compare are explained in Sect. 4. The results achieved are presented in Sect. 5. Section 6 indicates the conclusions and further developments.

2 Data and setup

2.1 Hardware

In the previous section, we have presented relevant works which have contributed significantly to our work. Each research group uses different sensors and experimental setups; therefore, we want to explain our approach.

For the data recording, we used two insoles. The insoles were made with a 3D printer and a flexible material. Ten force sensors (FSR 402 short from Interlink) are used per insole, see Fig. 1. The four force sensors at the heel and at the ball are arranged parallel to each other so that the postural stability within the foot can be measured. The BNO 055 sensor from Bosch is also mounted in the insole. This sensor is an inertial sensor consisting of a gyroscope, accelerometer and a magnetometer. This sensor has a co-processor for sensor fusion. The sensor fusion calculates absolute orientations and linear acceleration values directly. The output is therefore angle velocity, acceleration, quaternions, Euler angles and linear acceleration at a frequency of 100 Hz. The sensor is located in the middle of the insole, see Fig. 1.

2.2 Sensor data

Figure 2 shows data of gait. In the first graph (a) are shown the three-dimensional orientation data, in (b) the three-dimensional linear acceleration data, in (c) the force of three different zones (heel, metatarsus and toe) and in (d) the average of all force sensors. For our evaluation, we use the y- and z-axis of the orientation and linear acceleration data, as well as the mean value of all force sensors. We do not use the x-axis of the orientation and linear acceleration data, because it has already been determined in other work that these values contain hardly any information about the gait and we can confirm this from our experience [12]. Furthermore, we use the derivation of the orientation data y' and z'.
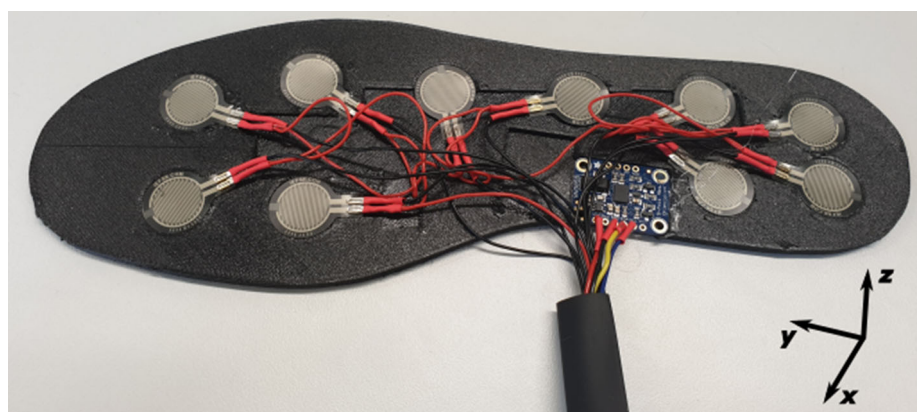
2.3 Data sets

2.3.1 Daily life activities

For the daily life activities dataset, we have a total of 7 recordings of 7 different healthy persons. The age of the persons was between 25 and 54 years. In total, each person passed the test one time. During the experiment, the candidates had to pass the following test, see Fig. 3. At the beginning of the test, the person sits on a chair for 1 min. Then, the person gets up from the chair and stands for 1 min. After that, the person walks back and forth for 1 min. Then, the person goes up stairs three floors and then down the stairs. Next, the person walks for another minute again and ends up in front of a chair. The person spends 1-min standing. In the second last step, the person changes repeatedly for 1 min from a standing to a sitting position. Finally, the person sits for 1 min on the chair.

2.3.2 Time up and go test

The time up and go (TUG) test dataset consists of total 50 subjects. Subjects suffer from 28 Parkinson's disease with a maximum stadium of 3 by Hohn and Yahr [26]. The healthy subjects without motoric disfunctions are used as control group.

The test subjects had to pass a gait test of the MDS-UPDRS [27]. For this purpose, the person sits on a chair with back and armrests. They get up from the chair and walk 10 m straight away. At a mark, the subject turns 180° and walks back to the chair. Then, the subject sits down again. The complete process of the TUG test is shown in Fig. 4.

Fig. 1 Insole with force and IMU sensors

Fig. 2 a Orientation data as Euler angles; **b** linear acceleration; **c** average force of heel (four sensors), metatarsus (two sensors) and bunion (four sensors); **d** average of all force sensors
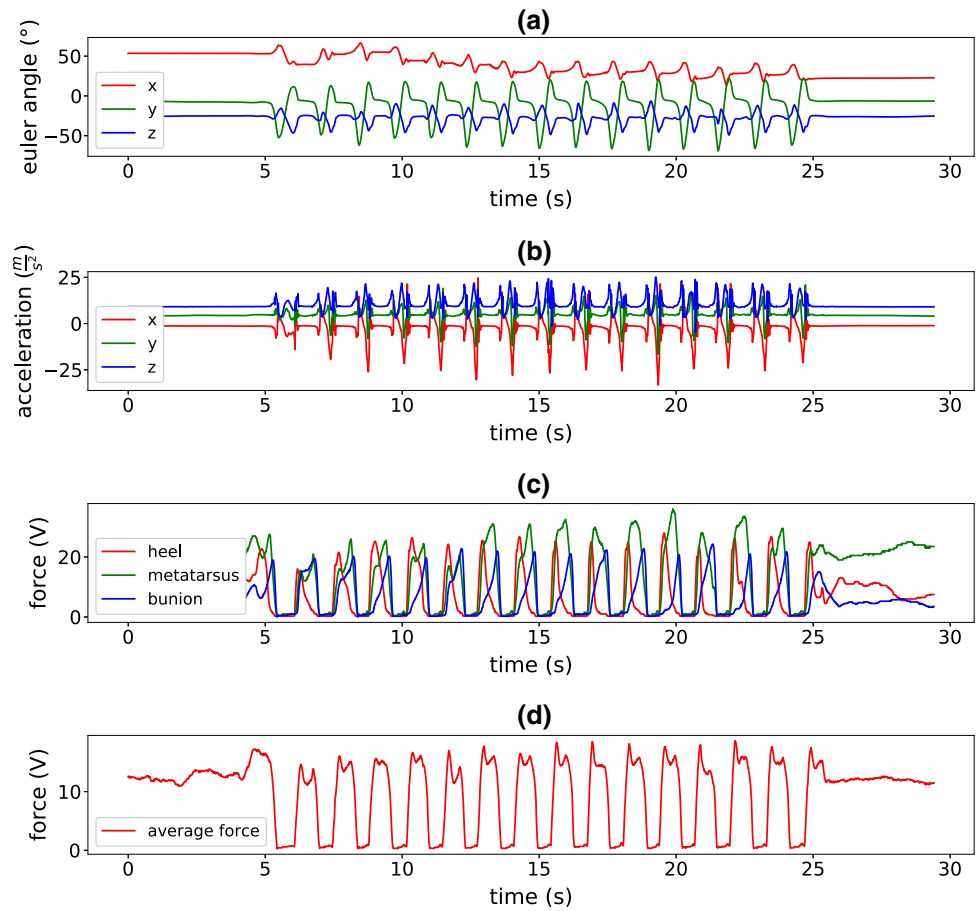
Fig. 3 Process of daily life activities test
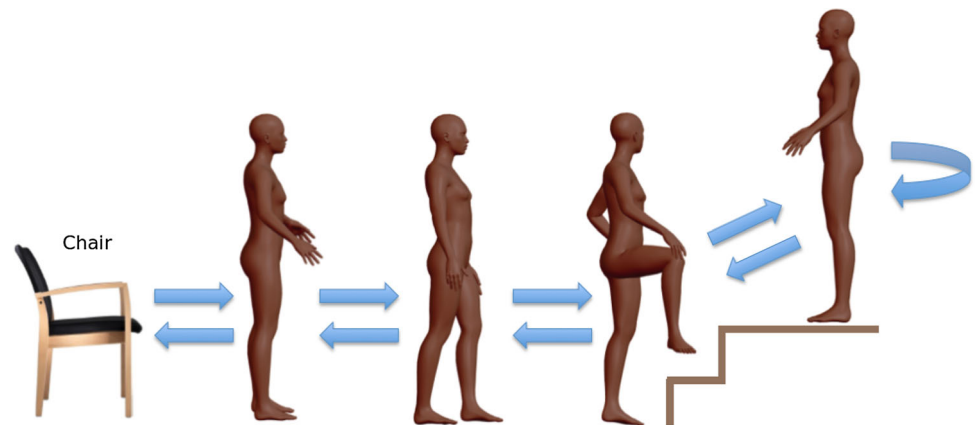
2.4 Training and test data

To create our training data, we label manually our daily life activities and TUG test datasets into strides and no strides, see Fig. 5.

Data are split into training and test data. In order to avoid biasing the results, we make sure that data assigned to an individual are either only in test data or only in training data. 70% of the data were used for training and 30% for testing. This type of separation makes the training data totally different from the test data. This means there are no redundant data to improve the results. Since there is a small dataset for the classification, we decided to use a k-fold cross-validation with mixing. We select seven folders

Fig. 4 Process of time up and go (TUG) test
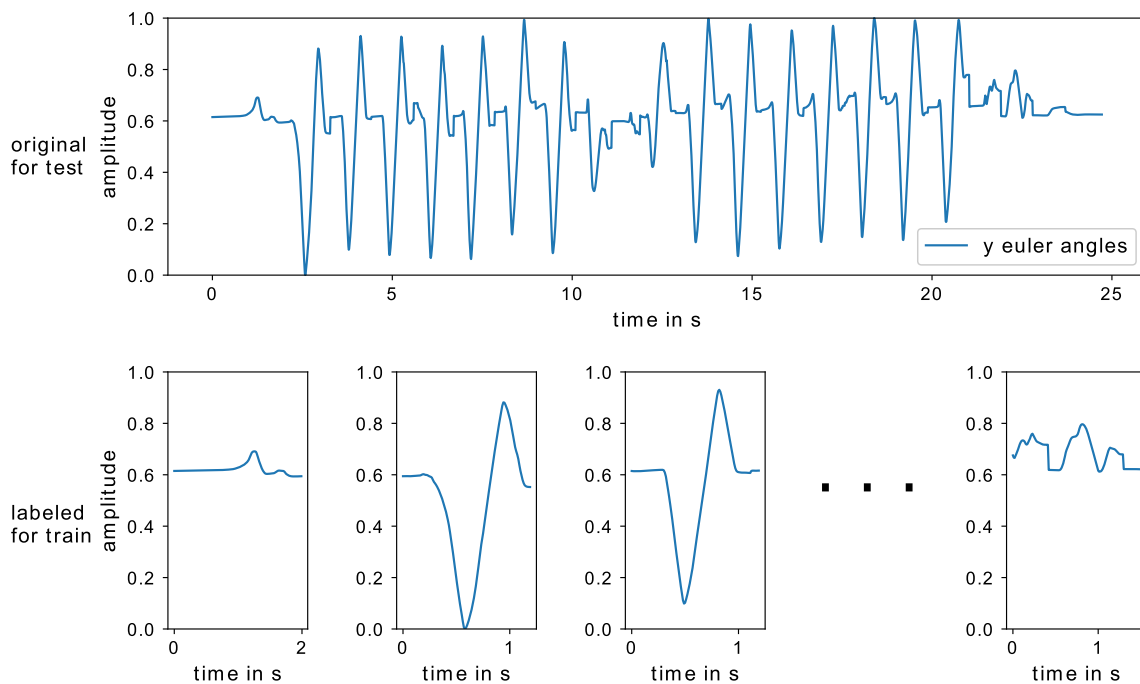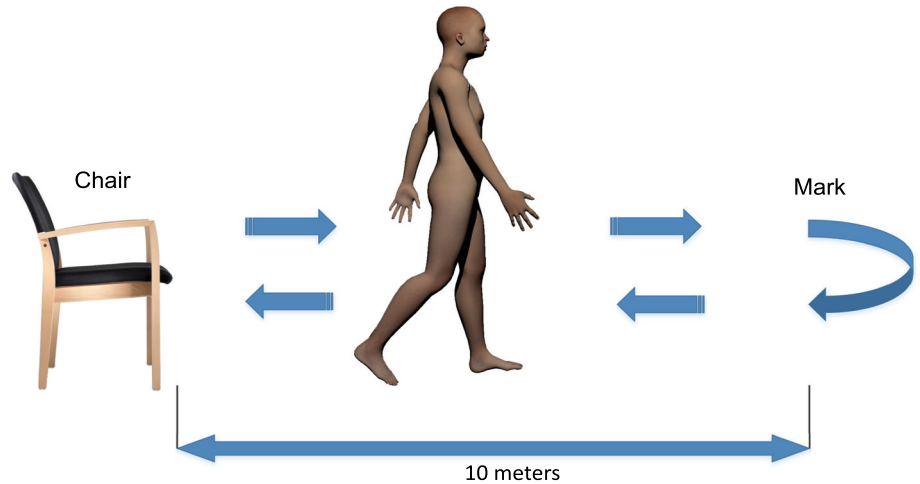
Fig. 5 Original and manually labelled data

for the daily life activity Test. We use five folders for training and two for the test.

3 Preprocessing

3.1 Normalization

In order to enable the classifiers to work with uniform values, we normalize the data. For the normalization of the data, we use the min–max normalization. Thus, our result vector has a value ranging from 0 to 1. The normalization is shown in Eq. 1. We calculate the normalization for every $x_i \forall i \in \{0, \ldots, N-1\}$ of the feature X where N is the length

of feature X. Functions $\min(X)$ and $\max(X)$ return the absolute minimum and maximum of the feature X. The result is a normalized value $x_i^{\mathrm{norm}} \in X^{\mathrm{norm}}$ [28].

$$x_i^{\mathrm{norm}} = \frac{x_i - \min(X)}{\max(X) - \min(X)} \tag{1}$$

3.2 Resampling

After normalization, the individual signals are transformed to a uniform length of 100 values. This step is necessary because classifiers such as CNN always require the same tensors as input. For resampling, we use the Python

function "resampling" in the library signal. This method is based on FFT.

3.3 Ideal stride template

For the stride detection with the DTW, we need an ideal stride as a template. For estimating the ideal stride, we also use the DTW in combination with the labelled training data. For this, we create a distance matrix $D_{\text{stride}}^{(M,N)}$, based on the costs for all strides to each other, where M is the number of rows and N the number of columns. The cost $D_{\text{stride}}^{(i,j)}$ is the distance between two strides by DTW. Then, we sum the costs of all columns for each row in vector Cost_i

$$\text{Cost}_i = \sum_{j=0}^{N-1} D_{\text{stride}}^{(i,j)}, \forall i \in \{0,\ldots,M-1\}, j \in \{0,\ldots,N-1\}.$$

(2)

After that, we choose the minimum of the vector Cost.

$$C_{\text{ideal\_stride}} = \min(\text{Cost}_i) \quad \forall i \in \{0,1,\ldots,M-1\}$$

(3)

This stride will be used as an ideal model for a stride. An example of our approach can be seen in Table 1. To choose the ideal stride [12], we resampled the signals to a uniform length and averaged each index over all the strides.

4 Methods

In the previous section, we presented the datasets, the hardware and the preprocessing. In this section, we want present two comparable methods, min–max-pattern (MMP) and dynamic time warping (DTW), and our method convolutional neural networks (CNN). This includes preprocessing, algorithms for stride detection, and the validation process. An overview of the different stride detection processes can be found in Fig. 6.

4.1 Min–max-pattern

The simplest way to detect strides is to trace a minimum–maximum-pattern (MMP). This pattern is typical in human gait. However, this pattern also occurs in other motion

Table 1 Example of a distance matrix for selecting the ideal stride

	Stride 1	Stride 2	Stride 3	$\sum$
Stride 1	0	2	3	**5**
Stride 2	2	0	5	7
Stride 3	3	5	0	8

The best choice is stride 1 with the minimum costs to all other strides (bold)
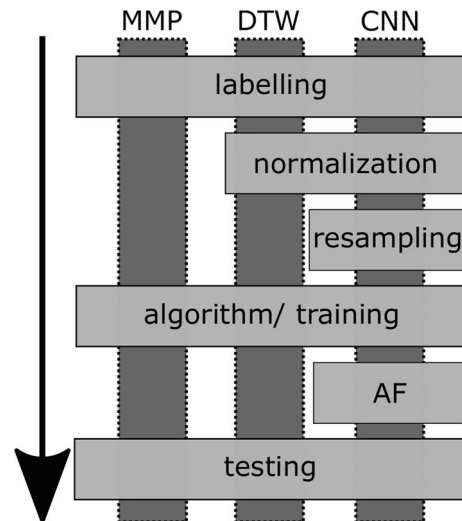
Fig. 6 Stride detection processes

sequences, e.g. climbing stairs. For this reason, this pattern is not an ideal choice [12]. Nevertheless, we have included the procedure for the sake of completeness.

The idea is that with a fixed window width the time series is traversed over the y-axis of the orientation data. The index of the minimum and maximum within the window is for each window stored. We have set the size of the window to 90 values, because this corresponds to 0.9 s, which is more than half duration of an average human stride. The average duration is about 1.1 s, 110 values [29]. Inside this window, all maxima and minima of a stride are expected to be included, without overlapping with a second stride.

The indices of all minima and maxima can then be displayed in a separate frequency table. All indices where the absolute frequency is greater than the average are potential strides. After that, a logical check is made, because each minimum must be followed by a maximum. This ensures that minima and maxima are always presented in pairs, see Fig. 7. Next, the distance from each minimum to the corresponding maximum is determined. If this distance is outside the 90% of the confidence interval of all strides used for training, it is assumed that it is not a stride. The 90% confidence interval was chosen to remove extremely short or long steps. This confidence interval has proven to be useful in our tests.

Now we want to determine the corresponding stand phase for each MMP. In the standing phase, the angle change is almost zero. We form the derivation of the y-axis of the orientation data y' and calculate the standard deviation $s_{y'}$ of the y' sequence. Now, the ranges are selected between $y'_i > -s_{y'} \cdot 0.25$ and $y'_i < +s_{y'} \cdot 0.25$. We have chosen the coefficient 0.25 because we only look for areas close to zero. The person's standing phase is located in this
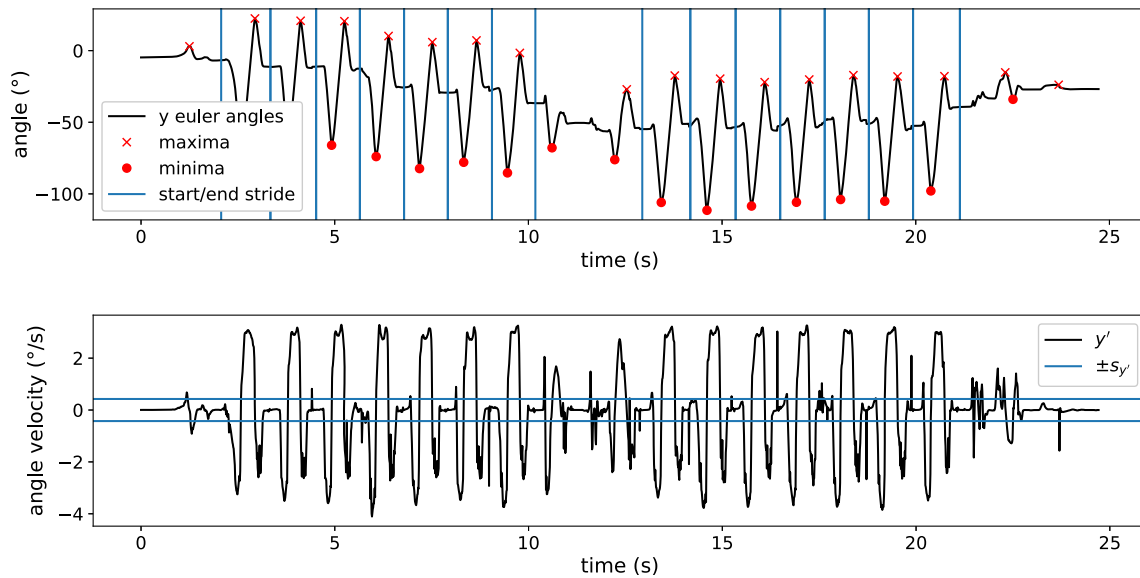
Fig. 7 Min–max-pattern recognition

area. Thus, we receive the areas of the standing phases. Finally, we select the mean index of the region within the standing phase between the minima–maxima patterns. This index indicates the start or end of a stride. We estimate the beginning of the first stride or the end of the last stride of a sequence of strides by the average length of the strides.

4.2 DTW

DTW is used to measure the similarity or distance of two signals based on the best path. The particular feature of the method is that the signals do not have to have the same length. In contrast, the Euclidean distance always determines the distance between two points directly. For stride detection, we use the force, orientation, derivative orientation and linear acceleration data. The DTW searches for the ideal path between two signals, see Fig. 8 [30]. The signals are first normalized before the algorithm for stride detection begins. Our algorithm is strongly based on the algorithm presented by Barth [12].

By using the ideal stride, see Sect. 3.3, we calculate the distance matrix $D(M, N)$ between the ideal stride and the test signal we want to analyse, see Fig. 9, where M is the length of the ideal stride and N the length of the test signal.

Then, we calculate the accumulated cost matrix $C(M, N)$. For this, we add the minimum costs from the distance matrix D. The lowest row of the matrix C results from the bottom row of the matrix D, see Eq. 4 [12].

$$C(0, n) = D(0, n) \forall n \in \{0, \ldots, N - 1\} \quad (4)$$

The first column of the cost matrix C results from the sum of the previous element of the matrix C and the current element of the matrix D, see Eq. 5.
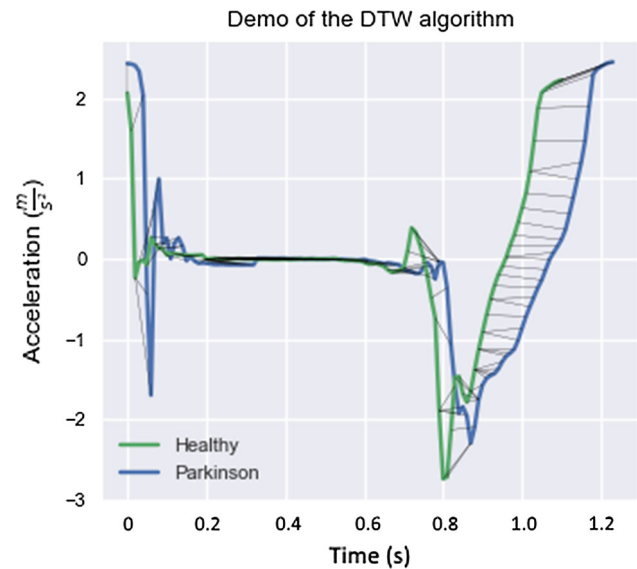
Fig. 8 DTW: ideal path between strides of healthy and PD subjects

$$C(m, 0) = C(m - 1, 0) + D(m, 0) \forall m \in \{0, \ldots, M - 1\} \quad (5)$$

All other elements of the cost matrix C are calculated from the minima of the neighbourhood summed with the distance of the current element, see Eq. 6. The result of the cost matrix C is shown in Fig. 9 in the second last row.

$$C(m, n) = \min(C(m - 1, n), C(m - 1, n - 1), C(m, n - 1)) + D(m, n) \forall m \in 0, \ldots, M - 1, n \in \{0, \ldots, N - 1\} \quad (6)$$

As a result of the cost matrix, the summed costs are displayed in the first row. The first line of the cost matrix is in
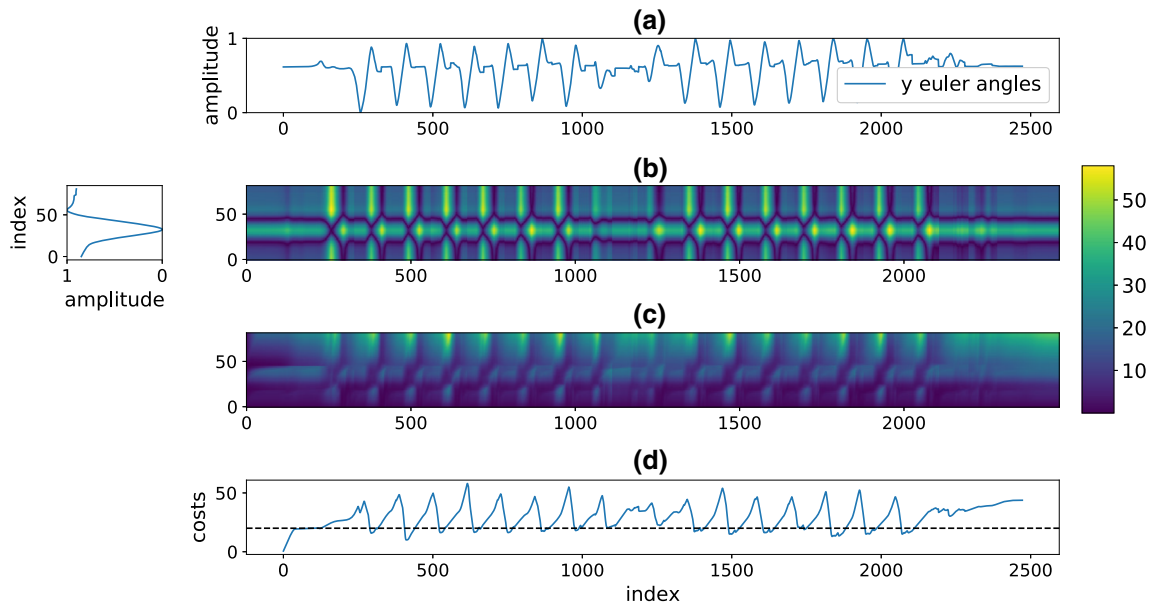
Fig. 9 DTW algorithm between ideal stride and a test signal. **a** Raw *y* orientation signal; **b** distance matrix between raw signal and template; **c** accumulated distance matrix; **d** summed costs of the accumulated distance matrix

Fig. 10 Path between stride start and end
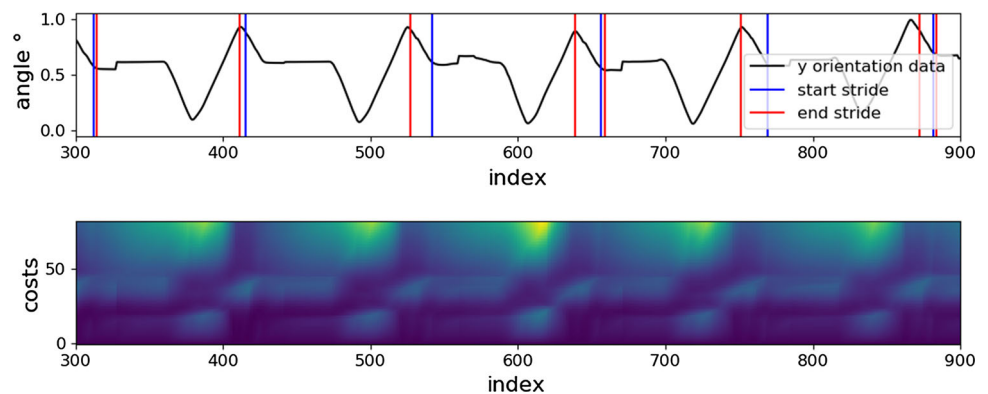
the last line of Fig. 9. It can be seen in the last line of the figure. In the next step, a threshold value is selected to mark the end of a step. In our case, we chose the threshold of 17. A threshold value of 20, as recommended by Barth, was not useful in our case, as steps at the turn were often detected during the TUG test [12].

Finally, we follow the minimal path beginning at the end of the stride. Thus, we get the beginning of a stride, see Fig. 10.

4.3 CNN

CNN are becoming more and more popular because they achieve significantly better results than traditional NN. CNN are used primarily for image recognition, but they are just as powerful at detecting signals. The difference between NN and CNN is that CNN learn local patterns. In contrast, traditional NN always use the entire input. The multilayer convolutional architecture allows you to increase the complexity of detection. Thus, it is possible to recognize in the first layer only patterns, and with the second or *n*-layer more and more complex objects [31, 32]. For our work with the CNN, we use the open source python library Keras with tensorflow.

Preprocessing for CNN includes normalization and resampling, see Fig. 11. Via resampling, all training data are resampled to a length of 100 values. For the classification with CNN, we use a sequential network. As an activation function, we use the rectified linear unit (ReLU) function with except at the output layer, see Eq. 7, where *x* is the input. At the output layer, we use the sigmoid function, see Eq. 8, because a ReLu function is not suitable. For output layer, it is recommended to use a Sigmoid or Softmax function. The first one-dimensional convolutional layer creates 100 filters with a kernel size of 3.
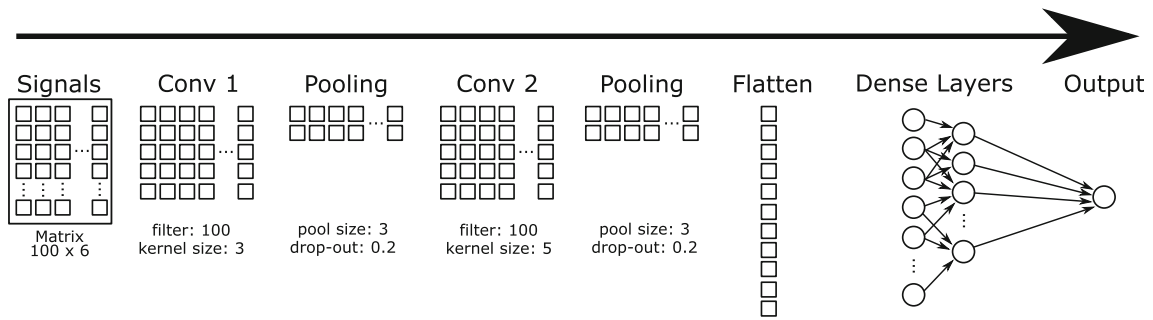
Fig. 11 Schema of the CNN layers

$$f(x) = \max(0, x) \tag{7}$$

$$f(x) = \frac{1}{1 + e^{-x}} \tag{8}$$

To reduce the filters, we apply a max pooling with a pool size of 3 and a dropout with probability 0.2. The second convolutional layer consists of 100 filters and a kernel size of 5. This is followed by max pooling again with a pool size of 3. This is followed by a so-called dropout with probability 0.2, where single connections are randomly deleted [33]. After that, we have a flattening layer to adjust the dimensions for the NN. Next, we have two dense layers. The first has 20 neurons and the second 30 neurons.

4.4 Automatic framing

In contrast to the MMP or DTW method, the CNN signals must have a uniform length. This is important that the classifier always has the same inputs. In this case, we develop an algorithm that systematically cuts out a small windows from our entire signal that the classifier can detect strides. The algorithm uses dynamic window sizes that even strides with different durations can be detected. The average duration of a stride is $1.1\,\mathrm{s} \pm 0.2\,\mathrm{s}$ [29], which corresponds to 110 ± 20 values. Therefore, we use average window size of 110 ± 30 values, so we capture all possible ranges. The window w can have the following sizes

$$w = \{80, 90, 100, 110, 120, 130, 140\}. \tag{9}$$

To increase performance, the algorithm always skips seven values when scanning the signal. This increases the performance, because not every single increment is classified seven times. If the classifier within a window detects a stride with a probability more than 70%, the stride is stored in a list with start index, end index and probability of the stride. A recognition probability of 70% is very low. In a later step, we select the stride with the highest probability. This deletes unnecessary strides. Based on the first detected stride, overlaps up to a maximum of

$$\text{Overlapping} = \text{Detected stride} + (\text{Average stride} \cdot 0.8) \tag{10}$$

are saved. The factor 0.8 was selected so that a large range is available for stride detection. Thus, a tolerance is given if a classification error has been made. Based on the average stride duration of $1.1\,\mathrm{s} \pm 0.2\,\mathrm{s}$ values [29]. Because multiple strides represent the same stride by overlapping, we need to select the best fitting stride. For this reason, we choose the area from the first detected stride to the end of the overlap. Then, we select from this range this stride with the highest probability of being a stride. This stride is then defined as a valid stride. An example of the result is shown in Fig. 12.

To check the results of the algorithm, we use two test procedures. With the first method, we use the labelled data. For the second method, we use the original signals. Here, we always mark the absolute minimum within one step $\pm 10\,\mathrm{ms}$. If the predicted stride lies within this range, it is marked as a correct detected stride [12].
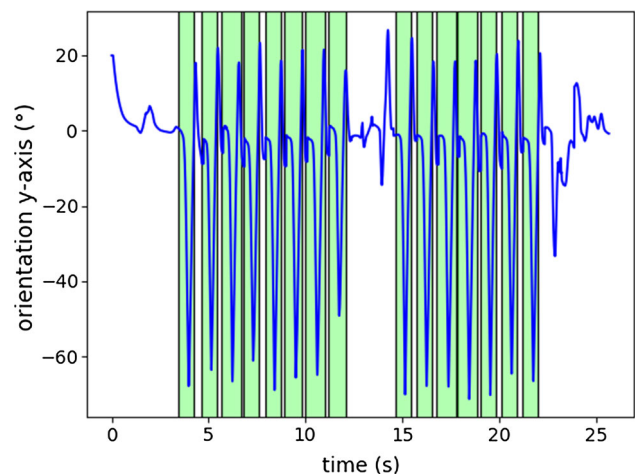
Fig. 12 Stride detection by CNN

Table 2 Binary confusion matrix

	Labelled class		
	Positive	Negative	$\sum$
Predicted positive	True positive	False positive	Total predicted positive
Predicted negative	False negative	True negative	Total predicted negative
$\sum$	Total labelled positive	Total labelled negative	Total

4.5 Measurement

In the previous sections, we have presented various methods for stride detection. In this section, we describe our methods for evaluating the results.

While we have a binary classification problem (stride, not stride), we present our results in a 2×2 confusion matrix, see Table 2. The table is used to help in the following sections to understand the equations.

For the true positive values, we have labelled the strides first. We used the minimum of the strides in the y-axis value from the orientation data. If the marking of a stride is included from the starting point and end point of the algorithms, it will be evaluated as True Positive. In order to be assigned to the true negative values, the average step duration of 110 values was assumed. This allowed us to calculate how many wrong decisions were made over time.

4.5.1 Sensitivity

Sensitivity (recall) is a widespread measurement in medicine. It indicates the ratio of predicted strides to all strides inside our test data, see Eq. 11.

$$\text{Sensitivity} = \frac{\sum \text{True positive}}{\sum \text{Total labelled positive}} \qquad (11)$$

4.5.2 Specificity

The specificity describes how well our system can distinguish steps from all other activities (no steps). It is the ratio of undetected strides in all test data where no steps were present, see Eq. 12.

$$\text{Specificity} = \frac{\sum \text{True negative}}{\text{Total labelled negative}} \qquad (12)$$

4.5.3 Precision

The precision is the proportion of correctly predicted steps to all predicted steps, see Eq. 13.

$$\text{Precision} = \frac{\sum \text{True positive}}{\sum \text{Predicted condition positive}} \qquad (13)$$

4.5.4 Accuracy

Accuracy is the ratio of all correctly recognized strides and all correctly recognized other activities (no stride) to all test data, see Eq. 14.

$$\text{Accuracy} = \frac{\sum \text{True positive} + \sum \text{True negative}}{\sum \text{Total population}} \qquad (14)$$

4.5.5 F1-score

The $F1$-Score is the harmonious average between precision and recall. In this way, both measures are combined into one value.

$$F_1 \text{ score} = 2 \cdot \frac{\text{Precision} \cdot \text{Recall}}{\text{Precision} + \text{Recall}} \qquad (15)$$

5 Results

In this section, we would like to present our results, which were achieved by using the data sets daily life activities and TUG test by using the presented methods.

5.1 Measured using IMU sensors

We do not use any force sensors to train the daily life activities 1 data sets. Because the TUG test data set was made with an older version of the insole (without force sensors). So the data are comparable.

Table 3 shows the results of the daily life activities data set. The MMP, DTW algorithm and AF + CNN classification were compared. For the test, the complete time series were used. The sensitivity shows that the MMP and AF + CNN algorithms perform best. The DTW algorithm performs comparatively well. From this, it can be assumed that the DTW algorithm does not always detect strides correctly. In contrast, the MMP and AF + CNN algorithms detect strides very well. The DTW algorithm has the highest specificity followed by the AF + CNN algorithm. The MMP algorithm performs worse. From this, it can be assumed that the DTW and AF + CNN algorithms detect other activities, e.g. standing or going stairs as well as no strides. However, the MMP algorithm has big problems

Table 3 Daily life activities 1 (IMU sensors)

	Sensitivity	Specificity	Precision	F1-score	Accuracy
MMP	0.990	0.771	0.658	0.791	0.838
DTW	0.896	**0.986**	**0.969**	0.931	0.956
AF + CNN	**0.992**	0.940	0.901	**0.944**	**0.958**

Best results are highlighted in bold

with this. This result is the identical to Barth's results [12]. With F1-score and accuracy, the AF + CNN algorithm performs best, closely followed by the DTW algorithm. For this reason, we would recommend the AF + CNN algorithm for stride detection.

5.2 Measured using IMU and force sensors

These results show the improvement in classification that is achieved when additional force sensors are used for classification. The force sensors have been reduced to three different measuring points. For this purpose, we have calculated the average value of heel, metatarsus and ball of foot, as already described in Sect. 2.2. Table 4 shows a comparison of the AF + CNN method with and without force sensors. It is clearly to seen that the classification result for our test data was completely correct. With the addition of force sensors, the gain in information increased significantly. This result can be related to the small data set of individuals tested and all did not have motor dysfunctions.

5.3 TUG test

The classifiers were not trained again during the test of the TUG test data set. We used the models from Sect. 5.1. This shows how independent the model is of motor dysfunctions or other appearance. In addition, the test took place in a completely different environment. The results are shown in Table 5. The results were grouped by classifiers with the subgroups PD and no PD.

The AF + CNN algorithm shows the best results for PD and no PD at F1-score and accuracy. From this, it can be concluded that the algorithm reacts well to changed data and is therefore very robust. However, it has a relatively weak specificity value. This is due to the fact that the AF + CNN algorithm wrongly counted other activities as a stride. The DTW algorithm scored worst in this test. This can be explained by the fact that the threshold was not optimized for the data. The algorithm can therefore react poorly to new data. This demonstrates the weakness of a fixed threshold in the algorithm. The same also applies to the MMP algorithm.

6 Discussion

The presented methods have shown that the problem of stride detection can be solved with many different methods. The best performance in our tests was achieved by AF-CNN. The advantage of the AF-CNN classifier is that it does not require a threshold value. Furthermore, the AF-algorithm makes it possible to analyse the data during recording.

Furthermore, we have shown that the combination of force and IMU sensors can increase the results even more, so that our test produces small errors.

Table 4 Daily life activities 2 (labelled data)

	Sensitivity	Specificity	Precision	F1-score	Accuracy
AF + CNN (IMU)	0.978	0.994	0.978	0.974	0.988
AF + CNN (IMU + force)	**1.0**	**1.0**	**1.0**	**1.0**	**1.0**

Best results are highlighted in bold

Table 5 Results of the data set TUG test (IMU sensors)

	Group	Sensitivity	Specificity	Precision	F1-score	Accuracy
MMP	PD	0.838	**0.895**	**0.925**	0.879	0.86
	No PD	0.844	0.778	0.871	0.857	0.820
DTW	PD	0.615	0.852	0.875	0.723	0.703
	No PD	0.663	**0.844**	0.887	0.759	0.727
AF + CNN	PD	**0.983**	0.812	0.899	**0.939**	**0.920**
	No PD	**0.968**	0.818	**0.91**	**0.938**	**0.916**

The best results separated by PD or no PD are highlighted in bold

In our opinion, the step recognition is the most important point in the analysis of the human gait, since all further parameters are inside this. If the step is not well recognized, further mistakes will occur in a more detailed analysis.

As comfortable to carry measuring instruments for persons with motoric dysfunctions as in Parkinson's disease, we propose a combination of force and IMU sensors. As an automatical stride detection process for daily life use, we propose a joint of automatic framing, normalization, resampling, and CNN.

References

1. Ball N et al (2019) Parkinson's disease and the environment. Front. Neurol. 10:218
2. Pachoulakis, I., Papadopoulos, N.: Exergames for Parkinson's disease patients: the balloon goon game. In: 2016 International Conference on Telecommunications and Multimedia (TEMU). IEEE (2016)
3. Kovač J, Štruc V, Peer P (2019) Frame-based classification for cross-speed gait recognition. Multimed. Tools Appl. 78(5):5621–5643
4. Kovač J, Peer P (2014) Human skeleton model based dynamic features for walking speed invariant gait recognition. Math Probl Eng 2014:484320
5. Kovač J, Peer P (2013) Transformation based walking speed normalization for gait recognition. KSII Trans Internet Inf Syst 7(11):2690–2701
6. Seckiner D, Mallett X, Maynard P, Meuwly D, Roux C (2019) Forensic gait analysis—morphometric assessment from surveillance footage. Forensic Sci Int 296:57–66
7. Ng H, Tong HL, Tan WH, Yap TTV, Chong PF, Abdullah J (2011) Human identification based on extracted gait features. Int. J. New Comput. Archit. Appl. (IJNCAA) 1(2):358–370
8. Rastegari, E., Azizian, S., Ali, H.: Machine learning and similarity network approaches to support automatic classification of Parkinson's diseases using accelerometer-based gait analysis. In: Proceedings of the 52nd Hawaii International Conference on System Sciences (2019)
9. Prakash, C., Sujil, A., Kumar, R., Mittal, N.: Linear prediction model for joint movement of lower extremity. In: Recent Findings in Intelligent Computing Techniques, pp. 235–243. Springer, Singapore (2019)
10. Gupta, U., Bansal, H., Joshi, D.: Gender specific and age dependent classification model for improved diagnosis in Parkinson's disease. arXiv preprint arXiv:1904.09651 (2019)
11. Espay AJ et al (2016) Technology in Parkinson's disease: challenges and opportunities. Mov. Disord. 31(9):1272–1282
12. Barth J et al (2015) Stride segmentation during free walk movements using multi-dimensional subsequence dynamic time warping on inertial sensor data. Sensors 15(3):6419–6440
13. Bobić, V.N., et al.: Challenges of stride segmentation and their implementation for impaired gait. In: 2018 40th Annual International Conference of the IEEE Engineering in Medicine and Biology Society (EMBC). IEEE (2018)
14. Tao X et al (2018) Precise displacement estimation from time-differenced carrier phase to improve PDR performance. IEEE Sensors J. 18(20):8238–8246
15. Koroglu, M.T., Yilmaz, A., Saul, C.J.: A deep learning strategy for stride detection. In: 2018 IEEE sensors. IEEE (2018)
16. Hannink J et al (2018) Mobile stride length estimation with deep convolutional neural networks. IEEE J. Biomed. Health Inf. 22(2):354–362
17. Watanabe, T., Miyazawa, T., Shibasaki, J.: A study on IMU-based stride length estimation for motor disabled subjects: a comparison under different calculation methods of rotation matrix. In: 2018 IEEE EMBS International Conference on Biomedical and Health Informatics (BHI). IEEE (2018)
18. Kim, Y., Eyobu, O.S., Han, D.S.: ANN-based stride detection using smartphones for Pedestrian dead reckoning. In: 2018 IEEE International Conference on Consumer Electronics (ICCE). IEEE (2018)
19. Jiang, X., et al.: Exploration of gait parameters affecting the accuracy of force myography-based gait phase detection. In: 2018 7th IEEE International Conference on Biomedical Robotics and Biomechatronics (Biorob). IEEE (2018)
20. Ince, O.F., et al.: Gait analysis and identification based on joint information using RGB-depth camera. In: 14th International Conference on Electrical Engineering/Electronics. Computer, Telecommunications and Information Technology (ECTI-CON). IEEE (2017)
21. Agostini V, Balestra G, Knaflitz M (2014) Segmentation and classification of gait cycles. IEEE Trans. Neural Syst. Rehabil. Eng. 22(5):946–952
22. Mazumder, O., et al.: Assessment of insole based gait feature variation with progression of Parkinson's disease. In: 2018 IEEE Sensors. IEEE (2018)
23. Steinmetzer, T., et al.: Clustering of human gait with Parkinson's disease by using dynamic time warping. In: 2018 IEEE International Work Conference on Bioinspired Intelligence (IWOBI). IEEE (2018)
24. Muheidat, F., et al.: Estimating walking speed, stride length, and stride time using a passive floor based electronic scavenging system. In: 2017 IEEE Sensors Applications Symposium (SAS). IEEE (2017)
25. Gwak, M., Sarrafzadeh, M., Woo, E.: Support for a clinical diagnosis of mild cognitive impairment using photoplethysmography and gait sensors. In: Proceedings, APSIPA Annual Summit and Conference, vol. 2018 (2018)
26. Hoehn MM, Yahr MD (1967) Parkinsonism: onset, progression, and mortality. Neurology 17(5):427–427
27. Goetz CG et al (2008) Movement disorder society-sponsored revision of the unified Parkinson's disease rating scale (MDS-UPDRS): scale presentation and clinimetric testing results. Mov. Disorders 23(15):2129–2170
28. Frochte J (2019) Maschinelles Lernen: Grundlagen und Algorithmen in Python. Carl Hanser Verlag GmbH Co KG, Munich
29. Hausdorff JM et al (1998) Gait variability and basal ganglia disorders: stride-to-stride variations of gait cycle timing in Parkinson's disease and Huntington's disease. Mov. Disorders 13(3):428–437
30. Keogh E, Ratanamahatana CA (2005) Exact indexing of dynamic time warping. Knowl. Inf. Syst. 7(3):358–386
31. Abadi, M., et al.: Tensorflow: a system for large-scale machine learning. In: 12th USENIX Symposium on Operating Systems Design and Implementation (OSDI 16) (2016)
32. Sze V et al (2017) Efficient processing of deep neural networks: a tutorial and survey. Proc. IEEE 105(12):2295–2329
33. Srivastava N et al (2014) Dropout: a simple way to prevent neural networks from overfitting. J. Mach. Learn. Res. 15(1):1929–1958

Analysis and Classification of Motor Dysfunctions in Arm Swing in Parkinson's Disease

Tobias Steinmetzer [1,2,†] , **Michele Maasch** [2,†] , **Ingrid Bönninger** [2,†] **and Carlos M. Travieso** [1,*,†]

1   Institute for Technological Development and Innovation in Communications, University of Las Palmas de Gran Canaria, Campus Universitario de Tafira, 35017 Las Palmas de Gran Canaria, Spain; tobias.steinmetzer@b-tu.de
2   Institute of Medical Technology, Brandenburg University of Technology Cottbus, 01968 Senftenberg, Germany; michele.maasch#1@b-tu.de (M.M.); ingrid.boenninger@b-tu.de (I.B.)
*   Correspondence: ctravieso@dsc.ulpgc.es
†   These authors contributed equally to this work.

Abstract: Due to increasing life expectancy, the number of age-related diseases with motor dysfunctions (MD) such as Parkinson's disease (PD) is also increasing. The assessment of MD is visual and therefore subjective. For this reason, many researchers are working on an objective evaluation. Most of the research on gait analysis deals with the analysis of leg movement. The analysis of arm movement is also important for the assessment of gait disorders. This work deals with the analysis of the arm swing by using wearable inertial sensors. A total of 250 records of 39 different subjects were used for this task. Fifteen subjects of this group had motor dysfunctions (MD). The subjects had to perform the standardized Timed Up and Go (TUG) test to ensure that the recordings were comparable. The data were classified by using the wavelet transformation, a convolutional neural network (CNN), and weight voting. During the classification, single signals, as well as signal combinations were observed. We were able to detect MD with an accuracy of 93.4% by using the wavelet transformation and a three-layer CNN architecture.

Keywords: wavelet transformation; gait analysis; inertial sensors; Parkinson's disease; machine learning; wearable sensors

1. Introduction

The life expectancy of humankind is increasing worldwide. Life expectancy is projected to increase in the 35 industrialised countries with a probability of at least 65% for women and 85% for men. There is a 90% probability that life expectancy at birth among South Korean women in 2030 will be higher than 86.7 years, the same as the highest worldwide life expectancy in 2012, and a 57% probability that it will be higher than 90 years [1]. Due to the increasing life expectancy, the number of old-age diseases is also increasing. One of them is PD. At present, there are 10 million people affected by this disease, and the trend is increasing [2]. Parkinson's disease is a neurodegenerative disease and is currently incurable. However, the progression of the disease can be delayed by medication. For this reason, an exact diagnosis is very important so that the medication can be adjusted as well as possible to the particular person. There are different rating scales for the uniform assessment, e.g., the Unified Parkinson's Disease Rating Scale (UPDRS) [3]. With the help of this rating scale, for example, cognitive and motor performance are assessed. One of the motor tests is the Timed Up and Go (TUG). The assessment is visual and therefore subjective. For this reason, many researchers are working on the objective evaluation of this test.

Most of the research on gait analysis deals with the analysis of leg motion [4–10]. However, the analysis of the arm movement is also important for the assessment of a gait disorder. Stationary systems that use cameras or ultrasound [11–19] and mobile systems with inertial sensors [20–22] are used to measure the arm swing.

In [11], the arm swings of Parkinson's patients and healthy persons with the help of a Kinect camera were compared. Significant differences in amplitude and speed were observed. The arm movements of Parkinson's patients also often showed asymmetry. The PD group showed significant reductions in arm swing magnitude (left, $p = 0.002$; right, $p = 0.006$) and arm swing speed (left, $p = 0.002$; right, $p = 0.004$) and significantly greater arm swing asymmetry (ASA) ($p < 0.001$). An accuracy of more than 90% in distinguishing healthy people from persons with PD was also achieved using a Kinect camera in [12]. Classification between healthy and non-healthy subjects is performed based on the five most relevant features and the two new obtained features from LDA, using four different classifiers, support vector machine (SVM), multilayer perceptron (MLP), the radial basis (RB) neural network, and k nearest neighbor (KNN). Using the motion capture system Motek CAREN in [13], it was detected that Parkinson's patients have a different jerk and arm swing length compared to healthy people. The fact that Parkinson's patients in the early stages have a larger ASA could be confirmed in [14] with the Vicon and the Baton Rouge motion lab system. The p-value for distinguishing healthy individuals from individuals with Parkinson's disease was 0.003. A Kinect system was used in [16] to detect the differences in speed, amplitude, and symmetry in arm movement between healthy people and people in the early stages of Parkinson's disease. In [17], it was investigated which model method provided the best results when using a Kinect to detect Parkinson's disease stages. The best results with an accuracy of 93.4% were obtained with a special Bayesian network classifier using 10-fold cross-validation. The relevant features were related to left shin angles, left humerus angles, frontal and lateral bends, left forearm angles, and the number of steps during a spin. For the recordings in [18], a Kinect system was used in combination with an e-Motion capture program. The proposed system classifies PD into three different stages related to freezing of gait (FoG). An accuracy of 93.4% was reached using the features of the movement and position of the left arm, the trunk position for slightly displaced walking sequences, and left shin angle for straight walking sequences. However, they obtained a better accuracy of 96.23% for a classifier that only used features extracted from slightly displaced walking steps and spin walking steps.

In [15], an automatic method for the treatment of levodopa-induced dyskinesia (LID) was developed. Gyroscopes were used on the abdomen and chest and the abdomen, chest, wrists, and ankles. In general, an average detection rate of 90% for Parkinson's patients was achieved, and the average detection rate and the precision of the individual classes (LID, Parkinson, healthy) were 80% and 77%, respectively. Several classification techniques have been used for LID assessment, including the naive Bayes classifier, KNN, fuzzy lattice reasoning (FLR), decision trees, random forests (RF), and neural networks using a multilayer perceptron (MLP).

The method used in [19] consisted of guiding patients with early Parkinson's on a treadmill and measuring their movements with an ultrasound device on each side. The results were a reduced arm swing amplitude in the patients and a longer stride length compared to healthy people.

In [20], a sensor unit was used on each forearm. This sensor unit consisted of two triaxial G-Link accelerometers that were attached to an aluminum bar. Arm swing asymmetry (ASA), maximal cross-correlation (MXC), and instantaneous relative phase (IRP) of bilateral arm swing were compared between PD and controls. PD subjects demonstrated significantly higher ASA ($p = 0.002$) and lower MXC ($p < 0.001$) than controls.

An accelerometer was placed on the upper arm, as well as a magnetic angular rate and gravity (MARG) device on the shoulder in [21]. The Denavit–Hartenberg model was used, and the algorithm was based on the pseudoinverse of the Jacobian by the acceleration of the upper arm. The accuracy of this method was demonstrated by the use of an optoelectronic system for control purposes.

A similar system was used in [22] with nearly the same sensors and sensor position. An eigenvector method was suggested to compare the axes of the left and right hand. The results showed a difference between people with Parkinson's disease and healthy people.

In our approach, we want to propose a medical wearable system that:

(a) classifies between subjects with motor dysfunctions and a control group based exclusively on arm motions
(b) uses 3D data from the accelerometer, gyroscope, and magnetometer
(c) includes new parameters
(d) is small and easy to use
(e) is not bound to a location
(f) requires a small number of sensors
(g) is low cost

According to the previously mentioned classification, this paper is organized as follows. Section 2 describes our materials. The section is divided into the medical experiment protocol, the hardware used, and the dataset. Then, in Section 3, a description of our methods and how we apply the methods to our data are described. Section 4 include the results. Finally, a discussion and comparison is found in Section 5.

2. Materials

2.1. Protocol

We decided to use the TUG test as a suitable test for recording gait data. Among other things, it is used to evaluate the motor performance of the UPDRS. For the test, only a chair with a backrest and armrests was needed. At first, the test person was sitting on a chair. Upon a command from the test leader, the test person stood up and walked straight ahead for ten meters at an appropriate speed to a mark. At the mark, the test person turned around and walked ten meters straight ahead, back to the chair. The test person sat down in the chair. The test and the recording were then finished. We divided the TUG into two different parts for later analysis of the data. Part (A) contained all data of the TUG including standing up and sitting down in the chair. Part (B) included going straight to the mark, turning around, and going straight back to the chair. Parts (A) and (B) are shown in Figure 1. The aim of this splitting was to extract the gait data from the complete recording.
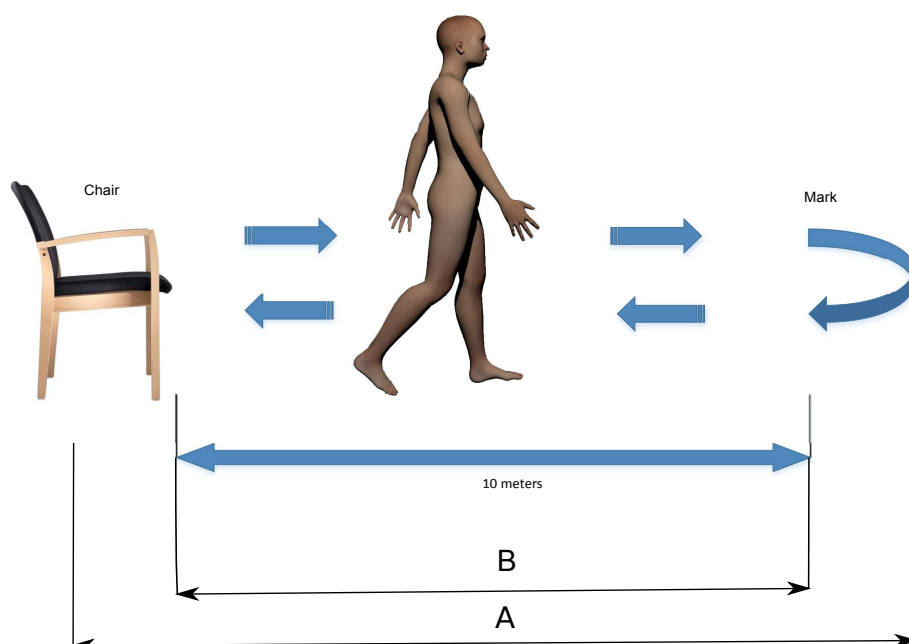
Figure 1. Process of the Timed Up and Go (TUG) test.

2.2. Hardware

For data recording, we used two wristbands with the Meta Motion Rectangle wearable sensors from Mbientlab; see Figure 2 [23]. This is an inertial measurement unit (IMU) sensor. It consists of a BMI 160 with a 3-axis gyroscope and a 3-axis accelerometer and a BMM 150 with a 3-axis magnetometer. By using the Bosch sensor fusion algorithm, the Euler angle and linear acceleration can be obtained [24]. The x-axis corresponds to the gait direction.
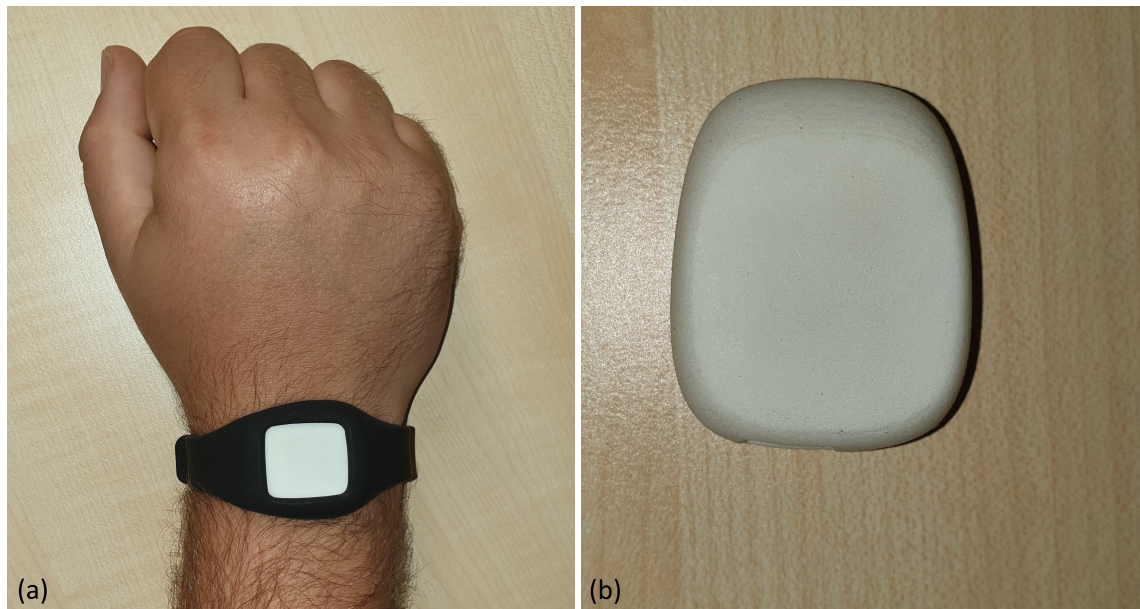
Figure 2. (**a**) Wristband with the Meta Motion Rectangle sensor. (**b**) Position of the sensor during the measurement.

2.3. Data

2.3.1. Dataset

To create a dataset for later analysis, we worked together with the Niederlausitz Clinic in the study "Development of a digitalParkinson Disease Assessment" (ethics request granted in December 2018 by Ethics Committee Brandenburg). All persons were evaluated by the physicians. A total of 39 different persons with 250 recordings were available for the dataset. Of these, there were 15 motor dysfunction patients with 80 recordings and 24 persons with 170 recordings as the control group. Table 1 summarizes the data.

Table 1. Amount of persons and records from the Parkinson's and control groups.

Label	Persons	Records
Motor dysfunction	15	80
Control	24	170

2.3.2. Sensor Data

While the subjects performed the TUG test, 3D Euler angles and 3D linear acceleration of the arms were captured. The signals for the Euler angles and the linear acceleration were the result of the sensor fusion algorithm from Bosch. Both signals were recorded at a frequency of 100 Hz. The algorithm for the sensor fusion used the data from the accelerometer, gyroscope, and magnetometer. Figure 3 shows at the top the 3D Euler angles and at the bottom the 3D linear acceleration signals. In Figure 3,

the complete signal of one wristband during the TUG test is shown. Furthermore, Part (A) contains all recorded data and Part (B) the data between the black dotted lines, the active walking parts.
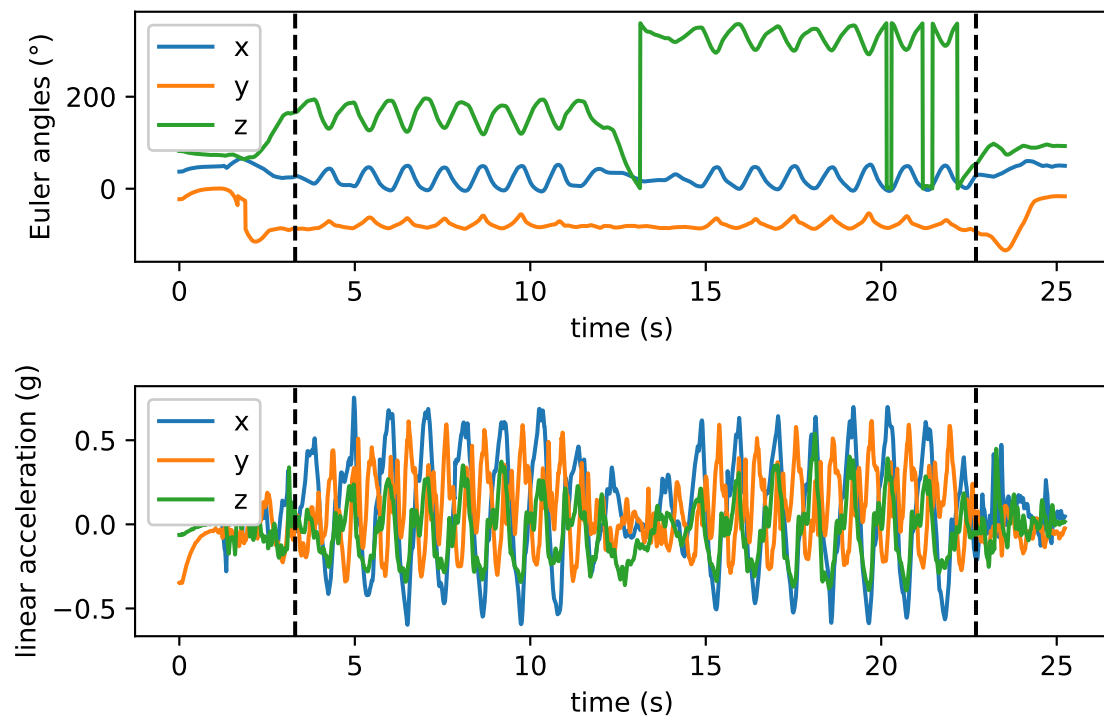
Figure 3. Euler angles and linear acceleration of one wristband for the TUG test.

3. Methods

3.1. Removing Jumps

Figure 3 shows that some jumps existed in the signal of the z-axis of the Euler angle. This was because the value range of the sensor was between $0°$ and $360°$. This made the signal unstable. To correct this, we removed all jumps that were greater than a threshold of $300°$. In Equation (1), our procedure is shown. If the absolute value of the difference of two successive sensor values $|x_i - x_{i+1}| > 300$, a correction of the signal was performed, where $i \in \{1, ..., N\}$. N indicates the length of the signal. The result of the cleanup are given in Figure 4.

$$x_{i+1} = \begin{cases} x_{i+1} - 360 & for \ x_i < x_{i+1} \\ x_{i+1} + 360 & for \ x_i > x_{i+1} \end{cases} \tag{1}$$
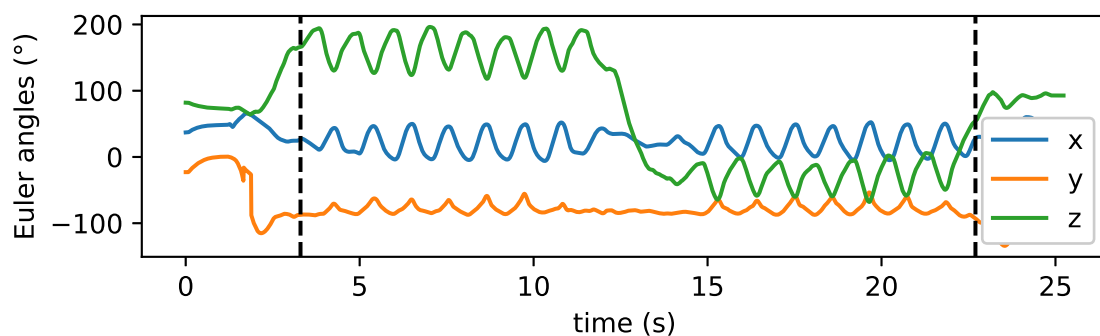
Figure 4. Euler angles without jumps.

3.2. Derivation

It was not possible to create a classifier that could classify the subjects with motor dysfunctions (MD) and no MD by using the Euler angles, because the Euler angles were measured in absolute values. This means that the angles were not calibrated to a starting value at the beginning of the recording. For this reason, we calculated the derivative of each axis of the Euler angles. For this purpose, we calculated the difference between two successive measured values. The equation of the first order discrete derivative can be seen in (2), where N is the length of the signal, x_i is the signal at index i, and x'_i is the value for the difference at i. The result of the derivation can be seen in Figure 5. The derivation makes the signals more comparable for different recordings. This is because the relative angle is used by the derivation.

$$X'_i = x_{i+1} - x_i, i \in \{1, 2, ..., (N-1)\} \tag{2}$$
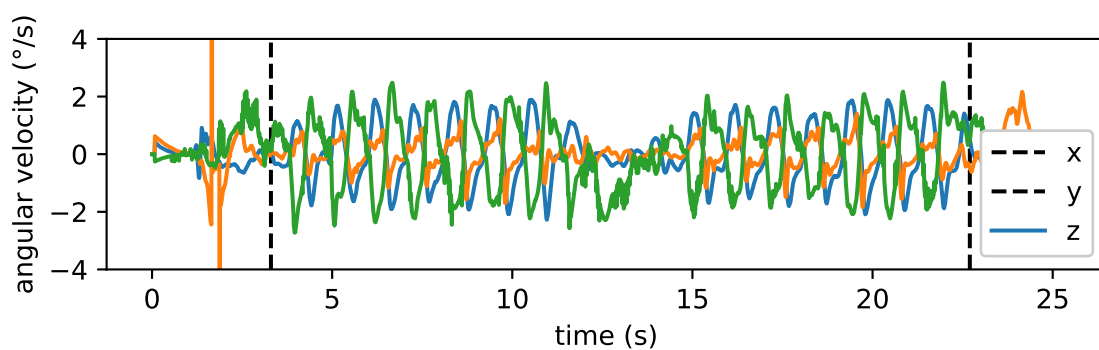
Figure 5. Derivation of the Euler angles.

3.3. Resampling

Before CNN can interpret the data, the signal must have a uniform length. To do this, we resampled the data to a length of 512 values. For resampling, we used the Python library SciPy [25].

3.4. Wavelet Transformation

When considering static signals, the Fourier transformation is very well suited. Unfortunately, there are hardly any static signals in the real world. Every signal changes its frequency dynamically in time. This also applies to the human gait. The gait is a dynamic process. For this reason, it does not make sense to use Fourier analysis.

The origin of the data was a temporal series; therefore, we preferred the use of the wavelet transform in order to increase the information, by decomposition of the time frequency. After the experiments, the accuracy showed a useful feature extracted from this transform. For the wavelet transformation, a signal was convoluted with a wavelet template. By selecting the kernel, we ensured that the ranges around 1.2 Hz (frequency of the arm swing [26]) had a high amplitude. With this template, we calculated the wavelet transformation over the complete signal. In our case, these were the x-, y-, and z-axes of the derived Euler angle and the x-, y-, and z-axes of the linear acceleration of both wristbands. Figure 6 shows the scalograms of the individual signals of one wristband. On the y-axis, the frequencies are shown in Hertz and on the x-axis the time in seconds. For the calculation of the wavelet transformations, we used the Python library PyWavelets [27].
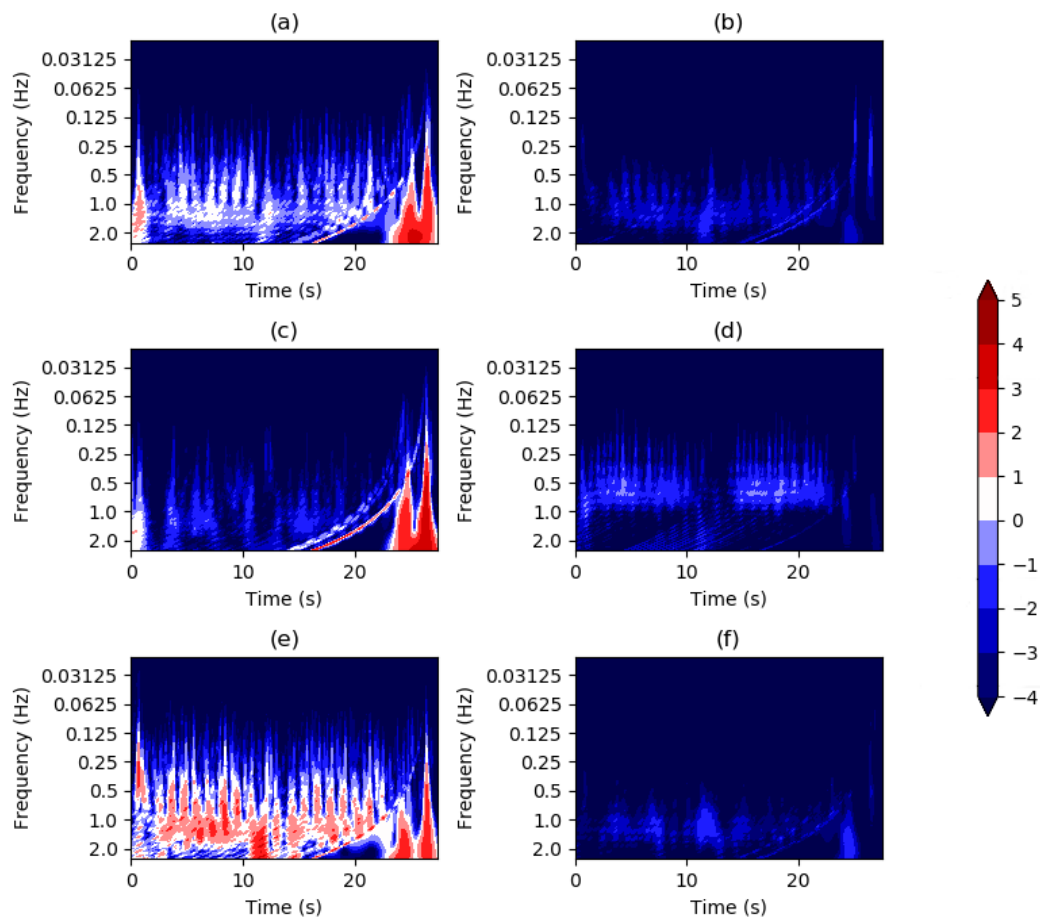
Figure 6. (**a**) x-axis of the derived Euler angle. (**b**) y-axis of the derived Euler angle. (**c**) z-axis of the derived Euler angle. (**d**) x-axis of linear acceleration. (**e**) y-axis of linear acceleration. (**f**) z-axis of linear acceleration.

Figure 6a,c,e corresponds to the x-, y-, and z-axes of the derived Euler angles. We calculated for each signal the continuous wavelet transformation with the Morlet wavelet. It can be seen that there was a high amplitude from 0.25 Hz. In the lower frequency data < 0.25, the individual arm swings can be seen.

Figure 6b,d,f reflects the x-, y-, and z-axes of linear acceleration. We calculated for each signal the continuous wavelet transformation with the Morlet wavelet. With these data, it can be seen that the largest amplitude was in the range of 1 Hz. This corresponds to the natural arm swing since this corresponds to a frequency of approximately 1.2 Hz [26].

3.5. CNN

In image classification, as well as other signals, the application of CNNs has been very successful. The difference from common NNs is that a CNN searches for a local pattern in the input signal. When using multiple CNN layers, one after the other, larger patterns can be detected [28,29]. Thus, a CNN often provides better classification results than NN. In our case, we achieved the best results with the use of three convolution layers. Then, we applied one NN with three encoders and one decoder. Our used CNN with the configuration is shown in Figure 7. We used Python and the Keras library to create the CNN [30]. We obtained the architecture for our CNN by systematically testing. We wanted to keep the number of CNN layers as small as possible. However, with less than three layers, no useful results were available.
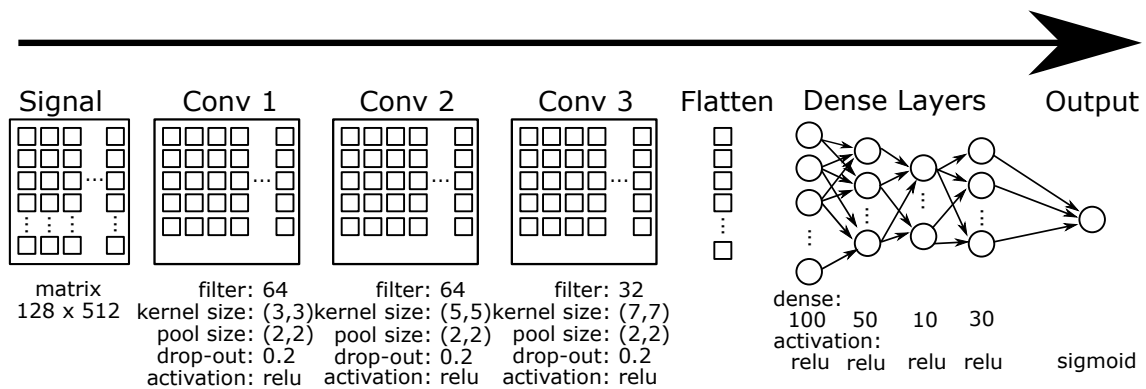
Figure 7. Construction of a single signal CNN for classification.

In order to have a useful input for the CNN, we resampled the signal to a uniform length of 512 values; see Section 3.3. We then applied a wavelet transformation to the signal; see Section 3.4. This gave us a 128×512 matrix for the signal. We used this matrix as input for the CNN. As the activation function, we used the ReLU function for all convolution layers. We also used the ReLU function in the hidden layers of the encoder and decoder. The equation of the ReLU function can be seen in Equation (3). The characteristic of the ReLU function is that the weight of the output is not negative. In the output layer, we used the sigmoid function; see Equation (4). After each convolution layer, we performed a two-dimensional max-pooling with a pool size of 2×2 and a drop out with a probability of 0.2.

$$f(x) = max(0, x) \tag{3}$$

$$f(x) = \frac{1}{1 + e^{-x}} \tag{4}$$

The first convolutional layer searched for the smallest pattern from the signal. For convolution, we used a 3×3 matrix. In total, we created 64 different filters in the first convolutional layer. In the second convolutional layer, we increased our kernel size to 5×5 and created 64 filters again. The third convolutional layer had a kernel size of 7×7, and the filters created were reduced to 32 pieces. After the convolutional layers, we used a flatten layer so that the signal could be interpreted by the dense layers. In the dense layers, we started with three encoder layers with 100, 50, and 10 neurons, followed by a decoder layer with 30 neurons. Finally, we obtained our prediction in the output layer. Since we had a binary problem, a single neuron was used. For the training of the models, we used a batch size of 50 and 50 epochs. For training, we used an Intel Core i7-6700HQ with 2.6 GHz with four cores. Furthermore, the system used 16 GB RAM. The computer required approximately 45 min to train a model.

3.6. Multi-Channel CNN

In the last section, we presented our architecture for a single signal. To achieve better and more robust results, we wanted to use multiple channels x, y Euler angles, and x of linear acceleration for classification. For this reason, we created an m-dimensional input. For the third dimension, we used the number of *m* different signals used. Figure 8 shows the construction. Another difference was that the first convolutional layer created 128 filters. The model was similar to the one in Figure 7. The computer required approximately 2 h to train a model.
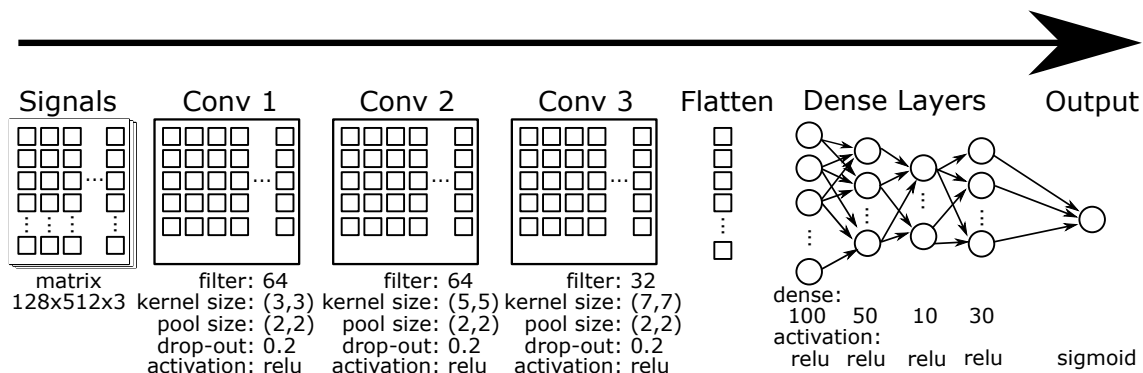
Figure 8. Construction of a 3-channel CNN to use three different signals for classification.

3.7. Weight Voting

The multi-channel CNN was trained with 3 signals at the same time. The difference in voting was that for each signal, a separate model was trained, which was independent of the other models. In our case, we had a binary problem, so the calculation for the voting was easy. We used the predicted classes and calculated the average of all predictions; see Equation (5), where m_i is the prediction of a model from a classifier and M is the number of classifiers.

$$v = \frac{1}{M} \sum_{i=1}^{M} m_i, i \in \{1, 2, ..., M\} \tag{5}$$

If $v \geq 0.5$, then the predicted class is MD and in all other cases, no MD; see Equation (6).

$$prediction = \begin{cases} MD, & v \geq 0.5 \\ noMD, & v < 0.5 \end{cases} \tag{6}$$

3.8. Evaluation

We decided to use 3-fold cross-validation for the classification to make the results of our applied methods reasonable. We used 66.6% of the data for training and 33.3% for testing. For each measurement, we calculated the sensitivity, specificity (precision), recall, F1-score, and accuracy. For this, we used the confusion matrix in Table 2.

Table 2. Binary confusion matrix.

	Classes	
	Positive	**Negative**
predicted positive	TP true positive	FP false positive
predicted negative	FN false negative	TN true negative

Sensitivity (recall) is a widespread measurement in medicine. It indicated the ratio of predicted MD to all MD inside our test data; see Equation (7). The specificity described how well our system can distinguish MD from the control group (no MD). It was the ratio of predicted non-MD persons in all test data where healthy persons were present; see Equation (8). Precision was the proportion of correctly predicted MD to all MD; see Equation (9). Accuracy was the ratio of all correctly recognized

MD and no MD to all test data; see Equation (10). The F1-score (F1) was the harmonious average between precision and recall; see Equation (11).

$$recall = sensitivity = \frac{TP}{TP + FN} \tag{7}$$

$$specificity = \frac{TN}{FP + TN} \tag{8}$$

$$precision = \frac{TP}{TP + FP} \tag{9}$$

$$accuracy = \frac{TP + TN}{TP + FP + FN + TN} \tag{10}$$

$$F1 = 2 \cdot \frac{precision \cdot recall}{precision + recall} \tag{11}$$

3.9. Methodology

After we have presented our material and methods, we will now discuss in this section how we applied these methods. In the presentation of the dataset, we already said that we divided our recording into two different parts. First, we classified Parts (A) and (B), which comprised the complete recording of the TUG test. The other scenario was that we only used Part (B). In Part (B), only the gait was used. Figure 9 shows the complete algorithm of the classification. In principle, we distinguished between the signals of the Euler angles and the linear acceleration. First, we removed the jumps within a signal of the Euler angles and then calculated the derivation of the signal. This made the signal more comparable. These steps were not necessary for linear acceleration. Then, we set the signals to a uniform length. This was necessary so that the signals could be interpreted by CNN later during classification. After resampling, we calculated the wavelet transformation for each individual signal. We used the resulting scalograms for the classification. In the classifications, we analyzed three different cases. At first, we classified each signal individually by CNN. This allowed us to show which axis of the sensors was very important. In the second case of classification, we used the three best signals for a multi-channel CNN. The third case was that we used the three best signals for classification by voting.

Figure 9. Classification process for detecting motor dysfunctions in arm swinging.

4. Results

4.1. Parts (A) and (B) of TUG

4.1.1. Single Layer

To find out which sensor data were particularly useful for classification, we first separated all signals from each other. The results are shown in Table 3. In the table, we applied three-fold cross-validation to the sensor data. Furthermore, we optically separated the results from the Euler angles and the linear acceleration with a double line. For each signal, we calculated the precision, specificity, recall, F1-score, and accuracy. In every cell, we show the mean $\bar{x} = \frac{1}{N} \sum_{i=1}^{N} x_i, i \in \{1, 2, ..., N\}$ plus or minus the standard deviation $s = \sqrt{\frac{1}{1-N} \sum_{i=1}^{N} (x_i - \bar{x})^2}, i \in \{1, 2, ..., N\}$, where N is the length of the signal. The columns with the best results are highlighted with bold. It can be seen that the x-axis of the Euler angle and the x-axis of the linear acceleration produced the best results. Furthermore, it can be seen that the z-axis of the Euler angle and linear acceleration provided the lowest results.

Table 3. Results of a single signal by CNN classification. Parts (A) and (B) of the TUG test are used.

Signal	Sensitivity	Specificity	Recall	F1-Score	Accuracy
x Euler angles	**0.918 ± 0.071**	**0.939 ± 0.043**	**0.887 ± 0.085**	**0.898 ± 0.017**	**0.928 ± 0.009**
y Euler angles	0.891 ± 0.014	0.874 ± 0.016	0.775 ± 0.072	0.829 ± 0.047	0.882 ± 0.009
z Euler angles	0.57 ± 0.505	0.844 ± 0.186	0.606 ± 0.527	0.587 ± 0.514	0.821 ± 0.173
x linear acceleration	**0.907 ± 0.101**	**0.901 ± 0.048**	**0.846 ± 0.036**	**0.873 ± 0.046**	**0.908 ± 0.015**
y linear acceleration	0.857 ± 0.031	0.888 ± 0.056	0.841 ± 0.066	0.848 ± 0.032	0.877 ± 0.027
z linear acceleration	0.795 ± 0.118	0.863 ± 0.044	0.74 ± 0.043	0.761 ± 0.037	0.841 ± 0.009

4.1.2. Signal Combination

To get better results in the classification, we decided to combine the individual layers. For the combination, there were several possibilities. On the one hand, it was possible to use an ensemble classifier like voting. On the other hand, we could use a multi-channel CNN. In Table 3, the x-axis of the Euler angles and the linear acceleration produced the best results. The third was the Euler angles of the y-axis. In this section, we used these three signals to improve our results. The results are shown in Table 4. We again used three-fold cross-validation for our results. Each cell represented the result as $\bar{x} \pm s$, as introduced in Section 4.1.1.

Table 4. Classification results by combining the x- and y-axis of Euler angles and the x-axis of linear acceleration. Parts (A) and (B) of the TUG test are used.

Layer	Sensitivity	Specificity	Recall	F1-Score	Accuracy
3 channel CNN	0.934 ± 0.047	0.932 ± 0.013	0.899 ± 0.026	0.928 ± 0.043	0.933 ± 0.024
3 signal voting	0.915 ± 0.078	0.9 ± 0.02	0.821 ± 0.052	0.862 ± 0.026	0.902 ± 0.018

Table 4 shows the results of the signal combination classification. The three channel CNN achieved better results than the three signal voting. The three channel CNN was also better than any signal in Table 3.

4.2. Part (B) of TUG

4.2.1. Single Layer

In this section, we present our results if only Part (B) of the TUG test was used for classification. In Table 5, you can see the results for a CNN classification for each axis of the sensors. As in Section 4.1.1, we used three-fold cross-validation and calculated the average $\bar{x}$ plus or minus the standard deviation s. The best results for each sensor and each column are marked with bold. Like the analysis of

the complete TUG test, the x-axis provided the best results for Euler angles and linear acceleration. However, the results were not as accurate as in Section 4.1.1.

Table 5. Results of a single signal by CNN classification. Only Part (B) of the TUG test is used.

Signal	Sensitivity	Specificity	Recall	F1-Score	Accuracy
x Euler angles	0.873 ± 0.027	0.899 ± 0.043	0.822 ± 0.088	0.844 ± 0.039	0.887 ± 0.018
y Euler angles	0.793 ± 0.037	0.855 ± 0.016	0.756 ± 0.046	0.772 ± 0.006	0.831 ± 0.015
z Euler angles	0.763 ± 0.202	0.943 ± 0.049	0.904 ± 0.088	0.809 ± 0.099	0.821 ± 0.138
x linear acceleration	0.909 ± 0.012	0.9 ± 0.044	0.822 ± 0.088	0.862 ± 0.053	0.903 ± 0.032
y linear acceleration	0.804 ± 0.041	0.832 ± 0.043	0.705 ± 0.078	0.748 ± 0.033	0.821 ± 0.024
z linear acceleration	0.563 ± 0.496	0.794 ± 0.147	0.508 ± 0.468	0.52 ± 0.453	0.774 ± 0.111

4.2.2. Signal Combination

Table 6 shows the results of the signal combination of Part (B) of the TUG test. For the results, three-fold cross-validation was applied and for each cell, and the average $\bar{x}$ plus or minus the standard deviation s was calculated. The three signal voting performed best. However, the results were marginally better than the single signal CNN classification in Table 5. Furthermore, the results were not as good as if the complete TUG test was used for the classification.

Table 6. Classification results by combining the x- and y-axis of Euler angles and the x-axis of linear acceleration. Only Part (B) of the TUG test is used.

Layer	Sensitivity	Specificity	Recall	F1-Score	Accuracy
3 layer CNN	0.888 ± 0.045	0.847 ± 0.027	0.677 ± 0.065	0.766 ± 0.042	0.856 ± 0.024
3 signal voting	0.914 ± 0.03	0.901 ± 0.043	0.822 ± 0.088	0.863 ± 0.04	0.903 ± 0.024

5. Discussion

In Tables 3 and 5, the x-axis always shows the best results. The x-axis corresponds to the movement in the sagittal plane. According to the literature, the most important characteristics of human gait are also present in this plane [31,32]. For this reason, it is a logical conclusion that the features with the highest significance are present on this axis.

We presented our results in the previous section. We compared the results when the complete TUG test, Parts (A) and (B), was used for the classification, as well as if we only used the gait, Part (B), for the classification. The results showed that for the classification of motor dysfunctions, the gait alone gave quite good results with an accuracy of 90.3%, but when looking at the complete test, we obtained even better results with an accuracy of 93.3%. From this, we concluded that the complete TUG test was necessary for the analysis of motor dysfunctions.

Furthermore, we classified each signal separately. During the classification, we found out that the x-axis of the Euler angle and linear acceleration gave the best results, independent of whether Parts (A) and (B), as well as only Part (B) were used for the classification. From this, we concluded that the x-axis was the most relevant.

The conclusion was that we obtained better results through the combination of the signals compared to single signals. In the classification of Parts (A) and (B), the three-channel CNN proved to be the best solution. When classifying with only Part (B), voting was the best choice.

Table 7 shows our classification results compared to the corresponding state-of-the-art works. Our results were comparable to the results from large, expensive, and stationary video based systems.

Table 7. Comparison of classification results with other works.

Reference	Description	Accuracy
Our System	IMU sensors	93.3%
[12]	Kinect camera	90%
[17]	Kinect, Bayesian network	93.4%
[18]	Kinect and e-Motion capture program	96.23%
[15]	Gyroscope	90%

Our system delivered better results than the wearable system that also classified the data [15]. We could not make a comparison with the other works because they focused on a statistical evaluation of the data. CNN in combination with wavelet transformations was a powerful technique for arm swing analysis.

References

1. Kontis, V.; Bennett, J.E.; Mathers, C.D.; Li, G.; Foreman, K.; Ezzati, M. Future life expectancy in 35 industrialised countries: Projections with a Bayesian model ensemble. *Lancet* **2017**, *389*, 1323–1335. [CrossRef]

2. Parkinson's Foundation. Available online: https://www.parkinson.org/Understanding-Parkinsons/Statistics (accessed on 1 October 2019).

3. Goetz, C.G.; Tilley, B.C.; Shaftman, S.R.; Stebbins, G.T.; Fahn, S.; Martinez-Martin, P.; Poewe, W.; Sampaio, C.; Stern, M.B.; Dodel, R.; et al. Movement Disorder Society-sponsored revision of the Unified Parkinson's Disease Rating Scale (MDS-UPDRS): Scale presentation and clinimetric testing results. *Mov. Disord.* **2008**, *23*, 2129–2170. [CrossRef] [PubMed]

4. Mazumder, O. Development and Control of Active Lower Limb Exoskeleton for Mobility Regeneration and Enhancement. Ph.D. Thesis, Indian Institute of Engineering Science and Technology, Shibpur, India, 2018.

5. Jasni, F.; Hamzaid, N.A.; Al-Nusairi, T.Y.; Yusof, N.H.M.; Shasmin, H.N.; Cheok, N.S. Feasibility of A Gait Phase Identification Tool for Transfemoral Amputees using Piezoelectric-Based In-Socket Sensory System. *IEEE Sens. J.* **2019**, *19*, 6437–6444. [CrossRef]

6. Stoelben, K.J.V.; Pappas, E.; Mota, C.B. Lower extremity joint moments throughout gait at two speeds more than 4 years after ACL reconstruction. *Gait Posture* **2019**, *70*, 347–354. [CrossRef] [PubMed]

7. Balzer, J.; Marsico, P.; Mitteregger, E.; van der Linden, M.L.; Mercer, T.H.; van Hedel, H.J. Influence of trunk control and lower extremity impairments on gait capacity in children with cerebral palsy. *Disabil. Rehabil.* **2018**, *40*, 3164–3170. [CrossRef] [PubMed]

8. Prakash, C.; Sujil, A.; Kumar, R.; Mittal, N. Linear Prediction Model for Joint Movement of Lower Extremity. In *Recent Findings in Intelligent Computing Techniques*; Springer: Singapore, 2019; pp. 235–243.

9. Steinmetzer, T.; Bonninger, I.; Priwitzer, B.; Reinhardt, F.; Reckhardt, M.C.; Erk, D.; Travieso, C.M. Clustering of Human Gait with Parkinson's Disease by Using Dynamic Time Warping. In Proceedings of the 2018 IEEE International Work Conference on Bioinspired Intelligence (IWOBI), San Carlos, Costa Rica, 18–20 July 2018; pp. 1–6.

10. Steinmetzer, T.; Bönninger, I.; Reckhardt, M.; Reinhardt, F.; Erk, D.; Travieso, C.M. Comparison of algorithms and classifiers for stride detection using wearables. *Neural Comput. Appl.* **2019**, 1–12. [CrossRef]

11. Ospina, B.M.; Chaparro, J.A.V.; Paredes, J.D.A.; Pino, Y.J.C.; Navarro, A.; Orozco, J.L. Objective arm swing analysis in early-stage Parkinson's disease using an RGB-D camera (Kinect). *J. Parkinson's Dis.* **2018**, *8*, 563–570. [CrossRef] [PubMed]

12. Spasojević, S.; Santos-Victor, J.; Ilić, T.; Milanović, S.; Potkonjak, V.; Rodić, A. A vision-based system for movement analysis in medical applications: The example of Parkinson disease. In *International Conference on Computer Vision Systems*; Springer: Cham, Switzerland, 2015; pp. 424–434.

13. Baron, E.I.; Koop, M.M.; Streicher, M.C.; Rosenfeldt, A.B.; Alberts, J.L. Altered kinematics of arm swing in Parkinson's disease patients indicates declines in gait under dual-task conditions. *Parkinsonism Relat. Disord.* **2018**, *48*, 61–67. [CrossRef] [PubMed]

14. Lewek, M.D.; Poole, R.; Johnson, J.; Halawa, O.; Huang, X. Arm swing magnitude and asymmetry during gait in the early stages of Parkinson's disease. *Gait Posture* **2010**, *31*, 256–260. [CrossRef] [PubMed]

15. Tsipouras, M.G.; Tzallas, A.T.; Rigas, G.; Tsouli, S.; Fotiadis, D.I.; Konitsiotis, S. An automated methodology for levodopa-induced dyskinesia: Assessment based on gyroscope and accelerometer signals. *Artif. Intell. Med.* **2012**, *55*, 127–135. [CrossRef] [PubMed]

16. Castaño, Y.; Navarro, A.; Arango, J.; Muñoz, B.; Orozco, J.L.; Valderrama, J. Gait and Arm Swing Analysis Measurements for Patients Diagnosed with Parkinson's Disease, using Digital Signal Processing and Kinect. In Proceedings of the SSN2018, Valdivia, Chile, 29–31 October 2018; pp. 71–74.

17. Dranca, L.; de Mendarozketa, L.D.A.R.; Goñi, A.; Illarramendi, A.; Gomez, I.N.; Alvarado, M.D.; Rodríguez-Oroz, M.C. Using Kinect to classify Parkinson's disease stages related to severity of gait impairment. *BMC Bioinform.* **2018**, *19*, 471. [CrossRef] [PubMed]

18. Castaño-Pino, Y.J.; Navarro, A.; Muñoz, B.; Orozco, J.L. Using Wavelets for Gait and Arm Swing Analysis. In *Wavelet Transform and Complexity*; IntechOpen: London, UK, 2019.

19. Roggendorf, J.; Chen, S.; Baudrexel, S.; Van De Loo, S.; Seifried, C.; Hilker, R. Arm swing asymmetry in Parkinson's disease measured with ultrasound based motion analysis during treadmill gait. *Gait Posture* **2012**, *35*, 116–120. [CrossRef] [PubMed]

20. Huang, X.; Mahoney, J.M.; Lewis, M.M.; Du, G.; Piazza, S.J.; Cusumano, J.P. Both coordination and symmetry of arm swing are reduced in Parkinson's disease. *Gait Posture* **2012**, *35*, 373–377. [CrossRef] [PubMed]

21. Bertomeu-Motos, A.; Lledó, L.; Díez, J.; Catalan, J.; Ezquerro, S.; Badesa, F.; Garcia-Aracil, N. Estimation of human arm joints using two wireless sensors in robotic rehabilitation tasks. *Sensors* **2015**, *15*, 30571–30583. [CrossRef] [PubMed]

22. Viteckova, S.; Kutilek, P.; Lenartova, J.; Kopecka, J.; Mullerova, D.; Krupicka, R. Evaluation of movement of patients with Parkinson's disease using accelerometers and method based on eigenvectors. In Proceedings of the 2016 17th International Conference on Mechatronics-Mechatronika (ME), Prague, Czech Republic, 7–9 December 2016; pp. 1–5.

23. MbientLab. MetaWear RG/RPro. 2016. Available online: https://mbientlab.com/docs/MetaWearRPROPSv0.8.pdf (accessed on 4 January 2016).

24. BOSCH Sensortec, Data Sheet BMI160. 2015. Available online: https://ae-bst.resource.bosch.com/media/_tech/media/datasheets/BST-BMI160-DS000-07.pdf (accessed on 2 December 2019).

25. Virtanen, P.; Gommers, R.; Oliphant, T.E.; Haberland, M.; Reddy, T.; Cournapeau, D.; Burovski, E.; Peterson, P.; Weckesser, W.; Bright, J.; et al. SciPy: Open Source Scientific Tools For Python. 2019. Available online: http://www.scipy.org/ (accessed on 2 December 2019).

26. Hausdorff, J.M.; Cudkowicz, M.E.; Firtion, R.; Wei, J.Y.; Goldberger, A.L. Gait variability and basal ganglia disorders: Stride-to-stride variations of gait cycle timing in Parkinson's disease and Huntington's disease. *Mov. Disord.* **1998**, *13*, 428–437. [CrossRef] [PubMed]

27. Lee, G.R.; Gommers, R.; Wasilewski, F.; Wohlfahrt, K.; O'Leary, A. PyWavelets: A Python package for wavelet analysis. *J. Open Source Softw.* **2019**, *4*, 1237. [CrossRef]

28. Abadi, M.; Abadi, M.; Barham, P.; Chen, J.; Chen, Z.; Davis, A.; Dean, J.; Devin, M.; Ghemawat, S.; Irving, G.; et al. Tensorflow: A system for large-scale machine learning. In Proceedings of the 12th USENIX Symposium on Operating Systems Design and Implementation (OSDI 16), Savannah, GA, USA, 2–4 November 2016.

29. Sze, V.; Chen, Y.H.; Yang, T.J.; Emer, J.S. Efficient processing of deep neural networks: A tutorial and survey. *Proc. IEEE* **2017**, *105*, 2295–2329. [CrossRef]

30. Chollet, F. Keras. 2015. Available online: https://keras.io (accessed on 11 October 2019).

31. Tafazzoli, F.; Safabakhsh, R. Model-based human gait recognition using leg and arm movements. *Eng. Appl. Artif. Intell.* **2010**, *23*, 1237–1246. [CrossRef]
32. Zhang, R.; Vogler, C.; Metaxas, D. Human gait recognition at sagittal plane. *Image Vis. Comput.* **2007**, *25*, 321–330. [CrossRef]

Analyzing gait symmetry with automatically synchronized wearable sensors in daily life

Tobias Steinmetzer*, Sandro Wilberg, Ingrid Bönninger, Carlos M. Travieso

Tobias Steinmetzer, Universitätsplatz 1, Senftenberg 01968, Germany

ABSTRACT

Gait deviations such as asymmetry are one of the characteristic symptoms of motor dysfunctions that contribute to the risk of falls. Our objective is to measure gait abnormalities such as asymmetry of the lower limbs in order to evaluate the diagnosis more objectively. For the measurement we use inertial measurement unit (IMU) sensors and force sensors, which are integrated in wristbands and insoles. To extend the battery life of wearable devices, we only save data of the activity *gait* within the wearables. Therefore we perform activity recognition with a smartphone. Using convolutional neural network (CNN) we achieved an accuracy of 94.7 % of the activity *gait* recognition. Before recording we synchronize the wearable sensors and reach a maximum latencies of 3 *ms*. Before the analysis of the symmetry we detect the strides by using a CNN with an accuracy of 98.8 %. For the symmetry evaluation we used dynamic time warping (DTW). The DTW enables us to calculate symmetry of the complete time series of human gait.

1. Introduction

One of the greatest achievements of modern medicine is that the life expectancy of the global population is continuously increasing [1]. However, it also creates new problems. The epidemiology of old-age diseases is a significant part of the problem. These include, for example, Parkinson's disease (PD) [2]. PD is often combined with motor dysfunctions. For this reason, it is essential to assess the patient's motor skills at regular intervals. Furthermore, the measurement of motor skills can be used for conclusions about the progress of the disease and treatment success. Bradykinesia, rigor, tremor, postural instability, and walking disorders are typical symptoms of the disease. The aim of our cooperation with the Niederlausitz Clinic Senftenberg is to measure gait abnormalities in PD, such as the asymmetry of the upper and lower limbs in daily life. Thus, the diagnosis can be more objective and therapy more effective. Furthermore, the continuous measurements should give the patient feedback to the therapy success and thus can be motivated for the therapy. For this reason, we created a mobile system that provides objective measurement data to the physician to be able to evaluate motor disease quantitatively. Gait deviations such as asymmetry are one of the characteristic symptoms of patients

with PD that contribute to the risk of falls [3]. For the continuous measurement of motion in daily life, we propose the use of wearable microcontroller-based systems. For this reason, we propose a system that:

1. uses sensors that the user can comfortably carry the whole day
2. records and transmits data in an energy-saving manner
3. synchronizes the arm and leg sensors in real-time
4. filters out the activity *gait* from any *other* movement activity
5. analyses the symmetry of legs individually and to each other

This work is divided into seven sections. Relevant works for this paper are introduced in section II. Section III describes the developed hardware, the test performed by the users. All carried out procedures we need for the analysis of the A-symmetry are described in Section IV. The results achieved are presented in Section V. Section VI indicates the discussion and Section VII the conclusion and further development.

2. Related works

For the symmetry analysis of the gait in daily life, time series must be recorded with the wearable sensors. Therefore it is necessary to extract the activity *gait* from all activities such as sitting, standing, climbing stairs, or walking. To be able to calculate symmetry values from this time series, the system must work synchronously.

* Corresponding author.
E-mail addresses: tobias.steinmetzer101@alu.ulpgc.es, tobias.steinmetzer@b-tu.de (T. Steinmetzer).

2.1. Sensors

Already in 1992, motion and symmetry of the lower extremities were recorded with cameras and markers [4]. Technological advances and the cost-effective development of depth cameras have opened up new possibilities for motion analysis by Kinect from 2010. The depth camera extended the RGB camera. Thus the gait could be analyzed with new methods [5]. The disadvantage of camera systems is that they are stationary.

In the following years, the use of gyroscopes, accelerometers magnetometers, and force sensors were further developed, and the popularity of the sensors increased, as the many smartphones and game console controllers are equipped with these sensors. The advantage of these sensors is that these are integrated into small devices and that they are wearable. Thus it is possible to analyze the human gait independent of location. These sensors are often used to determine strides or activities [6–15].

2.2. Activity recognition

Many smartphones have a gyroscope, accelerometer, and magnetometer. In many studies, this has been used to try to identify the activities of people [13–15]. One possibility to implement this is to choose a fixed window width and collect all statistical values for this window, which serve as a characteristic for the classification. The use of a neural network has proven to be useful here [14,15]. Another possibility is the use of CNN's [13].

Activity detection is usually used to reflect the time a person has been moving throughout the day. This is sufficient for an activity estimation of a person in general. The quality of smartphone sensors is adequate to estimate the activity of a person.

2.3. Symmetry

The situation is different when wearables assess diseases related to movement disorders. In this case, IMU sensors are attached to specific joints or integrated into clothing. To measure and store the time series of gait wearable containing microcontrollers in combination with IMU sensors are often used [6–11,16–22]. In most cases, the motion of the lower extremities is measured [6–11,22]. Thereby conclusions can be made about the stride length, cadence, stride duration, gait phases, and symmetry [6,10,11,23].

There are different methods for the calculation of symmetry. One approach is that different calculated features like step length, step duration, standing time, or swing time of the legs are put into relation [16,20,24]. The disadvantage of this method is that only average values of the calculated characteristics for the gait can be assessed, but not the entire time series. This is different for stationary systems, which are camera-based. With these systems, the complete body can be recorded synchronously [17]. Both types of symmetry evaluation are useful. However, in our opinion, a direct comparison of the time series is most useful, because differences in the related arms and strides can be measured directly.

The symmetry of arms and legs, as well as the symmetry of the upper and lower limbs with each other, investigate only a few papers [25–27]. Changes of interlimb coordination in individuals with PD and healthy older adults while systematically manipulating walking speed are compared to determine the impact of PD symptoms on interlimb coordination [25]. Markers were placed on the foot, heel, ankle, knee, hip, thigh, wrist, elbow, shoulder, and head. A point estimate of the relative phase (PERP) between body segments was calculated by using the moment at which the positive maxima were reached for the angle of each body segment. To assess change in asymmetry over time is the objective in [26]. The

changes in movements are assessed by a single neurologist specializing in movement disorders. A robust ordinal logistic regression model that includes a control for clustering due to repeated observations within-person for evaluating the relative change in asymmetry is used.

Another system focuses on the study of the impact of PD on synkinesias (i.e., the symmetry of movement) during walking, and the effect of medication on the gait symmetry [27]. Every patient was tested and measured using IMU-sensors in his ON and OFF state. The trend symmetry value is calculated as a ratio of the variabilities of two eigenvectors, which are calculated from the kinematic motion data of the left and right limb. An up-to-date overview of symmetry analysis systems for movements is shown in [28].

The use of identical time points for the determination of A-symmetry is of the highest importance. That means data transmission has to be synchronized.

2.4. Synchronization

The video-based systems have a synchronized recording of all extremity movements. The disadvantage is that the measurements cannot be carried out in daily life. Only camera systems for laboratory measurements were found in the literature [27]. Wearable systems, in contrast, could be an alternative for making symmetry measurements of gait in daily life, but they are not time-synchronized.

To closing this gap, the microcontrollers must be synchronized with each other. Several approaches have already been pursued this. A possible solution is to build up a sensor network in which the sensors are connected by wires [27]. Another work presents a system where a docking station serves as a charging station and for synchronization [18]. The docking station can synchronize four wearable sensors, but it has a time drift after a longer runtime. Others use the system of MbientLab [20]. To determine the symmetry of the gait, we need four synchronized sensors (one at each limb). In earlier works, we had tested the system of Mbientlab, but it can only record three synchronized sensors [20].

Advantages and disadvantages of current systems:

– Camera-based systems can measure synchronized time series of each limb. But they are stationary and therefore not suitable for measurements in everyday life.
– A smartphone is useful for detecting gait activities. But it's too imprecise for clinical measurement.
– IMU systems are an alternative to camera-based systems. But they have to be synchronized.

To calculate the gait symmetry of time series using wearable sensors in daily life, we propose a system with two wristbands with IMU sensors, two insoles each with one IMU and ten force sensors, and a smartphone for activity detection. For the measurements, we synchronize all sensors if the activity walk is detected in daily life. We propose a method to calculate the symmetry from all measured values of the gait cycle instead of the symmetry calculation with parameters. For our prototype, we only used data from healthy subjects.

3. Material

3.1. Hardware

3.1.1. Smartphone

For activity detection, we used various smartphones and tablets with the Android operating system. To be independent of a specific device. However, the device must be able to provide linear acceleration and rotation data. We recorded both sensor data with
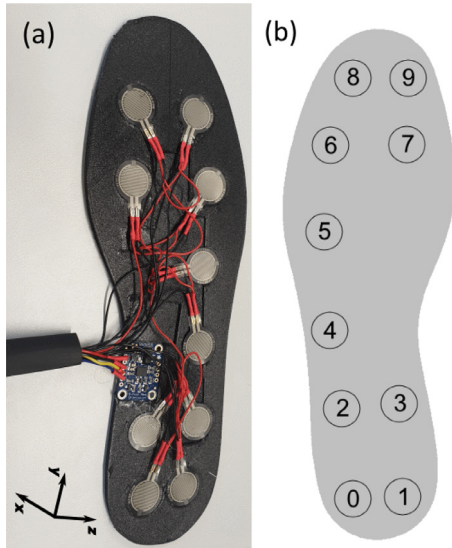
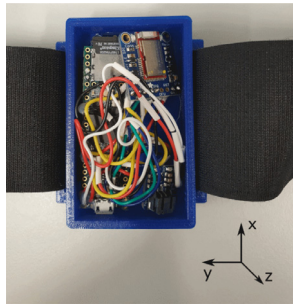**Fig. 1.** Insole with force and IMU sensor.

Fig. 2. Wristband and IMU sensor.

a frequency of 50 %. To make the system energy efficient, we use smartphones for activity detection. Only if the smartphone has detected the activity *gait*, the wearables record the data.

3.1.2. Wearables

For the motion measurement, we use Bosch BNO055 IMU sensors consisting of a gyroscope, accelerometer, and magnetometer [29]. The sensors are mounted in insoles, see Fig. 1, and in wristbands, see Fig. 2. The BNO 055 sensor has an integrated co-processor for the sensor fusion that calculates the absolute orientation and linear acceleration. So angle velocity, acceleration, quaternions, Euler angles, and linear acceleration values are received with 100 Hz. For force measurement, we use ten FSR 402 force sensors in the insoles [30]. Furthermore, the natural rolling motion can be measured by the horizontal arrangement of the sensors. The parallel arrangement of the sensors should later make it possible to calculate the balance, see (b) in Fig. 1. The insoles were printed with a 3D printer. We used flexible material to achieve a lower bias by using the insoles. To get a lower bias and higher comfort by a foreign insole, we made the insole out of flexible material.

3.2. Data set

3.2.1. Activity recognition

In this data set, we use recordings of 20 healthy subjects to test the system. For this propose, we developed an Android App. The subjects specified the start, end, and type of activity via the App before each recording. We recorded linear acceleration and rotation data of the Android operating system with a frequency of 50 Hz.

The users had to specify in which activity they performed. In total the following activities were recorded *gait, cycling, go stairs, lying, sitting, standing, smartphone lying around* (table or desk), *smartphone in use* (writing a message or play a game), and *use transport* (drive by car or train). We have reduced the problem to a binary problem and use in the following only the classes *gait* and *other*. The class *other* contains the activities *cycling, go stairs, lying, sitting, smartphone lying around, smartphone in use, standing,* and *use transport*.

3.2.2. Daily life

For the daily life data set, we have a total of 7 recordings of 7 different healthy persons. The age of the persons was between 25 and 54 years. The persons passed the following test:

1. sitting on a chair for 1 minute
2. stand up and standing for 1 minute
3. walking for 1 minute
4. ascending stairs over three floors
5. descending stairs over three floors
6. walking for 1 minute
7. standing for 1 minute in front of the chair
8. sit down
9. sitting on a chair for 1 minute

4. Methods

4.1. Methodology

The whole process for the recognition of gait data is based on the communication between our Android App and four wearable devices (two wristbands and two insoles). Fig. 3 shows the process. We have separated the functional tasks of the smartphone and wearables with a dotted line. However, the wearables work only as slaves, so the smartphone must always send a signal for starting a function. For this reason the tasks *Stop Recording, Data Transmission, Synchronization* and *Start Recording* are involved by both devices.

At the beginning of the workflow, we make an activity recognition. Thus, we want to distinguish the activity *gait* again, the activity *other*. The activity detection is designed to keep the wearable sensors in standby mode until the activity *gait* is detected. This activity detection extends the usage time of the wearable devices.

When a person does the activity *gait*, the app checks if a recording is in process. If not, the wearable devices have first synchronized, and then the recording of the movement starts. When
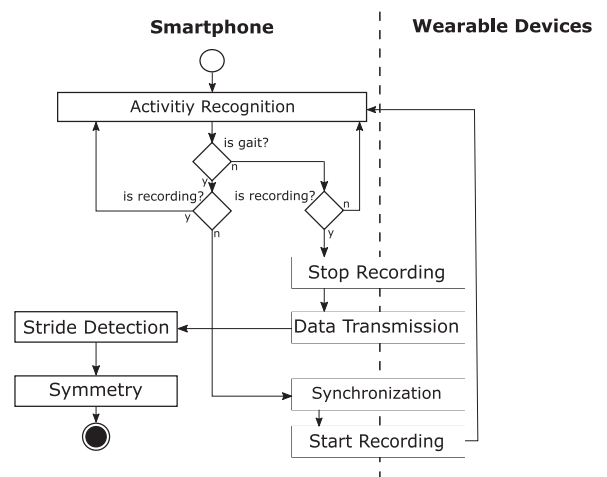
Fig. 3. Process of synchronize, record, and evaluate data.
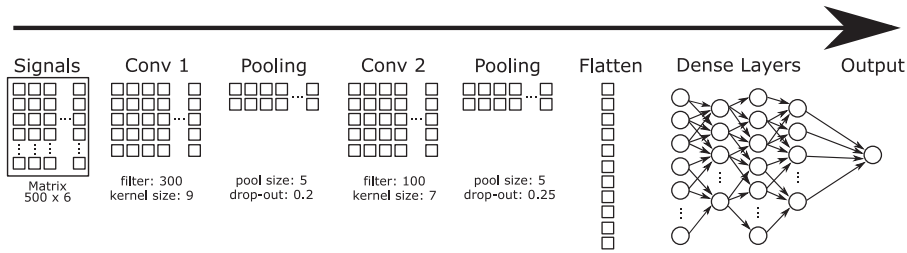
Fig. 4. Schema of the CNN layers for activity recognition.

the activity *other* as *gait* has been detected, and the recording is in process, the recording stopped, and the data transmitted to the smartphone.

For the symmetry calculation, we need a more accurate detection of the strides than with the activity recognition. For this reason, we perform a stride detection by using CNN to detect individual strides of the foot. After that, the symmetry of the strides can be calculated.

4.2. Activity recognition

To enable energy-efficient use of the wearable devices, they are only powered when they are in use. The energy-efficient use means that the wearable devices only have to be switched on during recording. For this reason, we decided to use a binary activity classifier in the smartphone device. This classifier enables us to distinguish the activity *gait* from *other* like cycling, go stairs, lying, sitting, smartphone lying around, smartphone in use, standing, and use transport.

For the activity detection, we use data of the linear acceleration and rotation data of the Android operating system (OS) at a frequency of 50 Hz. As features, we use a fixed window width of 10 s and an overlap of 50 %. We use as input the x-, y-, and z- axis of the linear acceleration and rotation data of the complete window as input for a 1D CNN classifier. Fig. 4 shows the design of the

CNN. We chose CNN because other researchers have also achieved good results with CNN [13,14].

For the construction of the model, we use the activation function rectified linear unit (ReLU) function except for the output layer. The first layer is a convolutional layer with 300 filters and a kernel size of 9. Next is a max pooling with a size of 5 and a drop-out with 0.2. Then follows another convolution layer with 100 filters and a kernel size of 7. Then again, a max pooling with a size of 5 and a drop-out with a probability of 0.25. Next comes a flatting layer. In the following, there are different dense layers with 30, then 10, and finally 50 neurons. The last layer is the output layer, which uses a sigmoid function as the activation function.

For training, we have separated the data by persons. This ensures that the same person is not included in the training and test data set. We split the data that 66 % (13 subjects) are used for training, and 34 % (7 subjects) for testing. During training, we use different epochs and batch sizes. In our case, the setting of 100 epochs and 100 batch sizes has proven good results.

4.3. Synchronization

4.3.1. Process

The synchronization takes place according to the following scheme, see Fig. 5. The master device is the smartphone, and the slaves are the four wearable devices.
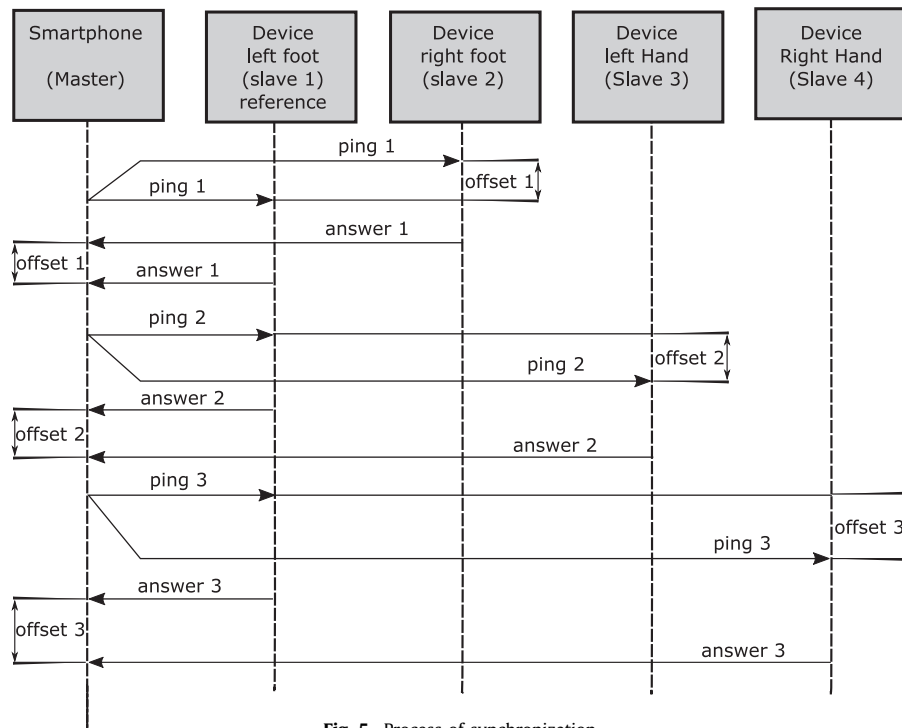
Fig. 5. Process of synchronization.

1. The master sends an empty Bluetooth packet to the first slave (reference slave) and the second slave.
2. Each slave replies with its device time (milliseconds since power-on) as soon as it receives the packet of the master.
3. The master receives the responses and measures the time difference between them.
4. To avoid random response times (e.g., caused by physical influences), the process is repeated multiple times.
5. The median is the time difference between the reception of the packets by the reference slave and the second slave.
6. The master calculates the offset of the second device (see formula 2) and sends it to the second device.
7. Now, the second slave knows its offset compared to the reference slave.
8. Steps 1 to 7 are repeated with the first slave and the third slave.
9. Steps 1 to 7 are repeated with the first slave and the fourth slave.

As a result, we get the offsets between the reference device and the other three measuring devices. The four measuring devices record data synchronously. Unfortunately, a drift can occur between the devices. To prevent this, the synchronization is repeated before each recording.

4.3.2. Verification test setup

To be able to measure the Bluetooth latency correctly, we have wired the microcontrollers to each other. Two microcontrollers are connected by wire using their serial output and input. The output pin of one device is connected with the input pin of the other device and vice versa. In the beginning, the outputs are set to "low". One of the two devices now initiates a "high" output and starts a timer. The other device registers this event by reading a "high" input and answers to the first device by setting its output pin to "high", too. The first device stops the timer as soon as it registers a "high" input. According to repeated measurements, the serial la-

tency is lower than 1 ms Because this latency measurement does not influence the synchronization latency, it is ignored in the following section.

4.3.3. Latency bluetooth

In the next step, we measure the latency and offset of the Android OS to send a Bluetooth packet to the microcontrollers. Furthermore, we also measure the time at which packets are received if the microcontrollers have sent them. For the measurement of the offset between the microcontrollers, we use the test setup from Section 4.3.2. For the test setup, the microcontrollers (M1) and (M2) were placed at the same distance to the Android smartphone (A) so that the same signal strength exists for all devices. Otherwise, this can corrupt the result. The results of the measurement can be seen in Table 1. The first and second columns *A send M1* and *A send M2* are the time stamps of the Android OS in milliseconds (*ms*) when the commands were executed. *Diff 1* is the difference in *ms* between column (*AsendM*2) − (*AsendM*1). The *RL* column is the wired offset between the two microcontrollers measured using the method in the 4.3.2 section. This offset is the real offset. *R1* and *R2* are the timestamps in *ms* of the received Bluetooth packets of the microcontrollers. The last column *l* reflects the difference of the columns *R2* − *R1* in *ms*. This offset, the Android OS uses to calculate the device offsets. Perfect synchronization is achieved when $RL = l$.

The measurement was repeated three times. Therefore each measurement is separated in the table by a double line. The columns *RL* and *l* show a correlation to each other. For this reason, it was written in bold.

The Table 1 shows that the packets are sent with different priorities by the Android OS. Thus the column *Diff 1* does not correlate with *RL*. The values of the three measurements of *A send M1* and *A send M2* by Pearson correlation give the following results 0.034, -0.272, -0.617. This means that there is no correlation. On

Table 1

Latency between Android and two microcontrollers between sending and receiving time for three different executions. *A send M1* and *A send M2* are the timestamps when the commands are executed by the Android OS. *Diff 1* is the difference of (*A send M2*) − (*A send M1*). *RL* is the wired latency between both microcontrollers when receiving the packets. *R1* and *R2* are the times when the Android OS has received the packets from the microcontrollers. *l* is the difference of *R2* − *R1*. Bold shows the correlation between wired *l* and calculated *l*.

A send M1	A send M2	DIFF 1	RL	R1	R2	l
1552473386320	1,552,473,386,332	12	**23**	1,552,473,386,373	1,552,473,386,396	**23**
1552473402974	1,552,473,402,985	11	**27**	1,552,473,403,025	1,552,473,403,054	**29**
1552473411800	1,552,473,411,804	4	**23**	1,552,473,411,851	1,552,473,411,872	**21**
1552473415820	1,552,473,415,829	9	**30**	1,552,473,415,863	1,552,473,415,897	**24**
1552473418088	1,552,473,418,100	12	**28**	1,552,473,418,131	1,552,473,418,160	**29**
1552473420520	1,552,473,420,527	7	**28**	1,552,473,420,564	1,552,473,420,593	**29**
1552473422598	1,552,473,422,604	6	**31**	1,552,473,422,638	1,552,473,422,672	**34**
1552473424513	1,552,473,424,523	10	**29**	1,552,473,424,557	1,552,473,424,585	**28**
1552473426282	1,552,473,426,295	17	**28**	1,552,473,426,327	1,552,473,426,355	**28**
1552473428201	1,552,473,428,209	8	**28**	1,552,473,428,239	1,552,473,428,267	**28**
1552475001845	1,552,475,001,849	4	**43**	1,552,475,001,888	1,552,475,001,929	**41**
1552475013106	1,552,475,013,111	5	**19**	1,552,475,013,159	1,552,475,013,179	**20**
1552475014617	1,552,475,014,624	7	**33**	1,552,475,014,658	1,552,475,014,730	**72**
1552475015951	1,552,475,015,964	13	**32**	1,552,475,015,996	1,552,475,016,029	**33**
1552475017448	1,552,475,017,460	12	**23**	1,552,475,017,495	1,552,475,017,517	**22**
1552475018910	1,552,475,018,920	10	**24**	1,552,475,018,958	1,552,475,018,979	**21**
1552475020302	1,552,475,020,309	7	**31**	1,552,475,020,346	1,552,475,020,380	**34**
1552475021704	1,552,475,021,713	9	**31**	1,552,475,021,751	1,552,475,021,780	**29**
1552475022982	1,552,475,022,995	13	**29**	1,552,475,023,021	1,552,475,023,049	**28**
1552475024662	1,552,475,024,670	8	**28**	1,552,475,024,709	1,552,475,024,737	**28**
1552477976517	1,552,477,976,523	6	**42**	1,552,477,976,564	1,552,477,976,605	**41**
1552477978212	1,552,477,978,222	10	**29**	1,552,477,978,258	1,552,477,978,287	**29**
1552477979992	1,552,477,980,003	11	**16**	1,552,477,980,046	1,552,477,980,067	**21**
1552477981607	1,552,477,981,616	9	**31**	1,552,477,981,651	1,552,477,981,685	**34**
1552477983153	1,552,477,983,165	12	**31**	1,552,477,983,193	1,552,477,983,227	**34**
1552477984567	1,552,477,984,581	14	**31**	1,552,477,984,611	1,552,477,984,645	**34**
1552477986029	1,552,477,986,036	7	**43**	1,552,477,986,078	1,552,477,986,120	**42**
1552477987445	1,552,477,987,455	10	**28**	1,552,477,987,486	1,552,477,987,515	**29**

the other hand, the columns *l* and *RL* correlate strongly by Pearson correlation with the following values 0.743, 0.580, 0.982.

This can be explained by the fact that the microcontrollers M1 and M2 process the commands sequentially, and thus all commands are equally authorized. Furthermore, it is possible to receive signals at the app in real-time because there are several threads available.

Out of this knowledge, we can say the receive time of the smartphone is the offset in which the microcontrollers sent the signal. We use this fact for synchronization. In summary, we can note that when sending packages of two microcontrollers at the same time, these also arrive simultaneously.

4.3.4. Synchronization algorithm

Based on the data from sections 4.3.2 and 4.3.3 we can now propose a solution to synchronize two microcontrollers via Bluetooth. The following steps describe the procedure of the algorithm:

1. The Android device *A* sends a packet to microcontrollers *M*1 and *M*2.
2. *M*1 sends a packet to *A*. The packet holds a timestamp of the system time *t*1 directly before sending it.
3. *M*2 sends a packet to *A*. The packet holds a timestamp of the system time *t*2 directly before sending it.
4. *A* receives a packet from *M*1 at a real-time *R*1.
5. *A* receives a packet from *M*2 at a real-time *R*2.

With this information we can calculate our receive latency *l* in formula (1) where *c* represents an possible error.

$$l = R2 - R1 + c \tag{1}$$

To determine the offset *o* from *M*2 to *M*1, we use the formula (2).

$$o = (t2 - t1) + l \tag{2}$$

Of course, in the proposed algorithm, errors can occur, which are the result of disturbances in the magnetic field or other physical effects. Therefore we perform the algorithm eleven times and use the median of the latency to determine the best synchronization between the devices *M*1 and *M*2.

4.4. Stride detection

After the activity recognition algorithm has identified the phases of the activity *gait*, we use the transmitted, synchronized sensor data of the wearable devices to perform a stride detection. In the version of our proposed system, we used only the insole data for the stride detection and symmetry calculation. To train the classifier, first, we manually labeled the data After labeling, the data was normalized and resampled to a uniform length. Then, we trained our CNN to get a model for stride detection.To detect strides from the daily life data set, we use automatic framing to extract fragments from the recording. By fragments, we mean different parts of a recording. These fragments we normalized and resampled. The CNN model classifies these fragments for possible strides. This process is shown in Fig. 6.
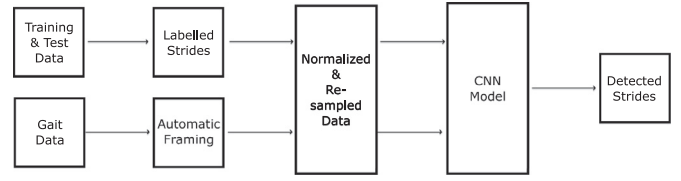
Fig. 6. Process of stride detection with CNN.

4.4.1. Normalization

We use a Min-Max-Normalization to normalize all data between range 0 to 1. The normalization were executed for every $x_i \; \forall \; i \in \{0, \ldots, N-1\}$ of the feature *X*, where *N* is the length of feature *X*, see formula 3. The result is a normalized vector X^{norm} with the values $x_i^{norm} \in X^{norm}$. The functions *min(X)* and *max(X)* return the minimum and maximum of the feature *X*.

$$x_i^{norm} = \frac{x_i - min(X)}{max(X) - min(X)} \tag{3}$$

4.4.2. Resampling

For using the CNN classifier, we need a uniform signal length. Therefore we transform all signals to a uniform length of 100 values. The Python function *resampling* in the library SciPy use a Fast Fourier Transformation (FFT) based method [31].

4.4.3. CNN

To build the CNNs model, we use a sequential network, see Fig. 7.

As the activation function, we use the rectified linear unit (ReLU) function with except at the output layer. As input we use the x-, y-, and z-axis of the linear acceleration and Euler angles. The first one-dimensional convolutional layer creates 100 filters with a kernel size of 3. To reduce the filters, we apply a max pooling with a pool size of 3 and a drop-out with probability 0.2. After the second convolutional layer consists of 100 filters and a kernel size of 5, this is followed by max-pooling again with a pool size of 3. A drop-out follows them with probability 0.2, where single connections are randomly deleted [32]. After that, we have a flattening layer to adjust the dimensions for the neural network (NN). Next, we have two dense layers. The first has 20 neurons, and the second 30 neurons. Last we have an output layer with a sigmoid function as the activation function. As a result, we obtain a probability of the signal being a stride.

4.4.4. Automatic framing

A real signal cannot be manually labeled. Thus, an algorithm should be that task. For this reason, we use automatic framing. The automatic framing creates dynamic window sizes, which we use as input for the CNN in the stride detection. For detection, we use dynamic window sizes. The average duration of a stride is 1.1 *s* [33] that is equivalent to 110 values of the data. Therefore we use an average window size of 110 ± 30 values. The window *w* can
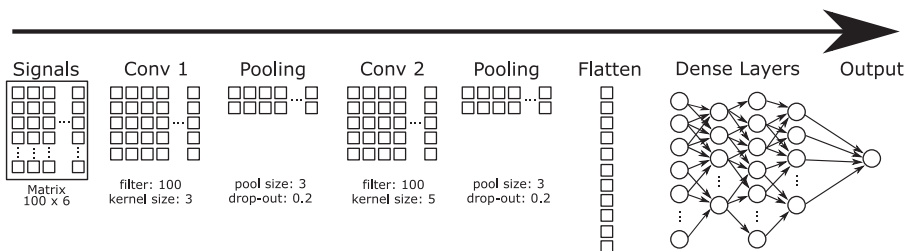
Fig. 7. Schema of the CNN layers.
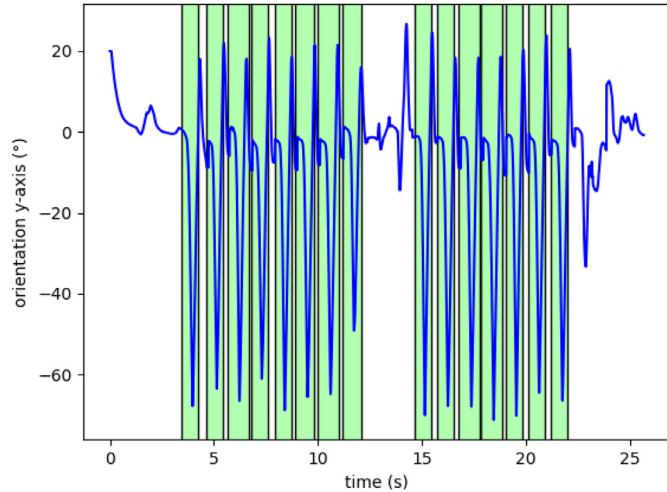
Fig. 8. Predicted strides.

have the following sizes

$$w = \{80, 90, 100, 110, 120, 130, 140\}. \tag{4}$$

From the signal to be classified, windows with all sizes are used.

All dynamic windows are resampled to a uniform length of 100 values and normalized with the functions from Section 4.4.1 and 4.4.2. If the CNN detects a stride with more than 70 % probabilities within a window, it is saved in a list. The stride with the highest probability from the list is only used and defined a valid stride. We mark the absolute minimum within a stride $\pm\ 10\ ms$. To distinguish the strides from each other, we use overlapping, see Eq. 5. Overlapping allows us to separate new strides from others. If the predicted stride lies within this range, it is marked as detected stride, see Fig. 8.

$$overlapping = detected\ stride + (average\ stride \cdot 0.8) \tag{5}$$

4.5. Symmetry

The calculation of the symmetry of two strides is possible by the previously performed synchronization in Section 4.3. To calculate the symmetry, we first do a stride detection like in Section 4.4.

So that we always have a fixed reference timestamp (e.g., right foot) point within a stride. We use the time stamp of the minimum inside a stride, see Fig. 9.

To measure the symmetry distance between the time series (strides) of the right and left foot, we use the DTW. DTW has be-
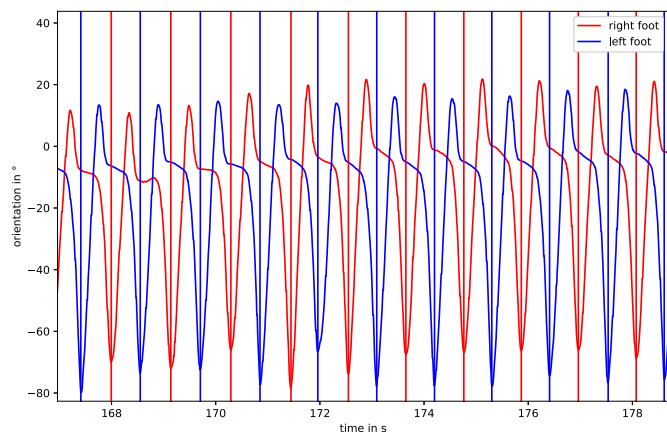
Fig. 9. Orientation data of the left and right foot with the corresponding minima.
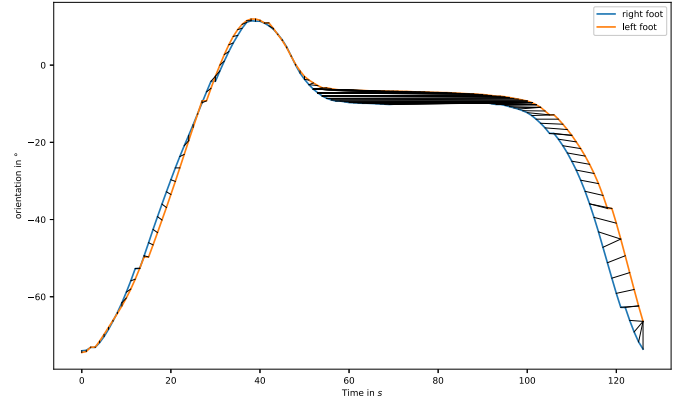
Fig. 10. DTW Symmetry result at person 1 with a distance value of 130.52.

come very well established in the analysis of time-series signals. In contrast to Euclidean distance, this method can compensate for time warping. Based on this flexibility, it is a popular method for the analysis of time series in medicine, science, and industry. The idea with DTW is that not the distance of two indices is calculated, but the distance to the most fitting one. Thus allows comparing time series with each other if they recorded with different duration or frequency.

In the first step, the algorithm calculates distances between the time series $(x_i)_{1 \leq i \leq n}$ (e.g. orientation angle of the right foot) of length n and $(y_j)_{1 \leq j \leq m}$ (e.g. orientation angle of the left foot) of length m, resulting in a n times m matrix $D = D_{ij}$ containing distances D_{ij} between y_j and x_i. The distances within the matrix are calculated by the sum of the current distance and the minimum distance of a previous neighboring element, see Eq. 6 [34].

$$D_{ij} = (x_i - y_j)^2 + min\{D_{i-1,j}, D_{i-1,j-1}, D_{i,j-1}\} \tag{6}$$

A distance D_{ij} of 0 means 100 % symmetry of the measured values. The higher the value D_{ij}, the lower is the symmetry of the two feet, see Fig. 10.

5. Results

5.1. Activity recognition

For recognition of activity *gait*, we have performed a five-fold cross-validation. The results are shown in Table 2. For the results we have specified precision, recall, F1-Score and Accuracy. For each column we have given the average value and standard deviation.

5.2. Synchronization

In the Tables 3, 4, and 5 the measured values of a synchronization are shown. In the tables, the first column is a numbered index. It is followed by the receiving time of the reference microcontroller and the third column of the to be synchronized microcontroller. Column four is the calculated latency of both microcontrollers, and column five is the wired measured latency over the wires. The last column shows the error from calculated to measured latency. For the most accurate timestamp, we calculate the median of the latencies *l*.

Table 2
Results for recognition of activity *gait*.

	precision	recall	F1-Score	accuracy
CNN	0.958 ± 0.031	0.683 ± 0.023	0.884 ± 0.011	0.947 ± 0.005

Table 3
Latency between microcontroller M1 and M2.

index	M1	M2	l	wired l	c
1	1,552,919,014,830	1,552,919,014,946	116	81	35
2	1,552,919,014,999	1,552,919,015,047	48	8	40
3	1,552,919,015,776	1,552,919,015,154	-622	-665	43
4	1,552,919,015,838	1,552,919,015,897	59	55	4
5	1,552,919,015,950	1,552,919,015,972	22	20	2
6	1,552,919,016,005	1,552,919,016,014	9	6	3
7	1,552,919,016,055	1,552,919,016,064	9	7	2
8	1,552,919,016,098	1,552,919,016,106	8	5	3
9	1,552,919,016,147	1,552,919,016,156	9	8	1
10	1,552,919,016,191	1,552,919,016,199	8	4	4
11	1,552,919,016,240	1,552,919,016,262	22	21	1

Table 4
Latency between microcontroller M1 and M3.

index	M1	M3	l	wired l	c
1	1,552,919,585,669	1,552,919,585,703	34	34	0
2	1,552,919,585,731	1,552,919,585,728	-3	-5	2
3	1,552,919,585,770	1,552,919,585,781	11	8	3
4	1,552,919,585,824	1,552,919,585,827	3	4	1
5	1,552,919,585,862	1,552,919,585,877	15	16	1
6	1,552,919,585,924	1,552,919,585,914	-10	-8	2
7	1,552,919,585,961	1,552,919,585,978	17	17	0
8	1,552,919,586,024	1,552,919,586,014	-10	-8	2
9	1,552,919,586,061	1,552,919,586,078	17	17	0
10	1,552,919,586,124	1,552,919,586,114	-10	-9	1
11	1,552,919,586,161	1,552,919,586,171	10	9	1

Table 5
Latency between microcontroller M1 and M4.

index	M1	M4	l	wired l	c
1	1,552,988,793,978	1,552,988,794,019	41	41	0
2	1,552,988,794,060	1,552,988,794,056	-4	5	9
3	1,552,988,794,110	1,552,988,794,119	9	8	1
4	1,552,988,794,154	1,552,988,794,145	-9	-4	5
5	1,552,988,794,203	1,552,988,794,199	-4	-5	1
6	1,552,988,794,227	1,552,988,794,236	9	9	0
7	1,552,988,794,258	1,552,988,794,262	4	3	1
8	1,552,988,794,295	1,552,988,794,313	18	17	1
9	1,552,988,794,359	1,552,988,794,348	-11	-10	1
10	1,552,988,794,395	1,552,988,794,404	9	11	2
11	1,552,988,794,451	1,552,988,794,442	-9	-8	1

Table 6
Latency between microcontroller M1 and M2.

index	l	c
3	-622	43
8	8	3
10	8	4
6	9	3
7	9	2
9	**9**	**1**
5	22	2
11	22	1
2	48	40
4	59	4
1	116	35

Table 7
Latency between microcontroller M1 and M3.

index	l	c
6	-10	2
8	-10	2
10	-10	1
2	-3	2
4	3	1
11	**10**	**1**
3	11	3
5	15	1
7	17	0
9	17	0
1	34	0

Table 8
Latency between microcontroller M1 and M4.

index	l	c
9	-11	1
4	-9	5
11	-9	1
2	-4	9
5	-4	1
7	**4**	**1**
3	9	1
6	9	0
10	9	2
8	18	1
1	41	0

Table 9
Daily life stride detection.

	recall	precision	F1-Score	Accuracy
CNN	0.978	0.978	0.974	0.988

Table 10
Results of the symmetry calculation.

subject	number strides	DTW median
1	90	130.52
2	45	309.91
3	86	576.42
4	37	351.40

5.3. Stride detection

For stride detection, we have performed a seven-fold cross-validation. The results are shown in Table 9. For the results we have specified precision, recall, F1-Score and Accuracy. For each column we have given the average value and standard deviation [35].

5.4. Symmetry

The Table 10 shows the results for the symmetry of four different healthy persons. The first column is the subject number. Column two is the number of strides used to calculate symmetry. In the last column, the median distance of the DTW is shown. All persons had no motor dysfunctions. Person 3 has the largest symmetry deviation. An earlier operation of one knee probably causes these motor dysfunction. The median distance of DTW from person 3 is shown in Fig. 11. In contrast, the median distance of DTW of person 1 in Fig. 10 is smaller than that of person 3. Thus, the gait symmetry of person 1 is more accurate than that of person 3.

In the Tables 6, 7, and 8 the latencies are shown in sorted and the median is printed bold. All three tables provide a positive error of 1 ms to the reference device. Thus, the total latency is 1 ms. In other measurements, we have a total error of 3 ms. Since we record the sensor data with 100 Hz, this error is tolerable for symmetry calculation.
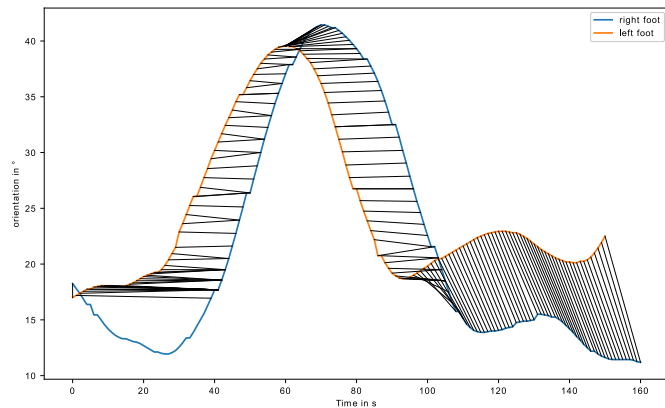
Fig. 11. DTW Symmetry result at person 3 with a distance value of 576.42.

6. Discussion

We have presented a system for real-time analysis of gait symmetry that can be used comfortably by people in their daily life and is independent of the location. The system can be used for measurement of human gait.

By developing an Android app for activity recognition, we were able to show that a smartphone can distinguish between activity *gait* and *other* activities such as standing, lying, cycling, or writing messages. With an accuracy of 94.7 % we obtain similar results to other researchers [13–15]. Activity recognition allows us to switch on the wearable sensors, and data recording only activity *gait* is recognized. This method is an energy-efficient solution.

Furthermore, we present a solution to synchronize several wearables sensors. In literature, this problem has already been recognized, and there were several approaches. However, the problem is that the devices of Mbientlab can only synchronize three devices [20]. We synchronize four wearables for four extremities. Another solution was to synchronize the time during charging by cable [18]. However, this solution has the disadvantage that in more extended use, a drift of the clock occurs. We synchronize the wearables before each recording (recognition of activity *gait*). This way, we start each recording without drift of the clock.

In most of the papers dealing with symmetry, they use the stride length, stride duration, and different gait phases to calculate the ratio of the left and right leg [6,10,11,23]. In contrast, our symmetry calculation considers the complete time series. However, the synchronization of the sensors is essential for this. For stride detection, we use a combination of automatic framing and CNN. The use of CNN's for stride detection has proven to be very useful for us. Other work has already been able to benefit from the technology [35]. The symmetry of the legs is analyzed with DTW.

7. Conclusion

With our work, we were able to present a complex system that can analyze the human gait symmetry with the help of wearable devices in daily life. For future work, we want to calculate further features from the time series. By synchronizing the wearable devices, more fundamental symmetry characteristics can be calculated, like cadence, cyclogram, mono pedal phase, or bipedal phase. Other features such as symmetry ratio, symmetry index, gait asymmetry, symmetry angle, stride length, or stride height are also possible. These additional features provide a wide range of features to evaluate human gait. With all these features, more accurate classification of PD stage in the use of machine learning should be possible.

Declaration of Competing Interest

The authors declare that they have no known competing financial interests or personal relationships that could have appeared to influence the work reported in this paper.

References

[1] World health organization, World report on ageing and health, World Health Organization, 2015.

[2] N. Ball, et al., Parkinson'S disease and the environment, Front. Neurol. 10 (2019) 218.

[3] M. Zhang, N. Artan, H. Gu, Z. Dong, L. Burina Ganatra, S. Shermon, E. Rabin, Gait study of parkinson's disease subjects using haptic cues with a motorized walker, Sensors 18 (10) (2018) 3549.

[4] G. Vagenas, B. Hoshizaki, A multivariable analysis of lower extremity kinematic asymmetry in running, International Journal of Sport Biomechanics 8 (1) (1992) 11–29.

[5] O.F. Ince, et al., Gait Analysis and Identification Based on Joint Information Using RGB-Depth Camera, in: 2017 14th International Conference on Electrical Engineering/Electronics, Computer, Telecommunications and Information Technology (ECTI-CON), IEEE, 2017.

[6] J. Barth, et al., Stride Segmentation During Free Walk Movements Using Multi-dimensional Subsequence Dynamic Time Warping on Inertial Sensor Data, in: Sensors 15.3, 2015, pp. 6419–6440.

[7] V.N. Bobić, et al., Challenges of Stride Segmentation and Their Implementation for Impaired Gait, in: 2018 40th Annual International Conference of the IEEE Engineering in Medicine and Biology Society (EMBC), 2018, p. IEEE.

[8] X. Tao, et al., Precise displacement estimation from time-differenced carrier phase to improve PDR performance, IEEE Sens. J. 18.20 (2018) 8238–8246.

[9] Koroglu, M. Taha, A. Yilmaz, C.J. Saul, A Deep Learning Strategy for Stride Detection, in: 2018 IEEE SENSORS, 2018, p. IEEE.

[10] J. Hannink, et al., Mobile stride length estimation with deep convolutional neural networks, IEEE J. Biomed. Health Inform. 22.2 (2018) 354–362.

[11] T. Watanabe, T. Miyazawa, J. Shibasaki, A Study on IMU-Based Stride Length Estimation for Motor Disabled Subjects: A Comparison under Different Calculation Methods of Rotation Matrix, in: 2018 IEEE EMBS International Conference on Biomedical & Health Informatics (BHI), 2018, p. IEEE.

[12] Y. Kim, O.S. Eyobu, D.S. Han, ANN-Based Stride Detection Using Smartphones for Pedestrian Dead Reckoning, in: 2018 IEEE International Conference on Consumer Electronics (ICCE), 2018, p. IEEE.

[13] M. Gadaleta, M. Rossi, Idnet: smartphone-based gait recognition with convolutional neural networks, Pattern Recognit. 74 (2018) 25–37.

[14] M.M. Hassan, M.Z. Uddin, A. Mohamed, A. Almogren, A robust human activity recognition system using smartphone sensors and deep learning, Future Generation Computer Systems 81 (2018) 307–313.

[15] L. Cao, Y. Wang, B. Zhang, Q. Jin, A.V. Vasilakos, GCHAR: An efficient group-based context'aware human activity recognition on smartphone, J. Parallel Distrib. Comput. 118 (2018) 67–80.

[16] S. Clemens, K.J. Kim, R. Gailey, N. Kirk-Sanchez, A. Kristal, I. Gaunaurd, Inertial Sensor-based Measures of Gait Symmetry and Repeatability in People with Unilateral Lower Limb Amputation, in: Clinical Biomechanics, 2019.

[17] S.J. Crenshaw, J.G. Richards, A method for analyzing joint symmetry and normalcy, with an application to analyzing gait, Gait & posture 24 (4) (2006) 515–521.

[18] M. Mancini, L. King, A. Salarian, L. Holmstrom, J. McNames, F.B. Horak, Mobility Lab to Assess Balance and Gait with Synchronized Body-worn Sensors, in: Journal of Bioengineering & Biomedical Science, volume 007, 2011.

[19] A.R. Anwary, H. Yu, M. Vassallo, An automatic gait feature extraction method for identifying gait asymmetry using wearable sensors, Sensors 18 (2) (2018a) 676.

[20] A.R. Anwary, H. Yu, M. Vassallo, Wearable Sensor Based Gait Asymmetry Visualization Tool, in: Twenty-Fourth Americas Conference on Information Systems, New Orleans, 2018.

[21] A.R. Anwary, H. Yu, M. Vassallo, Optimal foot location for placing wearable IMU sensors and automatic feature extraction for gait analysis, IEEE Sens. J. 18 (6) (2018c) 2555–2567.

[22] T. Steinmetzer, et al., Clustering of Human Gait with Parkinson's Disease by Using Dynamic Time Warping, in: 2018 IEEE International Work Conference on Bioinspired Intelligence (IWOBI), IEEE, 2018.

[23] X. Jiang, et al., Exploration of Gait Parameters Affecting the Accuracy of Force Myography-based Gait Phase Detection, in: 2018 7th IEEE International Conference on Biomedical Robotics and Biomechatronics (Biorob), IEEE, 2018.

[24] I. Loiret, C. Villa, B. Dauriac, X. Bonnet, N. Martinet, J. Paysant, H. Pillet, Are wearable insoles a validated tool for quantifying transfemoral amputee gait asymmetry? Prosthet. Orthot. Int. 43 (5) (2019) 492–499.

[25] C.C. Lin, R.C. Wagenaar, The impact of walking speed on interlimb coordination in individuals with parkinson's disease, J. Phys. Ther. Sci. 30 (5) (2018) 658–662.

[26] C. Miller-Patterson, R. Buesa, N. McLaughlin, R. Jones, U. Akbar, J.H. Friedman, Motor asymmetry over time in parkinson's disease, J. Neurol. Sci. 393 (2018) 14–17.

[27] S. Viteckova, P. Kutilek, J. Lenartova, J. Kopecka, D. Mullerova, R. Krupicka, Evaluation of movement of patients with parkinson's disease using accelerometers and method based on eigenvectors, in: In 2016 17th International Conference on Mechatronics-Mechatronika (ME), IEEE, 2016, pp. 1–5. December

[28] S. Viteckova, P. Kutilek, Z. Svoboda, R. Krupicka, J. Kauler, Z. Szabo, Gait symmetry measures: a review of current and prospective methods, Biomed. Signal Process. Control 42 (2018) 89–100.

[29] BNO055, Intelligent 9-axis absolute orientation sensor, in: BST-BNO055-DS000-14, Rev. 0273414209, Bosch Sensortec, 2016. June

[30] FSR 400, Series Data Sheet, in: Interlink Electronics, PDS-10004-C,

[31] P. Virtanen, R. Gommers, T.E. Oliphant, M. Haberland, T. Reddy, D. Cournapeau, E. Burovski, P. Peterson, W. Weckesser, J. Bright, et al. Scipy: Open source scientific tools for python, 2019, Available online: http://www.scipy.org/ (accessed on 2 December 2019).

[32] N. Srivastava, et al., Dropout: a simple way to prevent neural networks from overfitting, The Journal of Machine Learning Research 15.1 (2014) 1929–1958.

[33] J.M. Hausdorff, et al., Gait variability and basal ganglia disorders: stride–to-stride variations of gait cycle timing in parkinson's disease and huntington's disease, Movement disorders 13.3 (1998) 428–437.

[34] E. Keogh, C.A. Ratanamahatana, Exact indexing of dynamic time warping, Knowl Inf Syst 7.3 (2005) 358–386.

[35] T. Steinmetzer, I. Bönninger, M. Reckhardt, F. Reinhardt, D. Erk, C.M. Travieso, Comparison of Algorithms and Classifiers for Stride Detection Using Wearables, in: Neural Computing and Applications, 2019, pp. 1–12.

Tobias Steinmetzer Graduation 2013 - Bachelor of Science in Computer Science at Brandenburg University of Technology Cottbus - Senftenberg. Graduation 2016 - Master of Science in Computer Science at Brandenburg University of Technology Cottbus - Senftenberg. Since 11/2018 - PhD Student at Universidad de las Palmas de Gran Canaria

Clustering of Human Gait with Parkinson's Disease by using Dynamic Time Warping

Tobias Steinmetzer*, Ingrid Bönninger*, Barbara Priwitzer†, Fritjof Reinhardt*, Markus Christoph Reckhardt*, Dorela Erk‡ and Carlos M. Travieso§

*Brandenburg University of Technology Cottbus-Senftenberg
Institute of Medical Technology, Universitätsplatz 1, D-01968 Senftenberg, Germany
Email: tobias.steinmetzer@b-tu.de
†Hochschule Reutlingen, School of Engineering, Reutlingen, Germany
‡Niederlausitz Clinic, Center of Neurology and Pain Management, Senftenberg, Germany
§University of Las Palmas de Gran Canaria, Signals and Communication Department, IDeTIC, Las Palmas de Gran Canaria, Spain

Abstract—We present a new method for detecting gait disorders according to their stadium using cluster methods for sensor data. 21 healthy and 18 Parkinson subjects performed the Time Up and Go test. The time series were segmented into separate steps. For the analysis the horizontal acceleration measured by a mobile sensor system was considered. We used Dynamic Time Warping and Hierarchical Custering to distinguish the stadiums. A specificity of 92% was achieved.

Index Terms—DTW, clustering, parkinson disease, time series
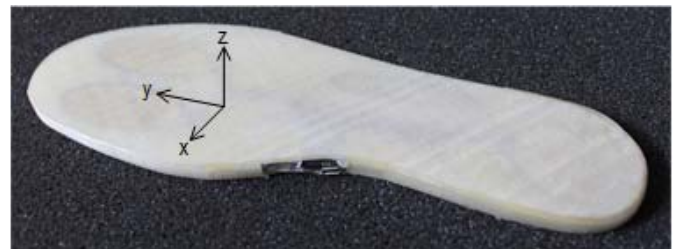
Fig. 1. Insole for gait analysis

I. INTRODUCTION

This work is intended to make a further contribution to the analysis of gait disorders in Parkinson's disease. The aim is to support the treating physician in diagnosis and in assessing the severity of the movement disorder. The use of different sensors has proven itself useful in the analysis of the human gait for many years [1]. In the first years, single or multiple cameras were often used to identify individuals by their gait [2] [3]. The Dynamic Time Warping (DTW) method has proven to be particularly effective in distinguishing the gait of individuals [4] [5]. Cameras were also used for the analysis of gait changes in neurodegenerative diseases. However, the accuracy is only sufficient to distinguish between healthy and sick persons [6]. In recent years sensors acceleration-, gyroscope- and magnetometersensors (inertial measurement unit - IMU) have been used for the analysis of movement disorders in Parkinson's disease [7] [8]. In [7] the Kalman filter is used to identify the gait asymmetry. The Fast Fourier transformation is used in [8] to detect the freezing phases. Newest research again uses DTW e.g. for the segmentation of gait sequences [9] and for recognition of asymmetry in gait [10]. For the detection of freezing phases, which occur especially during turns, the turn was analyzed [8] [9]. In this paper, the stage of the movement disorder is not to be determined on the basis of individual characteristics such as asymmetry or freezing, but rather as the combination of all single disorders. The IMU sensors have been mounted on the shoe [7] or on the ankle [8] [9] [10]. In this case, the sensor may slip during walking. This makes it difficult to detect the time point when the foot touches the ground. For a more robust step detection we have integrated the sensor into an insole.

In this work we use minimalistic sensor data to perform clustering based on the Parkinson's stadium. For this reason, we use only one axis from an insole. A problem with Parkinson's disease is that the stadium is often subjectively assessed. For this reason, we want to develop a system that supports the treating physician in his diagnosis and provides empirical measurement data. Because each person needs different length for each step, it would be impossible to work with the correlations without compressing or stretching the data, which would mean data manipulation. The advantage of the DTW algorithm is that you can measure a distance number between two time series of different lengths. The smaller this distance is, the more similar these time series are. The DTW algorithm searches for the ideal path between two time series.

This work is divided into four sections. Section II describes the developed hardware, the test performed by the patient and the procedures used for preprocessing, step analysis and clustering. The results achieved are presented in Section III. Section IV indicates the conclusions and further developments.

II. METHODS

A. Hardware

For data recording we use insoles produced by a 3D printer (see Fig. 1). Each insole is equipped with a microcontroller MetaMotionR from Mbientlab. This microcontroller has a gyroscope and an acceleration sensor (Bosch BMI160) and a magnetic sensor (Bosch BMM150). A major advantage of the microcontroller is that it integrates a sensor fusion from Bosch. This gives us absolute angles and linear acceleration. We use the insoles in combination with an Android app to control the recording and data transfer via Bluetooth. Euler angle and linear acceleration are recorded at 100 Hz. The data are saved to a flash memory and transferred to the Android app only after the exercise has been completed.

B. Test set-up

We used the Timed Up and Go test (TUG) [11], a standardized test for the Unified Parkinson's Disease Rating Scale (UPDRS) [12]. This test is used to estimate the motoric dysfunction of Parkinson's patients. It starts by sitting on a chair with armrests and a backrest. On command the subject stands up and walks 10m straight to a mark, turns around at the mark, walks back to the chair and sits down again.

C. Data

We collected 53 recordings from 21 healthy subjects (HS) and 45 recordings from 19 subjects suffering from Parkinson's disease. Out of the Parkinson patients 8 subjects were in hospital, denoted by PPH (hospital) in the following, and 10 were recruited form a self-help group, denoted by PPS (self-help group) in the following. For PPH the Parkinson level usually evaluated by a medical specialist on the scale of Hoehn-Yahr [13]. Levels between 1 and 3 were observed. For PPS patients the level was unkown, denoted by *nan* in table III and Fig. 7.

D. Preprocessing

For the present analysis we used only the data of the left insole, namely the linear acceleration of the y-axis (see Fig. 2), i.e. the forward acceleration (see Fig. 1). Step segmentation was performed with an algorithm detecting minima and maxima within a window of 100 frames. A step consists of a minimum followed by a maximum. We use this pattern to recognize the steps. The result of the step detection can be seen in Fig. 2. We have set the starting point of a step to the maximum of a step (black line). In addition, we have removed all steps exceeding or falling below 4 times the interquartile for step length.

For the later analysis in section III results we use the complete straight walking phase. Start or end points of the complete straight walking phase analysis are marked with red lines in Fig. 2, and are obtained by adding the average duration of a step to the first or last detected maximum, respectively.
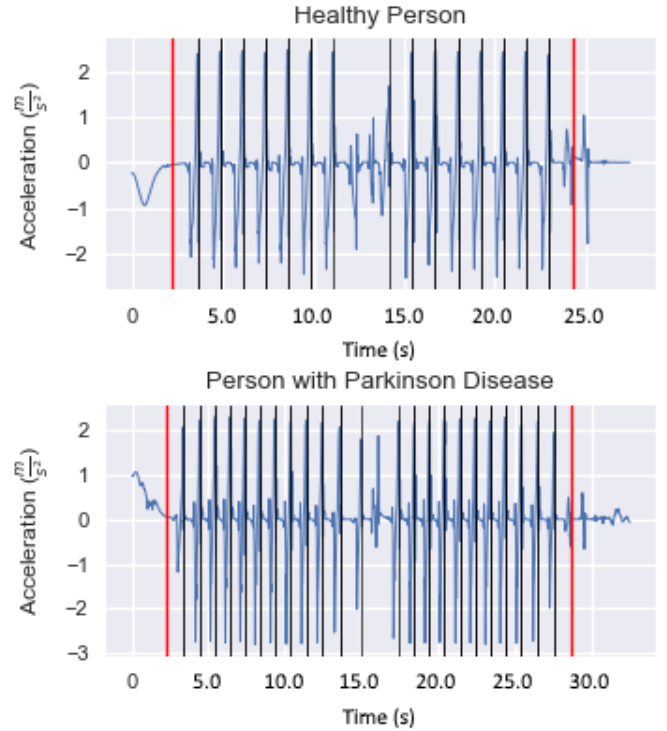
Fig. 2. Acceleration data of the y-axis and segmentation of the steps. The black lines indicate the start and end of a step. The red lines indicate the start and end of a recording.

E. Dynamic Time Warping

Standard distance measures like Euclidean distance are not suitable to measure the distance between two time series, since the measured values are displaced in time or the time series have a different length. For this reason we used the DTW algorithm. The DTW searches for the best path within a distance matrix. We use DTW to measure the distance between two steps or two recordings.

In the first step, the algorithm calculates distances between the time series $(x_i)_{1 \le i \le n}$ of length n and $(y_j)_{1 \le j \le m}$ of length m, resulting in a n times m matrix $D = D_{ij}$ containing distances D_{ij} between y_j and x_i. The distances within the matrix are calculated by the sum of the current distance and the minimum distance of an previous neighboring element, see formula 1 [14].

$$D_{ij} = |x_i - y_j| + min\{D_{i-1,j}, D_{i-1,j-1}, D_{i,j-1}\} \quad (1)$$

The resulting distance of the two time series can be found at the position D_{nm} in the matrix. The path leading from D_{11} to D_{nm} can be traced in the matrix D. Such a path is shown for a single step in Fig. 3. The figure shows one step for a HS (green) and one step for a PPS (blue). The black lines indicate the connections of both time series for distance formation. It can be seen that the PPS needs more time to complete the step. However, the pattern of both steps is very similar.
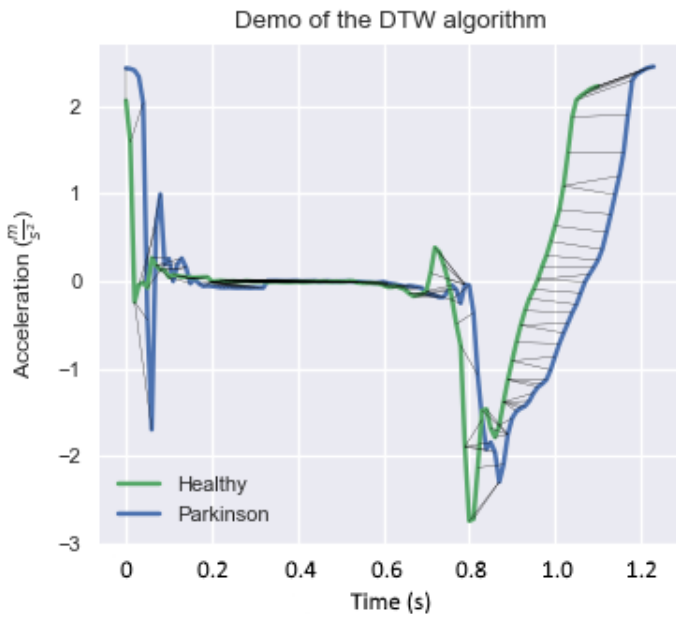
Fig. 3. The graphic shows one period of each step of HS and PPS with the path of the DTW algorithm.

F. Clustering

We performed hierarchical clustering [15]. Based on the distance of all single steps between two persons. This distance is obtained as the distance of all steps during the TUG for the two recordings. We performed hierarchical clustering according to the Complete-Linkage method as well as to the Single-Linkage method and use the agglomerative algorithm.

In Fig. 4 the result of clustering for steps with Single-Linkage of both subjects from section II-D can be seen. For easy understanding the start, turn and end of the recording are omitted (see Fig. 5, white line) and only single steps were used here. Here can be seen clearly that two large clusters were formed and one smaller one.

The result is shown in Fig. 5. The green and red clusters show that the persons can be clearly distinguished from each other. Furthermore, even incorrectly interpreted steps in the blue cluster could be marked. These data are outliers from segmentation. Only one step from HS is in the wrong cluster.

III. RESULTS

We clustered the data with the hierarchical clustering method using the complete linkage and the DTW for distance measurement. For the analysis we used all persons and the complete walking phase (see Fig. 2, red lines). The result is shown in the dendrogram in the appendix in Fig. 7. In the dendrogram we indicate the distances of the DTW algorithm of the clusters to each other on the y-axis. On the x-axis we have marked each data set with the id and the Parkinson stadium. This should help to understand better the coherence of the data. We have chosen the distance of 440 as the threshold for the forming of the clusters, because the results are very
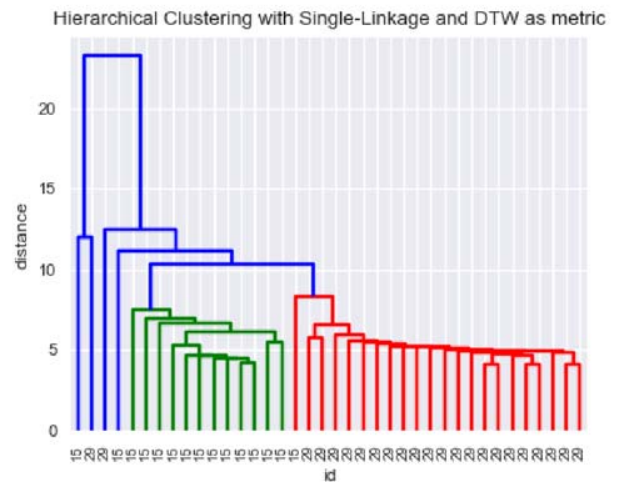
Fig. 4. The dendrogram shows the results of the cluster analysis. The steps of a healthy person (green) and a person with Parkinson's disease (red) were clustered. It can clearly be seen that two large clusters form and contain one smaller with outliers (blue).
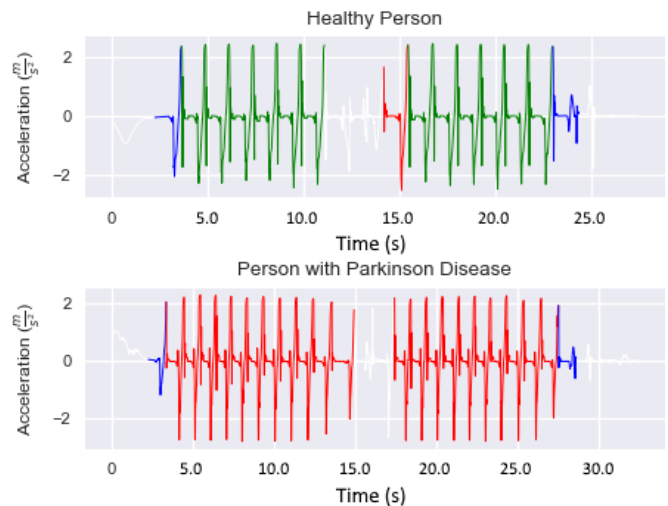
Fig. 5. Cluster result of HS (top), PPS (bottom) colored. the green cluster steps of HS; red steps of PPS; outliers are blue.

plausible in this constellation. This threshold gives us seven clusters as a result.

Table I and II show confusion matrices for the result of the clustering of persons (Table I) or recordings (Table II).

In Table I we have placed a confusion matrix for which only id's within clusters were displayed. It can be seen that the sensitivity is 57% and the specificity 90%. At first glance, the sensitivity appears very low. However, it must be taken into account that the majority of the test cases are PPS, which were very well adjusted and showed hardly any motor dysfunctions (Table III). The specificity, on the other hand, is very convincing.

The confusion matrix in Table II contains all recordings used during clustering. Here the sensitivity is 55% and the

TABLE I
CONFUSION MATRIX BY ID

	PD stadium positiv	PD stadium negativ	$\sum$
Clustering positiv	11	2	14
Clustering negativ	8	19	32
$\sum$	19	21	46

TABLE II
CONFUSION MATRIX BY RECORDING

	PD stadium positiv	PD stadium negativ	$\sum$
Clustering positiv	25	4	29
Clustering negativ	20	49	69
$\sum$	45	53	98

specificity 92%. The same reasoning applies here as to the confusion matrix in Table I.

In the following we will take a closer look at the individual clusters (see Table III) and discuss conspicous assingments of data sets to clusters. The first green cluster contains mostly HS and PPS which do not have any particular motor disorders. The only exception is data set (24,2.0), a PPH, recorded on the day of his discharge from hospital. As a result the PPH was optimally adjusted to the new medication and had no symptoms. The second (red) cluster consists of HS and PPS, which have no particular motor abnormalities. Here the PPH $(7, 3.0)$ stands out in particular. At the time of admission, this subject was newly adjusted to his medication. As a result, it was overdosed and over-movable. The third (turquoise) cluster consists only of test subjects of stadium one. According to our records, the subject $(10, 0)$ has a moderate tremor, but was set to Parkinson's stage zero by the medical doctor treating him. Cluster four (violet) contains only Parkinson's patients of stage 3, where the HS $(31, 0)$ is noticeable. The HS has artrosis in the legs and therefore had a high motor dysfunction. In clusters 5 blue, 6 yellow and 7 black all PPH are assigned to the correct cluster. In the appendix in Table III all results are summarized again.

In Fig. 6 all time series data of the respctive clusters are displayed jointly. The coincidence of pattern and time required to complete the TUG test within a cluster can be recognized in these diagrams.

IV. CONCLUSION

Finally it can be concluded that the sensor insole used for this study is very well suited for measuring motor dysfunctions. Hierachical clustering in combination with Single-Linkage and DTW is useful for detecting outliers within a recording. Hierachical clustering in combination with Complete-Linkage and DTW makes a clear distinction between subjects and the stadium of gait disorder. We also demonstrated that the linear acceleration data at a rate of $100Hz$ are sufficient to draw conclusions about a person's motor health. With this data rate it is theoretically even possible to evaluate the data in real time. It proved to be sufficient to use only data collected from one foot to distinguish the different levels of gait disorder. Further improvements could
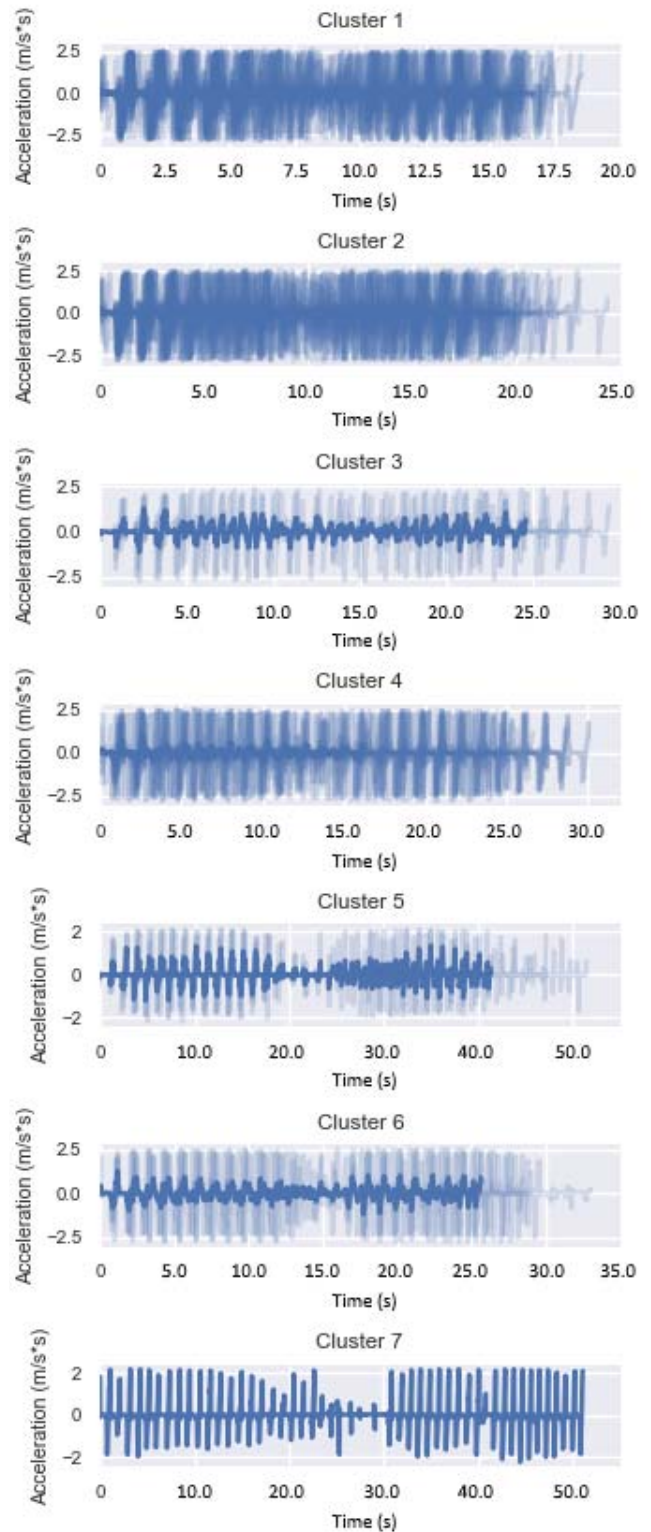
Fig. 6. Time series of the clusters separately according to their assignment

TABLE III
OUTSTANDING SUBJECTS

(Id, Stadium)	Cluster	Symptome
(48, nan)	1	no information about symptoms; fast-moving; no apparent gait disorder
(28, nan)	1	no information about symptoms; fast-moving; no apparent gait disorder
(24, 2)	1	light Hypokinesis ; Tremor slightly dominant on the right; light Postural instability new setting of medication recording on day of discharge from hospital
(51, nan)	1	Tremor hand right; no apparent gait disorder
(50, nan)	2	no information about symptoms; no apparent gait disorder
(8, 1)	2	Rigor ; Tremor
(7, 3)	2	Over-movable due to overdosing;
(47, nan)	2	no information about symptoms; no apparent gait disorder
(10, 0)	3	moderate tremor; Stadium 0 by doctor
(29, nan)	4	self-help group;
(49, nan)	4	self-help group; light Tremor left medium postural instability
(19, nan)	4	self-help group; Tremor left
(31, 0)	4	artrosis in the legs;

be achieved by using additional sensor data such as absolute angles and pressure data as well as by using the sensor data of both feet. Other possible classifications are k-Nearest-Neighbor or Neural Networks and so on. In addition, the number of dimensions could also be increased for practical use in order to boost the recognition rate.

REFERENCES

[1] Boix, J., von Hieber, D., & Connor, B. (2018). Gait Analysis for Early Detection of Motor Symptoms in the 6-OHDA Rat Model of Parkinson's Disease. Frontiers in behavioral neuroscience, 12, 39.

[2] Kale, A., Cuntoor, N., Yegnanarayana, B., Rajagopalan, A. N., & Chellappa, R. (2003, June). Gait analysis for human identification. In International Conference on Audio-and Video-Based Biometric Person Authentication (pp. 706-714). Springer, Berlin, Heidelberg.

[3] Boulgouris, N. V., Hatzinakos, D., & Plataniotis, K. N. (2005). Gait recognition: a challenging signal processing technology for biometric identification. IEEE signal processing magazine, 22(6), 78-90.

[4] Veeraraghavan, A., Chellappa, R., & Roy-Chowdhury, A. K. (2006). The function space of an activity. In Computer Vision and Pattern Recognition, 2006 IEEE Computer Society Conference on (Vol. 1, pp. 959-968). IEEE.

[5] Muscillo, R., Conforto, S., Schmid, M., Caselli, P., & D'Alessio, T. (2007, August). Classification of motor activities through derivative dynamic time warping applied on accelerometer data. In Engineering in Medicine and Biology Society, 2007. EMBS 2007. 29th Annual International Conference of the IEEE (pp. 4930-4933). IEEE.

[6] Rocha, A. P., Choupina, H., Fernandes, J. M., Rosas, M. J., Vaz, R., & Cunha, J. P. S. (2015, August). Kinect v2 based system for Parkinson's disease assessment. In Engineering in Medicine and Biology Society (EMBC), 2015 37th Annual International Conference of the IEEE (pp. 1279-1282). IEEE.

[7] Ferrari, A., Ginis, P., Hardegger, M., Casamassima, F., Rocchi, L., & Chiari, L. (2016). A mobile Kalman-filter based solution for the real-time estimation of spatio-temporal gait parameters. IEEE transactions on neural systems and rehabilitation engineering, 24(7), 764-773.

[8] Ferster, M. L., Mazilu, S., & Tröster, G. (2015, September). Gait parameters change prior to freezing in Parkinson's disease: a data-driven study with wearable inertial units. In Proceedings of the 10th EAI International Conference on Body Area Networks (pp. 159-166). ICST (Institute for Computer Sciences, Social-Informatics and Telecommunications Engineering).

[9] Haji Ghassemi, N., Hannink, J., Martindale, C. F., Gaßner, H., Müller, M., Klucken, J., & Eskofier, B. M. (2018). Segmentation of Gait Sequences in Sensor-Based Movement Analysis: A Comparison of Methods in Parkinsons Disease. Sensors, 18(1), 145.

[10] Barth, J. G. Development and Validation of a Mobile Gait Analysis System Providing Clinically Relevant Target Parameters in Parkinson's Disease.

[11] Podsiadlo, D., & Richardson, S. (1991). The timed "Up & Go": a test of basic functional mobility for frail elderly persons. Journal of the American geriatrics Society, 39(2), 142-148.

[12] Goetz, C. G., Tilley, B. C., Shaftman, S. R., Stebbins, G. T., Fahn, S., MartinezMartin, P., ... & Dubois, B. (2008). Movement Disorder Societysponsored revision of the Unified Parkinson's Disease Rating Scale (MDSUPDRS): Scale presentation and clinimetric testing results. Movement disorders, 23(15), 2129-2170.

[13] Hoehn, M. M., & Yahr, M. D. (1998). Parkinsonism: onset, progression, and mortality. Neurology, 50(2), 318-318.

[14] Keogh, E., & Ratanamahatana, C. A. (2005). Exact indexing of dynamic time warping. Knowledge and information systems, 7(3), 358-386.

[15] Handl, A. (2002). Multivariate Analysemethoden. Berlin uaO.

Hierarchical Clustering with Complete-Linkage and DTW as metric

Fig. 7.

(Id. Parkinson stadium)

E
Certificates

IEEE

CERTIFICATE

iwobi
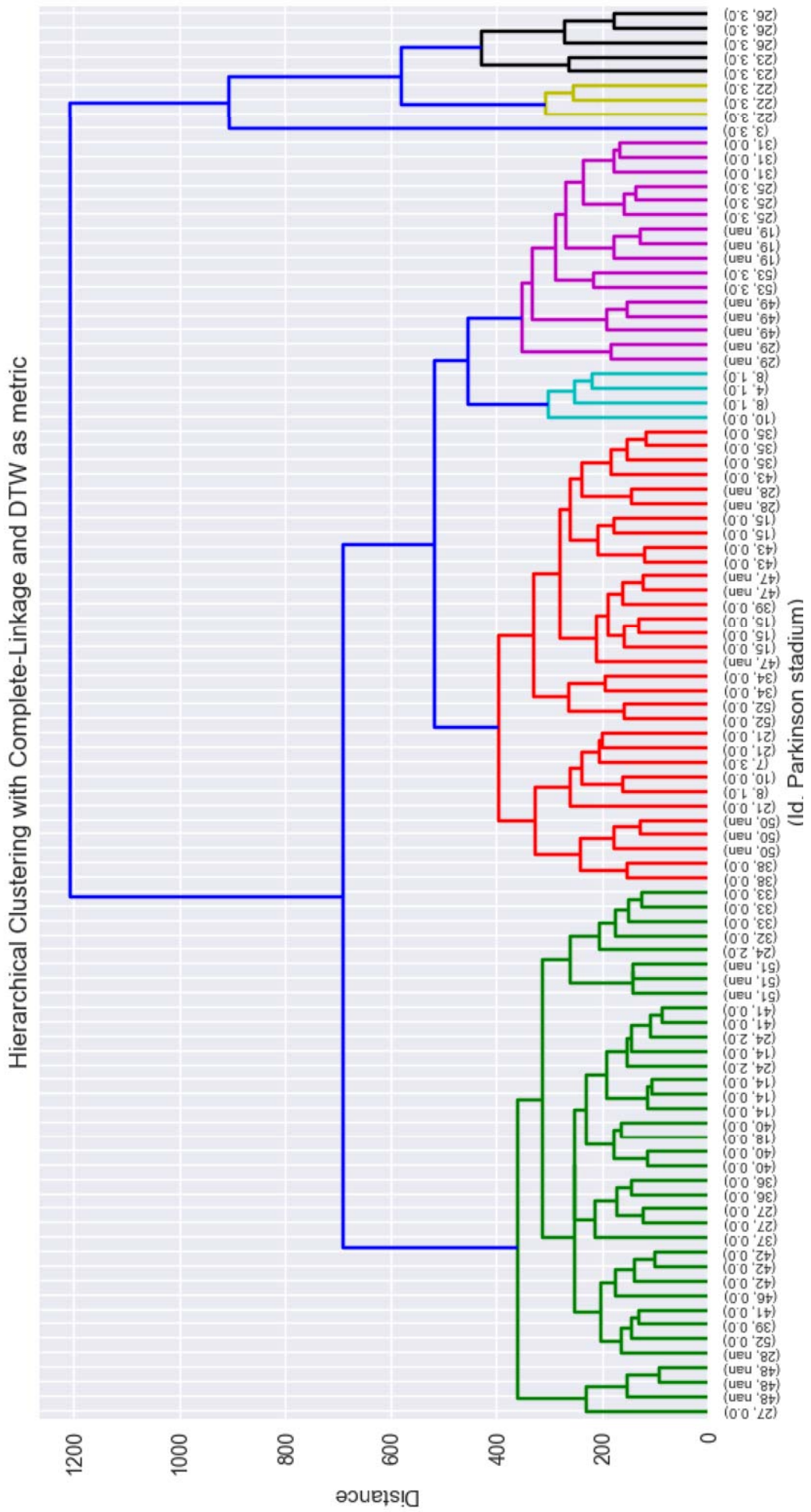
The organizing committee certificates that the work titled:

Clustering of Human Gait with Parkinson's Disease by using Dynamic Time Warping

has been presented by

Tobias Steinmetzer

as ORAL COMMUNICATION in the *2018 IEEE International Work Conference on Bioinspired Intelligence* (IWOBI 2018), which was held in the Instituto Tecnológico de Costa Rica, (COSTA RICA).

San Carlos, Costa Rica
July 18-20, 2018

Juan L. Crespo-Mariño
General Chair
Instituto Tecnológico de Costa Rica

Carlos M. Travieso-González
President of the IWOBI Steering Committee
Universidad de las Palmas de Gran Canaria

UNIVERSIDAD DE LAS PALMAS DE GRAN CANARIA UNIVERSIDAD DE COSTA RICA UNA UNIVERSIDAD NACIONAL COSTA RICA uTn Universidad Técnica Nacional TEC | Tecnológico de Costa Rica

BTU Graduate Research School (GRS)

Qualifikationsprogramm

TEILNAHMEBESTÄTIGUNG

Herrn Tobias Steinmetzer

wird die Teilnahme am Workshop

Überzeugend schreiben für Naturwissenschaftler, Informatiker & Ingenieure

am 22. und 23. März 2018 bestätigt.

Workshopleitung:	Till Hopfe & Adem Mulamustafić
Umfang:	16 Unterrichtseinheiten à 45 Minuten
Schwerpunkte:	

- Logisch überzeugende und rhetorisch wirkungsvolle wissenschaftliche Texte verfassen
- Klare und verständliche wissenschaftliche Texte durch einen verbesserten Text-, Absatz- und Satzaufbau verfassen
- Adäquates rekonstruieren und kritisieren von Gegenpositionen
- Abstracts auf den Punkt bringen
- Umgehen von Fallstricken im Double-Blind-Review-Verfahren
- Effizientes managen der Schreibzeit (z. B. für wissenschaftliche Aufsatz- und Buchprojekte)
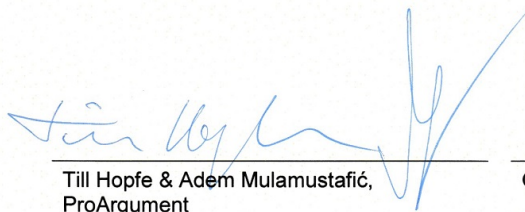
Till Hopfe & Adem Mulamustafić,
ProArgument
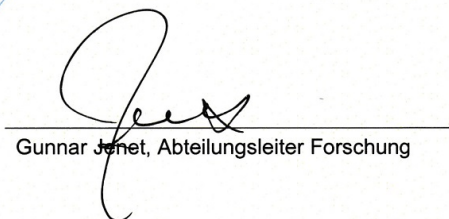
Gunnar Jenet, Abteilungsleiter Forschung

#6,953,105

CERTIFICATE NUMBER

STATEMENT OF ACCOMPLISHMENT

HAS BEEN AWARDED TO

Tobias Steinmetzer

FOR SUCCESSFULLY COMPLETING

Biomedical Image Analysis in Python Course

DataCamp

#6,793,030

CERTIFICATE NUMBER

STATEMENT OF ACCOMPLISHMENT

HAS BEEN AWARDED TO

Tobias Steinmetzer

FOR SUCCESSFULLY COMPLETING

Deep Learning in Python Course

DataCamp

#6,804,999
CERTIFICATE NUMBER

STATEMENT OF ACCOMPLISHMENT

HAS BEEN AWARDED TO

Tobias Steinmetzer

FOR SUCCESSFULLY COMPLETING

Introduction to Git for Data Science Course

DataCamp

#5,922,155
CERTIFICATE NUMBER

STATEMENT OF ACCOMPLISHMENT

HAS BEEN AWARDED TO

Tobias Steinmetzer

FOR SUCCESSFULLY COMPLETING

Intro to Python for Data Science Course
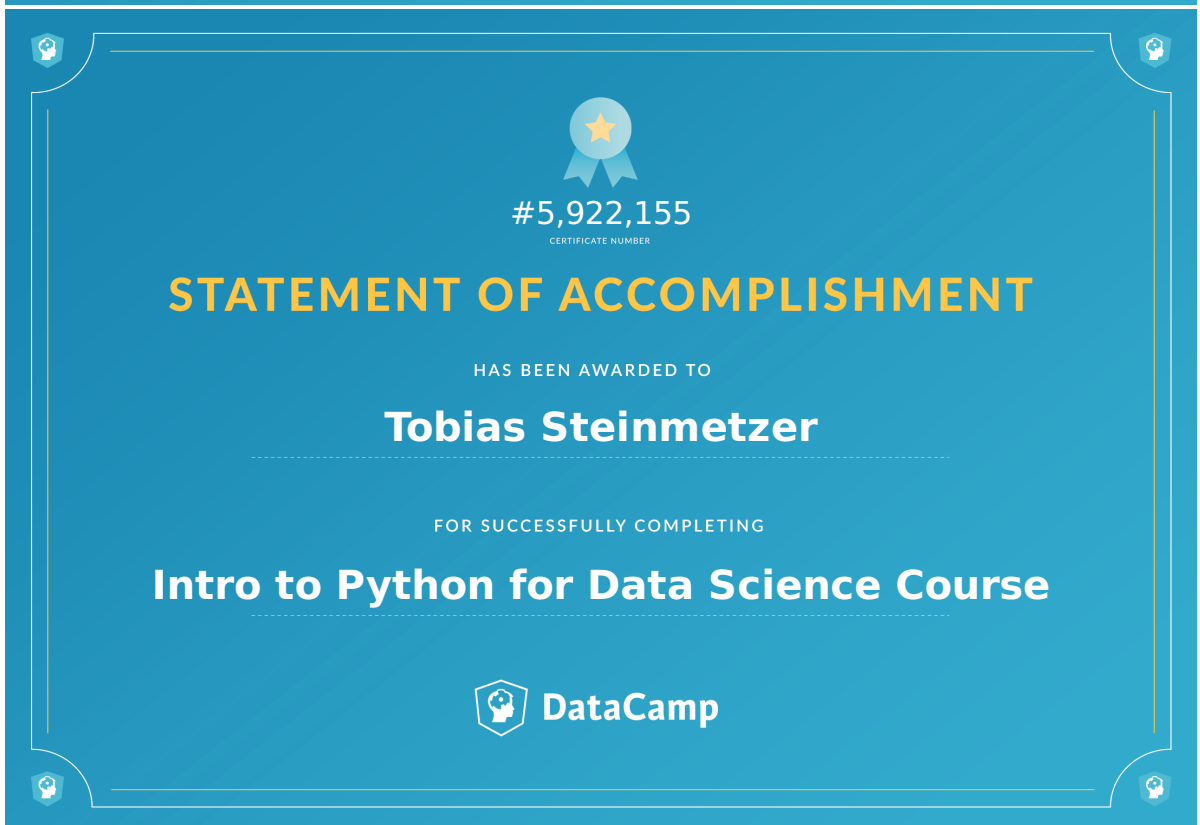
DataCamp

#6,884,970

CERTIFICATE NUMBER

STATEMENT OF ACCOMPLISHMENT

HAS BEEN AWARDED TO

Tobias Steinmetzer

FOR SUCCESSFULLY COMPLETING

Preprocessing for Machine Learning in Python Course

DataCamp

#6,790,382

CERTIFICATE NUMBER

STATEMENT OF ACCOMPLISHMENT

HAS BEEN AWARDED TO

Tobias Steinmetzer

FOR SUCCESSFULLY COMPLETING

Intermediate Python for Data Science Course

DataCamp

List of Figures

List of Tables

Bibliography

[Abadi2016] Abadi, M., Abadi, M., Barham, P., Chen, J., Chen, Z., Davis, A., Dean, J., Devin, M., Ghemawat, S., Irving, G., Isard, M., Kudlur, M., Levenberg, J., Monga, R., Moore, S., Murray, D.G., Steiner, B., Tucker, P., Vasudevan, V., Warden, P., Wicke, M., Yu Y., Zheng X., Tensorflow: A system for large-scale machine learning. In Proceedings of the 12th USENIX Symposium on Operating Systems Design and Implementation (OSDI 16), 2016.

[Aghanavesi2017] Aghanavesi, S., Memedi, M., Dougherty, M., Nyholm, D., & Westin, J. (2017). Verification of a method for measuring Parkinson's disease related temporal irregularity in spiral drawings. Sensors, 17(10), 2341.

[Agostini2014] Agostini, Valentina, Gabriella Balestra, and Marco Knaflitz, Segmentation and classification of gait cycles, IEEE Transactions on Neural Systems and Rehabilitation Engineering 22.5 (2014): 946-952.

[Ahlf2017] Ahlf, A. (2017). Klinische Parameter des essenziellen Tremors (Doctoral dissertation).

[Akyol2017] Akyol, K. (2017). A study on the diagnosis of Parkinson's disease using digitized wacom graphics tablet dataset. Int J Inf Technol Comput Sci, 9, 45-51.

[Andres1990] Andres, R. O., & Stimmel, S. K. (1990). Prosthetic alignment effects on gait symmetry: a case study. Clinical biomechanics, 5(2), 88-96.

[Anwary2018a] Anwary, A. R., Yu, H., & Vassallo, M. (2018). An automatic gait feature extraction method for identifying gait asymmetry using wearable sensors. Sensors, 18(2), 676.

[Anwary2018b] Anwary, A. R., Yu, H., & Vassallo, M. (2018). Wearable Sensor Based Gait Asymmetry Visualization Tool.

[Anwary2018c] Anwary, A. R., Yu, H., & Vassallo, M. (2018). Optimal foot location for placing wearable IMU sensors and automatic feature extraction for gait analysis. IEEE Sensors Journal, 18(6), 2555-2567.

[Appenrodt2009] Appenrodt, J., Al-Hamadi, A., Elmezain, M., & Michaelis, B. (2009, December). Data gathering for gesture recognition systems based on mono color-, stereo color-and thermal cameras. In International Conference on Future Generation Information Technology (pp. 78-86). Springer, Berlin, Heidelberg.

[Ashhar2017] Ashhar, K., Soh, C. B., & Kong, K. H. (2017, July). A wearable ultrasonic sensor network for analysis of bilateral gait symmetry. In 2017 39th Annual International Conference of the IEEE Engineering in Medicine and Biology Society (EMBC) (pp. 4455-4458). IEEE.

[Ball2018] Ball, Nicole, et al., Parkinson's disease and the environment, Frontiers in neurology 10 (2019): 218.

[Balzer2018] Balzer, J., Marsico, P., Mitteregger, E., van der Linden, M.L., Mercer, T.H., van Hedel, H.J. Influence of trunk control and lower extremity impairments on gait capacity in children with cerebral palsy. *Disabil. Rehabil.* **2018**, *40*, 3164–3170.

[Bamberg2008] Bamberg, S. J. M., Benbasat, A. Y., Scarborough, D. M., Krebs, D. E., & Paradiso, J. A. (2008). Gait analysis using a shoe-integrated wireless sensor system. IEEE transactions on information technology in biomedicine, 12(4), 413-423.

[Baron2018] Baron, E.I., Koop, M.M., Streicher, M.C., Rosenfeldt, A.B., Alberts, J.L. Altered kinematics of arm swing in Parkinson's disease patients indicates declines in gait under dual-task conditions. *Parkinsonism Relat. Disord.* **2018**, *48*, 61–67.

[Barth2017] Barth, J. G. (2017). Development and Validation of a Mobile Gait Analysis System Providing Clinically Relevant Target Parameters in Parkinson's Disease.

[Barth2015] Barth, Jens, et al. Stride segmentation during free walk movements using multi-dimensional subsequence dynamic time warping on inertial sensor data. Sensors 15.3 (2015): 6419-6440.

[Beauchet2009] Beauchet, O., Annweiler, C., Dubost, V., Allali, G., Kressig, R. W., Bridenbaugh, S., ... & Herrmann, F. R. (2009). Stops walking when talking: a predictor of falls in older adults?. European journal of neurology, 16(7), 786-795.

[Berg1992] Berg, K., Wooddauphinee, S., Williams, J. I., Maki, B., & Gayton, D. (1991, August). Measuring balance in the elderly-Validation of an instrument. In Journal of the American Geriatrics Society (Vol. 39, No. 8, pp. A65-A65). 351 WEST CAMDEN ST, BALTIMORE, MD 21201-2436: WILLIAMS & WILKINS.

[Berlit2011] Berlit, P. (2012). Klinische Neurologie (Vol. 3). Springer Berlin Heidelberg.

[Bertomeu2015] Bertomeu-Motos, A., Lledó, L., Díez, J., Catalan, J., Ezquerro, S., Badesa, F., Garcia-Aracil, N. Estimation of human arm joints using two wireless sensors in robotic rehabilitation tasks. *Sensors* **2015**, *15*, 30571–30583.

[Bishop2010] Bishop, E., & Li, Q. (2010, May). Walking speed estimation using shank-mounted accelerometers. In 2010 IEEE International Conference on Robotics and Automation (pp. 5096-5101). IEEE.

[Blazkiewicz2014] Blazkiewicz, M. I. C. H. A. L. I. N. A., Wiszomirska, I., & Wit, A. (2014). Comparison of four methods of calculating the symmetry of spatial-temporal parameters of gait. Acta of bioengineering and biomechanics, 16(1).

[Bobic2018] Bobic, Vladislava N., et al.,Challenges of Stride Segmentation and Their Implementation for Impaired Gait, 2018 40th Annual International Conference of the IEEE Engineering in Medicine and Biology Society (EMBC). IEEE, 2018.

[Boer2006] Boer, J. (2006). Charakterisierung des Balanceverhaltens von Gesunden, Hüft-und Kniepatienten auf dem Posturomed.

[Boix2018] Boix, J., von Hieber, D., & Connor, B. (2018). Gait Analysis for Early Detection of Motor Symptoms in the 6-OHDA Rat Model of Parkinson's Disease. Frontiers in behavioral neuroscience, 12, 39.

[Bortz2011] Bortz, J., & Schuster, C. (2011). Statistik für Human-und Sozialwissenschaftler: Limitierte Sonderausgabe. Springer-Verlag.

[Bosch2015] BOSCH Sensortec, Data Sheet BMI160. 2015. Available online: `https://ae-bst.resource.bosch.com/media/_tech/media/datasheets/BST-BMI160-DS000-07.pdf` (accessed on 2/12/2019).

[Bosch2016] BNO055 Intelligent 9-axis absolute orientation sensor, BST-BNO055-DS000-14, Rev. 0273414209, Bosch Sensortec, June 2016

[Boulgouris2005] Boulgouris, N. V., Hatzinakos, D., & Plataniotis, K. N. (2005). Gait recognition: a challenging signal processing technology for biometric identification. IEEE signal processing magazine, 22(6), 78-90.

[Buckley2019] Buckley, C., Alcock, L., McArdle, R., Rehman, R. Z. U., Del Din, S., Mazzà , C., ... & Rochester, L. (2019). The role of movement analysis in diagnosing and monitoring neurodegenerative conditions: Insights from gait and postural control. Brain sciences, 9(2), 34.

[Cao2018] Cao, L., Wang, Y., Zhang, B., Jin, Q., & Vasilakos, A. V. (2018). GCHAR: An efficient Group-based Context—Aware human activity recognition on smartphone. Journal of Parallel and Distributed Computing, 118, 67-80.

[Castano2018] Castaño, Y., Navarro, A., Arango, J., Muñoz, B., Orozco, J.L., Valderrama, J. Gait and Arm Swing Analysis Measurements for Patients Diagnosed with Parkinson's Disease, using Digital Signal Processing and Kinect. In Proceedings of the SSN2018, Valdivia, Chile, 2018, pp. 71–74.

[Castano2019] Castaño-Pino, Y.J., Navarro, A., Muñoz, B., Orozco, J.L. Using Wavelets for Gait and Arm Swing Analysis. In *Wavelet Transform and Complexity*, IntechOpen: 2019.

[Chen2011] Chen, X., & Dai, W. (2011). Maximum entropy principle for uncertain variables. International Journal of Fuzzy Systems, 13(3), 232-236.

[Chelius2011] Chelius, G., Braillon, C., Pasquier, M., Horvais, N., Gibollet, R. P., Espiau, B., & Coste, C. A. (2011). A wearable sensor network for gait analysis: A six-day experiment of running through the desert. IEEE/ASME Transactions On Mechatronics, 16(5), 878-883.

[Chen2018] Chen, H., Liu, X., & Zhao, G. (2018, August). Temporal Hierarchical Dictionary with HMM for Fast Gesture Recognition. In 2018 24th International Conference on Pattern Recognition (ICPR) (pp. 3378-3383). IEEE.

[Chollet2015] Chollet, F., Keras. 2015. Available online: `https://keras.io` (accessed on 11 10 2019).

[Clemens2019] Clemens, S., Kim, K. J., Gailey, R., Kirk-Sanchez, N., Kristal, A., & Gaunaud, I. (2019). Inertial sensor-based measures of gait symmetry and repeatability in people with unilateral lower limb amputation. Clinical Biomechanics.

[Crea2014] Crea, S., Cipriani, C., Donati, M., Carrozza, M. C., & Vitiello, N. (2014). Providing time-discrete gait information by wearable feedback apparatus for lower-limb amputees: usability and functional validation. IEEE Transactions on Neural Systems and Rehabilitation Engineering, 23(2), 250-257.

[Crenshaw2006] Crenshaw, S. J., & Richards, J. G. (2006). A method for analyzing joint symmetry and normalcy, with an application to analyzing gait. Gait & posture, 24(4), 515-521.

[Dempsey2018] Dempsey, A. F., Pyrznawoski, J., Lockhart, S., Barnard, J., Campagna, E. J., Garrett, K., ... & O'Leary, S. T. (2018). Effect of a health care professional communication training intervention on adolescent human papillomavirus vaccination: a cluster randomized clinical trial. JAMA pediatrics, 172(5), e180016-e180016.

[Dennis2016] Dennis, S. (2016). Secondary prevention of chronic health conditions in patients with multimorbidity: what can physiotherapists do?.

[Diaz2020] Díaz, S., Stephenson, J. B., & Labrador, M. A. (2020). Use of Wearable Sensor Technology in Gait, Balance, and Range of Motion Analysis. Applied Sciences, 10(1), 234.

[Domhardt2019] Domhardt, M., Geßlein, H., von Rezori, R. E., & Baumeister, H. (2019). Internet-and mobile-based interventions for anxiety disorders: A meta-analytic review of intervention components. Depression and anxiety, 36(3), 213-224.

[Dranca2018] Dranca, L., de Mendarozketa, L.D.A.R., Goñi, A., Illarramendi, A., Gomez, I.N., Alvarado, M.D., Rodríguez-Oroz, M.C. Using Kinect to classify Parkinson's disease stages related to severity of gait impairment. *BMC Bioinform.* **2018**, *19*, 471.

[Duncan1990] Duncan, P. W., Weiner, D. K., Chandler, J., & Studenski, S. (1990). Functional reach: a new clinical measure of balance. Journal of gerontology, 45(6), M192-M197.

[Ebert2018] Ebert, D. D., Van Daele, T., Nordgreen, T., Karekla, M., Compare, A., Zarbo, C., ... & Kaehlke, F. (2018). Internet-and mobile-based psychological

interventions: applications, efficacy, and potential for improving mental health. European Psychologist.

[Elble1996] Elble, R. J., Brilliant, M., Leffler, K., & Higgins, C. (1996). Quantification of essential tremor in writing and drawing. Movement disorders: official journal of the Movement Disorder Society, 11(1), 70-78.

[Espay2016] Espay, Alberto J., et al., Technology in Parkinson's disease: Challenges and opportunities, Movement Disorders 31.9 (2016): 1272-1282.

[Ferrari2013] Ferrari, A., Rocchi, L., van den Noort, J., & Harlaar, J. (2013). Toward the use of wearable inertial sensors to train gait in subjects with movement disorders. In Converging clinical and engineering research on neurorehabilitation (pp. 937-940). Springer, Berlin, Heidelberg.

[Ferrari2015] Ferrari, A., Ginis, P., Hardegger, M., Casamassima, F., Rocchi, L., & Chiari, L. (2015). A mobile Kalman-filter based solution for the real-time estimation of spatio-temporal gait parameters. IEEE transactions on neural systems and rehabilitation engineering, 24(7), 764-773.

[Ferrari2016] Ferrari, A., Ginis, P., Hardegger, M., Casamassima, F., Rocchi, L., & Chiari, L. (2016). A mobile Kalman-filter based solution for the real-time estimation of spatio-temporal gait parameters. IEEE transactions on neural systems and rehabilitation engineering, 24(7), 764-773.

[Ferster2015] Ferster, M. L., Mazilu, S., & Tröster, G. (2015, September). Gait parameters change prior to freezing in Parkinson's disease: a data-driven study with wearable inertial units. In Proceedings of the 10th EAI International Conference on Body Area Networks (pp. 159-166). ICST (Institute for Computer Sciences, Social-Informatics and Telecommunications Engineering).

[Floryan2019] Floryan, M. R., Ritterband, L. M., & Chow, P. I. (2019). Principles of gamification for Internet interventions. Translational behavioral medicine, 9(6), 1131-1138.

[Frenkel2005] Frenkel-Toledo, S., Giladi, N., Peretz, C., Herman, T., Gruendlinger, L., & Hausdorff, J. M. (2005). Treadmill walking as an external pacemaker to improve gait rhythm and stability in Parkinson's disease. Movement disorders: official journal of the Movement Disorder Society, 20(9), 1109-1114.

[Frochte2019] Frochte, J. (2019). Maschinelles Lernen: Grundlagen und Algorithmen in Python. Carl Hanser Verlag GmbH Co KG.

[Gadaleta2018] Gadaleta, M., & Rossi, M. (2018). Idnet: Smartphone-based gait recognition with convolutional neural networks. Pattern Recognition, 74, 25-37.

[Goetz2008] Goetz, C.G., Tilley, B.C., Shaftman, S.R., Stebbins, G.T., Fahn, S., Martinez-Martin, P., Poewe, W., Sampaio, C., Stern, M.B., Dodel, R., et al. Movement Disorder Society-sponsored revision of the Unified Parkinson's Disease Rating Scale (MDS-UPDRS): Scale presentation and clinimetric testing results. *Mov. Disord.* **2008**, *23*, 2129–2170.

[Goldberger2003] Goldberger AL, Amaral LAN, Glass L, Hausdorff JM, Ivanov PCh, Mark RG, Mietus JE, Moody GB, Peng C-K, Stanley HE. PhysioBank, PhysioToolkit, and PhysioNet: Components of a New Research Resource for Complex Physiologic Signals (2003). Circulation. 101(23):e215-e220.

[Goswami2009] Goswami, A. (2009). U.S. Patent No. 7,503,900. Washington, DC: U.S. Patent and Trademark Office.

[Gotz2006] Götz-Neumann, K. (2006). Gehen verstehen: Ganganalyse in der Physiotherapie, 18 Tabellen. Georg Thieme Verlag.

[Grangeia2018] Grangeia, T. D. A. G., de Jorge, B., Cecílio-Fernandes, D., Tio, R. A., & de Carvalho-Filho, M. A. (2018). Learn+ Fun! Social Media and Gamification sum up to foster a community of practice during an Emergency Medicine Rotation. Health Professions Education.

[Guo2018] Guo, D., Zhou, W., Li, H., & Wang, M. (2018). Online early-late fusion based on adaptive hmm for sign language recognition. ACM Transactions on Multimedia Computing, Communications, and Applications (TOMM), 14(1), 8.

[Gupta2019] Gupta, U., Bansal, H., & Joshi, D. (2019). Gender specific and Age dependent classification model for improved diagnosis in Parkinson's disease. arXiv preprint arXiv:1904.09651.

[Gwak2018] Gwak, Migyeong, Majid Sarrafzadeh, and Ellen Woo. "Support for a Clinical Diagnosis of Mild Cognitive Impairment Using Photoplethysmography and Gait Sensors." Proceedings, APSIPA Annual Summit and Conference. Vol. 2018. 2018.

[Haji2018] Haji Ghassemi, N., Hannink, J., Martindale, C. F., Gaßner, H., Müller, M., Klucken, J., & Eskofier, B. M. (2018). Segmentation of Gait Sequences in Sensor-Based Movement Analysis: A Comparison of Methods in Parkinson's Disease. Sensors, 18(1), 145.

[Handl2002] Handl, A. (2002). Multivariate Analysemethoden. Berlin uaO.

[Hanlon2009] Hanlon, M., & Anderson, R. (2009). Real-time gait event detection using wearable sensors. Gait & posture, 30(4), 523-527.

[Hannink2018] Hannink, Julius, et al., Mobile stride length estimation with deep convolutional neural networks. IEEE journal of biomedical and health informatics 22.2 (2018): 354-362.

[Hassan2014] Hassan, M., Kadone, H., Suzuki, K., & Sankai, Y. (2014). Wearable gait measurement system with an instrumented cane for exoskeleton control. Sensors, 14(1), 1705-1722.

[Hassan2018] Hassan, M. M., Uddin, M. Z., Mohamed, A., & Almogren, A. (2018). A robust human activity recognition system using smartphone sensors and deep learning. Future Generation Computer Systems, 81, 307-313.

[Hausdorff1998] Hausdorff, J. M., Cudkowicz, M. E., Firtion, R., Wei, J. Y., Goldberger, A. L., Gait variability and basal ganglia disorders: Stride-to-stride variations of gait cycle timing in Parkinson's disease and Huntington's disease. *Mov. Disord.* **1998**, *13*, 428–437.

[Hausdorff2007] Hausdorff, J. M., Lowenthal, J., Herman, T., Gruendlinger, L., Peretz, C., & Giladi, N. (2007). Rhythmic auditory stimulation modulates gait variability in Parkinson's disease. European Journal of Neuroscience, 26(8), 2369-2375.

[Helms2017] Helms, T., Pharmawissen aktuell. Cardio News 2017,11–12

[Herzog1989] Herzog, W. A. L. T. E. R., Nigg, B. M., Read, L. J., & Olsson, E. (1989). Asymmetries in ground reaction force patterns in normal human gait. Med Sci Sports Exerc, 21(1), 110-114.

[Hirvensalo2000] Hirvensalo, M., Rantanen, T., & Heikkinen, E. (2000). Mobility difficulties and physical activity as predictors of mortality and loss of independence in the community-living older population. Journal of the American Geriatrics Society, 48(5), 493-498.

[Hoehn1967] Hoehn, Margaret M., and Melvin D. Yahr, Parkinsonism: onset, progression, and mortality. Neurology 17.5 (1967): 427-427.

[Hoehn1998] Hoehn, M. M., & Yahr, M. D. (1998). Parkinsonism: onset, progression, and mortality. Neurology, 50(2), 318-318.

[Hsu2014] Hsu, Y. L., Chung, P. C., Wang, W. H., Pai, M. C., Wang, C. Y., Lin, C. W., ... & Wang, J. S. (2014). Gait and balance analysis for patients with Alzheimer's disease using an inertial-sensor-based wearable instrument. IEEE journal of biomedical and health informatics, 18(6), 1822-1830.

[Huang2012] Huang, X., Mahoney, J.M., Lewis, M.M., Du, G., Piazza, S.J., Cusumano, J.P. Both coordination and symmetry of arm swing are reduced in Parkinson's disease. *Gait Posture* **2012**, *35*, 373–377.

[Hubble2015] Hubble, R. P., Naughton, G. A., Silburn, P. A., & Cole, M. H. (2015). Wearable sensor use for assessing standing balance and walking stability in people with Parkinson's disease: a systematic review. PloS one, 10(4).

[Ince2017] Ince, Omer Faruk, et al., Gait analysis and identification based on joint information using RGB-depth camera. 2017 14th International Conference on Electrical Engineering/Electronics, Computer, Telecommunications and Information Technology (ECTI-CON). IEEE, 2017.

[Interlink2016] FSR 400 Series Data Sheet, Interlink Electronics, PDS-10004-C

[Isenkul2014] Isenkul, M., Sakar, B., & Kursun, O. (2014, May). Improved spiral test using digitized graphics tablet for monitoring Parkinson's disease. In Proc. of the Int'l Conf. on e-Health and Telemedicine (pp. 171-5).

[Jagt2018] van't Jagt, R. K., Tan, S. L., Hoeks, J., Spoorenberg, S., Reijneveld, S. A., de Winter, A., ... & Jansen, C. J. (2018). Using photo stories to support doctor-patient communication. Three studies into a communicative health literacy intervention for older adults. Show, don't just tell., 163.

[Jasni2019] Jasni, F., Hamzaid, N.A., Al-Nusairi, T.Y., Yusof, N.H.M., Shasmin, H.N., Cheok, N.S. Feasibility of A Gait Phase Identification Tool for Transfemoral Amputees using Piezoelectric-Based In-Socket Sensory System. *IEEE Sens. J.* **2019**, *19*, 6437–6444.

[Jelen2008] Jeleń, P., Wit, A., Dudziński, K., & Nolan, L. (2008). Expressing gait-line symmetry in able-bodied gait. Dynamic Medicine, 7(1), 17.

[Jiang2018] Jiang, X., et al. "Exploration of Gait Parameters Affecting the Accuracy of Force Myography-Based Gait Phase Detection." 2018 7th IEEE International Conference on Biomedical Robotics and Biomechatronics (Biorob). IEEE, 2018.

[Johnson1967] Johnson, S. C. (1967). Hierarchical clustering schemes. Psychometrika, 32(3), 241-254.

[Kale2003] Kale, A., Cuntoor, N., Yegnanarayana, B., Rajagopalan, A. N., & Chellappa, R. (2003, June). Gait analysis for human identification. In International Conference on Audio-and Video-Based Biometric Person Authentication (pp. 706-714). Springer, Berlin, Heidelberg.

[Keogh2005] Keogh, E., & Ratanamahatana, C. A. (2005). Exact indexing of dynamic time warping. Knowledge and information systems, 7(3), 358-386.

[Kim2018] Kim, Youngwoo, Odongo Steven Eyobu, and Dong Seog Han, ANN-based stride detection using smartphones for Pedestrian dead reckoning. 2018 IEEE International Conference on Consumer Electronics (ICCE). IEEE, 2018.

[Klucken2013] Klucken, J., Barth, J., Kugler, P., Schlachetzki, J., Henze, T., Marxreiter, F., ... & Winkler, J. (2013). Unbiased and mobile gait analysis detects motor impairment in Parkinson's disease. PloS one, 8(2).

[Kontis2018] Kontis, V., Bennett, J.E., Mathers, C.D., Li, G., Foreman, K., Ezzati, M. Future life expectancy in 35 industrialised countries: Projections with a Bayesian model ensemble. *Lancet* **2017**, *389*, 1323–1335.

[Koroglu2018] Koroglu, M. Taha, Alper Yilmaz, and Can Jozef Saul, A Deep Learning Strategy for Stride Detection. 2018 IEEE SENSORS. IEEE, 2018.

[Kovac2013] Kovač, J., & Peer, P. (2013). Transformation based walking speed normalization for gait recognition. KSII Trans Internet Inf Syst, 7(11), 2690-2701.

[Kovac2014] Kovač, J., & Peer, P. (2014). Human skeleton model based dynamic features for walking speed invariant gait recognition. Mathematical Problems in Engineering, 2014.

[Kovac2019] Kovač, Jure and Štruc, Vitomir and Peer, Peter, P. (2019). Frame–based classification for cross-speed gait recognition. Multimedia Tools and Applications, 78(5), 5621-5643.

[Laertius1925] Laertius, D. (1925). Lives of Eminent Philosophers in Two Volumes, trans. RD Hicks, vol. 2.

[Lauziere2014] Lauziere, S., Betschart, M., Aissaoui, R., & Nadeau, S. (2014). Understanding spatial and temporal gait asymmetries in individuals post stroke. Int J Phys Med Rehabil, 2(3), 201.

[Leakey1981] Leakey, R. E. (1981). The making of mankind (No. 573.2 L43).

[Lee1999] Lee, H. K., & Kim, J. H. (1999). An HMM-based threshold model approach for gesture recognition. IEEE Transactions on pattern analysis and machine intelligence, 21(10), 961-973.

[Lee2019] Lee, G.R., Gommers, R., Wasilewski, F., Wohlfahrt, K., O'Leary, A. PyWavelets: A Python package for wavelet analysis. *J. Open Source Softw.* **2019**, *4*, 1237.

[Levandowsky1971] Levandowsky, M., & Winter, D. (1971). Distance between sets. Nature, 234(5323), 34.

[Lewek2010] Lewek, M.D., Poole, R., Johnson, J., Halawa, O., Huang, X. Arm swing magnitude and asymmetry during gait in the early stages of Parkinson's disease. *Gait Posture* **2010**, *31*, 256–260.

[Li2009] Li, Q., Young, M., Naing, V., & Donelan, J. M. (2009, June). Walking speed and slope estimation using shank-mounted inertial measurement units. In 2009 IEEE International Conference on Rehabilitation Robotics (pp. 839-844). IEEE.

[Li2014] Li, G., Liu, T., Gu, L., Inoue, Y., Ning, H., & Han, M. (2014, November). Wearable gait analysis system for ambulatory measurement of kinematics and kinetics. In SENSORS, 2014 IEEE (pp. 1316-1319). IEEE.

[Liao2008] Liao, F., Wang, J., & He, P. (2008). Multi-resolution entropy analysis of gait symmetry in neurological degenerative diseases and amyotrophic lateral sclerosis. Medical engineering & physics, 30(3), 299-310.

[Lin2018a] Lin, P. C., Chen, K. H., Yang, B. S., & Chen, Y. J. (2018). A digital assessment system for evaluating kinetic tremor in essential tremor and Parkinson's disease. BMC neurology, 18(1), 25.

[Lin2018b] Lin, C. C., & Wagenaar, R. C. (2018). The impact of walking speed on interlimb coordination in individuals with Parkinson's disease. Journal of physical therapy science, 30(5), 658-662.

[Liu2005] Liu, X., Carroll, C. B., Wang, S. Y., Zajicek, J., & Bain, P. G. (2005). Quantifying drug-induced dyskinesias in the arms using digitised spiral-drawing tasks. Journal of neuroscience methods, 144(1), 47-52.

[Lohse2019] Lohse, P., Gamification in der ambulanten Langzeitbetreuung, , 8. Lausitzer Schlaganfalltag, Neuronetz Lausitz, Klinikum Niederlausitz, 2019, pp. 44-46

[Lohse2020] Lohse, P., Steinmetzer, T., Reichmann, H., Reckhardt, M., Bönninger, I., & Reinhardt, F. (2020). Optimierung der Langzeitbetreuung von neurologischen Patienten durch internet-und mobile-basierte Interventionen ohne und mit persuasiven Elementen einschließlich der Gamification. Fortschritte der Neurologie· Psychiatrie.

[Loiret2019] Loiret, I., Villa, C., Dauriac, B., Bonnet, X., Martinet, N., Paysant, J., & Pillet, H. (2019). Are wearable insoles a validated tool for quantifying transfemoral amputee gait asymmetry?. Prosthetics and orthotics international, 43(5), 492-499.

[Lord2013] Lord, S., Galna, B., Verghese, J., Coleman, S., Burn, D., & Rochester, L. (2013). Independent domains of gait in older adults and associated motor and nonmotor attributes: validation of a factor analysis approach. Journals of Gerontology Series A: Biomedical Sciences and Medical Sciences, 68(7), 820-827.

[Lovejoy1981] Lovejoy, C. O. (1981). The origin of man. Science, 211(4480), 341-350.

[Maetzler2016] Maetzler, W., Klucken, J., & Horne, M. (2016). A clinical view on the development of technology-based tools in managing Parkinson's disease. Movement Disorders, 31(9), 1263-1271.

[Mancini2011] Mancini, M., King, L., Salarian, A., Holmstrom, L., McNames, J., & Horak, F. B. (2011). Mobility lab to assess balance and gait with synchronized body-worn sensors. Journal of bioengineering & biomedical science, 007.

[Mariani2010] Mariani, B., Hoskovec, C., Rochat, S., Büla, C., Penders, J., & Aminian, K. (2010). 3D gait assessment in young and elderly subjects using foot-worn inertial sensors. Journal of biomechanics, 43(15), 2999-3006.

[Martinez1994] Martinez-Martin, P., Gil-Nagel, A., Gracia, L. M., Gomez, J. B., Martinez-Sarries, J., & Bermejo, F. (1994). The Cooperative Multicentric Group. Unified Parkinson's disease rating scale characteristics and structure. Mov Disord, 9(1), 76-83.

[Mazumder2018a] Mazumder, O. Development and Control of Active Lower Limb Exoskeleton for Mobility Regeneration and Enhancement. Ph.D. Theses, Indian Institute of Engineering Science and Technology, Shibpur, 2018.

[Mazumder2018b] Mazumder, Oishee, et al. Assessment of Insole Based Gait Feature Variation with Progression of Parkinson's Disease. 2018 IEEE SENSORS. IEEE, 2018.

[Mbientlab2016] MbientLab. 2016. MetaWear RG/RPro. 2016. Available online: `https://mbientlab.com/docs/MetaWearRPROPSv0.8.pdf` (accessed on 4 January 2016).

[Mead2017] Mead, R. (2017, January). Semio: Developing a cloud-based platform for multimodal conversational AI in social robotics. In Consumer Electronics (ICCE), 2017 IEEE International Conference on (pp. 291-292). IEEE.

[Melecky2019] Melecky, R., Rasev, E., Kutilek, P., Jerabek, J., Janatova, M., Hana, K., ... & Kaspar, J. (2019). Assessment of Postural Stability Using the Method of Postural Somatooscilography. In World Congress on Medical Physics and Biomedical Engineering 2018 (pp. 697-701). Springer, Singapore.

[Memedi2016] Memedi, M., Aghanavesi, S., & Westin, J. (2016, February). A method for measuring Parkinson's disease related temporal irregularity in spiral drawings. In 2016 IEEE-EMBS International Conference on Biomedical and Health Informatics (BHI) (pp. 410-413). IEEE.

[Miller2018] Miller-Patterson, C., Buesa, R., McLaughlin, N., Jones, R., Akbar, U., & Friedman, J. H. (2018). Motor asymmetry over time in Parkinson's disease. Journal of the neurological sciences, 393, 14-17.

[Milligan1985] Milligan, G. W., & Cooper, M. C. (1985). An examination of procedures for determining the number of clusters in a data set. Psychometrika, 50(2), 159-179.

[Mills2013] Mills, K., Hettinga, B. A., Pohl, M. B., & Ferber, R. (2013). Between-limb kinematic asymmetry during gait in unilateral and bilateral mild to moderate knee osteoarthritis. Archives of Physical Medicine and Rehabilitation, 94(11), 2241-2247.

[Miralles2006] Miralles, F., Tarongi, S., & Espino, A. (2006). Quantification of the drawing of an Archimedes spiral through the analysis of its digitized picture. Journal of neuroscience methods, 152(1-2), 18-31.

[Mojena1977] Mojena, R. (1977). Hierarchical grouping methods and stopping rules: An evaluation. The Computer Journal, 20(4), 359-363.

[Montavon2012] Montavon, G., Orr, G., & Müller, K. R. (Eds.). (2012). Neural networks: tricks of the trade (Vol. 7700). springer.

[Muheidat2017] Muheidat, Fadi, et al. Estimating walking speed, stride length, and stride time using a passive floor based electronic scavenging system. 2017 IEEE Sensors Applications Symposium (SAS). IEEE, 2017.

[Muro2014] Muro-De-La-Herran, A., Garcia-Zapirain, B., & Mendez-Zorrilla, A. (2014). Gait analysis methods: An overview of wearable and non-wearable systems, highlighting clinical applications. Sensors, 14(2), 3362-3394.

[Muscillo2007] Muscillo, R., Conforto, S., Schmid, M., Caselli, P., & D'Alessio, T. (2007, August). Classification of motor activities through derivative dynamic time warping applied on accelerometer data. In Engineering in Medicine and Biology Society, 2007. EMBS 2007. 29th Annual International Conference of the IEEE (pp. 4930-4933). IEEE.

[Ngokingha2018] Mireille Ngokingha Tchouto (2018): Mobile Ganganalyse mit Inertialsensoren in Einlegesohlen: Implementierung und Validierung von Gangparametern bei Gesunden und bei Parkinson-Patienten. Bachelor thesis, Brandenburg University of Technology Cottbus-Senftenberg

[Ntoumanis2018] Ntoumanis, N., Quested, E., Reeve, J., & Cheon, S. H. (2018). Need supportive communication: Implications for motivation in sport, exercise, and physical activity. Persuasion and communication in sport, exercise, and physical activity, 155-169.

[Ospina2018] Ospina, B.M., Chaparro, J.A.V., Paredes, J.D.A., Pino, Y.J.C., Navarro, A., Orozco, J.L. Objective arm swing analysis in early-stage Parkinson's disease using an RGB-D camera (Kinect). *J. Parkinson's Dis.* **2018**, *8*, 563–570.

[Pacholakis2016] Pachoulakis, Ioannis, and Nikolaos Papadopoulos. Exergames for Parkinson's Disease patients: The balloon goon game. 2016 International Conference on Telecommunications and Multimedia (TEMU). IEEE, 2016.

[Paganini2018] Paganini, S., Teigelkoetter, W., Buntrock, C., & Baumeister, H. (2018). Economic evaluations of internet-and mobile-based interventions for the treatment and prevention of depression: a systematic review. Journal of affective disorders, 225, 733-755.

[Patel2009] Patel, S., Lorincz, K., Hughes, R., Huggins, N., Growdon, J., Standaert, D., ... & Bonato, P. (2009). Monitoring motor fluctuations in patients with Parkinson's disease using wearable sensors. IEEE transactions on information technology in biomedicine, 13(6), 864-873.

[Parkinson1817] Parkinson, J. (1817). An Essay on the Shaking Palsy (London: Sherwood, Neely and Jones).

[Patterson2010] Patterson, K. K., Gage, W. H., Brooks, D., Black, S. E., & McIlroy, W. E. (2010). Evaluation of gait symmetry after stroke: a comparison of current methods and recommendations for standardization. Gait & posture, 31(2), 241-246.

[Pham2019] Pham, H. N., Do, T. T., Chan, K. Y. J., Sen, G., Han, A. Y., Lim, P., ... & Chua, M. C. (2019, July). Multimodal Detection of Parkinson Disease based on Vocal and Improved Spiral Test. In 2019 International Conference on System Science and Engineering (ICSSE) (pp. 279-284). IEEE.

[Pirker2017] Pirker, W., & Katzenschlager, R. (2017). Gait disorders in adults and the elderly. Wiener Klinische Wochenschrift, 129(3-4), 81-95.

[Plotnik2009] Plotnik, M., Giladi, N., & Hausdorff, J. M. (2007). A new measure for quantifying the bilateral coordination of human gait: effects of aging and Parkinson's disease. Experimental brain research, 181(4), 561-570.

[Podsiadlo1991] Podsiadlo, D., & Richardson, S. (1991). The timed "Up & Go": a test of basic functional mobility for frail elderly persons. Journal of the American geriatrics Society, 39(2), 142-148.

[Prakash2019] Prakash, C., Sujil, A., Kumar, R., Mittal, N. Linear Prediction Model for Joint Movement of Lower Extremity. In *Recent Findings in Intelligent Computing Techniques*, Springer: Singapore, 2019, pp. 235–243.

[Prasad2009] Prasad, J. S., & Nandi, G. C. (2009, October). Clustering method evaluation for hidden markov model based real-time gesture recognition. In Advances in Recent Technologies in Communication and Computing, 2009. ARTCom'09. International Conference on (pp. 419-423). IEEE.

[Pullman1998] Pullman, S. L. (1998). Spiral analysis: a new technique for measuring tremor with a digitizing tablet. Movement Disorders, 13(S3), 85-89.

[Rabiner1989] Rabiner, L. R. (1989). A tutorial on hidden Markov models and selected applications in speech recognition. Proceedings of the IEEE, 77(2), 257-286.

[Rampp2014] Rampp, A., Barth, J., Schülein, S., Gaßmann, K. G., Klucken, J., & Eskofier, B. M. (2014). Inertial sensor-based stride parameter calculation from gait sequences in geriatric patients. IEEE transactions on biomedical engineering, 62(4), 1089-1097.

[Rastegari2019] Rastegari, E., Azizian, S., & Ali, H. (2019, January). Machine Learning and Similarity Network Approaches to Support Automatic Classification of Parkinson's Diseases Using Accelerometer-based Gait Analysis. In Proceedings of the 52nd Hawaii International Conference on System Sciences.

[Reichmann2018] Reichmann H, Gerber M, Reckhardt M et al. Dynamische Posturographie zur Quantifizierung der posturalen Kontrolle. AktNeurol 2018, 45: 714-725

[Reid2018] Reid, M., Walsh, C., Raubenheimer, J., Bradshaw, T., Pienaar, M., Hassan, C., ... & Le Roux, M. (2018). Development of a health dialogue model for patients with diabetes: A complex intervention in a low-/middle income country. International journal of Africa nursing sciences, 8, 122-131.

[Richards1994] Richards, M., Marder, K., Cote, L., & Mayeux, R. (1994). Interrater reliability of the Unified Parkinson's Disease Rating Scale motor examination. Movement Disorders, 9(1), 89-91.

[Rocha2015] Rocha, A. P., Choupina, H., Fernandes, J. M., Rosas, M. J., Vaz, R., & Cunha, J. P. S. (2015, August). Kinect v2 based system for Parkinson's disease assessment. In Engineering in Medicine and Biology Society (EMBC), 2015 37th Annual International Conference of the IEEE (pp. 1279-1282). IEEE.

[Roggendorf2012] Roggendorf, J., Chen, S., Baudrexel, S., Van De Loo, S., Seifried, C., Hilker, R. Arm swing asymmetry in Parkinson's disease measured with ultrasound based motion analysis during treadmill gait. *Gait Posture* **2012**, *35*, 116–120.

[Sabatini2005] Sabatini, A. M., Martelloni, C., Scapellato, S., & Cavallo, F. (2005). Assessment of walking features from foot inertial sensing. IEEE Transactions on biomedical engineering, 52(3), 486-494.

[Sadeghi2000] Sadeghi, H., Allard, P., Prince, F., & Labelle, H. (2000). Symmetry and limb dominance in able-bodied gait: a review. Gait & posture, 12(1), 34-45.

[Salarian2004] Salarian, A., Russmann, H., Vingerhoets, F. J., Dehollain, C., Blanc, Y., Burkhard, P. R., & Aminian, K. (2004). Gait assessment in Parkinson's disease: toward an ambulatory system for long-term monitoring. IEEE transactions on biomedical engineering, 51(8), 1434-1443.

[San2016] San Luciano, M., Wang, C., Ortega, R. A., Yu, Q., Boschung, S., Soto-Valencia, J., ... & Saunders-Pullman, R. (2016). Digitized spiral drawing: A possible biomarker for early Parkinson's disease. PloS one, 11(10).

[Sant2011] Sant'Anna, A., Salarian, A., & Wickstrom, N. (2011). A new measure of movement symmetry in early Parkinson's disease patients using symbolic processing of inertial sensor data. IEEE Transactions on biomedical engineering, 58(7), 2127-2135.

[Saunders2008] Saunders-Pullman, R., Derby, C., Stanley, K., Floyd, A., Bressman, S., Lipton, R. B., ... & Pullman, S. L. (2008). Validity of spiral analysis in early Parkinson's disease. Movement disorders: official journal of the Movement Disorder Society, 23(4), 531-537.

[Schattauer2016] Schattauer, S. (2016). Die Archimedesspirale-ein potentielles Werkzeug in der Früherkennung neurodegenerativer Erkrankungen?: Testung von Tremores in der TREND-Studie (Doctoral dissertation, Eberhard Karls Universität Tübingen).

[Schlomer2008] Schlömer, T., Poppinga, B., Henze, N., & Boll, S. (2008, February). Gesture recognition with a Wii controller. In Proceedings of the 2nd international conference on Tangible and embedded interaction (pp. 11-14). ACM.

[Schultz2018] Schultz, P. W., Nolan, J. M., Cialdini, R. B., Goldstein, N. J., & Griskevicius, V. (2018). The constructive, destructive, and reconstructive power of social norms: Reprise. Perspectives on psychological science, 13(2), 249-254.

[Seckiner2019] Seckiner, D., Mallett, X., Maynard, P., Meuwly, D., & Roux, C. (2019). Forensic gait analysis—Morphometric assessment from surveillance footage. Forensic science international.

[Shorter2008] Shorter, K. A., Polk, J. D., Rosengren, K. S., & Hsiao-Wecksler, E. T. (2008). A new approach to detecting asymmetries in gait. Clinical Biomechanics, 23(4), 459-467.

[Shumway1995] Shumway-Cook, A., & Woollacott, M. (1995). Assessment and treatment of the patient with mobility disorders. Shumway-Cook A, Woolacott MH. Motor control theory and practical applications. Maryland: Williams & Wilkins, 315-54.

[Sijobert2015] Sijobert, B., Benoussaad, M., Denys, J., Pissard-Gibollet, R., Geny, C., & Coste, C. A. (2015). Implementation and validation of a stride length estimation algorithm, using a single basic inertial sensor on healthy subjects and patients suffering from Parkinson's disease. ElectronicHealthcare, 704-714.

[Sokolova2009] Sokolova, M., & Lapalme, G. (2009). A systematic analysis of performance measures for classification tasks. Information Processing & Management, 45(4), 427-437.

[Spasojevic2015] Spasojević, S., Santos-Victor, J., Ilić, T., Milanović, S., Potkonjak, V., Rodić, A. A vision-based system for movement analysis in medical applications: The example of Parkinson disease. In *International Conference on Computer Vision Systems*, Springer: Cham, Switzerland, 2015, pp. 424–434.

[Sprager2015] Sprager, S., & Juric, M. B. (2015). Inertial sensor-based gait recognition: A review. Sensors, 15(9), 22089-22127.

[Srivastava2014] Srivastava, Nitish, et al. Dropout: a simple way to prevent neural networks from overfitting. The Journal of Machine Learning Research 15.1 (2014): 1929-1958.

[Stangor2019] Stangor, C., & Walinga, J. (2019). 1.2 The Evolution of Psychology: History, Approaches, and Questions. Introduction to Psychology.

[Steinmetzer2018] Steinmetzer, T., Bonninger, I., Priwitzer, B., Reinhardt, F., Reckhardt, M.C., Erk, D., Travieso, C.M. Clustering of Human Gait with Parkinson's Disease by Using Dynamic Time Warping. In Proceedings of the 2018 IEEE International

Work Conference on Bioinspired Intelligence (IWOBI), San Carlos, Costa Rica, 2018, pp. 1–6.

[Steinmetzer2019a] Steinmetzer, T., Bönninger, I., Reckhardt, M., Reinhardt, F., Erk, D., Travieso, C.M. Comparison of algorithms and classifiers for stride detection using wearables. *Neural Comput. Appl.* **2019**, 1–12, doi:10.1007/s00521-019-04384-6.

[Steinmetzer2019b] Steinmetzer, T., Maasch, M., Bönninger, I., & Travieso, C. M. (2019). Analysis and Classification of Motor Dysfunctions in Arm Swing in Parkinson's Disease. Electronics, 8(12), 1471.

[Steinmetzer2019c] T. Steinmetzer, S. Piatraschk, I. Bönninger, C. M. Travieso and B. Priwitzer, "Gesture Recognition with 3D Sensors using Hidden Markov Models and Clustering," 2019 IEEE International Work Conference on Bioinspired Intelligence (IWOBI), Budapest, Hungary, 2019, pp. 000127-000132, doi: 10.1109/IWOBI47054.2019.9114513.

[Steinmetzer2020] Steinmetzer, T., Wilberg, S., Bönninger, I., & Travieso, C. M. (2020). Analyzing gait symmetry with automatically synchronized wearable sensors in daily life. Microprocessors and Microsystems, 103118.

[Steubl2019] Steubl, L., Sachser, C., Baumeister, H., & Domhardt, M. (2019). Intervention components, mediators, and mechanisms of change of Internet-and mobile-based interventions for post-traumatic stress disorder: protocol for a systematic review and meta-analysis. Systematic reviews, 8(1), 265.

[Stoelben2019] Stoelben, K.J.V., Pappas, E., Mota, C.B. Lower extremity joint moments throughout gait at two speeds more than 4 years after ACL reconstruction. *Gait Posture* **2019**, *70*, 347–354.

[Sun2017] Sun, T., Nie, S., Yeung, D. Y., & Shen, S. (2017, May). Gesture-based piloting of an aerial robot using monocular vision. In Robotics and Automation (ICRA), 2017 IEEE International Conference on (pp. 5913-5920). IEEE.

[Sze2017] Sze, V., Chen, Y. H., Yang, T. J., Emer, J. S., Efficient processing of deep neural networks: A tutorial and survey. *Proc. IEEE* **2017**, *105*, 2295–2329.

[Taborri2016] Taborri, J., Palermo, E., Rossi, S., & Cappa, P. (2016). Gait partitioning methods: A systematic review. Sensors, 16(1), 66.

[Tafazzoli2010] Tafazzoli, F., Safabakhsh, R. Model-based human gait recognition using leg and arm movements. *Eng. Appl. Artif. Intell.* **2010**, *23*, 1237–1246.

[Takeda2014] Takeda, R., Lisco, G., Fujisawa, T., Gastaldi, L., Tohyama, H., & Tadano, S. (2014). Drift removal for improving the accuracy of gait parameters using wearable sensor systems. Sensors, 14(12), 23230-23247.

[Tao2018] Tao, Xianlu, et al. Precise Displacement Estimation From Time-Differenced Carrier Phase to Improve PDR Performance. IEEE Sensors Journal 18.20 (2018): 8238-8246.

[Thumler2002] Thümler, R. (2013). Morbus Parkinson: ein Leitfaden für Klinik und Praxis. Springer-Verlag.

[Tong2011] Ng, H., Tong, H. L., Tan, W. H., Yap, T. T. V., Chong, P. F., & Abdullah, J. (2011). Human identification based on extracted gait features. International Journal on New Computer Architectures and Their Applications (IJNCAA), 1(2), 358-370.

[Trojaniello2014] Trojaniello, D., Cereatti, A., Pelosin, E., Avanzino, L., Mirelman, A., Hausdorff, J. M., & Della Croce, U. (2014). Estimation of step-by-step spatio-temporal parameters of normal and impaired gait using shank-mounted magneto-inertial sensors: application to elderly, hemiparetic, parkinsonian and choreic gait. Journal of neuroengineering and rehabilitation, 11(1), 152.

[Tsipouras2012] Tsipouras, M.G., Tzallas, A.T., Rigas, G., Tsouli, S., Fotiadis, D.I., Konitsiotis, S. An automated methodology for levodopa-induced dyskinesia: Assessment based on gyroscope and accelerometer signals. *Artif. Intell. Med.* **2012**, *55*, 127–135.

[Tunca2017] Tunca, C., Pehlivan, N., Ak, N., Arnrich, B., Salur, G., & Ersoy, C. (2017). Inertial sensor-based robust gait analysis in non-hospital settings for neurological disorders. Sensors, 17(4), 825.

[Urban2016] Urban, T. (2016). Veränderungen der medizinischen Bedarfsstruktur bei ausgewählten neurologischen Erkrankungen und Funktionsstörungen durch den Einsatz moderner Informations-und Kommunikationstechnologien im Rahmen einer Personalisierten Medizin (Doctoral dissertation, Technische Universität Dresden, Medizinische Fakultät).

[Vagenas1992] Vagenas, G., & Hoshizaki, B. (1992). A multivariable analysis of lower extremity kinematic asymmetry in running. International Journal of Sport Biomechanics, 8(1), 11-29.

[vanVelsen2019] van Velsen, L., Broekhuis, M., Jansen-Kosterink, S., & op den Akker, H. (2019). Tailoring Persuasive Electronic Health Strategies for Older Adults on the Basis of Personal Motivation: Web-Based Survey Study. Journal of medical Internet research, 21(9), e11759.

[Veeraraghavan2006] Veeraraghavan, A., Chellappa, R., & Roy-Chowdhury, A. K. (2006). The function space of an activity. In Computer Vision and Pattern Recognition, 2006 IEEE Computer Society Conference on (Vol. 1, pp. 959-968). IEEE.

[Verghese2007] Verghese, J., Wang, C., Lipton, R. B., Holtzer, R., & Xue, X. (2007). Quantitative gait dysfunction and risk of cognitive decline and dementia. Journal of Neurology, Neurosurgery & Psychiatry, 78(9), 929-935.

[Verkerk1990] Verkerk, P. H., Schouten, J. P., & Oosterhuis, H. J. G. H. (1990). Measurement of the handcoordination. Clinical neurology and neurosurgery, 92(2), 105-109.

[Virtanen2019] Virtanen, P., Gommers, R., Oliphant, T.E., Haberland, M., Reddy, T., Cournapeau, D., Burovski, E., Peterson, P., Weckesser, W., Bright, J., et al. SciPy: Open Source Scientific Tools For Python. 2019. Available online: `http://www.scipy.org/` (accessed on 02/12/2019).

[Viteckova2016] Viteckova, S., Kutilek, P., Lenartova, J., Kopecka, J., Mullerova, D., & Krupicka, R. (2016, December). Evaluation of movement of patients with Parkinson's disease using accelerometers and method based on eigenvectors. In 2016 17th International Conference on Mechatronics-Mechatronika (ME) (pp. 1-5). IEEE.

[Viteckova2016] Viteckova, S., Kutilek, P., Lenartova, J., Kopecka, J., Mullerova, D., Krupicka, R. Evaluation of movement of patients with Parkinson's disease using accelerometers and method based on eigenvectors. In Proceedings of the 2016 17th International Conference on Mechatronics-Mechatronika (ME), Prague, Czech Republic, 7–9 December 2016, pp. 1–5.

[Viteckova2018] Viteckova, S., Kutilek, P., Svoboda, Z., Krupicka, R., Kauler, J., & Szabo, Z. (2018). Gait symmetry measures: A review of current and prospective methods. Biomedical Signal Processing and Control, 42, 89-100.

[Wahab2011] Wahab, Y., & Bakar, N. A. (2011, June). Gait analysis measurement for sport application based on ultrasonic system. In 2011 IEEE 15th international symposium on consumer electronics (ISCE) (pp. 20-24). IEEE.

[Wall2019] Wall, H. J., Campbell, C. C., Kaye, L. K., Levy, A., & Bhullar, N. (2019). Personality profiles and persuasion: An exploratory study investigating the role of the Big-5, Type D personality and the Dark Triad on susceptibility to persuasion. Personality and Individual Differences, 139, 69-76.

[Wang2010] Wang, M., Wang, B., Zou, J., Chen, L., Shima, F., & Nakamura, M. (2010, October). A new quantitative evaluation method of parkinson's disease based on free spiral drawing. In 2010 3rd International Conference on Biomedical Engineering and Informatics (Vol. 2, pp. 694-698). IEEE.

[Wang2015] Wang, Z., & Ji, R. (2015, June). Estimate spatial-temporal parameters of human gait using inertial sensors. In 2015 IEEE International Conference on Cyber Technology in Automation, Control, and Intelligent Systems (CYBER) (pp. 1883-1888). IEEE.

[Wang2018] Wang, L. (2018). Personalized Dynamic Hand Gesture Recognition.

[Watanabe2018] Watanabe, Takashi, Tasuku Miyazawa, and Jun Shibasaki. A study on IMU-based stride length estimation for motor disabled subjects: A comparison under different calculation methods of rotation matrix. 2018 IEEE EMBS International Conference on Biomedical & Health Informatics (BHI). IEEE, 2018.

[Westin2010] Westin, J., Ghiamati, S., Memedi, M., Nyholm, D., Johansson, A., Dougherty, M., & Groth, T. (2010). A new computer method for assessing drawing impairment in Parkinson's disease. Journal of neuroscience methods, 190(1), 143-148.

[WHO2015] World Health Organization. (2015). World report on ageing and health. World Health Organization.

[Yamato1992] Yamato, J., Ohya, J., & Ishii, K. (1992, June). Recognizing human action in time-sequential images using hidden markov model. In Computer Vision and Pattern Recognition, 1992. Proceedings CVPR'92., 1992 IEEE Computer Society Conference on (pp. 379-385). IEEE.

[Yang1994] Yang, J., & Xu, Y. (1994). Hidden markov model for gesture recognition (No. CMU-RI-TR-94-10). Carnegie-Mellon Univ Pittsburgh Pa Robotics Inst.

[Yang2010] Yang, C. C., & Hsu, Y. L. (2010). A review of accelerometry-based wearable motion detectors for physical activity monitoring. Sensors, 10(8), 7772-7788.

[Yang2011] Yang, C. C., Hsu, Y. L., Lu, J. M., Shih, K. S., & Chan, L. (2011, June). Real-time gait cycle parameters recognition using a wearable motion detector. In Proceedings 2011 International Conference on System Science and Engineering (pp. 498-502). IEEE.

[Yogev2005] Yogev, G., Giladi, N., Peretz, C., Springer, S., Simon, E. S., & Hausdorff, J. M. (2005). Dual tasking, gait rhythmicity, and Parkinson's disease: which aspects of gait are attention demanding?. European journal of neuroscience, 22(5), 1248-1256.

[Zham2017] Zham, P., Kumar, D. K., Dabnichki, P., Poosapadi Arjunan, S., & Raghav, S. (2017). Distinguishing different stages of Parkinson's disease using composite index of speed and pen-pressure of sketching a spiral. Frontiers in Neurology, 8, 435.

[Zhang2007] Zhang, R., Vogler, C., Metaxas, D. Human gait recognition at sagittal plane. *Image Vis. Comput.* **2007**, *25*, 321–330.

[Zhang2018] Zhang, M., Artan, N., Gu, H., Dong, Z., Burina Ganatra, L., Shermon, S., & Rabin, E. (2018). Gait Study of Parkinson's Disease Subjects Using Haptic Cues with A Motorized Walker. Sensors, 18(10), 3549.

[Zhou2018] Zhou, Z., Dai, Y., & Li, W. (2018). Gesture recognition based on Global Template DTW for Chinese Sign Language. Journal of Intelligent & Fuzzy Systems, (Preprint), 1-10.

[Zifchock2008] Zifchock, R. A., Davis, I., Higginson, J., & Royer, T. (2008). The symmetry angle: a novel, robust method of quantifying asymmetry. Gait & posture, 27(4), 622-627.